An Evaluation of Potential Applications of Low-cost Air Quality Sensors

Dissertation

Presented in Partial Fulfillment of the Requirements for the Degree Doctor of Philosophy in the Graduate School of The Ohio State University

By

Yangyang Zou

Graduate Program in Civil Engineering

The Ohio State University

2021

Dissertation Committee

Dr. Andrew May, Advisor

Dr. Mark McCord

Dr. Rabi Mishalani

Dr. Jordan Clark

Abstract

Air pollution is a great concern for public health, and it has been linked to impacts such as cardiovascular disease and premature death. Traditional air quality monitoring instruments are well-established for quantifying outdoor air pollution, but these instruments are expensive in terms of both capital and operation and maintenance costs. Conversely, low-cost air quality sensors have recently emerged in the market for air quality monitoring due to their inexpensive price and portability. Many researchers across government, academia, and industry have been working to evaluate these sensors in order to understand their performance. One major challenge is that the reliability (e.g., accuracy, robustness) and appropriate applications (e.g., exposure estimates, pattern detection) of these sensors are still uncertain. In this study, we explore the possibility of using low-cost gaseous sensors to characterize spatial patterns of air pollution in an urban area. We also evaluate factors influencing the performance of low-cost particle sensors within indoor environments.

This thesis described the application of using low-cost gaseous sensors to characterize air pollution patterns in an urban area. Because regulatory air monitoring stations are sparsely distributed, they may be unable to detect spatial variability in air pollution. Consequently, we used low-cost sensors deployed on a transit bus to characterize this spatial variability on The Ohio State University campus. Carbon

monoxide, nitrogen dioxide, and ozone sensors were installed on bus and collected data over several days on different bus routes that follow a regular and repeated pattern. The repeated measurement from the sensors demonstrated a systematic underlying spatial pattern in these three air pollutants after accounting for temporal effects.

To understand the detection of indoor particle emission events using low-cost particle sensors in indoor environments, we collocated the sensors with reference instruments in a real indoor environment for two and half months. During this time, we conducted 27 particle emission events of several different types (incense, candle, toast, spray, cooking, humidifier, and opening a window to introduce outdoor particles). All sensors demonstrated the ability to respond to different PM sources, although the magnitude of their responses varied.

In laboratory experiments, we explored the concentrations between which low-cost particle sensors can be expected to provide reliable data. We proposed definitions of upper and lower bounds of the functional range (i.e., the maximum and minimum particle concentrations bounding the range of reliable outputs) based on the relationship between a given sensor's output and that of a reference instrument during controlled laboratory experiments. Our results show that the lower bound ranges from 3 to 15 $\mu g/m^3$. At greater concentrations, the sensors' outputs begin to degrade between approximately 300 – 3,000 $\mu g/m^3$ (e.g., the detector appears to saturate). Therefore, some sensors will provide reliable information in most indoor environments (i.e., when operating within their functional ranges), but the use of these sensors in very clean indoor environments would be limited in effectiveness.

We evaluated how particle size and particle composition can affect the performance of low-cost particle sensors by conducting laboratory experiments with five different particle sources, including ammonium sulfate, propane-torch-generated soot, Arizona Test Dust, incense-generated particles, and burnt toast smoke. We attempted to separate the contribution of particle size and particle composition to the variance in the sensors' outputs and found that particle size appears to have a more dominant effect than composition, although the interaction between size and composition appears to be more important than size or composition alone.

Lastly, we investigated the impact of environmental conditions such as temperature and relative humidity on a particle sensors' accuracy. In this study, we conducted a series of laboratory experiments in which temperature and relative humidity are varied in a precisely-controlled chamber within the range of values that might be expected for typical indoor environments. Using incense and burnt toast smoke as particle sources, we determined that temperature does not appear to have a significant effect on the magnitude of the sensors' outputs, but relative humidity does, which suggests that the operation of these low-cost particle sensors likely requires a correction to account for this effect.

In general, low-cost sensors have potential as an alternative approach for air quality monitoring under outdoor and indoor environments. Gaseous sensors have the potential to provide high spatial resolution data to identify air pollution spatial patterns in urban areas when deployed on mobile platforms. Particle sensors have the ability to detect different indoor emission events. However, the performance of particle sensors is impacted by multiple factors such as particle size, particle composition and

environmental factors. Therefore, additional work is needed to further understand these effects and to propose a proper calibration method that accounts for the influence of these variables.

Acknowledgments

I would like to sincerely thank Dr. Andrew May, my PhD advisor, for his great support and guidance during my PhD study in the Ohio State University (OSU). His patience, motivation and enthusiasm act as a model for me not only for my research study but also my personal life.

Beside my advisor, I would like to thank my thesis committee: Dr. Jordan Clark, Dr. Mark McCord, and Dr. Rabi Mishalani for their insightful comments and great support for me during all my projects and thesis.

I am truly grateful to all of people with whom I have been working during my time in OSU. Specifically, I would like to thank Emma van Dommelen, Bennett Wildey, and Sachinda Liyanaarachchi who all contributed to the development and testing of the low-cost gaseous sensors, and Matthew Young, Morgan Wickey, Melissa Ryan, Jiaqi Liu, and Jiawei Chen all contributed to various aspects of the work with low-cost particle sensors. I would like to thank OSU Transportation and Traffic Management and Campus Area Bus Service for making bus 1105 available to serve as a platform and for supporting the installation of the sensor casing and the data collection. Vehicle location data were processed by Jakob zumFelde, Mohammad Hafiz bin Gulam Mohd Khan, and Gio Hansel. Declan McCord and Roisin McCord provided valuable assistance in preliminary data collection efforts.

And finally, I want to thank my family for their unconditional love to me.

Vita

Education

Ph.D. in Environmental Engineering…….. The Ohio State University
2016 – present

Master's degree in Environmental Engineering…….. Texas A&M University Kingsville
2010-2012

Bachelor degree in Architectural Engineering……..Beijing University of Civil Engineering and Architecture
2004-2008

Publications

Yangyang Zou, Matthew Young, Morgan Wickey, Andrew May, Jordan D. Clark (2019) " Response of eight low-cost particle sensors and consumer devices to typical indoor emission events in a real home (ASHRAE 1756-RP)", *Science and Technology for the Built Environment*, doi: 10.1080/23744731.2019.1676094

Yangyang Zou, Matthew Young, Jiawei Chen, Jiaqi Liu, Andrew May, Jordan Clark (2019) "Examining the Functional Range of Commercially Available Low-cost Airborne Particle Sensors and Consequences for Monitoring of Indoor Air Quality in Residences", *Indoor Air*, doi:10.1111/ina.12621

Yangyang Zou, Jordan D. Clark, Andrew A. May (2021). " A systematic investigation on the effect of temperature and relative humidity on the performance of eight low-cost particle sensor and devices", *Journal of Aerosol Science*, doi:10.106/j.aerosci.2020.105715

Yangyang Zou, Jordan D. Clark, Andrew A. May (2021). " Laboratory evaluation of the effects of particle size and composition on the performance of integrated devices containing Plantower particle sensors". *Aerosol Science and technology*. doi.org/10.1080/02786826.2021.1905148

Field of study

Air quality monitoring, low-cost air quality sensor

Table of Contents

List of Tables

List of Figures

Chapter 1. Introduction: An Overview of Air Quality Sensor Deployment

1.1 Air quality and health

Air pollutants are contaminants that can have harmful effect to human health and the environment. The United States Environmental Protection Agency (EPA) has set National Ambient Air Quality Standards (NAAQS) for six criteria air pollutants including carbon monoxide (CO), nitrogen dioxide (NO_2), ozone (O_3), sulfur dioxide (SO_2), lead, and particulate matter (PM) (Kolb, 2018). In this study we mainly focus on CO, NO_2, O_3 and PM. Unlike CO, NO_2, and O_3, which are gases, "PM is a complex mixture of many chemicals composed of extremely small solid particles and liquid droplets" (EPA,2019). There are two categories of PM, which are based on size, from a regulatory perspective. Particles with a diameter from 2.5 to 10 micrometers are considered as "coarse" particles and designated as PM_{10}. These particles are released from anthropogenic and natural sources. Particles with less than 2.5 micrometers in diameter are considered as "fine" particles and designated as PM2.5. PM2.5 likely to be generated from combustion or atmospheric chemistry process (Kim et al., 2015).

Air pollution is responsible for premature deaths, with an estimated 4 million premature deaths globally related to air pollution on an annual basis, including respiratory infections, heart disease and cancer among others (WHO, 2019). For example, exposure to high level NO_2 and O_3 may have a negative impact on the respiratory system,

leading to serious lung diseases after long-term exposure (Atkinson et al., 2018; Beckett, 1991). The impact of PM is related to its size, which affects where it can deposit within the respiratory system. PM10 will likely deposit in the nose and throat and may lead to respiratory diseases (Kim et al., 2015). PM2.5 is able to penetrate deeper into the lungs, from which it may be absorbed into the blood stream, and consequently, lead to cardiovascular disease or lung cancer (Xing et al., 2016). Because of these adverse health impacts, air pollution monitoring is necessary and critical to assess human exposure and prevent exposure to high concentrations of air pollutant.

In this study, we mainly focus on two locations that may pose higher health risk: near-road outdoor environments and indoor environments. Combustion processes are a major source of outdoor air pollution, e.g., from motor vehicles; from power plants and industry; and from forest fires. For example, CO, NO_2 and O_3 are generated directly or indirectly from traffic (Miller et al., 2020). Indoor air pollutants can also be generated from combustion sources (e.g., cooking, tobacco use, fireplaces), but some household products release gases that can form PM into the indoor environment (Singer et al., 2006).

1.2 Traditional approaches to air quality monitoring

Air quality monitoring has been traditionally conducted by regulatory organizations. In the United States, this is overseen by federal and state EPAs, which mostly focuses on urban environments where there are high populations and/or large number of pollution sources. EPA monitoring instruments follow federal reference method (FRM) and federal equivalent method (FEM) requirements, and they represent "gold standards" for exposure assessment, air quality management, and policy

development (Munir et al., 2019). These instruments are deployed as networks throughout each state. For example, as shown in Figure 1.1, there are numerous monitoring stations in Ohio providing information on ambient O_3 (as an "air quality index"). The distribution of the monitoring stations is relatively sparse, even within areas having a greater density of monitoring sites. For example, in Columbus Ohio, there are only two stations that monitor both O_3 and PM concentration. The collected air quality data from outdoor monitoring stations are provided through online databases for the public to access. For example, O_3 hourly AQI data are provided on the Ohio EPA's website (http://wwwapp.epa.ohio.gov/gis/mapportal/), and 24h PM data are provided through the Air Quality System database (https://www.epa.gov/outdoor-air-quality-data).

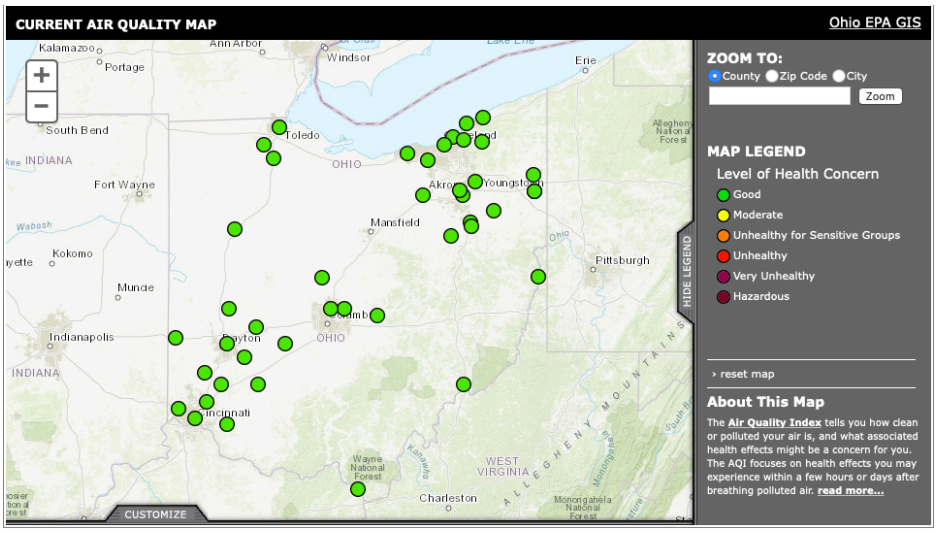

Figure 1.1: Air quality map from Ohio EPA website shows the Ozone AQI in Ohio (http://wwwapp.epa.ohio.gov/gis/mapportal/)

As a result, this traditional monitoring provides accurate data, but it is insufficient to capture spatial differences that may exist between monitoring sites; for example, urban environments represent a complex array of pollution sources that may mix unequally due to differences in land use. In addition, if people are interested in exposure to air pollution within micro-environments in an urban area (e.g., the OSU Campus located within Columbus, Ohio), there is no empirical air quality information because there are no monitoring stations in this location. Similarly, traditional air quality monitoring provides data using either 1 h or 24 h time resolution; therefore it may fail to capture the rapid changes in air quality that may occur over shorter timescales. Moreover, these instruments are expensive in terms of both capital and operation/maintenance costs. One additional limitation is that these traditional monitors represent outdoor air, meaning that there is no direct method for estimating for indoor air pollution exposure, where people spend 90% of their time (Klepeis et al., 2001). Therefore, additional monitoring approaches are necessary in order to provide more complete exposure assessments for air pollution in both the outdoor and the indoor environment.

1.3 Low-cost air quality sensors as an alternative

Low-cost air quality sensors have been recently emerging in the market and can potentially provide information that can supplement traditional air quality monitoring due to their inexpensive price and portability (A. Lewis & Edwards, 2016). Advanced computer algorithms and wireless communication technology enable air quality sensors to become user-friendly in terms of usage and data visualization. The use of these sensors can enhance the spatial and temporal resolution on monitoring pollutants, which makes it

possible to assess the changes in air pollution over smaller spatial scales with higher temporal resolution.

The US EPA defines two classes of low-cost sensors (Morawska et al., 2018). The first is a "measuring component", which always requires an additional data processing system (configured by the end-user) to make the raw signal usable. The second class is a "low-cost monitor", which are pre-packaged systems available from manufacturers and are comprised of at least one measuring component and supporting components including data processing, a power source, and occasionally, a data display. To be considered as "low-cost", the cost of a measuring component must be less than 100 US dollars, and the cost of a low-cost monitor must be less than 1000 US dollars (Williams, Kilaru, et al., 2014). In this study, we use "bare sensor" in reference to "measuring component", and use "integrated device" in reference to "low-cost monitor".

Because of their affordable price, low-cost sensors have become popular to measure personal exposure to air pollutants in both outdoor and indoor environments. For example, real time hourly air quality data (CO, SO_2 and NO_2) measured by low-cost sensors deployed on buses can be easily visualized through websites and even accessed from a smartphone (Varela et al., 2009). PM sensors have been used to assess personal exposure as individuals go about their daily routines (Steinle et al., 2013). Low-cost particle sensors have been used to create a network of PM data worldwide (https://www.purpleair.com/map), and these data have been used by numerous end-users to analyze air quality trends. Low-cost sensors can also be utilized in pollution source identification (Roberts et al., 2014) and warning systems (Kumar et al., 2015). However,

previous studies on low-cost sensor have not fully explored factors influencing the sensors' performance for certain applications and under some environmental conditions.

1.3.1 Working mechanisms of low-cost sensors

Briefly, low-cost gaseous sensors operate by detecting the interactions between the gaseous pollutant and material within the sensor, and low-cost particle sensors are based on particle interactions with light. Bare gaseous and particle sensors need to be integrated with a microcontroller (e.g., Arduino) or a single-board computer (e.g., Raspberry Pi) to receive signal from the sensor to calculate a concentration in real time. The following sections elaborate on how these sensors function.

1.3.1.1 Gaseous sensor

The widely used gaseous sensors on the market are electrochemical sensors and metal oxide semiconductor sensors. In a semiconductor sensor, the impedance capacity changes when the sensing layer contacts the target gas. In electrochemical sensors, the target gas reacts at an electrode, and an oxidation or reduction reaction generates a current which is proportional to the gas concentration (Hasenfratz, 2015). In this work, we use electrochemical gas sensors. The major components are the working electrode, the counter electrode, and an electrolyte solution. Figure 1.2 shows a schematic of the CO sensor (Alphasense CO-A4) used in this study. The reactions happening at the working electrode can be explained as:

$$CO + H_2O \rightarrow CO_2 + 2H^+ + 2e^- \qquad \text{eq 1}$$

A chemical reaction at the counter electrode can be explained as:

$$½\ O_2 + 2H^+ + 2e^- \rightarrow H_2O \qquad \text{eq 2}$$

In general the reaction is:

$$CO + ½\ O_2 \rightarrow CO_2 \qquad \text{eq 3}$$

The current generated between the working electrode and counter electrode is proportional to the concentration of CO. Other electrochemical sensors follow the same process but different chemical reactions. The generated current of electrons results in an electrical signal output, which can be converted to a gas-phase concentration of a target analyte through either the manufacturer-recommended calibration or a user-developed calibration against FEM/FRM reference instruments.

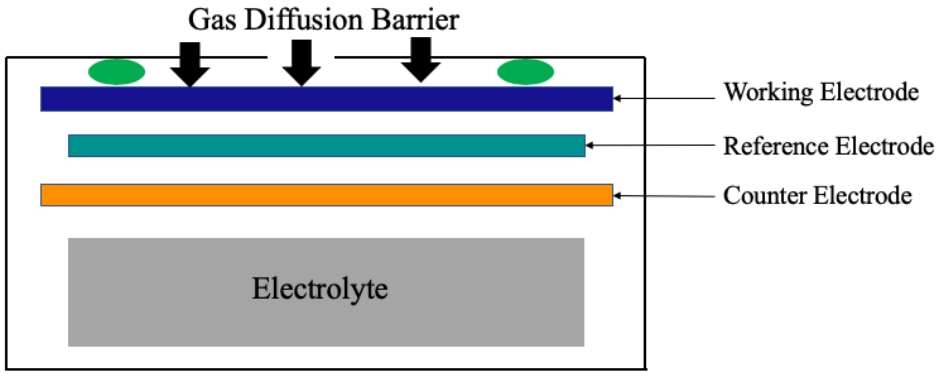

Figure 1.2: Schematic of CO electrochemical sensor used in this study

1.3.1.2 Particle sensor

Most commercially available PM sensors quantify particles based on the light scattered by the entire particle population rather than counting individual particles. Figure 1.3 provides a diagram that represents what occurs within one particle sensor (Honeywell HPM), but this is similar for other light-scattering sensors. The sensors emit light from a small LED, and this light is scattered by particles that pass through the sensing zone. A photodetector detects the scattered light intensity at a certain angle, and this intensity is then translated into particle number or mass concentration through a calibration equation (Yu el al, 2017, Shao et al, 2017). Several PM sensors provide analog output (e.g., Sharp GP2Y1010AU0F and Shinyei PPD41), and the manufacturers provide calibration curves to translate the analog signal to particle concentration in the technical sheet. Other PM sensors provide digital output (e.g., PlantowerS5003 and Honeywell HPM) that includes the translation of signal from the photodetector into mass concentration through an internal data processing system.

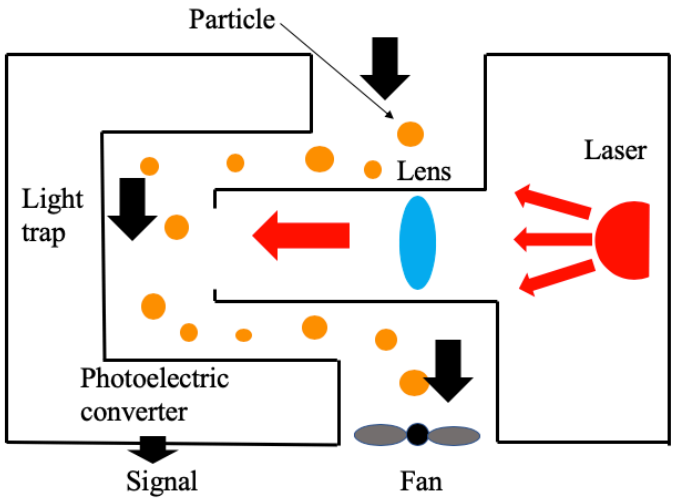

Figure 1.3: Schematic of low-cost particle sensor

1.4 Low-cost sensor evaluation and application

Prior research studies for low-cost air quality sensors have focused on a variety of topics, but these studies can all be grouped into one of four broad categories: laboratory evaluations of gas sensors; laboratory evaluations of particle sensors; field studies with gas sensors; and field studies with particle sensors. These studies can be sub-categorized into specific research foci. (Table 1.1). Specific results from the studies listed in Table 1 will be discussed in later sections.

Table 1.1: Summary of previous studies on low-cost air quality sensors

Category	Focus of study	Literature paper
Gas sensor (lab)	Assess accuracy	(EPA, 2010) (Mead et al., 2013) (Rai et al., 2017) (Karagulian et al., 2019)
	Assess temperature and RH effect	(Piedrahita et al., 2014) (Lin et al., 2015) (Sun et al., 2016)
Particle sensor (lab)	Assess accuracy	(Austin et al., 2015) (Sun et al., 2016) (Polidori et al., 2016b) (Zamora et al., 2019)
	Assess size effect	(Wang et al., 2015) (Manikonda et al., 2016) (Sousan et al., 2016) (Liu et al., 2017) (Zamora et al., 2019) (He et al., 2020) (Kuula et al., 2019)
	Assess composition effect	(Wang et al., 2015) (Sousan et al., 2016) (Sousan et al., 2017) (Liu et al., 2017) (Zamora et al., 2019) (Hagan & Kroll, 2020)
	Assess temperature and RH effect	(Wang et al., 2015) (Zamora et al., 2019)

		(Tryner et al., 2020) (Bulot et al., 2020)
Gas sensor (field)	Mobile monitoring/pollution dynamic	(Gil-Castiñeira et al., 2008) (Varela et al., 2009) (Wen et al., 2013) (Mead et al., 2013) (Patton et al., 2014) (Suriano et al., 2015) (Velasco et al., 2016) (Gao et al., 2016) (C. H. Yu et al., 2016) (Apte et al., 2017) (Jerrett et al., 2017) (Miller et al., 2020)
	Compare with reference instrument	(Moltchanov et al., 2015) (Castell et al., 2017)
	Compare with reference instrument (correction)	(Masson et al., 2015) (Spinelle et al., 2015) (Sun et al., 2016) (Cross et al., 2017) (Sadighi et al., 2018) (Zimmerman et al., 2018) (Lim et al., 2019)
Particle sensor (field)	Compare with reference instrument	(Mukherjee et al., 2017) (Mukherjee et al., 2017) (Kelly et al., 2017) (Zikova et al., 2017) (Zheng et al., 2018) (Badura et al., 2018) (Liu et al., 2019) (Sayahi et al., 2019)
	Compare with reference instrument (temperature and RH correction)	(Holstius et al., 2014) (Han et al., 2017) (Hojaiji et al., 2017) (Mukherjee et al., 2019) (Crilley et al., 2019) (Malings et al., 2020)
	Personal exposure	(Steinle et al., 2013) (A. C. Lewis et al., 2016) (Mazaheri et al., 2018) (Barkjohn et al., 2020)
	Indoor PM detection	(Dacunto et al., 2015) (Patel et al., 2017) (Li et al., 2018) (Singer & Delp, 2018) (Curto et al., 2018)

1.4.1 Laboratory evaluations of low-cost gaseous sensor

Laboratory evaluations of gaseous sensors usually compare the sensor's reported concentration (based on manufacturer calibrations) to a reference instrument or develop new calibrations using the raw signal output by the sensors. These laboratory experiments typically use either steady or transient concentrations by controlling the calibration gas flow into a testing chamber, and sensors and collocated reference instruments monitor the gas concentration simultaneously. Several studies use the calibration equation provided by the manufacturer (Christian Kjær Jensen, 2016; Gonzalez et al., 2019; Shum et al., 2011) to convert raw signal output to concentration (pre-calibration) and compare the results to reference instruments. Other studies (EPA, 2010; Piedrahita et al., 2014) directly compared the sensors' raw signal with a reference instrument in laboratory experiments and evaluated the relationship to develop their own calibration curve. There is often a linear relationship between sensors' signal /concentration and the reference instrument. Typically, the slope, intercept and coefficient of determination (R^2) from these estimated linear relationships are used to assess the accuracy and precision of the sensors. For gaseous sensors (CO, NO_2 and O_3), slope and intercept may vary slightly in the laboratory test under the same experimental conditions for different units of the same sensor model, yet R^2 are typically greater than 0.9 for most of the laboratory studies (Mead et al., 2013; Piedrahita et al., 2014; Sun et al., 2016). Due to the excellent performance of gaseous sensor based on prior work, we did not conduct a rigorous

laboratory evaluation within this study beyond the development of calibration curves, and our focus is on field applications of these sensors.

1.4.2 Laboratory evaluation for low-cost particle sensor

Laboratory evaluation for particle sensor use approaches similar to those used to evaluate gaseous sensor. Either the sensors' raw signal is compared directly to the reference instrument (Wang et al., 2015), or the concentration (through the manufacturer recommended calibration equation) is compared to the reference (Sun et al., 2016). Different than gas sensors, most particle sensors, especially those found in integrated devices, internally convert the electrical signal to provide particle number and/or particle mass concentration as an output (Sousan et al., 2017). During the calibration process, a simple linear regression is applied to sensor raw/calibrated concentration with the reference instrument. R^2, slope and intercept from this linear regression are considered to be the key indicators of particle sensors' performance (Karagulian et al., 2019). Other research studies use calculated bias (Austin et al., 2015; Sousan et al., 2017) and root mean square error (Zheng et al., 2018) to evaluate sensors' accuracy, and use coefficient of variation to evaluate sensors' precision (Zamora et al., 2019).

However, due to the complex interactions of the particles' size and composition (which influences the particles' complex refractive index) on light scattering, this regression relationship can vary significantly for the same sensor when monitoring different types of particles under different environmental conditions. Previous research

has explored the effect that these two properties have on a particle sensor's performance. Regarding particle composition, prior laboratory studies have used variety of particles source to evaluate these effects including polystyrene latex spheres (Liu et al., 2017a; Northcross et al., 2013; Wang et al., 2015); salt particles (Sousan et al., 2017; Wang et al., 2015); Arizona Test Dust (Manikonda et al., 2016; Sousan et al., 2017); and oleic acid (Zamora et al., 2019). In these studies, the slopes of the regression fit between sensors' output and the reference instruments varied for different particle sources. However, among these particle sources, particle size may co-vary with particle composition depending on the source of the particles. Thus, there is need to separate compostion and size effects. In Chapter 5 of this work, we describe experiments to de-couple composition and size effects to better understand these impacts.

Secondly, environmental factors may also significantly impact sensors' performance. Changes in temperature and/or relative humidity (RH) may change the properties of the particles; for example, condensation of water vapor to the particles can both increase the size of the particles and alter the complex refractive index. Prior work has suggested that RH is a more important effect than temperature (Liu et al., 2017; Wang et al., 2015). However, these studies are lacking in repeatability for the same temperature and RH condition as they conducted one replicate at each temperature or RH condition. In addition, the evaluation of environmental effects has mainly been conducted using outdoor field tests (Budde et al., 2013; Han et al., 2017; Jayaratne et al., 2018), in which temperature and RH may be correlated, resulting in difficulties in de-coupling the effects of each and potentially affecting the conclusions. As for the indoor environment, temperature and RH may not necessarily be correlated because they can be controlled

independently (to some extent). Therefore, we apply an optimized experimental matrix spanning a range of temperature and RH conditions likely to be encountered in indoor environments to evaluate these two factors separately in Chapter 6.

1.4.3 Field studies for gaseous sensor

For field studies of gaseous sensors, researchers deployed sensors for both stationary and mobile monitoring. Under both approaches, various studies concluded that low-cost sensors can provide reliable data on outdoor air pollutants under different applications. To understand real-time air pollution spatial pattern in urban environment, researchers have used sensors for stationary air pollution monitoring (Spinelle et al., 2014; Sun et al., 2016). These studies demonstrated that a network of stationary sensors can provide a method to detect spatial variations in air quality at a fine resolution in urban areas. However, stationary monitoring requires a dense sensor network (a large number of units) to capture this spatial variation, and this approach may be difficult to manage for long-term measurements without the right personnel. Consequently, others have explored the use of mobile monitoring to provide an alternative approach to investigate the spatial variations in air pollution . Several studies applied sensors on mobile platforms such as bicycles and cars (Apte et al., 2017; Mead et al., 2013; Miller et al., 2020; Moltchanov et al., 2015; Velasco et al., 2016), and they found spatial variations of air quality within the microenvironment sampled by their mobile sensors. However, these studies only included

one data collection period per day on the same route across several days, and therefore, are insufficient to capture diurnal temporal variations without a more labor-intensive approach. In this work, we explored the use of low-cost gas sensors deployed on a transit bus, which are common to any urban environment, because they follow a regular and repeated route, overcoming the spatial and temporal limitations that exist in various prior studies, in Chapter 2.

1.4.4 Field studies for particle sensor

Field studies for particle sensors include both indoor and outdoor monitoring. The majority of research to date has focused on outdoor applications, while only a few studies investigate the usage of these sensors for indoor environments. Chapters 3 though 6 focus on understanding the performance of particle sensors under realistic indoor environments.

Indoor particle sources are different than outdoor sources. The composition of particles can be significantly different. For example, Geller et al (2002) found that organic carbon indoors is 77% higher than outdoors, while Long et al (2000) demonstrate that the indoor activity generates more ultrafine particles (< 0.1 microns). These differences in particle characteristics may affect the response of the particle sensors to the particles. Therefore, whether particle sensors can be reliable in detecting indoor particle concentrations remains under question. In Chapter 3, we address this question by evaluating particle sensors' performance in the detection of various residential PM sources.

One further challenge is that indoor PM may be difficult for the particle sensors to detect when the concentrations are small (e.g., in a "clean room" environment or in a building with a high-efficiency particle filter). Thus, the ability of particle sensors to detect low particle concentrations is important. However, there is no standardized definition for this metric for continuous PM monitoring by low-cost sensors (Wallace et al. 2011). Similarly, when an extremely-high particle concentration event occurs (e.g., some cooking events, indoor smoking), particle sensors need to be accurately report concentrations as well. Therefore, both the minimum and maximum limits of functional range, or equivalently, the limits of quantification (LOQ), need to be evaluated to determine a sensor's usefulness in building applications. Chapter 4 evaluates both lower and upper LOQ for particle sensors under laboratory environment using different particle sources.

1.5 Overview of objectives and contributions of chapters

In this study, we explore the possibility of using low-cost gaseous sensors to characterize spatial patterns of air pollution in an urban area. We also evaluate factors influencing the performance of low-cost particle sensors within indoor environments. This section summarizes both the objectives and the main contributions of each chapter.

Chapter 2 objectives:

1) Investigate how the air pollution varies in space across different bus route using low-cost sensors.

2) Determine whether a consistent, underlying spatial pattern exists after accounting for temporal variations.

Chapter 2 contribution:

Among the research studies for monitoring on-road air pollutants, there is a lack of repeated mobile monitoring using low-cost sensors over the same locations; thus, spatial trends have not been sufficiently characterized. We deployed low-cost gaseous sensors on a transit bus to monitor on-road traffic-related air pollutants, and we observed a consistent spatial pattern from this regular and repeated monitoring.

Chapter 3 objectives:

1) Assess the ability of low-cost particle sensor to detect different types of indoor particle emission events in a real indoor environment.
2) Assess the consistency in performance of multiple instances of sensors from the same manufacturer.

Chapter 3 contribution:

Low-cost particle sensors have been widely used for outdoor PM monitoring; only few studies focus on particle sensors and indoor applications. Indoor particles are diverse and often different than outdoor particles, and whether particle sensors can reliably detect indoor particle sources needs to be evaluated. We are one of the few studies who utilized low-cost particle sensors to quantify residential particles in a semi-controlled manner. We find that particle sensors can identify various indoor particle sources; however, some factors may impact the sensor performance,

including particle size and particle composition, which are explored in the subsequent chapters.

Chapter 4 objectives:

1) Propose several definitions of an upper and lower bound of the range of particle concentrations between which a low-cost particle sensor can be expected to provide reliable data and assess the appropriateness of each.
2) Quantify this range for several low-cost particle sensors under laboratory experiments using different particle sources.

Chapter 4 contribution:

Particle sensors need to be able to detect both low and high particle concentrations indoors. Some indoor environments may be relatively particle-free, but the lower limit of the concentration that is detectable by these sensors has not yet been sufficiently characterized in previous work. Similarly, some indoor activities may create high particle concentrations (e.g., cooking, burning incense), and whether a particle sensor can detect and accurately report this high concentration needs to be investigated. We propose new methods to define lower and upper limits of the concentration between which the sensors can provide reliable data and find that some particle sensors can reliably quantify particles spanning very low (~5 $\mu g\ m^{-3}$) and very high concentrations (~500 $\mu g\ m^{-3}$) using proxies for indoor particle sources.

Chapter 5 objectives:

1) Investigate the effects of particle composition on the sensors' performance by conducting laboratory experiments using different particle sources.
2) Evaluate the influence of particle size to sensors' performance using size-selected particles between the range of 100 nm to 700 nm and distributions of particles with mass-median diameters ranging from ~200 nm to ~2 μm.
3) Quantify how size and composition contribute to variability in the sensors' response.

Chapter 5 contribution:

From previous research, the performance of low-cost particle sensors appears to vary when sampling different particle sources, and in the majority of that work, particle composition was inherently related to particle size due to the experimental methods. In this study, we separate composition and size effects and provide supplemental information for the evaluation of the influence of particle size and particle composition on a sensor's performance. We find that there was a source effect on the performance of sensors, and we quantify the influence that size, composition, and the interaction between size and composition have on the variance in the sensors' output.

Chapter 6 objectives:

1) Investigate the relationship between temperature and low-cost particle sensors' performance for the range of temperature expected in indoor environments.
2) Investigate the relationship between RH and sensors' performance for the range of RH expected in indoor environments.

Chapter 6 contribution**:**

Previous studies suggest that temperature may have an effect and that RH does have an effect on particle sensors' performance. However, these studies either lack repeatability (i.e., there are few replicates of the experiments) under the same laboratory conditions or are based on outdoor sampling, where temperature and RH are often correlated. However, under indoor environments, temperature and RH may not be correlated because they can be controlled independently. In this study, we conducted laboratory experiments under optimized temperature and RH conditions and find that there is a significant linear relationship between the slopes of the linear fit between sensors and research grade instruments as RH varies, but no evidence that temperature has such an effect.

Chapter 2: Using Low-Cost Air Quality Sensors to Understand the Spatial Pattern of CO, NO_2 and O_3 over Urban Roadways

2.1 Introduction

Motor vehicles are a major source for urban air pollution that can have harmful effects on human health and the environment. The direct and indirect air emissions from motor vehicles include carbon monoxide (CO), nitrogen dioxide (NO_2), and ozone (O_3) as well as particulate matter (which will not be a focus here). These emissions are collectively referred to as traffic-related air pollution (TRAP) (Patton et al., 2014; C. H. Yu et al., 2016). To monitor the air quality impacts of TRAP and other air pollution, the Environmental Protection Agencies (EPA) conducts regulatory air pollution measurements at sparsely distributed monitoring stations, typically with a reporting interval of 1 hr. One limitation of this existing approach is that the sparse distribution of the regulatory monitors does not allow them to capture spatial changes of air pollution at a high resolution (Morawska et al., 2018). High-resolution air pollution models at the urban scale have high computational requirements, given the large complexity of urban environments (Kumar et al., 2015); this complexity requires smaller step sizes in space (and possibly in time), which greatly increases the computational time of the model, implying that a purely model-based approach may be impractical to obtain.

In this work, we consider low-cost air quality sensors as an approach to supplement the existing TRAP measurements. Low-cost air quality sensors may provide

an inexpensive solution for air quality monitoring with higher sampling frequency, but the ability of these sensors to provide reliable air pollution data in urban areas remains under evaluation.

Various research studies have used mobile or stationary sensor platforms to monitor spatial and temporal variation of air pollution in urban areas. Several studies (Brienza et al., 2015; Guo et al., 2018; Jiao et al., 2016; Masson et al., 2015; Moltchanov et al., 2015; Roberts et al., 2014; Spinelle et al., 2014; Zimmerman et al., 2018) evaluate the sensors performance against collocated reference instruments or nearby monitoring stations in order to conduct in situ calibrations. Those studies found that the correlations between the sensors and the reference instruments are high, although some studies developed correction methods to account for biases related to temperature and relative humidity. However, even though low-cost sensors may provide an approach to overcome some of the spatial limitations faced by regulatory monitors, a high-density network of sensors may be required to capture location-specific features, e.g., at traffic intersections or within so-called “urban canyons”.

In order to gain high spatial resolution monitoring while reducing the number of sensors deployed, researchers have used various transportation modes as the sensors’ platforms. Mead et al. (2013) utilized CO, nitric oxide (NO), and NO_2 sensors carried by pedestrians and observed variability of these pollutants over a small spatial scale during a short period of sampling time. Velasco et al. (2016) deployed O_3 and particulate matter (PM) sensors on a public bike-sharing system and identified similar spatial pattern on the

same route over five consecutive days. In Yu et al. (2016)'s study, PM and CO were monitored by pedestrians carrying the sensor devices on two parallel streets at the same time across multiple days. They found CO and PM were significantly different between two parallel routes, and they also demonstrated significant differences between days. However, the measurements were only conducted once per day on each pass, so they lack information about temporal variations throughout the day. This may indicate that short-term monitoring over small spatial scales are insufficient to provide information on air quality in urban environments. In addition, long-term monitoring by pedestrians and cyclists (Mead et al., 2013; Velasco et al., 2016; C. H. Yu et al., 2016) may become burdensome for the data collectors. A transit system, however, is a transportation mode that can provide routinely-collected, high-time-resolution data by repeatedly traversing a fixed route throughout a broad region.

Therefore, to achieve high resolution of spatial and temporal coverage, we use a transit system to perform as the platform carrying air quality sensors because transit provides broader spatial coverage in a repeated pattern. Previous studies have used buses as the sensor platform in Europe. Gil-Castineira et al. (2008) mounted a carbon dioxide (CO_2) sensor on a transit bus equipped with a GPS system with the objective of developing a real-time monitoring and dynamic mapping system in an open service website. Varela (2009) also deployed CO_2, CO, NO_2, and sulfur dioxide (SO_2) sensors on buses and developed an air quality network capable of visualizing the air pollution data. However, these studies were mainly focused on visualizing the air quality data on a map for public use; our study focuses on the analysis of spatial patterns within the data.

2.2 Objectives

This study aims to explore the possibility of using air quality sensors and a transit platform to measure on-road air pollution patterns. The goal is to characterize the patterns of CO, NO_2 and O_3 in an urban area by deploying low-cost sensors on a transit bus as a mobile platform. The objectives are to: 1) investigate how the air pollution varies in space along routes; and 2) determine whether a consistent, underlying spatial pattern exists after accounting for temporal variations with the low-cost sensors being used.

2.3 Materials and method

A custom-built sensor unit was fabricated through the assistance of other lab members using three low-cost gas sensors including a carbon monoxide (CO) sensor (Model CO-A4F, Alphasense Ltd), an ozone (O_3) + nitrogen dioxide (NO_2) sensor (Model OX-A431), and a standalone NO_2 sensor (Model NO2-A43F). These sensors are electrochemical sensors. The target gas reacts at the working electrode, and the electrical charge generated by this chemical reaction is directly proportional to the concentration of the target gas. We used Raspberry Pi 2 as the data acquisition system to record and store time-stamped sensor data onto a 16GB micro-SD card via executable code written in the Python programming language; new sensor data were recorded every 3 seconds during operation.

The three gas sensors were calibrated against EPA-grade monitoring instruments including a Carbon Monoxide (CO) Analyzer (Teledyne Model T300, Teledyne API, San Diego, CA), Nitrogen Oxide (NOx) Analyzer (Model T200), and a Photometric Ozone (O_3) Analyzer (Model T400). The CO and O_3 analyzers detect the targeted air pollutants using a system based on the Beer-Lambert law (KS., 2014) for measuring target gas concentration, in which a light is passed through the sampling cell, and the quantity of light that is absorbed by the sample is proportional to the target gas concentration. In the NOx analyzer, NOx concentration is determined from the light intensity that is generated from chemical reactions between NOx and O_3.

To calibrate the sensors, they were placed into a 0.71 m x 0.48 m x 0.38 m (0.130 m^3) enclosed chamber. First, we injected "zero air" (ProSpec Inc.) having "0" ppbv concentration of any air pollutant. We injected "zero air" to obtain a stable sensor signal for "0" ppbv. We then injected CO calibration gas (ProSpec Inc., 9.6 ppmv) from the inlet of the chamber and monitored the CO concentration from the outlet through a sampling port using a CO analyzer and a data logger. The output concentration from the CO analyzer and the signal from the CO sensors both increased during this process, following a linear relationship. We then converted the signal to concentration using a linear regression calibration equation (reference concentration = slope x sensors' signal + intercept). This calibration was repeated multiple times for each individual sensor to obtain the values of slope and intercept; the average of the values from repeated calibration experiments for each individual sensor was then used to determine the calibration equation. We then used this calibration equation to convert the sensor's signal

into concentration when it was deployed in the field. In all of these equations, y is the concentration of a given gas-phase pollutant and x is the digital signal obtained from the appropriate sensor.

Table 2.1 Calibration equations for sensors deployed on bus 1105. Numerical values represent the average ± one standard deviation of the slopes and intercept among all repeated calibration experiments of each individual sensor.

Sensors	Calibration equations	R^2
CO	y = (0.0156 ± 0.001) x – 2.574 ± 0.24	0.92 ± 0.04
NO_2	y = (24.38 ± 3.21) x – 2201 ± 562	0.62 ± 0.18
O_3	y = (15.68 ±2.32) x – 480.30 ± 24.42	0.73 ± 0.09

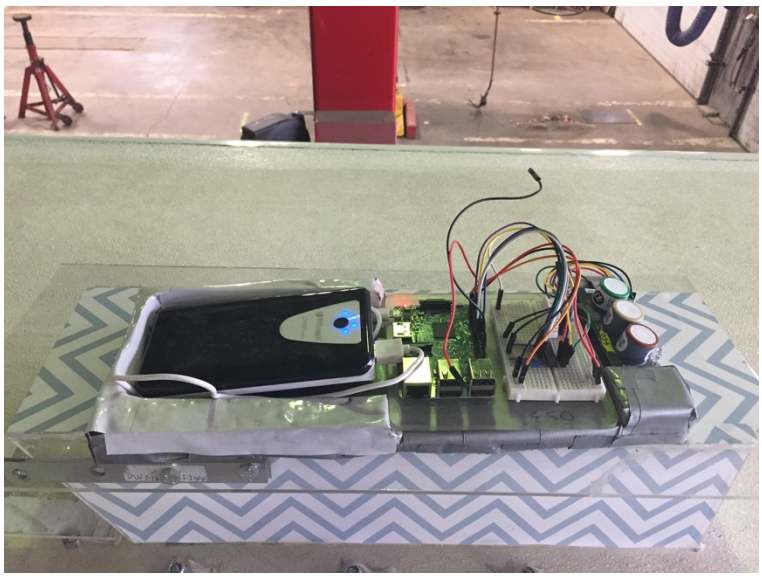

Figure 2.1: The air quality sensor unit installed on CABS bus 1105.

The air quality sensor unit was placed inside a 0.50 m x 0.25 m x 0.17 m (0.02 m^3) custom-built acrylic box (Figure 2.1) which allows air to flow through the sensor unit via openings in the leading and trailing edges. The design of the box can also reduce direct exposure to solar radiation because it is covered by a non-transparent paper on the three sides of the box; and the angled design on the front of the box can reduce entry of water in the event of rain. The box is securely attached on the top of the bus (near the emergency exit) by screws. As the bus drives, the sensor unit is located upwind of the exhaust pipe, so it is unlikely that the sensors are simply sampling from the exhaust pipe under typical operation. The sensor unit was powered by a USB power bank (10,000mAh) that provided for at least 24 hours of operation.

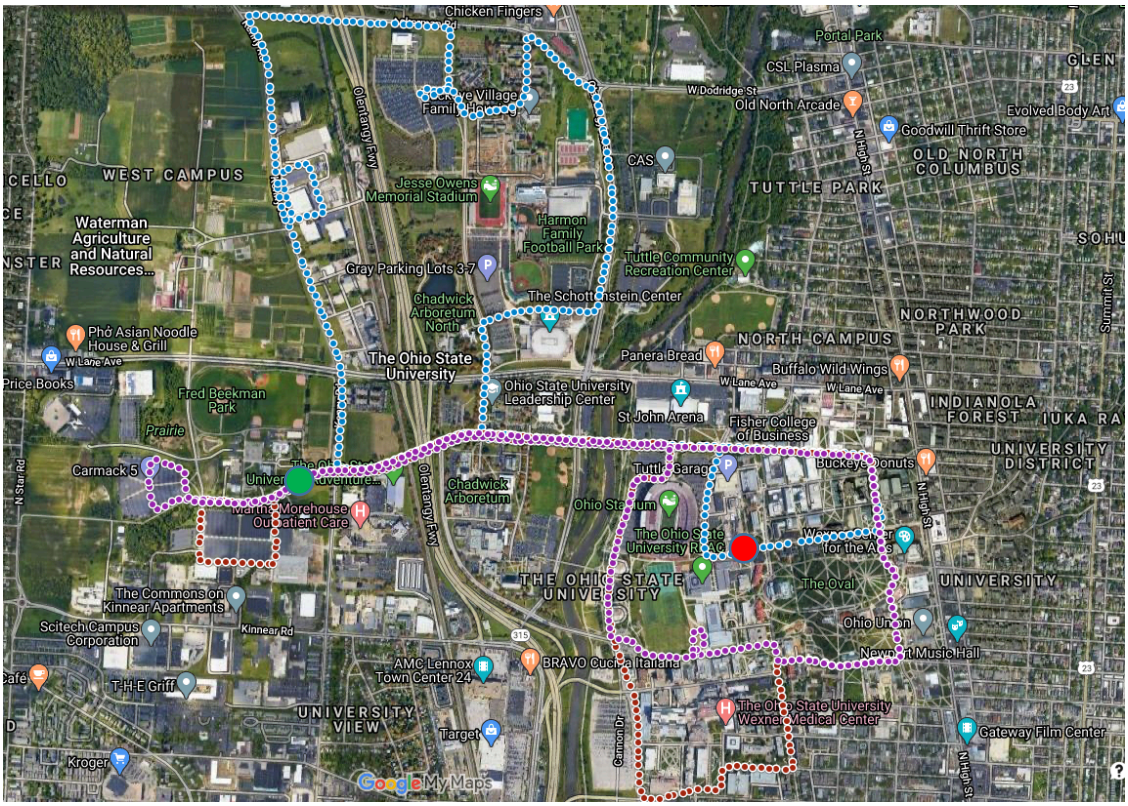

Figure 2.2: OSU CABS bus routes map for CLN (red), BV (blue) and WC (purple) routes. The large green dot represents the starting point (distance = 0) for CLN and WC, and the large red dot represents the starting point for BV.

We used the OSU Campus Area Bus Service (CABS) bus 1105 as our mobile air quality sensing platform. At the time of the data collection, OSU Campus Area Bus Service (CABS) served approximately 5 million passengers annually with seven major bus routes for the service of public transportation on and around OSU campus that traverse varied land uses including core academic campus, park-and ride facilities, a large medical campus, administrative facilities and residential and commercial neighborhoods. There are also numerous potential sources of TRAP including large surface parking lots and parking garages for employees and students, a state highway with multiple ramps that serves the campus, and a large medical campus that serves a large number of visitors on a

daily basis. Bus 1105 served three routes -- Campus Loop North (CLN), Buckeye Village (BV) and West Campus (WC), as depicted in Figure 2.2 -- during the period in which this study was conducted. The CLN route was approximately 28,300 ft (~8630 meter) and had a 35 min cycle time (the duration of one bus trip), the BV route was approximately 34,500 ft (10,520 meter) and had a 25 min cycle time, and the WC route was approximately 26,420 feet (8,050 meter) long and had a 30 minutes cycle time. The sampling times common to all sampling days were 7:00 to 18:00, so we have removed data outside of that time window.

In addition to the air quality sensor data, we also obtained location data through the Automatic Vehicle Location (AVL) system data. The AVL data provide time-stamped information in the form of coordinates (latitude and longitude). The AVL data were processed by students in the Campus Transit Lab (CTL) to provide distances along the route with respect to the start points. Using AVL data, we can assign a specific location to a given record of air quality data. We used linear distance (X = x) from the beginning of the bus trips (X = 0) to identify the sensor's location from the coordinate information. This linear distance also allows for separating sensors readings into bus trips (a bus trip is a complete traversal or a route by a bus, typically starting and ending from the same reference location, commonly the route's terminal) because the linear distance begins anew for the next trip at the starting points shown in Figure 2.2.

Due to a large number of maintenance issues experienced by the bus on which we deployed the sensors, we have somewhat limited data – 5 days (total of 83 bus trips) for CLN, 3 days (total of 60 bus trips) for BV, and 5 days (total of 100 bus trips) for WC.

2.4 Data analysis

We conducted some data pre-processing prior to analysis. For example, some of the sensor data may be influenced by localized, transient pollution events (e.g., following a heavy-duty diesel truck on the road; being stopped at an intersection behind another transit bus). Thus, the data were smoothed using windows of 1,000 ft (305 meter) with a step size of 100 ft (30.5 meter) in order to dampen these effects; effectively, this approach was a running median. For example, on CLN route, the median value of CO between 0 to 1,000 ft is assigned at the mid-point (X = 500 ft) to define the first observation along the route; this process was repeated by stepping forward 100 ft and repeating until the upper bound of the window is reached at X = 28,300 ft. The result is a smoothed dataset that is gridded to 283 fixed locations (every 100 ft along the route) for all 83 bus trip vectors on CLN (i.e., a 283 by 83 matrix). Similarly, we obtained matrices that are 264 by 100 for BV and 345 by 60 for WC.

In order to visualize the spatial pattern as a function of locations and associated factors (e.g. traffic, land use) that impact the spatial pattern, the average of CO, NO_2 and O_3 concentration across all trips for each data matrix is plotted with distance (as is done in Figure 2.3 below).

To determine if there is a consistent spatial pattern for the three air pollutants along each route, we computed the correlation coefficient between each pair of bus-trip

vectors of three air pollutant concentration on the three bus routes. The Pearson correlation coefficient is used to determine this correlation between gridded pollutant values for 1) all pairs of trips; 2) pairs of consecutive trips; and 3) the median value of 50% of the trips randomly sampled from the population and the median value of the remaining trips.

Considering the temporal effect, the median CO, NO_2 and O_3 value at each gridded location can be affected by day-to-day and time-of-day factors. For example, if the CO concentration on one day is substantially higher than the other days, this could raise the median CO concentration across all locations. To investigate the temporal effect, we calculate the average concentration for each trip and plot the concentration with the beginning of that trip on different sampling days. To partially control for these temporal effects, we compared the median value of each pollutant for each bus trip to the gridded locations on the same bus trip. To understand whether air quality values at some locations is significantly different than other locations across all trips, a proportion is used to represent this information.

At a specific location (distance from the beginning of the bus trip), we determine if a given pollutant value is greater than the median value for that trip; the proportion is then calculated as the number of times that the pollutant value is greater than the median value across all trips, divided by the total number of trips. Under the null hypothesis (of systematic spatial pattern), the probability that the concentration value at a location on any given trip would be above the trip median is 0.5. To test the significance of this proportion for all locations, the following equation is used:

$$z = \frac{P - P_0}{\sqrt{\frac{(1-P_0)P_0}{n}}} \qquad \text{eq.2.1}$$

In the equation, P_0 is the proportion under the null hypothesis (in this case is 50%), n is the total number of bus trips, and z, the z-score, is determined from a z-table at a significance level of 0.05. The value of P (the sample proportion) can then be calculated as proportions that are statistically different from the hypothesized proportion at 5% significance level.

2.5 Results and discussion

In this study, we are interested to determine the spatial pattern of three air pollutants over the three transit routes by using low-cost sensors deployed on one bus as it traverses each of the three routes. We first visualize the spatial pattern of each pollutant on each route, and we subsequently analyze the consistency of these spatial patterns. We then investigate the general underlying spatial pattern for each pollutant on each route.

2.5.1 Characterizing spatial variations

Figure 2.3 shows the mean CO concentration values at each grid point over all bus trips as a function of route distance from the beginning of the route on CLN, BV and WC respectively. Mean concentrations of CO clearly varied with location on a given route. Local maxima and minima of mean CO concentrations across all trips for all routes suggests a strong spatial pattern, which may be associated with land use. For example, on CLN, the built environment at 18,000 ft is comprised of a large parking lot and several parking garages for employees and visitors to the OSU Medical Center, and this location is adjacent to an off-ramp to State Route 315; both of these factors may contribute to

generally higher CO concentrations at this location. On the contrary, the location at 22,000 ft on CLN is near the north end of Cannon Drive, in close proximity to green space and the Olentangy River; although it is adjacent to a large surface parking lot, this is primarily used by OSU staff and students, so we expect traffic to only be heavier during the morning and afternoon rush hours. In addition, CO spatial patterns are different among three routes because of difference in sampling days, land use and traffic patterns. For BV and WC, more local maxima (where the CO concentration is high) and local minima (where the CO concentration is low) for CO were observed compared to CLN, potentially indicating more local features influencing the CO on these routes, which may be related to different land use, traffic patterns, and intersection control. For example, the location at 6,000 ft on BV and WC both show a local maximum for CO; this is located near a signalized intersection near OSU's Agricultural Campus area, with bus stops on both sides of the road and several nearby parking lots.

Similar figures to Figure 2.4 for NO_2 and O_3 concentration on CLN, BV and WC routes are provided in Figure 2.6 to Figure 2.11. However, the spatial pattern of NO_2 and O_3 cannot be clearly explained by land use and traffic pattern. For example, there is no local maximum in NO_2 at 18,000ft on the CLN route (a local maximum for CO), while O_3 has a local maximum at 22,000 ft on CLN (a local minimum for CO). The spatial pattern of NO_2 and O_3 may not be explained by the traffic pattern as CO, because CO is directly emitted from vehicles, but O_3 is formed through atmospheric chemistry; NO_2 may be directly emitted or formed in the atmosphere through chemical reactions. Moreover, NO_2 and O_3 can also be depleted due to atmospheric chemistry or reactive uptake on surfaces. However, we cannot fully explain the atmospheric chemistry that

may have occurred due to a lack of the complementary measurements that would be required for this.

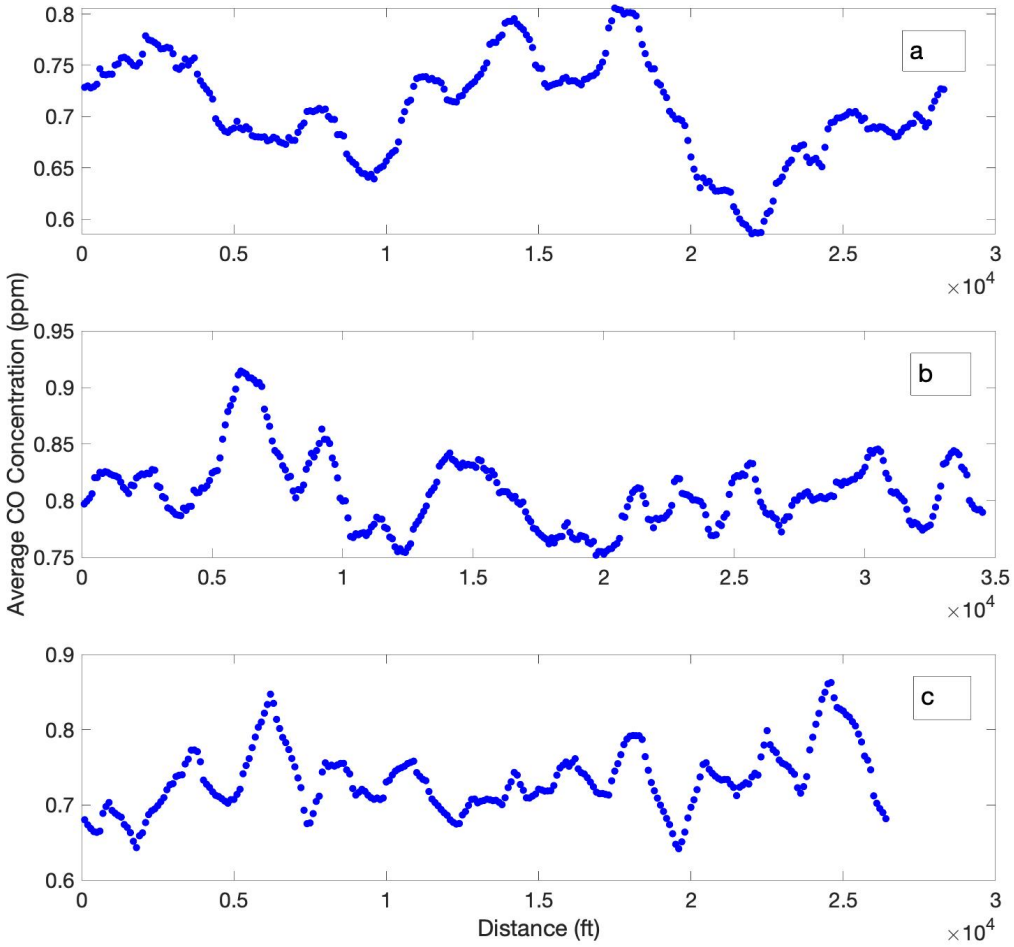

Figure 2.3: Mean CO (n = 83, 60,100 respectively for CLN (a), BV (b) and WC (c)) in ppm as a function of route distance from the beginning of bus route

2.5.2 Investigating an underlying spatial pattern

To investigate whether an underlying spatial pattern existed throughout the bus routes for each of three pollutants, the correlation coefficient was computed between each pair of the trip vectors within each route. The median, mean, standard deviation, 10% percentile, and 90% percentile of the correlation values for all pairwise comparisons across all trips on each route and for each pollutant are presented in the Table 2.2. Both the mean and median correlation coefficient of all bus trips are close to zero (ranging between 0.001 and 0.09 across all routes and pollutants), suggesting that a small positive correlation may exist, on average. Moreover, the absolute values of both the 10th and 90th percentiles are relatively low. These low correlation coefficients suggest that no spatial pattern is consistent across all trips. However, correlations from these pairwise comparisons across all trips are likely influenced by temporal variations due to time-of-day and day-to-day effects. For example, Figure 2.4 demonstrates that a time-of-day temporal pattern exists for CO. Therefore, the comparison between, e.g., an 8:00 trip and a 14:30 trip on the same day, is likely not appropriate due to the likelihood of different traffic patterns and different meteorological conditions. These differences may be amplified if comparing an 8:00 trip to one day to a 14:30 trip on a different day.

Table 2.2: Summary statistics of correlations between all pairs of bus-trip vectors. N is the total number of bus trips sampled on each route.

	CLN (N = 83)			**BV (N = 60)**			**WC (N = 100)**		
All pairs of bus trips	**CO**	**NO_2**	**O_3**	**CO**	**NO_2**	**O_3**	**CO**	**NO_2**	**O_3**
Mean	0.055	0.040	0.043	0.020	0.022	0.031	0.090	0.043	0.041
Median	0.048	0.040	0.039	0.011	0.001	0.015	0.076	0.034	0.036
Standard deviation	0.199	0.282	0.250	0.179	0.272	0.252	0.234	0.210	0.230
10^{th} quantile	-0.196	-0.340	-0.284	-0.207	-0.306	-0.253	-0.199	-0.228	-0.203
90^{th} quantile	0.311	0.419	0.371	0.254	0.357	0.323	0.402	0.402	0.390
Sample size	3403	3403	3403	1770	1770	1770	4950	4950	4950

To remove these day-to-day effects and reduce the time-of-day effects, the sample size was reduced to only consider consecutive trip vectors occurring on the same day (Table 2.3) in the correlation analysis. For example, the air pollutant concentration during the approximately 30 minute cycle time between consecutive bus trips (e.g., trip *n* and trip *n*+1) at a certain location is likely to have more similar traffic and meteorological conditions, and hence, a more consistent underlying spatial pattern, than any two randomly-selected trips from a given route. The statistics in Table 2.3 show that the

correlations between consecutive pairs of bus-trip vectors are generally higher than those presented in Table 2.2. However, both the mean and the median values are still relatively low in magnitude (ranging from 0.07-0.31). The large value of the standard deviation and the large difference between the 90 percentile and 10 percentile values may indicate the presence of some variability that affects the systematic location patterns. This may be due to changes in the spatial pattern during the 30-minute time window. The correlation for CO is slightly higher than for NO_2 and O_3 for consecutive bus trip vectors, which may indicate a more similar spatial pattern for this pollutant compared to NO_2 and O_3.

Table 2.3: Summary statistics of correlations between all pairs of consecutive bus-trip vectors on same day. N is the total number of bus trips sampled on each route.

	CLN (N = 83)			**BV (N = 60)**			**WC (N = 100)**		
consecutive	**CO**	**NO_2**	**O_3**	**CO**	**NO_2**	**O_3**	**CO**	**NO_2**	**O_3**
Mean	0.272	0.187	0.172	0.137	0.068	0.114	0.321	0.162	0.186
Median	0.309	0.200	0.173	0.126	0.050	0.101	0.279	0.144	0.222
Standard deviation	0.246	0.278	0.279	0.161	0.257	0.241	0.341	0.250	0.271
10^{th} quantile	-0.078	-0.180	-0.208	-0.070	-0.197	-0.171	-0.023	-0.139	-0.213
90^{th} quantile	0.580	0.420	0.525	0.374	0.487	0.473	0.657	0.517	0.493
Sample size	78	78	78	57	57	57	95	95	95

In order to further reduce the presence of variability caused by temporal effects, we investigated average spatial profiles and adopted a random sampling method to generate "representative" trips. We divided the bus trips for a given route into two groups by randomly selecting half of the trip vectors, calculating a mean vector for both the first set and the second set of bus trips. We then computed the correlation coefficient between these two mean vectors. This process was repeated 5,000 times. While this could result in repeats in the selected trip vectors, there are roughly 10^{17} unique combinations for selecting 30 trips out of 60 for BV (the lowest sample size); thus, the probability of a repeat is effectively negligible. However, two selected sets share many trips in common.

The summary statistics of this process (Table 2.4) demonstrates that the mean correlation coefficient substantially increases and that even the 10-percentile value shows strong positive correlation for most of the air pollutants. For these randomly subsampled bus trip vectors, the large positive correlation statistics indicate strong spatial pattern consistency for air pollutants when the temporal effects have been minimized through this averaging process.

Table 2.4: Summary statistics of correlations between all pairs of subsampled vectors. N is the total number of bus trips sampled on each route.

	CLN (N = 83)			**BV (N =60)**			**WC (N = 100)**		
Random 50%	**CO**	**NO_2**	**O_3**	**CO**	**NO_2**	**O_3**	**CO**	**NO_2**	**O_3**
Mean	0.832	0.485	0.656	0.648	0.552	0.634	0.867	0.632	0.718
Median	0.845	0.561	0.664	0.659	0.596	0.673	0.874	0.641	0.732
Standard deviation	0.053	0.208	0.131	0.129	0.401	0.158	0.046	0.085	0.086
10^{th} quantile	0.764	0.133	0.508	0.480	0.261	0.482	0.806	0.521	0.601
90^{th} quantile	0.890	0.688	0.796	0.812	0.667	0.792	0.920	0.738	0.811
Sample size	5000	5000	5000	5000	5000	5000	5000	5000	5000

2.5.3 Identifying temporal patterns

From the analysis described in previous section, there appears to be temporal effects that influenced our analysis of underlying spatial patterns, but in that analysis, it is not clear whether these were driven by time-of-day or day-to-day differences in the measurements. In this section, we investigate the presence of temporal patterns for all three air pollutants (CO, O_3, and NO_2).

Figure 2.4 represents the trip-averaged values of CO, NO_2 and O_3 for each sampling day, using the start time of each bus trip (the timestamp associated with X= 0)

to represent the trips' time-of-day. These results suggest that both day-to-day effects and time-of-day effects exist in the data.

Consistent time-of-day patterns of CO were identified in Figure 2.4a, in which higher mean CO concentrations were observed in the morning, noon and afternoon likely due to heavier traffic activity during those times (e.g., am and pm rush hours and lunch hour). The generally decreasing trend of CO in Figure 2.4a (e.g., negative slopes are obtained for a linear regression on 3 of the 5 days) is likely related to dilution induced by an expansion of the atmospheric boundary layer; at night, the boundary layer tends to be more shallow, resulting in a smaller volume for mixing, but during the day, the boundary layer height increases, largely due to daytime warming of the surface. NO_2 shows a similar pattern (Figure 2.4b) to CO, with morning, noon and afternoon peaks. NO_2 also has a generally decreasing trend (again, 3 of the 5 days have a negative slope), which may be related to atmospheric dilution and/or atmospheric chemistry. However, O_3 has a general increasing trend (5 out of 5 positive slopes) from the morning to the afternoon (Figure 2.4c). The lowest O_3 concentration occurred around 7 AM and increased steadily throughout the day; O_3 is produced during the daytime when volatile organic compounds (VOCs) and NO_x are exposed to sunlight, and the O_3 subsequently will react away overnight. The temporal trend of NO_2 and O_3 in this study are consistent with Sadighi et al. (2018) where they use stationary monitoring instruments to detect diurnal trend of NO_2 and O_3 near a road way. Consequently, our results suggest that low-cost sensors deployed on transit buses are able to capture the diurnal trend in these air pollutants. Temporal patterns of CO, NO_2 and O_3 on BV, and WC routes were shown in Figure 2.12 to Figure 2.17. The temporal trends for CO, NO_2 and O_3 on BV and WC are consistent

with the temporal trends on CLN route. In BV and WC, CO and NO_2 show a general decreasing trend with local peak at morning, noon and afternoon. O_3 show a general increasing trend with peak in the later afternoon. This suggests that the temporal patterns are consistent and that they are not affected by the spatially-different sampling locations across the different routes.

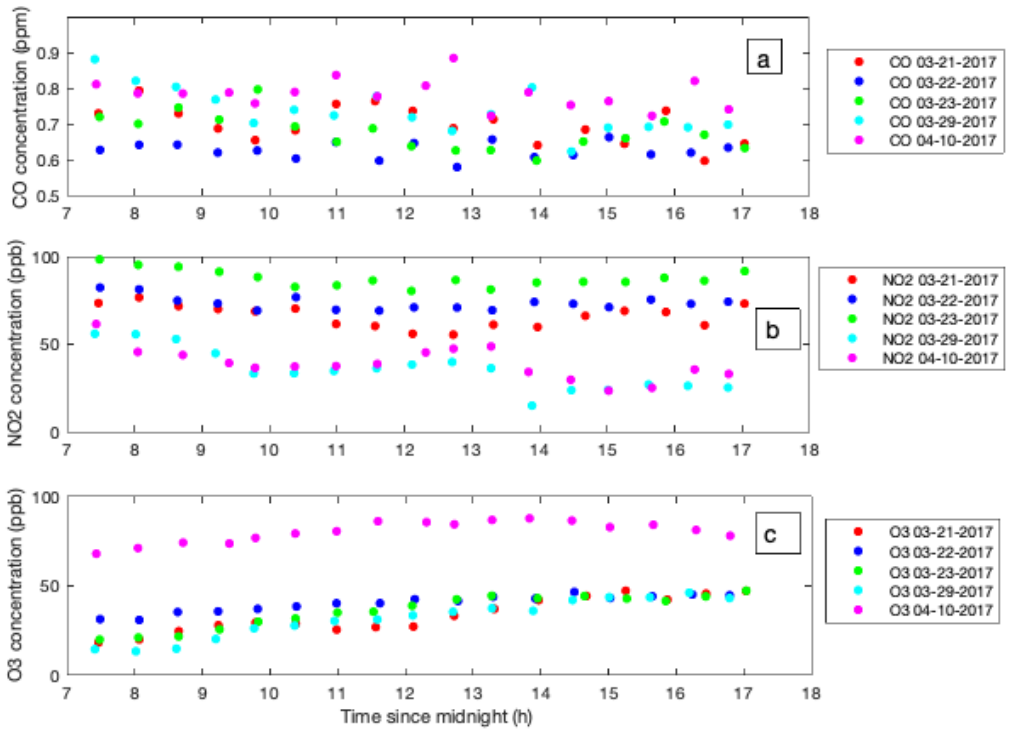

Figure 2.4: Average CO, NO_2 and O_3 (N =83) on CLN route for each trip with time of day. The y-axis in the top panel ranges from 0.5 to 1 ppm to allow for better visualization.

2.5.4 Identify features of spatial pattern after removing temporal effects

As mentioned in the previous section, temporal effects exist both within days and across days. To partially control for the large day-to-day and time-of-day variation when investigating the underlying spatial pattern of air pollutants, the gridded air pollutant values are compared to the median value of each trip. As discussed in data analysis section, the median value of each trip was used as a representative air pollution level for a given trip. The proportions of times that the CO values at each gridded location is greater than the median CO values for the corresponding bus trips are presented with distance for all locations in Figure 2.5. We used $z = \frac{P - P_0}{\sqrt{\frac{(1-P_O)P_0}{n}}}$ (equation 2.1) to test the significance of these proportion values to investigate an underlying spatial pattern accounting for temporal differences. The confidence interval (CI) of [0.4 0.6] can be calculated with a significance level of 5%, which is presented in Figure 2.5 by dashed horizontal lines. If the calculated proportion at any location falls outside out of these confidence intervals, this suggests that a significant spatial pattern is likely to exist. The result in Figure 2.5, 50 gridded 100-ft intervals along the route (17% of the 283 total) are above and 68 of these intervals (24% of the 283 total) are below this CI. From this calculation, a 5% significance level implies that roughly 5% of locations would be above or below this interval under the null hypothesis of no systematic spatial pattern. However, approximately 42% of locations are outside this interval, which indicates a statistically significant location-specific pattern after controlling for the temporal effect.

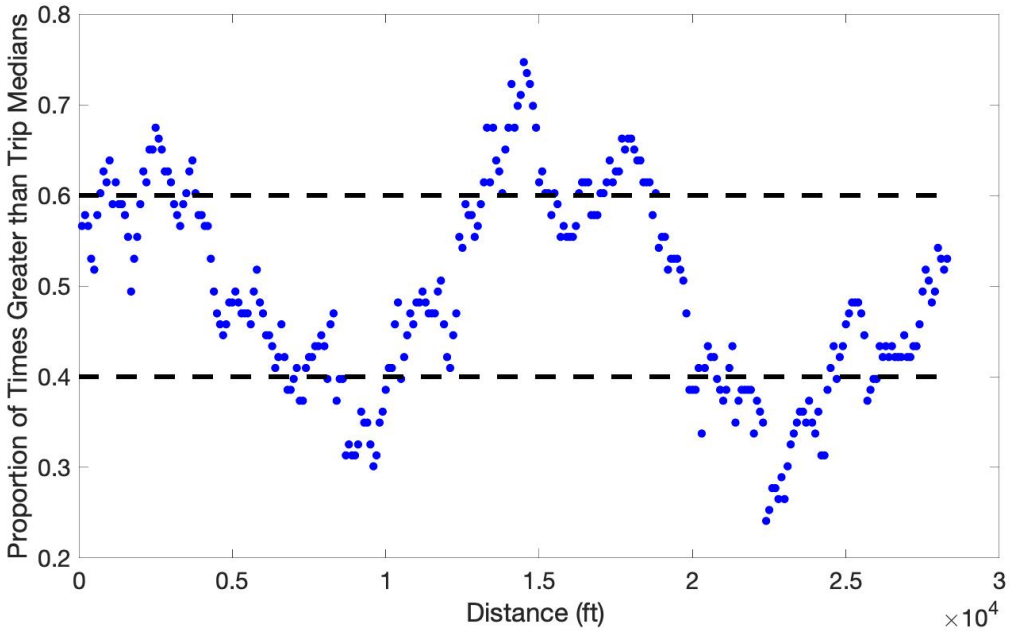

Figure 2.5: Proportion of times CO values at a location (each 100ft) are greater than median of all CO values on the same bus trip

Table 2.5 summarizes the calculated proportions for the three pollutants (CO, NO_2 and O_3) across all three routes (CLN, BV and WC). For all three pollutants, more than 5% of the locations are above or below the thresholds for each of the three routes. This indicates that a location-specific pattern can be observed for these pollutants on all routes. By comparing the proportion of the same pollutant on three routes, we observe that there are more locations outside the 5% significant CI on CLN but fewer locations on BV and WC (except CO on WC). This may indicate that the spatial variation is more evident in CLN than BV and WC due to the characteristics of the route itself (e.g., traffic activity, built environment). By comparing the proportion of the three pollutants on the same route, CO tends to have more locations outside the 5% significant CI than NO_2 and O_3, with an exception of the BV route. This may indicate that the variation of CO has a more stable underlying pattern than NO_2 and O_3, because CO emission are more related

to direct traffic emissions and are less influenced by atmospheric chemistry than NO_2 and O_3.

Table 2.5: Number of locations (percentage) falling outside the confidence interval for CO, NO_2 and O_3 on CLN, BV and WC route

	CLN (# of location = 283)			**BV (# of location = 264)**			**WC (# of location = 345)**		
	CO	**NO_2**	**O_3**	**CO**	**NO_2**	**O_3**	**CO**	**NO_2**	**O_3**
<lower	68 (24%)	53 (19%)	50 (18%)	50 (15%)	29 (7%)	72 (6%)	63 (23%)	34 (13%)	43 (16%)
>higher	50 (17%)	62 (21%)	70 (25%)	26 (8%)	24 (8%)	21 (20%)	85 (31%)	53 (20%)	50 (19%)
<lower & >higher	118 (42%)	115 (41%)	120 (43%)	76 (22%)	53 (15%)	93 (27%)	148 (54%)	87 (33%)	93 (35%)

2.6 Conclusion

In this study, spatial air pollution patterns were observed by using low-cost air quality sensors deployed on a transit bus. The mean concentration of CO along three bus routes suggested that these spatial patterns can be detected even on a relatively small spatial scale (i.e., the OSU campus). This spatial pattern may be associated with land use, the built environment, and traffic activity. The spatial pattern of NO_2 and O_3 also suggested a location-specific dependency, but the patterns may not be directly related to traffic activity. We lack information to fully explain the spatial variations of NO_2 and O_3 on these routes.

To investigate the consistency of the spatial pattern of each pollutant, correlation coefficients between any two of individual bus trip vectors were calculated. Low correlation coefficient in this pair-wise comparison was likely related to a temporal effect. After averaging bus trip vectors through a random subsampling method to for temporal effects, strong correlations were obtained, indicating consistent spatial pattern.

The temporal pattern of CO, NO_2 and O_3 on three routes show day-to-day and time-of-day variation. After removing this temporal effect, for the three pollutants on the three routes, greater than 5% of locations are outside the 0.05 confidence intervals for each route and for each pollutant, which indicated underlying spatial pattern independent of time. In summary, low-cost sensor deployed on transit buses as sensing platforms has potential to provide long-term observations of air pollution in an urban area, and therefore, provide a means to explore the consistency of the underlying spatial pattern.

2.7 Future work

In the future, we could expand sensors installation to more buses to create a denser air quality network in an urban area to confirm and strengthen the results arrived at in this study and eventually to provide more extensive and reliable information.

Air pollution models base on sensors' network have been studied (Hankey and Marshall 2015, Apte et al 2017, Hasenfratz et al 2015). These models require high spatial resolution data which can be obtained from low-cost sensors. In a future study, we could build upon these efforts to develop models in order to further understand air pollution patterns within an urban environment. Such models could provide predictions of air quality in areas based on sensors' data as well as explore which land-use factors may contribute to elevated air pollution.

2.8 Additional Tables and Figures

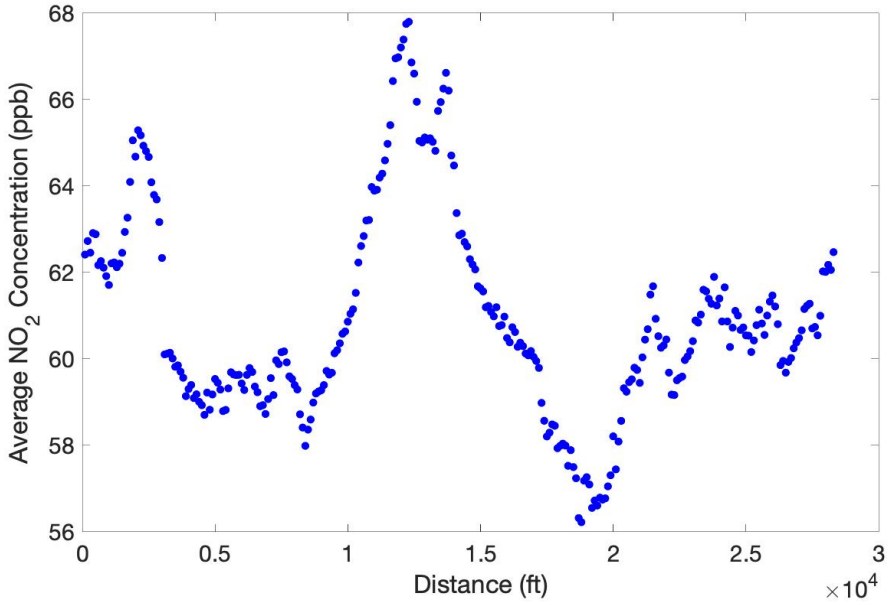

Figure 2.6: Average NO_2 concentration in CLN route as a function of route distance from the beginning of bus route

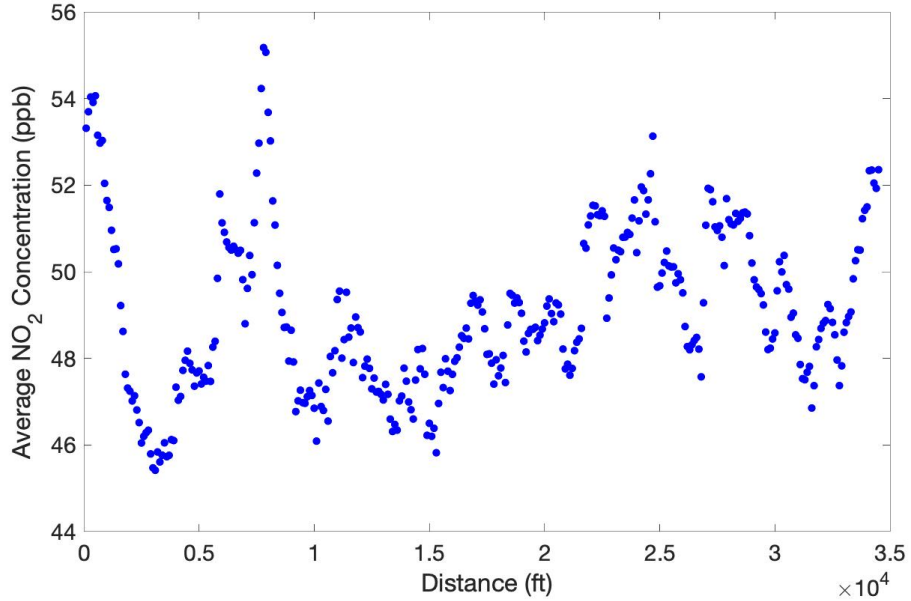

Figure 2.7: Average NO_2 concentration in BV route as a function of route distance from the beginning of bus route

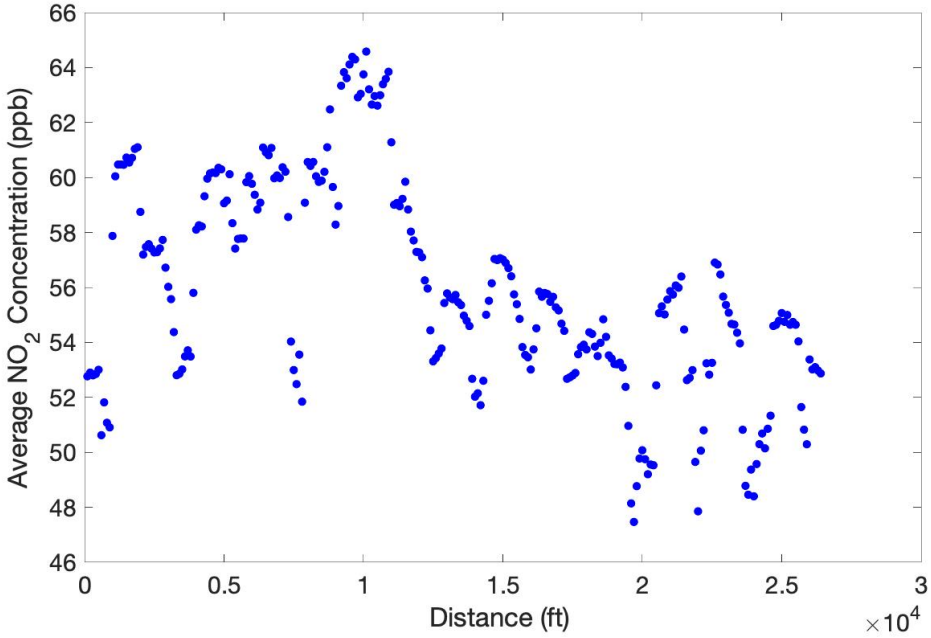

Figure 2.8: Average NO_2 concentration in WC route as a function of route distance from the beginning of bus route

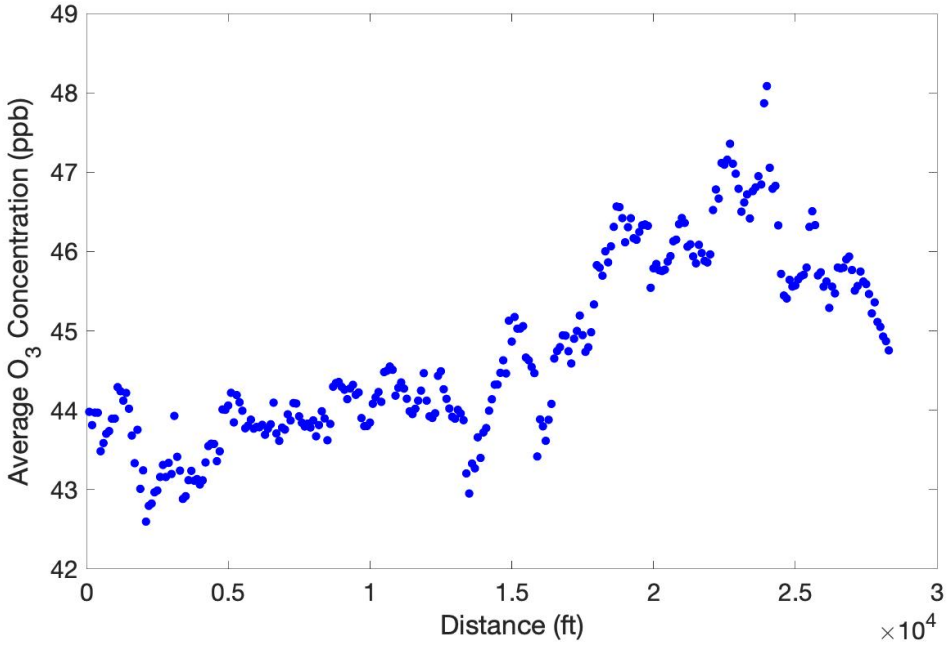

Figure 2.9:Average O_3 concentration in CLN route as a function of route distance from the beginning of bus route

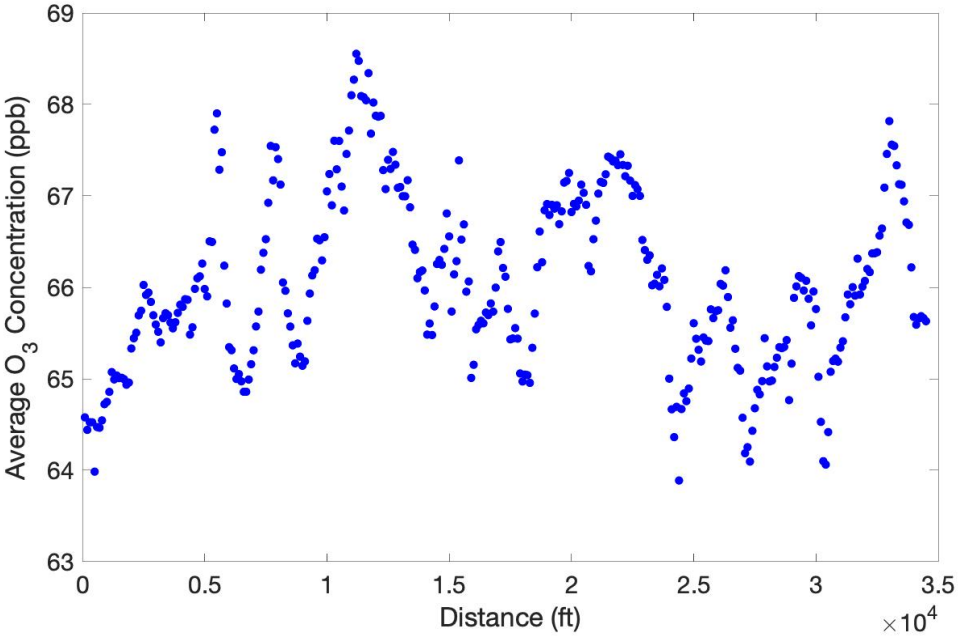

Figure 2. 10: Average O_3 concentration in BV route as a function of route distance from the beginning of bus route

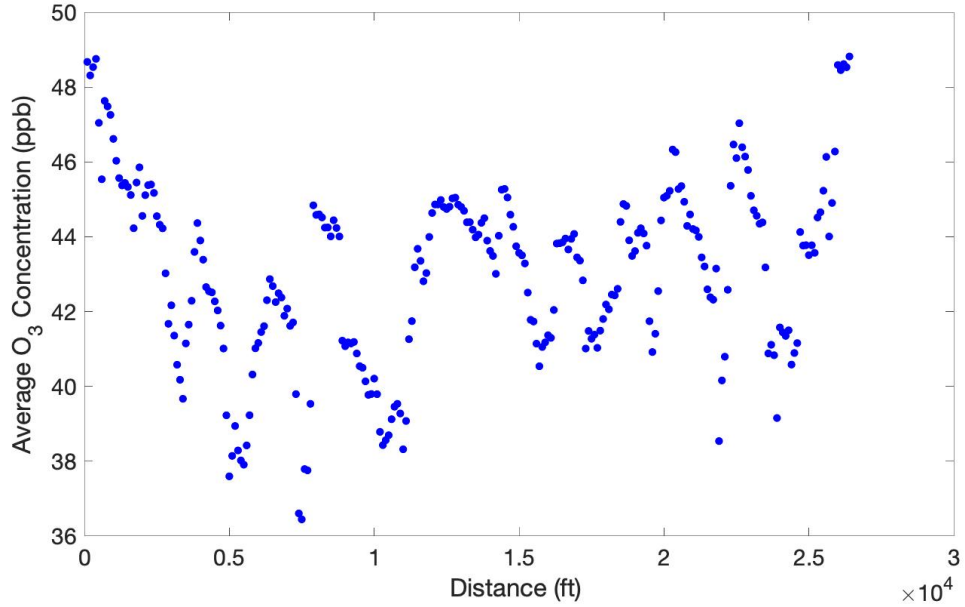

Figure 2.11: Average O_3 concentration in WC route as a function of route distance from the beginning of bus route

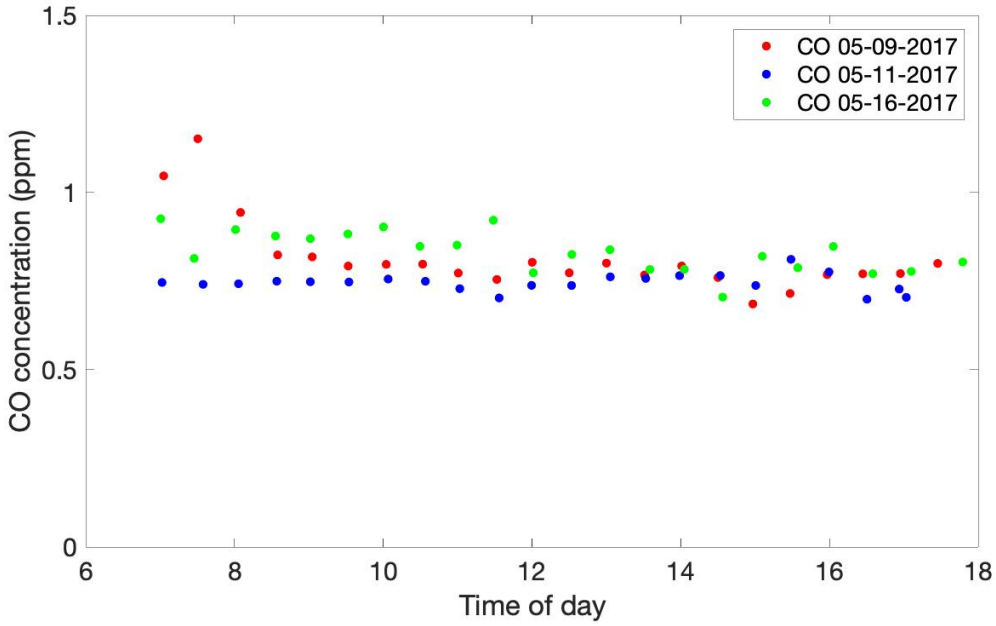

Figure 2.12: Average CO (n =60) on BV route for each trip with time of day

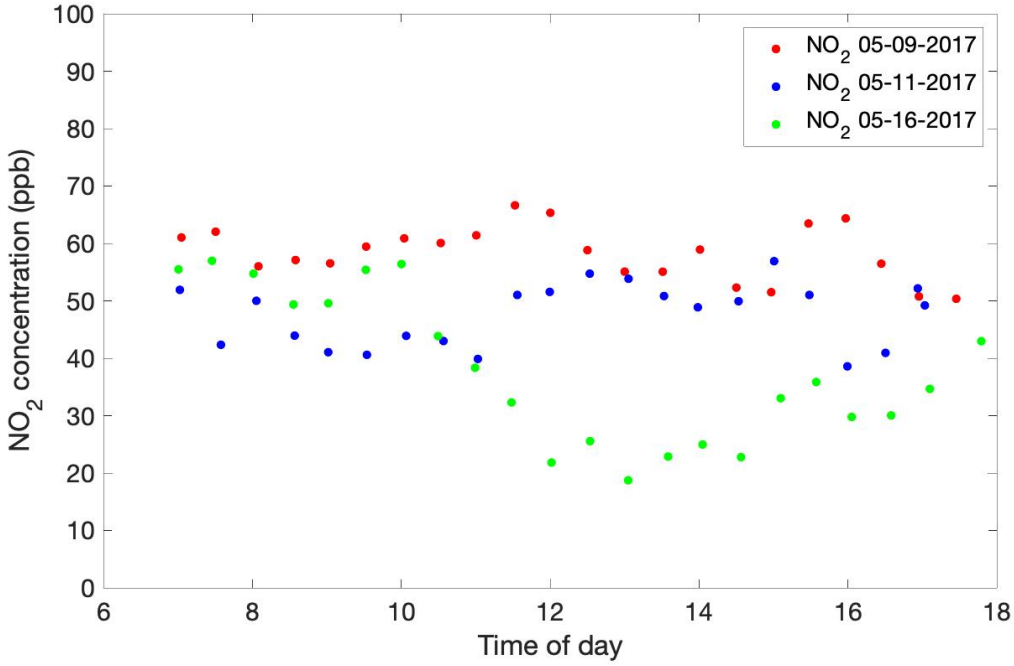

Figure 2.13: Average NO_2 (n =60) on BV route for each trip with time of day

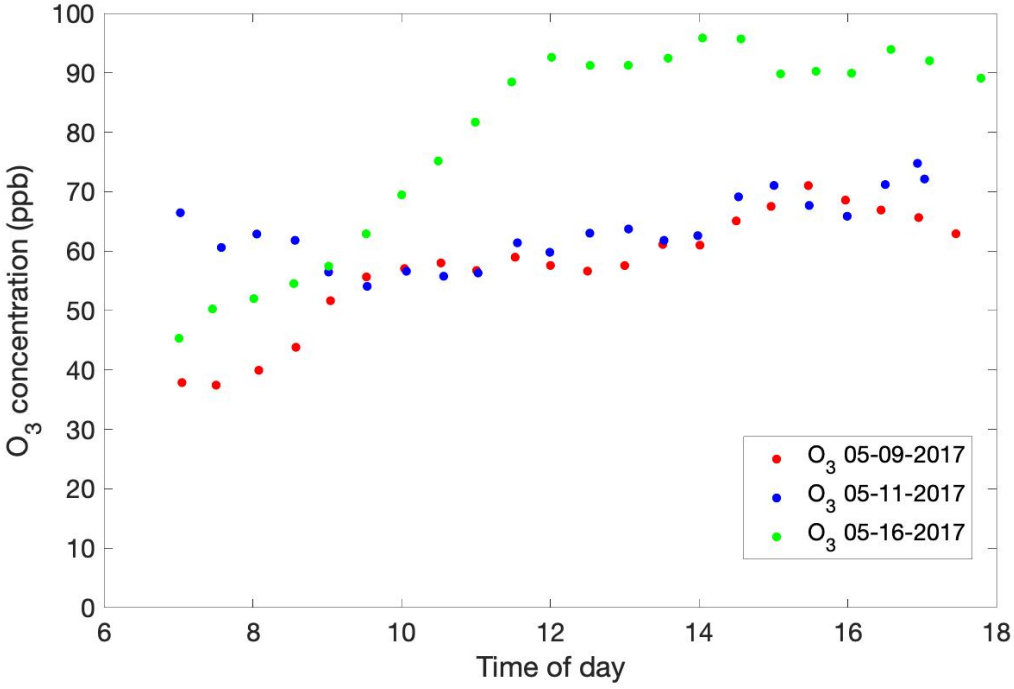

Figure 2.14: Average O_3 (n =60) on BV route for each trip with time of day

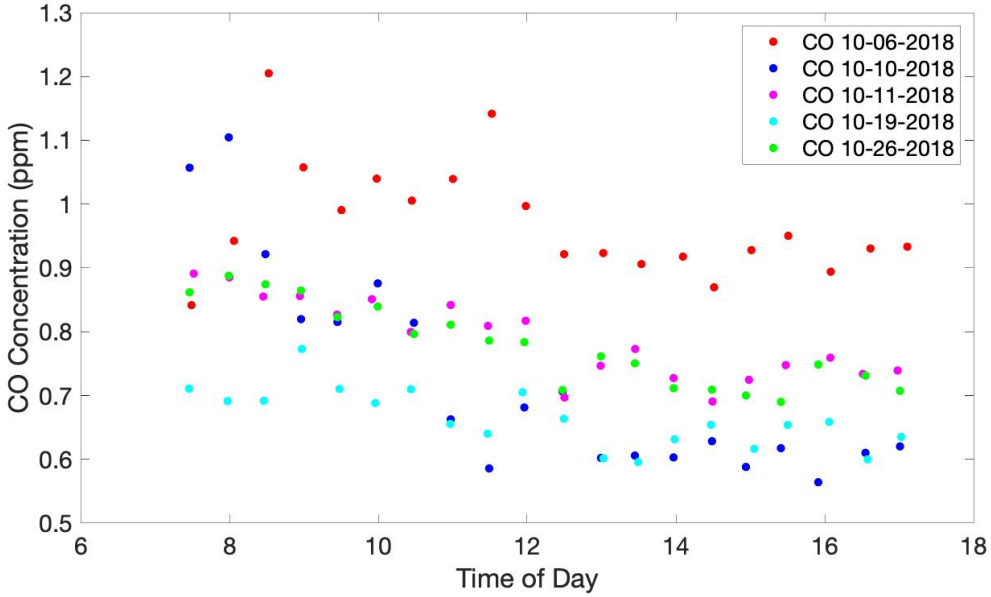

Figure 2.15: Average CO (n =100) on WC route for each trip with time of day

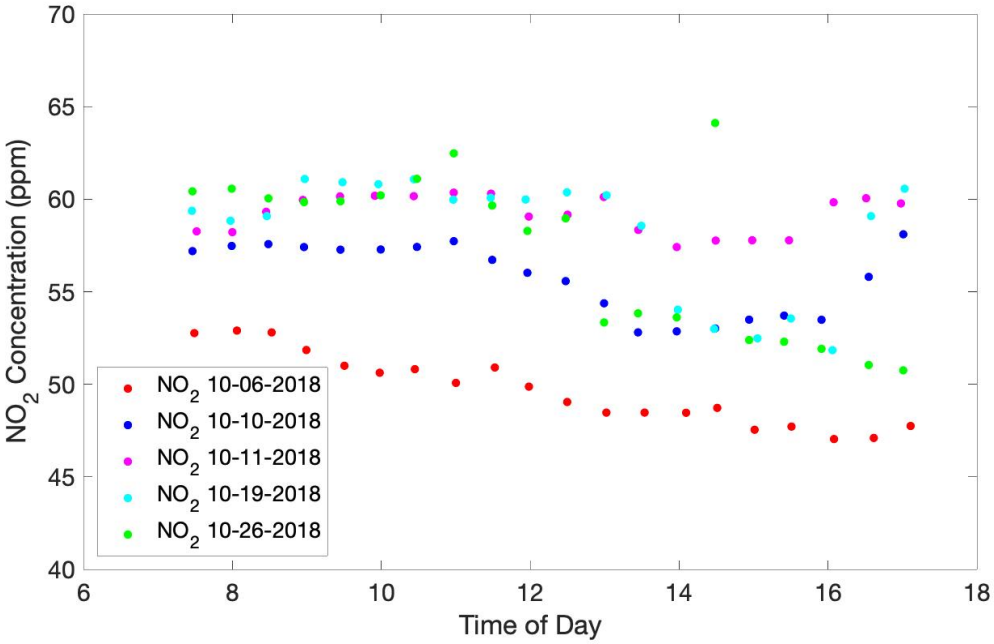

Figure 2.16: Average NO_2 (n =100) on WC route for each trip with time of day

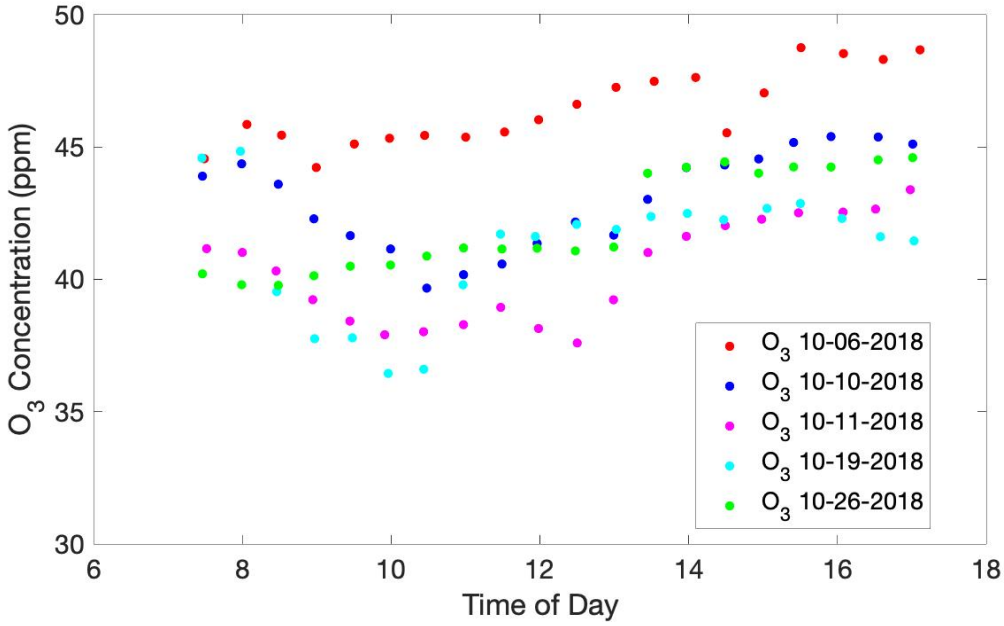

Figure 2.17: Average O_3 (n =100) on WC route for each trip with time of day

Chapter 3: Response of eight low-cost particle sensors and consumer devices to typical indoor emission events in a real home (ASHRAE 1756-RP)[1]

3.1 Introduction

Recent improvements in the performance of commercially-available low-cost air quality sensors are preparing the way for large changes in air quality monitoring and control of indoor environments (Karami et al., 2018; Morawska et al., 2018; Schieweck et al., 2018). Specifically, the ability to measure particulate matter concentration using only low-cost devices (<$20 for a bare sensor or <$250 for a packaged device) has undergone great improvements in recent years, but many shortcomings have been identified. Numerous studies have evaluated different aspects of the performance of these sensors (Kelly et al., 2017; Nieuwenhuijsen et al., 2018; Zikova et al., 2017). We focus on the two aspects of performance with which this paper is concerned, namely the ability of the sensors to detect indoor particle emission events and the consistency between different sensors from the same manufacturer.

3.1.1 Event detection

Different studies have defined emission events in different ways. Wallace et al (2006) defined the beginning of an event as an increase of 7 μg m^{-3} above the baseline

[1] This chapter is a published paper at https://doi.org/10.1080/23744731.2019.1676094

concentration and the end as the running average falling below 10 μg m^{-3} and the time rate of change in concentration becoming negative. Similarly, Chan et al. (2018) defined events as a 10 μg m^{-3} increase above the baseline concentration. Event start time was defined as the time when there are three consecutive measurements that have zero or positive change from the previous measurement, and the end time was defined as three consecutive measurements with zero or negative change from the previous measurement.

Several studies have investigated the ability of low-cost particle sensors to register indoor emission events and to recover to the correct background concentration after an event. Singer & Delp (2018) evaluated response to indoor sources including dust, toast, incense, and cooking in a laboratory. They found some sensors can track rapid changes in concentrations with accuracy close to that of research-grade instruments, while some miss events completely. Performance was particularly poor for events that emitted mostly particles smaller than 0.3 μm. Similarly, Manikonda et al (2016) used Arizona Test Dust to evaluate low-cost particle sensors and reported peak concentrations 30% higher than reference instruments in some sensors and 50% less in others. Zikova et al. (2017) tested 66 low-cost sensors and compared them to a reference instrument in an indoor residential setting for 3 days. The reference instrument identified two peaks exceeding 20 μg m^{-3}, and in both instances, the average of the 66 sensors was greater than the concentrations reported by the reference instrument.

3.1.2 Consistency between multiple instances of a single sensor model

Several studies collocated multiple sensors of the same model to evaluate consistency. Mukherjee et al (2017) showed that one type of particle sensor demonstrated very high manufacturing consistency throughout the test period in an outdoor environment (R^2 = 0.99) while other types had greater discrepancies. Polidori et al. (2016a) tested sensors in triplicate to determine their intra-model variability, and showed intra-model variability greater than 20% in some cases. Zikova et al. (2017) showed varying performance among 66 low-cost sensors. Manikonda et al. (2016) tested several sensors and found that one model reported similar concentrations during particle events, while another model differed by 30% between the duplicates.

3.2 Objectives

In this study, we subject several low-cost particle sensors from several manufacturers to typical emission events in a real home and compare their response with research-grade instrument response. Our objectives in this work were to:

1. Assess ability of low-cost sensors to characterize different types of typical indoor particle emission events in a real indoor environment.

2. Assess the consistency of multiple instances of sensors fabricated by the same manufacturer.

3. Investigate the effect of averaging time on apparent performance.

3.3 Devices Tested

We evaluated eight commercial products: three bare sensors (BS) and five integrated devices (ID). We tested multiple instances of each as indicated in Table 3.1. Bare sensors are small sensors usually less than 10 cm along their longest edge. Their output is an electrical signal that must be then translated into usable information by the end user or device in which it is housed. Conversely, integrated devices contain one or more sensors, housing, and storage/communication capability. All sensors (both BS and ID) tested in this study operate using a light scattering principle. Light is generated by a light-emitting diode, then often focused by one or more lenses, and scattered by suspended particles in the air stream. A photodetector detects light scattered by the particle stream and this signal is converted to either number of particles in the stream or an estimate of mass concentration. Particles are introduced into the sensor either by natural convective flows caused by a resistor (e.g., BS2) or by forced advection driven by a fan inside the sensor (e.g., BS1 and BS3).

We refer to these sensors and devices by the designations listed in Table 3.1 from here forward. Table 3.1 also includes manufacturer-reported detectable size range, sampling time, data acquisition and communication method. No specific product names are used in order to be compliant with the ASHRAE Commercialism Policy. We briefly describe each sensor as well as two reference instruments: a scanning mobility particle sizer (SMPS) and an aerodynamic particle sizer (APS) in Additional Tables and Figures.

Table 3.1. Specifications of tested integrated sensors and bare sensors

Sensor	No. of Units	Cost (USD)	Mass Concentration Range (µg m^{-3})	Size	Communication (Output Method)	Sampling time	Bare sensors used
ID1	1	$699	0-500	PM1, 2.5, 10	Cloud-based storage	1 min	unknown
ID2	3	$200	0-1000	PM1, 2.5, 10	Bluetooth, Wi-Fi Serial connector	1 s	BS3
ID3	3	$290	Number concentration	PM0.5-2.5, PM>2.5	Serial connector, software	1 min	unknown
ID4	2	N/A	0 -1000	PM1, 2.5, 10	Serial connector	~900 milliseconds	BS3
ID5	3	$299	0 -1000	PM1, 2.5, 10	SD card storage, Wi-Fi	80 s	BS3
BS1	2	$30	0 -1000	PM 2.5, 10	Serial connector (UART)	2 s	N/A
BS2	3	$15	0 -500	N/A	Serial connector (Analog)	1 s	N/A
BS3	2	$25	0 -1000	PM1, 2.5, 10	Serial connector (UART)	~ 900 milliseconds	N/A

3.4 Experimental Methodology

We deployed the BS and ID, along with the SMPS and APS as reference instruments, in an on-campus building. The reference instruments are counting the aerosol particles while the low-cost particle sensors are using aggregated light scattering to attempt to deduce how many particles there are, so we consider that the instruments are more accurate than the low-cost particle sensors. This building is a test house that includes a working kitchen, dining and living areas, two bedrooms, and a bathroom. We mimicked operation in a typical residence by conducting indoor particle-generating activities such as cooking, burning incense, lighting candles, spraying room deodorizer, and opening windows to promote outdoor-to-indoor penetration. All of the reference instruments, ID, and BS were located in the living room, marked with an X in Figure 3.1. ID and BS were placed inside a cage with three elevated wire racks to allow for air flow. All bare sensors were operated with a microcontroller (e.g., Arduino) using a program written in the C language. This program also recorded the data into a real-time output file. We used a serial communication software to access all data from sensors' serial connectors. SMPS and APS data were merged using an approach similar to Khlystov et al. (2004b), and we use the notation "SMPS+APS" to indicate combined data. Particle mass concentrations were calculated by integrating across the entire combined particle size distribution, assuming spherical particles and a particle density of 1 g cm^{-3}. Although these assumptions may not be strictly true for all particle sources, it is common in the absence of known particle shapes and densities (L. Wallace, 2007) .

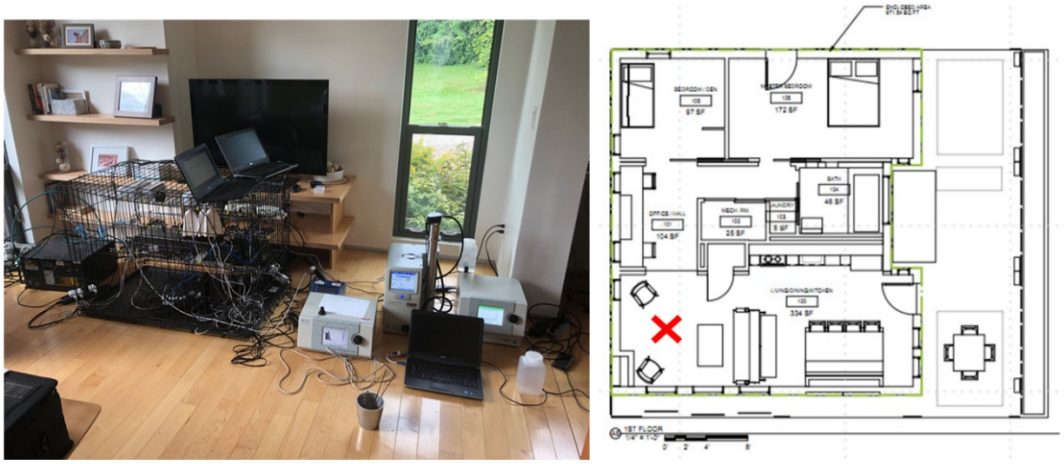

Figure 3.1: Sensors and reference instrument inside the test house

The sources were generated either in the living room or in the adjacent open kitchen. Concentrations naturally decayed in the room via air exchange with the outdoor environment, gravitational settling, and other loss mechanisms. During this testing, we used multiple sources (27 total events) every one or two days over approximately three months. Detailed information about particle sources can be found in Table 3.2. For each event, the start time was defined as the time after we introduced the PM source and measured concentration increased for five consecutive data points. The end time was defined as the time at which the concentration decreased for five consecutive data points and fell below 10 μg m^{-3}.

In Table 3.2, each event is described. The mode of the particle size distribution is determined from the combined SMPS and APS (SMPS+APS) data, where we can observe that the mass-mode particle sizes are different for different PM source types. Most sources

have only one size mode that is fairly repeatable. Room spray always has a size mode of 8-9 μm. Burning toast always provides a mode in the range of 300-500 nm. Similarly, burning candles always generate particles with a mode of 300-700 nm. Burning incense mostly generates 200-300 nm particles, but it also frequently has a larger mode that may be related to differences in the combustion process (e.g., "smouldering" rather than "flaming"). Opening a window can also have two modes, around 300 nm and 2 μm; this may be because both coarse particles from a nearby gravel road and fine particles from a nearby highway can enter the house through the window.

Table 3.2. List of emission events, duration, and particle size information.

Date	**Time**	**Duration Time(min)**	**PM source**	**Mode of Averaged Particle Size Distribution during Event**
09/25	11:05-13:20	135	Burning incense	300 nm
09/28	11:15-13:00	105	Open door	345 nm
09/28	15:50-16:30	40	Deodorizer	9.3 μm
10/02	9:30-11:00	90	Open window	2.4 μm
10/02	11:30 -13:00	90	Burning candle	290 nm
10/03	11:05-13:00	115	Open window	346 nm
10/05	11:20-13:00	100	Cooking	135 nm, 2.5 μm
10/08	10:20-10:40	20	Open window	300 nm

Date	Time	Duration Time(min)	PM source	Mode of Averaged Particle Size Distribution during Event
10/09	12:00-13:00	60	Burning incense	180 nm, 700 nm, 8 μm
10/11	10:45-11:20	35	Burning toast	445 nm
10/12	12:50-13:05	15	Deodorizer	8.1 μm
10/16	11:46-15:20	214	Burning incense	200 nm, 600 nm
10/18	11:40-12:00	20	Burning candle	370 nm
10/19	10:25-11:40	75	Open window	271 nm, 7.2 μm
10/19	16:20-17:20	60	Deodorizer	7.7 μm
10/23	11:20-16:20	300	Burning toast	500 nm
10/25	11:36-12:20	44	Deodorizer	7.6 μm
10/30	11:10-15:20	250	Burning incense	253 nm, 630 nm
11/10	13:33-15:20	107	Deodorizer	7.7 μm
11/13	11:47-15:00	193	Humidifier	200 nm
11/16	11:47-12:53	66	Deodorizer	8.1 μm
11/20	11:40-12:40	60	Deodorizer	8.3 μm
11/30	11:36-12:00	24	Burning candle	496 nm
12/03	11:45-13:00	75	Burning candle	700 nm

Date	Time	Duration Time(min)	PM source	Mode of Averaged Particle Size Distribution during Event
12/06	11:35-12:20	45	Burning toast	543 nm
12/07	13:23-17:00	217	Burning toast	325 nm
12/11	13:23-15:34	131	Burning toast	472 nm

The output data from ID and BS were mostly recorded at 0.5 or 1 Hz (based on the sensor capability) using serial communication software with corresponding computer time logged. The raw data included text files and comma-separated variable files. We used a script to post-process the raw data. The raw data had timestamps to enable time alignment among all sensors (if needed), and the aligned data were then averaged into 1 minute bins to align with the SMPS+APS. The 1-minute time series data were processed using a moving averaging method with a window of 30 minutes and step size of 1 minute.

Performance is most often quantified in the literature with R^2, slope, intercepts, linearity, or an integrated approach. In most cases, a linear regression analysis is the most commonly used method to evaluate sensor accuracy (Brauer, 2010; Budde & Beigl, 2016; Holstius et al., 2014; D. Liu et al., 2017; Northcross et al., 2013; Zheng et al., 2018). In this study, we have focused primarily on R^2, slope and intercepts to quantify relationship between the sensors and reference instruments. We also use two other metrics, ratio of integrated mass concentrations over event duration and peak concentration ratios, to quantify the ability of sensors to capture events.

3.5 Results

In the following section we present the results of the field study. First, we present an overall summary of low-cost sensor response and reference-grade instrument response. We then characterize the integrated response of the low-cost devices and compare to reference-grade instruments in order to assess the low-cost sensors' ability to quantify exposure. We then distinguish the response of each sensor by source type. Lastly, we compare multiple instances of devices from the same manufacturer to assess the consistency of performance among devices from the same manufacturer.

3.5.1 Event Detection

Figure 3.2 shows the typical response of sensors and reference instruments to different event types, both as a time series of all sensors and the average mass size distribution.

Figure 3.2a1 shows performance during incense-burning events. All ID and BS detect the event, possibly because this event generates a mass concentration of particles greater than 500 μg m^{-3}. They also all recover to the background concentration. All ID and BS follow trends similar to the SMPS+APS, but the magnitude of the response varies with some responses greater and some less than the reference instruments. Figure 3.2a2 shows the averaged particle mass size distribution during this event. Burning incense has a multi-modal particle mass distribution, with peaks at 180 nm, 700 nm, and 8 μm.

In Figure 3.2b1, burning toast also generates high mass concentrations approaching 500 μg m^{-3}. Similar to the incense burning event, BS1 and BS3 record greater mass concentrations than the SMPS+APS. ID4, ID1, ID5 are closer to SMPS+APS. ID2, ID3, and BS2 show only 50% of the mass concentration of the SMPS+APS, consistent with the incense burning event. From Figure 3.2b2, a unimodal size distribution is observed during this event with a mass mode diameter at 445 nm.

All ID and BS display similar trends when the window is opened (Figure 3.2c1), despite much lower mass concentrations; the peak mass concentration from the SMPS+APS is 27 μg m^{-3}. Opening a window can produce increased concentrations of both fine and coarse particles, depending on nearby outdoor sources. However in this event, higher concentrations of smaller particles with a mass mode at 346 nm can be observed in Figure 3.2c2. This indicates that most sensor types respond even under relatively low particle mass concentrations and for relatively small particle sizes.

The response of ID and BS to the deodorizing spray is different than other events, as shown in Figure 3.2d1. There was a sharp increase in concentrations shortly after the spray was introduced. ID3, BS1 and BS2 showed higher mass concentrations than the SMPS+APS. Figure 3.2d2 demonstrates that during spray events only coarse particles with a mode at 8 μm were produced. The relatively poor performance of the low-cost sensors for this source may be due to uneven mixing of spray particles and the relatively fast settling of these particles and/or challenges associated with sampling these relatively large

particles. The performance of the sensors may also be different for liquid particles, although they did respond relatively well to humidifier-generated particles.

Figure 3.2e1 shows sensors' response to the burning candle event. All sensors exhibited similar behavior. Burning a candle produced mass concentrations less than 15 $\mu g\ m^{-3}$. Figure 3.2e2 demonstrates that burning the candle produced particles with a size mode around 300 nm.

During the cooking event shown in Figure 3.2f1, all sensors display similar trends except for ID5. All show lower mass concentration than the SMPS+APS. From Figure 3.2f2, a bimodal size distribution is again observed during this event with mass mode diameters of 135 nm and 2.5 μm.

The humidifier generated a mass concentration greater than 200 $\mu g\ m^{-3}$ (Figure 3.2g1), with a mass mode at 200 nm. All sensors responded to the humidifier with varying magnitudes of response, and each recovered to background concentrations.

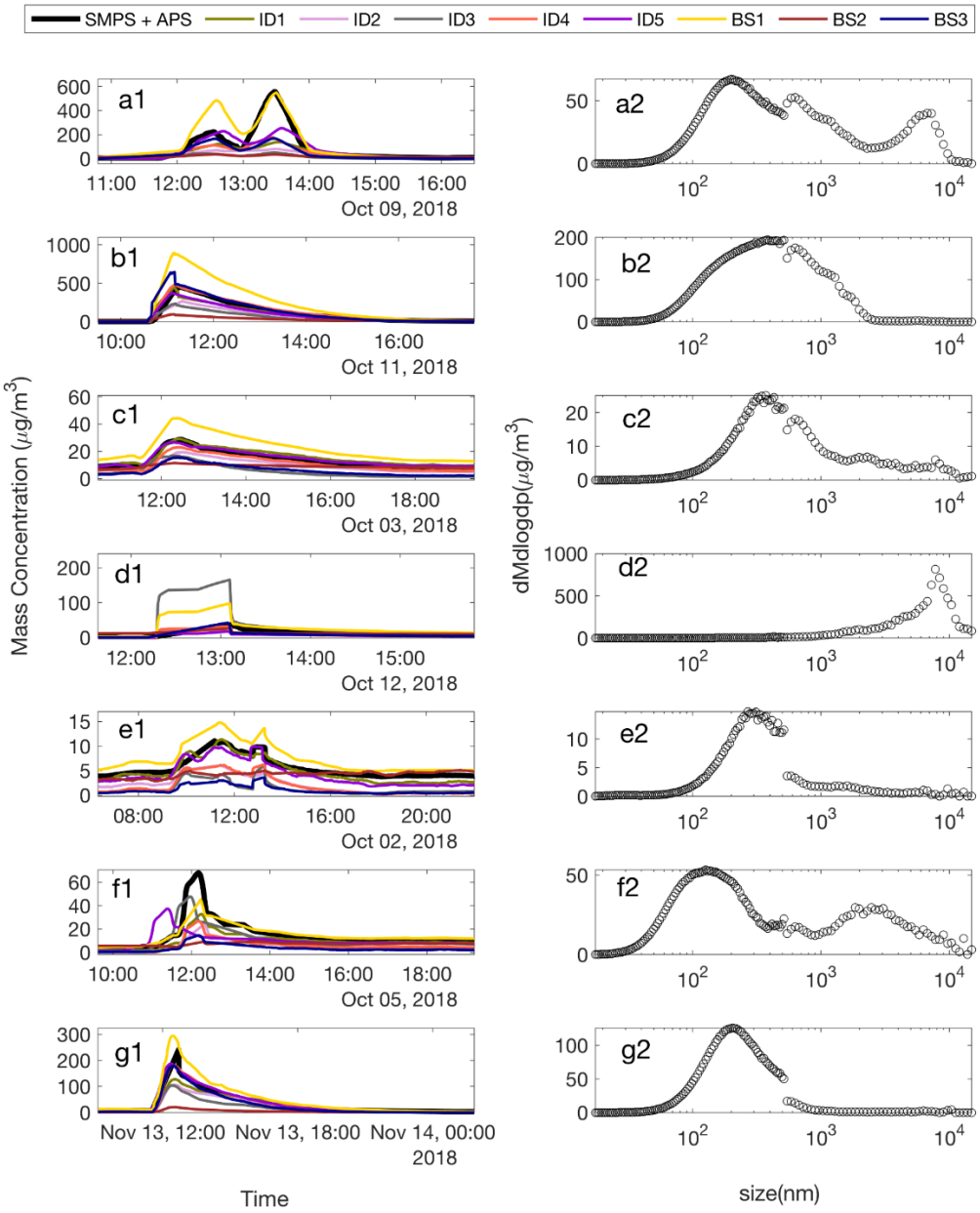

Figure 3.2: Typical response of sensors and reference instruments to different event types

Figure 3.3 shows the ratio of integrated mass concentration over the events to the SMPS+APS for each device and for each PM source, which provides a metric describing how well a given sensor estimates time-integrated exposure. In general, there is large

variability both among different sensor types and between different particle sources, ranging from close to zero to more than three. For example, the deodorizing spray almost always resulted in the lowest ratio for a given sensor. However, most of the sensors (except for BS2) have ratios greater than 0.5 for most of the events. Surprisingly, even though BS3 is used in ID2, ID4, and ID5, the integrated devices have lower mass ratios; this may be related to particle losses in the housing of the IDs, but it could be related to some other mechanism that we have not identified.

Figure 3.4 shows the ratio of the maximum particle mass concentration as output by a sensor during an event to the maximum concentration as reported by the SMPS+APS for that event, aggregated across all events of a given type. Results are similar to Figure 3.3. Most devices show ratios greater than 0.5 for most sources, indicating that most sensors reliably detect most indoor events. Deodorizing spray is an exception, and the cooking event falls within 0.3 - 0.5 for most sensors. Again, we see that even though BS3 is used in ID2, ID4, and ID5, the integrated devices have lower peak ratios. Differences in Figure 3 and 4 likely exist because the "decay rate" that a given sensor captures for a given event differs from that of the SMPS+APS (e.g., Figure 3.2). This is particularly pronounced when looking at ID1 in the burning toast event, with a peak ratio greater than 1 but an integrated mass ratio less than 1.

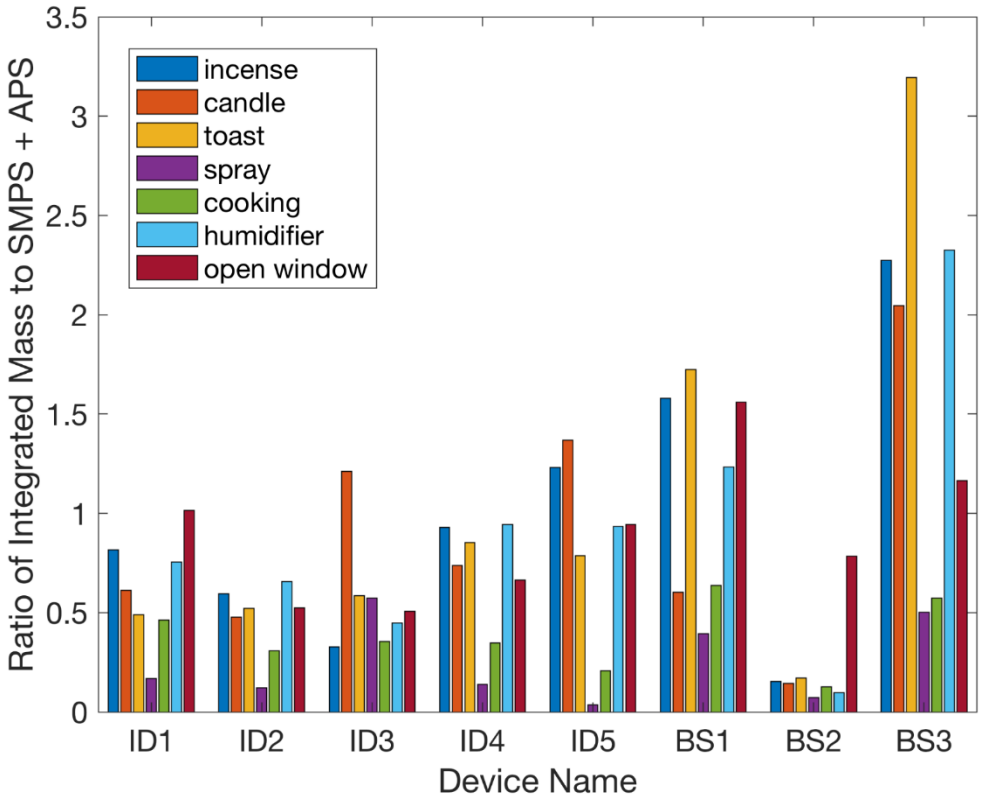

Figure 3.3: Ratio of integrated mass concentration over the events to the SMPS+APS for each device and for each PM source

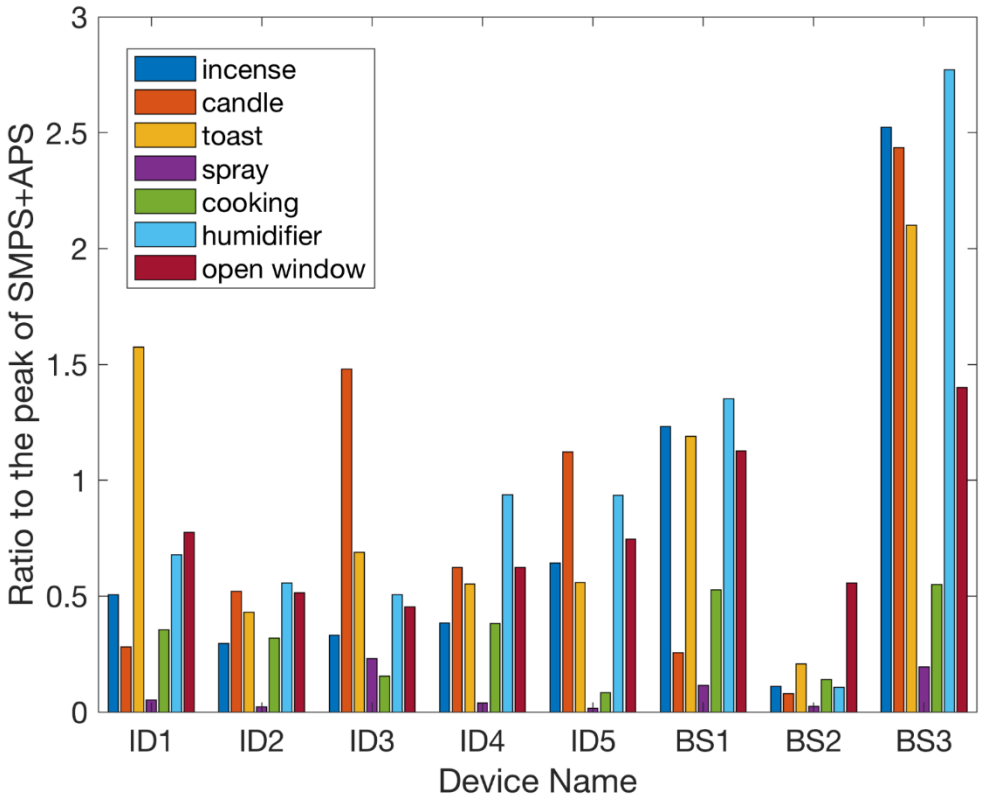

Figure 3.4: Ratio of the maximum particle mass concentration as output by a sensor during an event to the maximum concentration as reported by the SMPS+APS for that event

The denominators of the ratios presented in Figures 3.3 and 3.4 may be influenced by our assumption that all particles have a density of 1 g cm^{-3}. If the true density of the particles was greater than 1 g cm^{-3}, then we have under-estimated the mass concentration using the SMPS+APS, while if the true density of the particles was less than 1 g cm^{-3}, then we have over-estimated the mass concentration using the SMPS+APS. Consequently, these ratios could shift up or down based on the "true" density of the particles. However, the numerator for each sensor will also effectively treat density as a constant, which is embedded in the manufacturer calibration for each sensor. Therefore, there is some

uncertainty in Figures 3.3 and 3.4, but we cannot quantify this due to the unknown source for the manufacturer calibration and the unknown true densities of the particles that we generated.

However, we have explored using densities different from 1 g cm^{-3} (taken from the literature) for various particle events in Additional Tables and Figures. Briefly, literature results suggest that the density of particles generated from incense and candle burning, meat cooking, toast, and urban aerosols (as a proxy for opening the window) are greater than 1 g cm^{-3}, while the density of particles generated by a humidifier is less than 1 g cm^{-3}. Therefore, in Figures B.3.3 and B.3.4, the bars for each of these sources shift up or down accordingly with the change in the assumed density in the conversion of SMPS+APS number concentration to mass concentration. While this affects the magnitude of the values reported, it does not change our general conclusions.

3.5.2 Correlation of time series response by source type

We now present an analysis of the time series response of the low-cost devices and their correlation with reference instruments. Figure 3.5 shows the 1-minute-averaged data from ID4, BS3 and BS2 compared to the SMPS+APS when exposed to seven different PM sources. Also included in Figure 3.5 are solid black 1:1 lines showing the behavior of a "perfect" sensor. In each row of Figure 3.5, the left panel shows the entire mass concentration range for both sensors and the reference instruments during this event, while the right panel shows the subset of the same data with mass concentration < 100 $\mu g/m^3$ for

both sensors and the reference instruments. We present these three representative examples here and include plots of the response of the other devices tested in Figure 3.5.

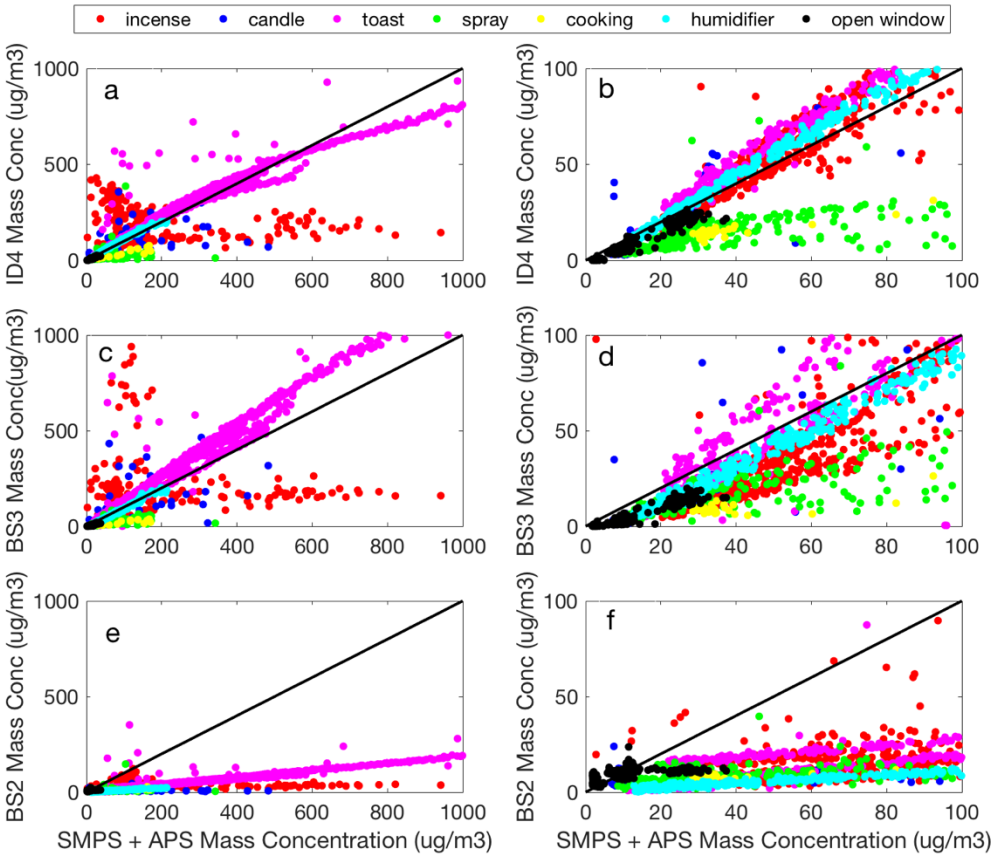

Figure 3.5: ID4, BS3 and BS2 compared to the SMPS+APS when exposed to seven different PM sources

In Figure 3.5, we highlight several features of the responses of the sensors tested. First, some sensors showed responses very similar to reference instruments, but only under certain circumstances. Namely, there is a range of concentrations in which response is very similar to the reference instruments but most responses deviate from a linearly proportional response at some higher concentration. For example, this is evident in Figure 3.5a in which the ID4 deviation from linearity for toast occurs at approximately 500 μg m^{-3}. It should be

noted that this deviation from linearity is source-specific. For example, there is an observable drift from linearity for ID4 that occurs around 80 μg m^{-3} when incense is the source.

The slope of the response line is also very source-specific in most cases. For BS3, we see the slope of response during cooking events, spray events, and incense deviate substantially from that of, for example, toast. Scatter around the linear response curve is also somewhat greater for this particular sensor. This may have consequences for application in indoor environments in that a simple linear calibration of many sensors available on the market would only be valid under certain event types.

Lastly, several sensors under several event types had responses that were very weak, or correlated very poorly to reference instruments. This is evident in the graphs for sensor BS2 for most events, and in the response of most sensors to spray, incense and cooking events. Hypotheses for why this occurs include that the optical properties of liquid particles emitted during spray and cooking events may deviate greatly from those with which the sensor was calibrated, and spatial variations within the room for some sources (we suspect that this is the case for incense) may mean that the response of the sensor is highly dependent on location.

A numerical quantification of the information in these plots is given in Table 3.3 as the parameters defining linear regression between sensors and reference instrument. For an ideal sensor, the slope should be equal to “1”, and the intercept should equal to “0”. We

used t-test to determine if the slope is significantly different than 1 and if the intercept is significantly different than 0 (both at a 5% significance level). However, before we tested if the slopes are different than "1", we first tested if the slopes are significantly different than "0". The vast majority of the slopes are significantly different than "0", strengthening our claim that the sensors can be used for event detection. Sensors with a linear relationship (i.e., slopes significantly different than zero and also different than one) can be corrected using a multiplication factor. Next we test if the slopes are significantly different than "1". From Table 3.3, we observed that the slopes are significantly different than "1" for the majority of the sources and for the majority of the sensors. With an exceptions of ID5, which have slopes that not significantly different than "1" for burning candle, humidifier and open window events, and ID4 have slopes that are not significantly different than "1" for humidifier and open window events. Regarding the intercepts, the majority of these are significantly different than zero, suggesting an offset in the sensors' responses when the reference instruments are reading a concentration approaching 0 $\mu g\ m^{-3}$.

Table 3.3: Linear regression coefficient for all events of all sensors (Values with # for slope indicate that this coefficient is not significantly different than "0". Values with * for slope indicate that this coefficient is not significantly different than "1", and the p-value is provided in parentheses. Values with * for intercept indicate that this coefficient is not significantly different than "0", and the p-value is provide in parentheses.)

PM Emission Type		ID1	ID2	ID3	ID4	ID5	BS1	BS2	BS3
Incense	R^2	0.30	0.12	0.07	0.23	0.14	0.31	0.23	0.20
	slope	0.20	0.10	0.10	0.24	0.32	0.91* (0.96)	0.06#	0.33
	intercept	66.41	54.55	25.22	74.16	98.32	82.61	10.95	48.37
Candle	R^2	0.30	0.20	0.66	0.47	0.43	0.36	0.05#	0.47
	slope	0.21	0.20	1.41	0.53	1.10* (0.78)	0.17	0.02	0.69
	intercept	18.08	13.43	-1.72* (0.76)	11.70	19.47	18.92	5.72	3.02
Toast	R^2	0.62	0.91	0.89	0.92	0.92	0.94	0.90	0.78
	slope	0.53	0.50	0.72	0.78	0.78	1.89	0.18	1.20
	intercept	72.72	34.20	-7.93* (0.09)	60.28	38.11	40.08	6.06* (0.08)	13.82
Spray	R^2	0.01	0.34	0.43	0.30	0.003	0.43	0.30	0.50
	slope	0.02#	0.04	0.25	0.06	0.001#	0.15	0.03#	0.12
	intercept	22.72	14.04	54.32	13.91	0.004* (0.98)	36.95	7.00	12.34
Cooking	R^2	0.30	0.30	0.06	0.87	0.41	0.77	0.70	0.74
	slope	0.21	0.26	0.02	0.36	0.02	0.43	0.09#	0.16
	intercept	18.08	11.06	24.83	2.11* (0.51)	12.05	16.87	4.46	3.13* (0.47)
Humidifier	R^2	0.92	0.92	0.91	0.92	0.97	0.87	0.67	0.95
	slope	0.61	0.57	0.53	1.02*	1.02* (0.76)	1.86	0.12	1.18* (0.72)
	intercept	17.62	13.57	0.27* (0.30)	1.05* (0.14)	3.99	7.29	6.78	-6.29
Open Window	R^2	0.90	0.94	0.81	0.94	0.91	0.95	0.31	0.89
	slope	0.97* (0.04)	0.71	0.58	0.85* (0.94)	0.95* (0.99)	1.51	0.19	0.56
	intercept	0.60	-1.23	-0.54	-1.68	0.98	1.02	7.08	-1.88
Background	R^2	0.34	0.49	0.48	0.49	0.45	0.52	0.43	0.41
	slope	0.27	2.56	0.35	0.40	0.42	0.93* (0.42)	0.08	0.60
	Intercept	3.21	0.27* (0.04)	1.23	1.96	4.43	4.62	2.34	0.06* (0.75)

3.5.3 Manufacturing consistency

Table 3.4 shows linear regression models and fit metrics between 1-minute data of all possible combinations of sensor pairs in our study. ID2, ID4, ID5, BS1 and BS3 demonstrate very high consistency between the same sensors, as seen by slopes and R^2 values closer to one. However, the correlations between the ID3 and BS2 pairs are relatively low. We do not speculate on the mechanism for these discrepancies or lack thereof, but our results are consistent with previous studies indicating that some sensor types may have high intra-model variability (D. Liu et al., 2017; Manikonda et al., 2016; Morawska et al., 2018; Mukherjee et al., 2017; Zheng et al., 2018; Zikova et al., 2017).

Table 3.4. Linear regression and correlation between sensors from the same manufacturer. The "underscore" notation represents duplicates of the same sensor type (e.g., we tested three of ID2, three of ID3). (Kumar et al., 2016; Wang et al., 2015)

X Axis sensor	Y Axis sensor	Least square	R^2	Reduced major axis	r
ID2-1	ID2-2	Y = 0.937 x + 0.20	0.97	Y = 0.950x+ 0.142	0.97
ID2-1	ID2-3	Y = 0.974 x+ 0.828	0.96	Y= 0.992x + 0.728	0.95
ID2-2	ID2-3	Y = 1.03x + 0.65	0.99	Y = 1.044x + 0.620	0.98
ID3-1	ID3-2	Y = 0.797x + 1.425	0.64	Y = 1.00x + 0.402	0.62
ID3-1	ID3-3	Y = 0.692x + 0.440	0.80	Y = 0.773x – 0.014	0.81
ID3-2	ID3-3	Y = 0.626x + 0.560	0.65	Y = 0.779x – 0.351	0.62

X Axis sensor	Y Axis sensor	Least square	R^2	Reduced major axis	r
ID4-1	ID4-2	Y = 1.065x – 0.298	0.99	Y = 1.070x – 0.327	0.99
ID5-1	ID5-2	Y = 1.012x – 0.116	0.99	Y = 1.0144x – 0.1007	0.99
ID5-2	ID5-3	Y = 0.95x – 0.094	0.98	Y = 0.9671 – 0.0317	0.96
ID5-1	ID5-3	Y = 0.981x + 0.075	0.98	Y = 0.9896x – 0.0446	0.99
BS2-1	BS2-2	Y = 0.95x + 11.70	0.77	Y = 1.080x + 11.167	0.75
BS2-1	BS2-3	Y = 1.31x + 11.76	0.36	Y = 2.183x + 7.921	0.34
BS2-2	BS2-3	Y = 1.36x – 3.73	0.45	Y = 2.02x – 13.992	0.45
BS1-1	BS1-2	Y = 0.974x + 0.452	0.93	Y = 1.00x - 0.046	0.93
BS3-1	BS3-2	Y = 0.927x + 0.69	0.91	Y =0.968x - 0.245	0.92

3.5.4 Effect of Averaging Time

Lastly, we investigate the effect of averaging time on the apparent performance of low-cost sensors as compared to the reference instruments. To do this, we took the time series of all data taken over the course of the 2.5 month investigation and averaged it over different lengths of time. In Figure 3.6, we then plot the coefficient of determination of the linear fit of the data of each low-cost sensor and the reference instruments versus the time over which the data was averaged. For example, 10-minutes on the abscissa implies data was averaged over ten minutes and then compared to similar reference instrument data

averaged over the same time period. We used 1 minute, 10 minutes, 30 minutes, 1 hour, 6 hours, 12 hours and 24 hours as the averaging times to examine the correlation between sensors and the reference instruments. While the longer averaging times are well beyond the length of an event, they may give some insight into how these sensors may function as indicators of overall air quality in a given building, assuming they are calibrated correctly. We show the same information with two different abscissas for clarity. We see that for all devices there exists a distinct time scale at which apparent performance begins to decline rapidly. Using this R^2 metric this occurs for most sensors at an approximately one-hour averaging time. This may point to a possible time scale at which control decisions could be executed with sensors in their current form.

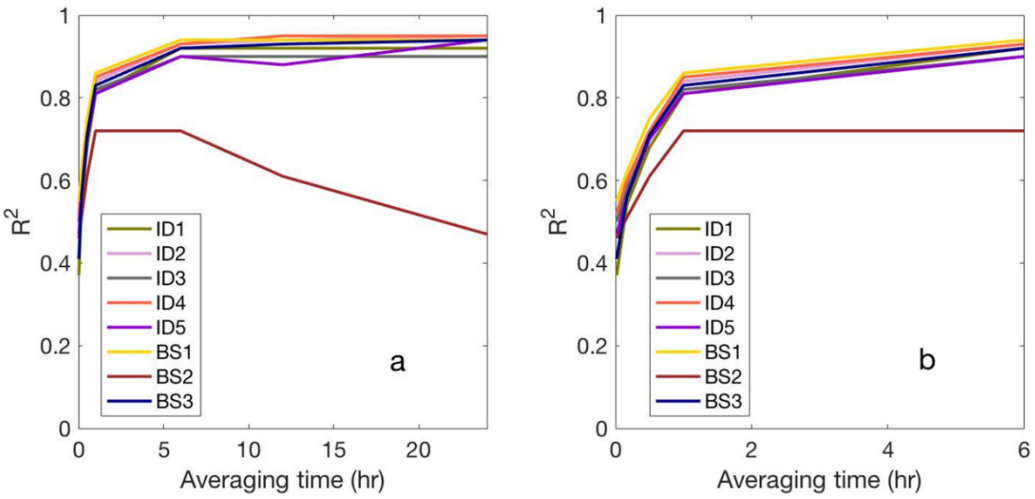

Figure 3.6: Coefficient of determination R^2 of the linear fit of the data of each low-cost sensor and the reference instruments versus the time over which the data was averaged

3.6 Discussion and Conclusion

In this study we evaluated three BS and five ID along with a SMPS and APS as reference instruments in a test house subjected to seven typical indoor particle-generating activities over two and half months. In general, the consumer devices showed large variability as quantified by several metrics. Specifically:

- All events tested in this work resulted in measurable and significant responses of all devices tested, although magnitude of responses varied widely.
- The ratios of the integrated signals and peak signals to the reference instruments over the course of an event range from near zero to three.
- All low-cost products showed responses less than reference instruments for spray and cooking events, with peak and integrated ratios less than 0.5. Correlations between reference instruments and low-cost products for these events were also lower than for other events. Incense burning also resulted in lower concentrations, possibly due to large spatial variations.
- We did not witness an inability of any sensor to return to baseline concentrations after an event.
- While some devices showed nearly linear response to multiple types of particle emission events, the slope of the linear response varied significantly, meaning simple linear calibration may only be appropriate for certain event types.
- Most sensors showed a distinct functional range of mass concentrations in which response was linear and consistent. The boundaries of this range varied significantly between products.

- Intra-model consistency was generally good for the sensors used, with five models showing intra-model correlations, R^2, of 0.92-0.99, while two models had significantly lower intra-model consistency (R^2 = 0.34-0.75). It should be noted that the small sample size measured precludes any statistically significant conclusions from being drawn from this data.
- When assessing sensor performance over the entire experimental campaign, it appears averaging time affects apparent performance dramatically, as is consistent with previous work. In the experiments done in this work, at a time scale of approximately one hour, correlation to reference device performance appears to decrease significantly. It should be noted that much of the data used to find this correlation was under low-concentration conditions, and emission event frequency was not necessarily representative of the operation of a real home. We do not assert a mechanism for this apparent decline in performance at shorter time scales.

Further laboratory studies will examine the size-specific response of these sensors to different PM source, and also evaluate the response of these sensors to particles of different composition in Chapter 5.

3.7 Additional Tables and Figures

Devices Tested

BS1 uses a fan to drive the intake and exhaust of particles. Particles enter through the sensing area and pass through a light beam produced using a laser as the light source and a lens positioned across from a photodetector. As particles pass through, the sensor light intensity varies, and the photodetector then produces a 32-byte signal, from which, 4 bytes are used in a proprietary algorithm process to produce serial outputs for particle sensors for PM 2.5 and PM10. BS1 has a sampling time of 2 second.

BS2 uses a thermal resistor to drive particle flow through the detector area, comprised of LED and photodetector both utilizing individual lenses to magnify the light intensity. The LED is turned on for 280µs and then switched off for 40µs. The light intensity will differ based on particle density, which in turn effects the voltage output read by the photodetector. The intensity of the voltage between pulsed widths is used to interpret sensor outputs, which can be assessed using a manufacture calibration curve to produce total PM mass density ($\mu g/m^3$). BS2 has a sampling time of 1 second.

BS3 uses a fan to drive airflow and also includes a laser-based light source and a photodetector. It produces a 32-byte digital signal in which 12 -bytes are used in a proprietary algorithm to provide serial output of number concentration for particles in different size ranges (>0.3, >0.5, >1.0, >2.5, >5 and > 10 μm). The mass concentration can then be calculated in those size bins by assuming a particle density. BS3 has a sampling time of approximately 900 milliseconds.

Integrated devices combine bare sensors and a microcontroller in a compact enclosure, and they nearly always provide PM mass concentration.

ID1 has a variety of unique measures such as cellular, Wi-Fi, and Bluetooth capabilities. ID1 implements a cloud-based system for continuous long-term monitoring with a wireless device monitoring PM_1, $PM_{2.5}$, PM_{10}, CO_2, CH_2O, VOCs, Temperature, humidity and pressure. ID1 has a sampling time of 1 minute.

ID2 communicates over Wi-Fi and Bluetooth, and a serial connector. It also has weather-resistant features. It requires an Android device to configure the device. Measurements are transmitted to an Android app and can be added to a map. ID2 has a sampling time of 1 minute.

ID3 detects two size ranges: $PM_{0.5\text{-}2.5}$ and $PM_{2.5\text{-}10}$. It uses a fan to drive the airflow, and baffles to direct the particles into a beam trap that incorporates a laser and a photodetector. ID3 has its own software which can visualize the time series plot of particle

number concentration. It also communicates via a serial connector. ID3 has a sampling time of 1 minute.

ID4 has two BS3 inside the enclosure. It uses serial communication to provide number concentration of > 0.3, > 0.5, > 1.0, > 2.5, > 5 and > 10 μm. It also provides PM_1, $PM_{2.5}$ and PM_{10} mass concentration. Because ID4 is still in development, it has a sampling time of approximately 900 milliseconds, similar to BS3.

ID5 also uses two BS3 inside a weather resistant enclosure. It communicates with Wi-Fi, and it has a built-in 16 GB microSD card to store the data and a real-time clock for offline logging. The output data structure is similar to ID4 but the sampling time is 80 s.

In terms of the cost of IDs and BSs, Most IDs have a price in the range of $200-$300. BSs have a price in the range of $15-$30. In terms of size resolution, ID1, ID2, ID4, ID5 and BS3 all provide mass concentration for PM_1, $PM_{2.5}$, and PM_{10}. Among them, ID4, ID5 and BS3 also present number concentration over different size bins. ID3 only provides two channels ($PM_{0.5\text{-}2.5}$, > $PM_{2.5}$) of number concentration. Similarly, BS1 only provides mass concentration in two size bins ($PM_{2.5}$, PM_{10}). BS2 only presents overall mass concentration of $PM_{2.5}$.

We co-located two reference instruments with the low-cost devices in all experiments. These are described below:

Scanning Mobility Particle Sizer

A Scanning Mobility Particle Sizer system contains several components. In the first step, sometimes optional, an aerosol sample passes through an impactor, which removes particles larger than a certain diameter. In the second step, the aerosols pass through a neutralizer, which establishes an equilibrium charge distribution on the particles; in this work, we used a soft X-ray diffusion charger to impart this charge distribution. In the third step, the particles enter a Differential Mobility Analyzer (DMA) where the aerosols are classified according to their electrical mobility. When a given voltage is applied to the center of the DMA, only a specific particle diameter will be able to exit the column; by scanning through a range of voltages between roughly 10 V and 10,000 V, a distribution of particle diameters can be characterized. The final component is a Condensation Particle Counter, which counts the particles and provides a particle number concentration.

In this work, our typical scan time was 60 seconds between voltages corresponding to roughly 18 to 532 nm. Figure A3-1 provides sample data for a single scan through the voltages as a histogram of 95 size "bins" (x-axis). The y-axis is a normalized concentration ($dN/dlogD_p$), which represents the number concentration of particles dN between diameter $D_{p,n}$ and $D_{p,n+1}$; hence, the units on the y-axis are $\#/cm^3/nm$.

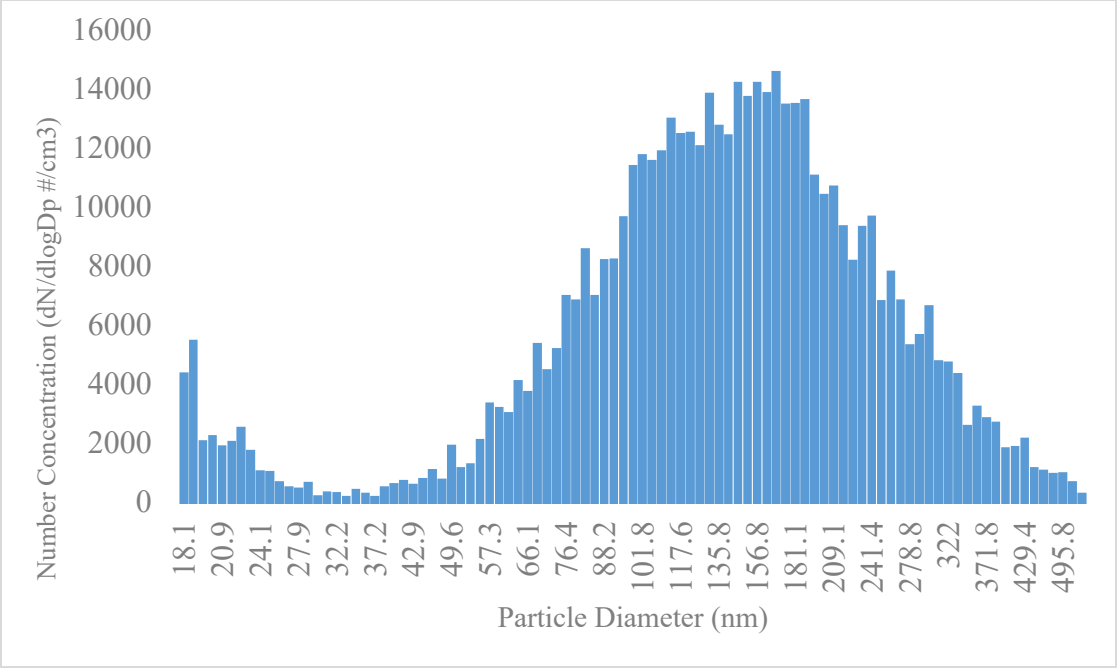

Figure 3.7: Example SMPS data for a single scan when monitoring particles

Aerodynamic Particle Sizer Spectrometer

The Aerodynamic Particle Sizer spectrometer combines the technology of light scattering measurement and time-of-flight measurement technology. It accelerates the particles into the detection area, where two partially overlapping laser beams are emitted causing particles to generate two peak electrical signals. Analyzing the length between the two peaks gives aerodynamic size information, by measuring the time when particle traverse between the laser beams. By analyzing the intensity of the peak, it provides the particle size and concentration information because the intensity of the electrical signal is proportional to the particle concentration. The measured particle aerodynamic size is range from 523 nm to 19.8 μm.

Response of individual sensors to multiple types of particle emission events

We show the response of the sensors and integrated devices not already presented in the body text in Figure 3.8. Responses are color-coded by particle emission event type. Also included are 1:1 solid lines showing the behavior of a "perfect" sensor. In each row of Figure 3.8, the left panel shows the entire mass concentration range for both sensors and the reference instruments during this event, while the right panel shows the subset of the same data with mass concentration < 100 $\mu g/m^3$ for both sensors and the reference instruments.

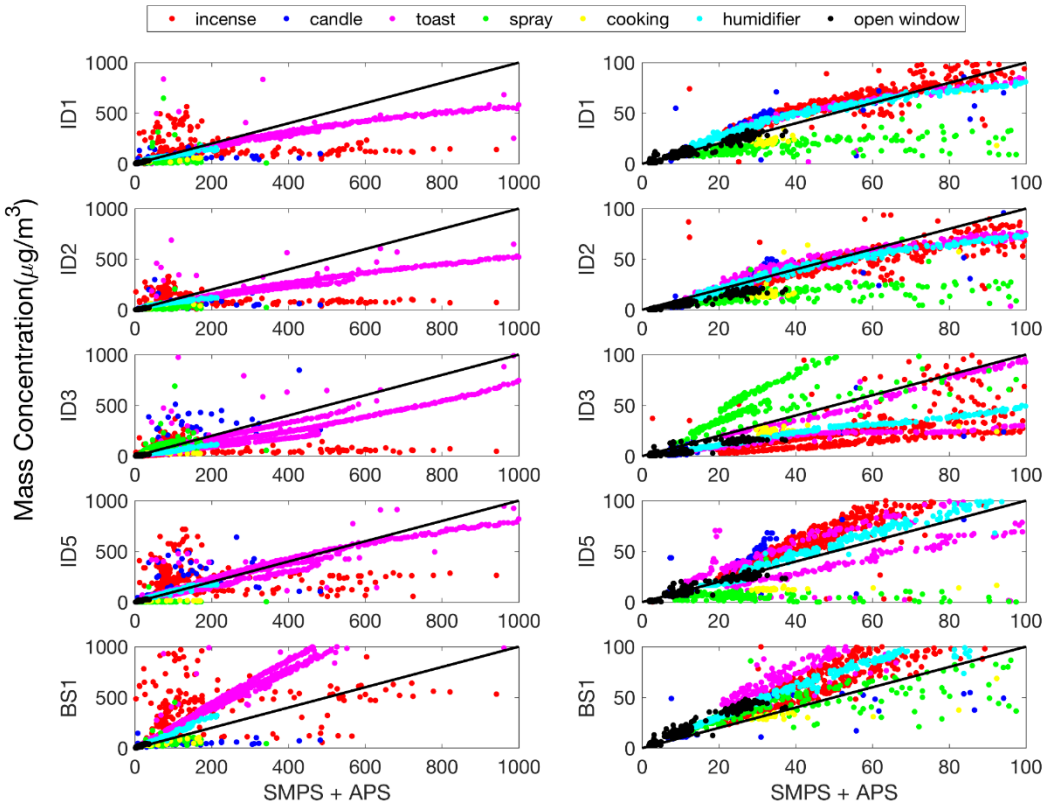

Figure 3.8: ID1, ID2, ID3, ID5 and BS1 compared to the SMPS+APS when exposed to seven different PM sources

Responses using a different density for each particle sources

In order to convert the output of reference instruments to a mass concentration that could then be compared to the output of the low-cost sensors (given as a mass concentration for all but one sensor), we first assumed a density of 1 g/cm^3 for all particle sources. This is the assumption for all data reported in the body of this article. In order to assess the effect of this assumption, we analysed the same data using particle density values previously reported in the literature. In cases where multiple values were reported for the same source, we averaged the reported values. This gave the following density values:

- Incense: 1.19g/cm^3 (Ji, Bihan, Ramalho, Martinon, & Nicolas, 2010; Singer & Delp, 2018).
- Candle: 1.25 g/cm^3 (Rissler et al., 2013; B. C. Singer & Delp, 2018; Vu et al., 2017).
- Cooking meat: 1.006 g/cm^3 (Pan & Singh, 2001).
- Burning toast: 1.28 g/cm^3 (B. C. Singer & Delp, 2018).
- Humidifier: 0.94 g/cm^3 (Umezawa et al. 2013; Singer and Delp 2018).
- Urban aerosol during window opening: 1.5g/cm^3 (Rissler et al., 2013; P. Taylor et al., 2010).
- Deodorizer spray is hypothesized to be 1g/cm^3.

Figure 3.9 shows the ratio of integrated mass concentration over each event as measured by the low-cost sensor to that measured by the SMPS+APS, which provides a

metric describing how well a given sensor estimates time-integrated exposure. Most of the ratios of integrated mass of sensors to the SMPS and APS decreased compared to Figure 3, which assumed particle density equal to 1g/cm^3.

Figure 3. 10 shows the ratio of the maximum particle mass concentration as output by a sensor during an event to the maximum concentration as reported by the SMPS+APS for that event and aggregated across all events of a given type after using different densities for different events. Similar to Figure 3.9, most of the ratios decreased while the ratio for humidifier increased.

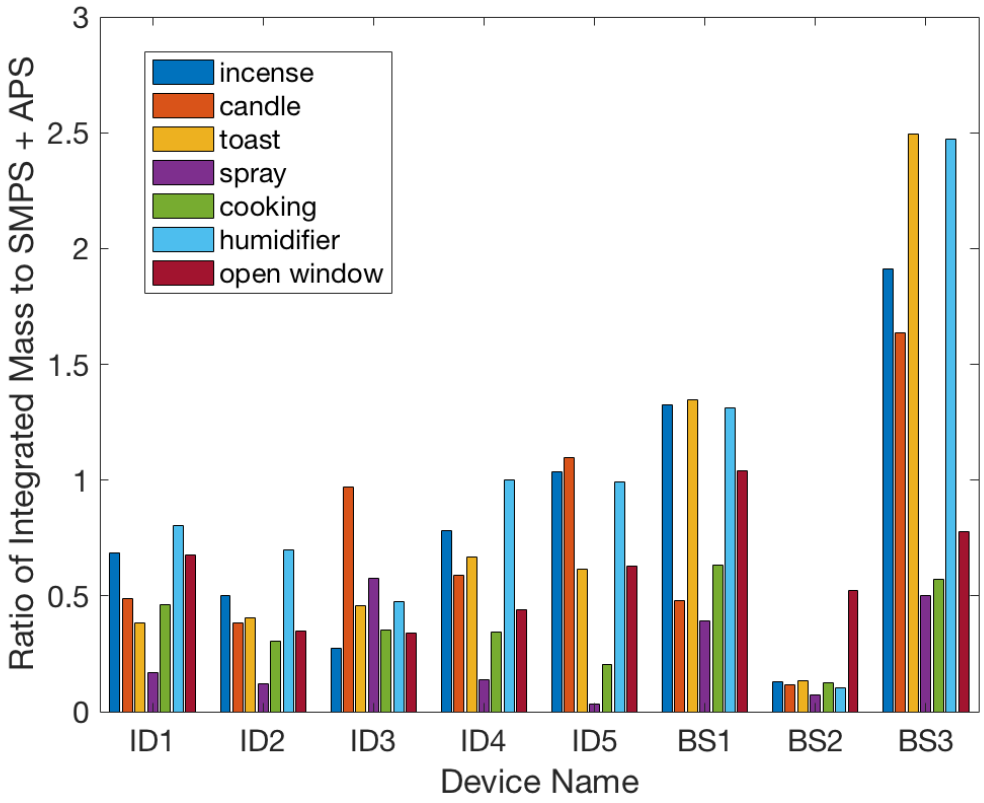

Figure 3.9: Ratio of integrated mass concentration over the events to the SMPS+APS for each device and for each PM source

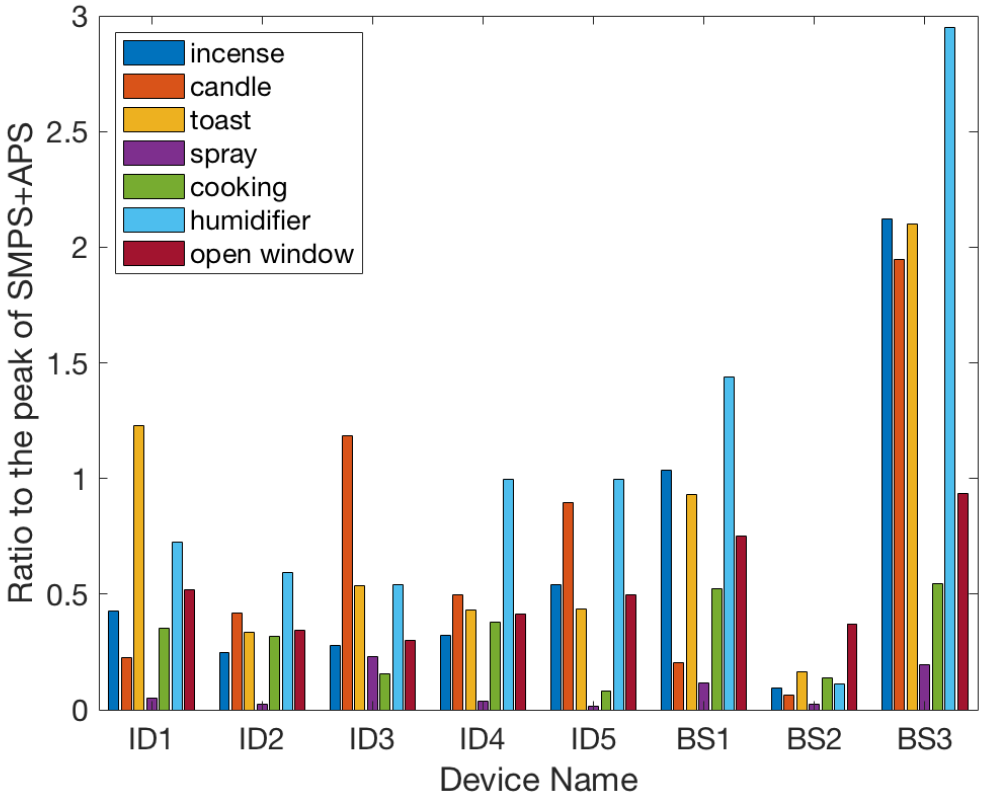

Figure 3.10: Ratio of the maximum particle mass concentration as output by a sensor during an event to the maximum concentration as reported by the SMPS+APS for that event

Chapter 4: Examining the functional range of commercially available low-cost airborne particle sensors and consequences for monitoring of indoor air quality in residences[2]

4.1 Introduction

Interest in low-cost sensors for indoor environmental monitoring and control of ventilation and air cleaning systems in smart buildings has increased recently. Many such devices are available from several manufacturers, and performance of such devices has been widely documented. In particular, low-cost particle sensors that measure airborne particle concentrations with only a small light-emitting diode and a small photocell are available from more than a dozen manufacturers and have been studied extensively in laboratory and field studies for both outdoor and indoor applications.

However, the conclusions drawn from the various studies investigating performance of these low-cost particle sensors vary. In some cases the conclusions are in direct contradiction with those of other investigations. Several mechanisms have been identified as a cause of the variation in performance of these sensors. These include effects of humidity(Han et al., 2017; Jayaratne et al., 2018; McMurry & Stolzenburg, 1989; Rai et al., 2017; Wang et al., 2015), ambient light, particle composition(Northcross et al., 2013; Sousan et al., 2017; Wang et al., 2015), manufacturing consistency(Polidori et al., 2016b; Zikova et al., 2017) , particle size effects (D. Liu et al., 2017; B. C. Singer & Delp, 2018;

[2] This chapter is a published paper at https://doi.org/10.1111/ina.12621

Sousan et al., 2016; Wang et al., 2015), and drift or degradation over time (Crilley et al., 2018; Polidori et al., 2016b; M. D. Taylor et al., 2016).

One effect that has not been sufficiently investigated is the effect of the concentration of particulate matter in the environments in which these sensors operate. In other words, we assume that as with any sensor, there is a distinct functional range in which these low-cost particle sensors function well, and both a low-concentration and high-concentration range in which performance declines significantly. Wang et al (Wang et al., 2015)showed evidence indicating a decrease of slope of sensor response as at concentrations as low as 160 $\mu g/m^3$ and a saturated signal near 5000 $\mu g/m^3$. Austin et al (2015) defined the upper limit of functional range as the concentration at which a 10 increase in the reference monitor (APS) resulted in less than 0.2 change in the Lo Pulse occupancy of the Shinyei PPD42NS sensors. Most manufacturers report a lower bound of operating range of "0 $\mu g/m^3$", but we seek to assess whether this is truly zero or if the lower limit is actually some non-zero value. We hypothesize that the definition of this functional range is important in understanding the performance of these devices, and that failure to take this functional range into account can explain some of the variance in reported performance and variance in preliminary observations we previously made in the field.

For these reasons we pursue three objectives over the course of an experimental campaign and associated simulations in this work:

1. Put forward a definition of an upper and lower bound of a range in which a low-cost particle sensor can be expected to perform comparably to more expensive instruments.

2. Define this range for several widely available low-cost sensors and integrated devices.

4.2 Materials and Methods

4.2.1 Sensors Tested

We tested three bare sensors (BSs) and five integrated devices (IDs) in this work. We define bare sensors as small stand-alone sensors measuring approximately five centimeters along their longest edge that output an electrical signal only, which then must be interpreted by the device in which it is housed or by its user via additional hardware. We define an integrated device as a packaged off-the-shelf consumer product that includes at least one bare particle sensor, a means of communication and/or storage, housing, and in some cases other sensors, a user interface, and/or an auxiliary fan or fans.

Table 4.1 lists the bare sensors tested in this work along with some relevant information (including number tested), while Table 4.2 provides the same information for the integrated devices. We have provided the manufacturer and model names in the spirit of reproducibility; no endorsement by the authors or the sponsor should be inferred. In this work, we make no efforts to calibrate these sensors; rather, we are simply using them "off-the-shelf" in order to mimic how they might be used in a typical residential or commercial setting.

Table 4.1: Bare sensors tested, along with information from the manufacturer and prior testing reported in the literature

Sensor	Type (Manufacturer)	Cost	Intake	Manufacturer Reported Range	Use in Integrated Device(s)	Previous Studies	No. of Units
BS1	HPMA115S0 (Honeywell)	$30	Fan	0 µg/m3 to 1000 µg/m3	None		2
BS2	GP2Y1010AU0f (Sharp)	$15	Resistor	0 µg/m3 to 500 µg/m3	Used in commercially available devices that were not tested in this work	(Budde et al., 2013; Hojaiji et al., 2017; Liu et al., 2017; Sousan et al., 2016; Wang et al., 2015; Weekly et al., 2013*)	3
BS3	PMS5003 (Plantower)	$25	Fan	Effective 0 µg/m3 to 500 µg/m3 Max 0 µg/m3 to 1000 µg/m3	ID2, ID4; ID5	(Jayaratne et al., 2018; Kelly et al., 2017*; Zheng et al., 2018*)	2

*different version of sensor from same manufacturer tested in previous work

Table 4.2: Integrated devices tested, along with information from the manufacturer and prior use reported in the literature

Sensor	Type	Cost	Sensor	Previous Studies	No. of Units
ID1	AirThinx	N/A	unknown		1
ID2	Airbeam2	$200	Previous version of BS3	(B. C. Singer & Delp, 2018; Sousan et al., 2017)	3
ID3	Dylos DC1100 PRO	$290	unknown	(Han et al., 2017; Hojaiji et al., 2017; Jiao et al., 2016*; Manikonda et al., 2016; Northcross et al., 2013; Polidori et al., 2016; Sousan et al., 2016*; Steinle et al., 2013)	3
ID4	TSI Bluesky	N/A	Dual BS3		2
ID5	Purple Air II	$229	Dual BS3	(Polidori et al., 2016*; Singer & Delp, 2018)	3

*different version of sensor from same manufacturer tested in previous work

4.2.2 Experimental Methodology

We conducted two phases of experimental work. In the first phase, we first placed all sensors into a 0.71 m x 0.48 m x 0.38 m (0.130 m^3) enclosed chamber. We then closed the chamber and injected as close to "zero air" as we were able to achieve by filtering room air with HEPA and activated carbon filters. We achieved a particle number concentration less than 200 #/cm^3 during these experiments in all cases but were not able to achieve exactly zero, most likely due to some re-suspension within the chamber and/or possible generation by the sensors themselves. We maintained these conditions in the chamber for two hours during which concentrations were logged for each device either through its native storage or through interfacing with micro-computers in the case of the bare sensors. As a reference, we also characterized particles in the chamber through a sampling port using a Scanning Mobility Particle Sizer (SMPS) and an Aerodynamic Particle Sizer (APS). For each device we then define the limit of detection (LOD) according to the International Union of Pure and Applied Chemistry (IUPAC) definition for an "instrument detection limit", where $LOD = M_{blank} + 3\sigma_{blank}$. M_{blank} is the average mass concentration for a given sensor under "zero air" conditions and σ_{blank} is the standard deviation for these conditions. This is similar to the definition used by others (Northcross et al., 2013; L. A. Wallace et al., 2011; Wang et al., 2015).

In the second phase of experiments we subjected both the low-cost devices and the APS and SMPS to decay tests by injecting one of three different particle sources into the chamber, closing the chamber, and recording the concentration as it decayed in the chamber. We used incense, atomized ammonium sulfate [$(NH_4)_2SO_4$] particles (solution

concentration of 10 g/L), and burnt toast smoke as the three particle sources in these decay tests. For each source, we generated a high concentration and passed them through a diffusion drier prior to entering the chamber. We then removed the source, letting the concentration in the chamber naturally decay (mainly via extraction of chamber air by the reference instruments) until all sensors' concentration reached near zero. The only sinks within the chamber were gravitational settling, deposition on chamber walls and sensors, and removal of chamber air by the reference instruments. We repeated these decay experiments four times for each source. The average temperature across all experiments was 26.01 ± 0.34 °C, and the relative humidity was 20.89 ± 4.36 %.

Because the low-cost devices and reference instruments had different sampling and averaging frequencies, we then averaged all data into one-minute bins to allow direct comparison between all events. SMPS and APS data were merged using the approach of Khlystov (2004). We assumed a spherical shape for particles from incense (C. C. Yu & Hung, 1995), for atomized $(NH_4)_2SO_4$ particles (Zelenyuk et al., 2006), and for burnt toast smoke (Lattimer, 2008). To convert SMPS+APS data to mass concentrations, we assumed the density of $(NH_4)_2SO_4$ particles is 1.77g/cm^3 (Zelenyuk et al., 2006), that of particles generate by incense is 1.06 g/cm^3 (B. C. Singer & Delp, 2018), and toast is 0.94 g/m^3 (B. C. Singer & Delp, 2018). An example of the averaged sensor data compared to merged SMPS and APS data is provided in Figure 4.1.

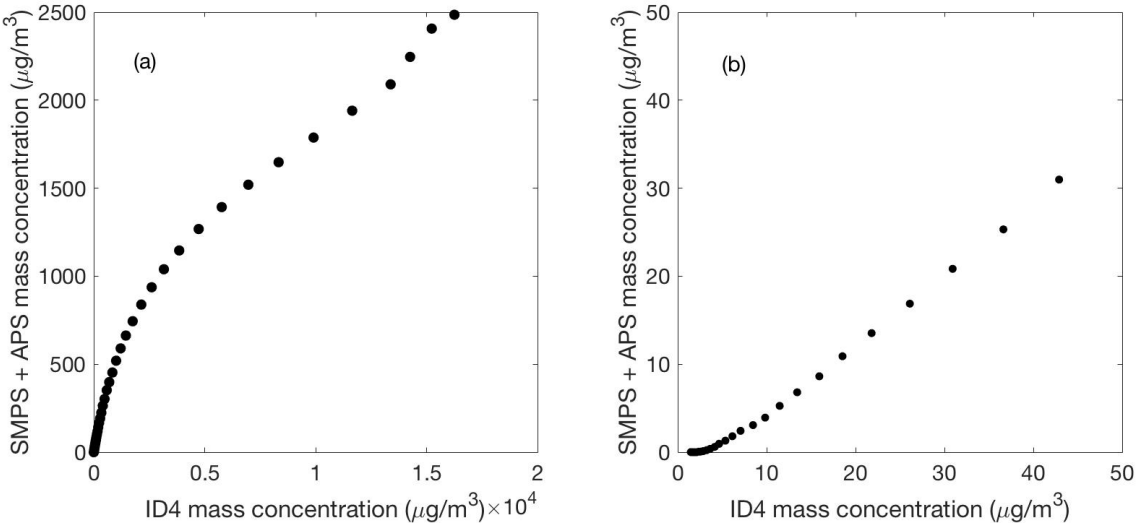

Figure 4.1: a) Response of low-cost device compared to SMPS and APS during the decay test. b) Magnified view of data from panel a) for concentrations < 50 μg/m^3.

By looking at Figure 4.1b closely we can see that below some low concentration, which we refer to here forward as the lower limit of quantification (LOQ), the signal from the low-cost sensor becomes nearly constant and no longer responds to changes in chamber concentration as detected by the reference. We defined a "running R^2" metric to understand at what concentration the correlation between reference instrument and low-cost device breaks down. This running R^2 method is analogous to a running mean using a window of 10 minutes and a step size of 1 minute. The concentration at which this running R^2 falls below a certain threshold, say 0.8, is a possible definition of the LOQ which we sought to establish.

Similar to running R^2, we also defined a "running slope" metric to evaluate the linearity of the relationship between reference instrument and low-cost devices. The running slope is also calculated from the linear regression using a window of 10 minutes

and a step size of 1 minute data between the sensors and the reference. By calculating a running slope, we can gain some insights into the concentration at which sensor response deviates from linearity and the point at which the sensor begins to approach saturation; these two points are candidates for definitions of the upper bound of the sensors' function range (UB). Visually, this UB appears to occur at roughly 500 $\mu g/m^3$ in Figure 1a, but we wanted a quantitative definition for this value. Austin et al (Austin et al., 2015) previously suggested defining the UB as the concentration at which a 10 increase in the reference monitor (APS) resulted in less than 0.2 change in the Lo Pulse occupancy of the Shinyei PPD42NS sensors.

4.3 Results

We first examined the effect of averaging time on the apparent limit of quantification of the sensors. In Figure 4.2 we show the concentration at which the coefficient of determination between ID1 and the reference instruments falls below 0.8, as a function of the number of points averaged. In other words we average the sensor concentrations at different time intervals (one point is one minute of sampling) and analyze the effect on apparent limit of quantification. We see that apparent limit of quantification is a strong function of averaging time at averaging times less than approximately ten minutes. Similar phenomena were measured by others (Budde et al., 2013; Zheng et al., 2018). This ten-minute threshold was consistent for all sensors tested. For this reason, we adopt the convention of averaging data over ten minutes for the remainder of this work.

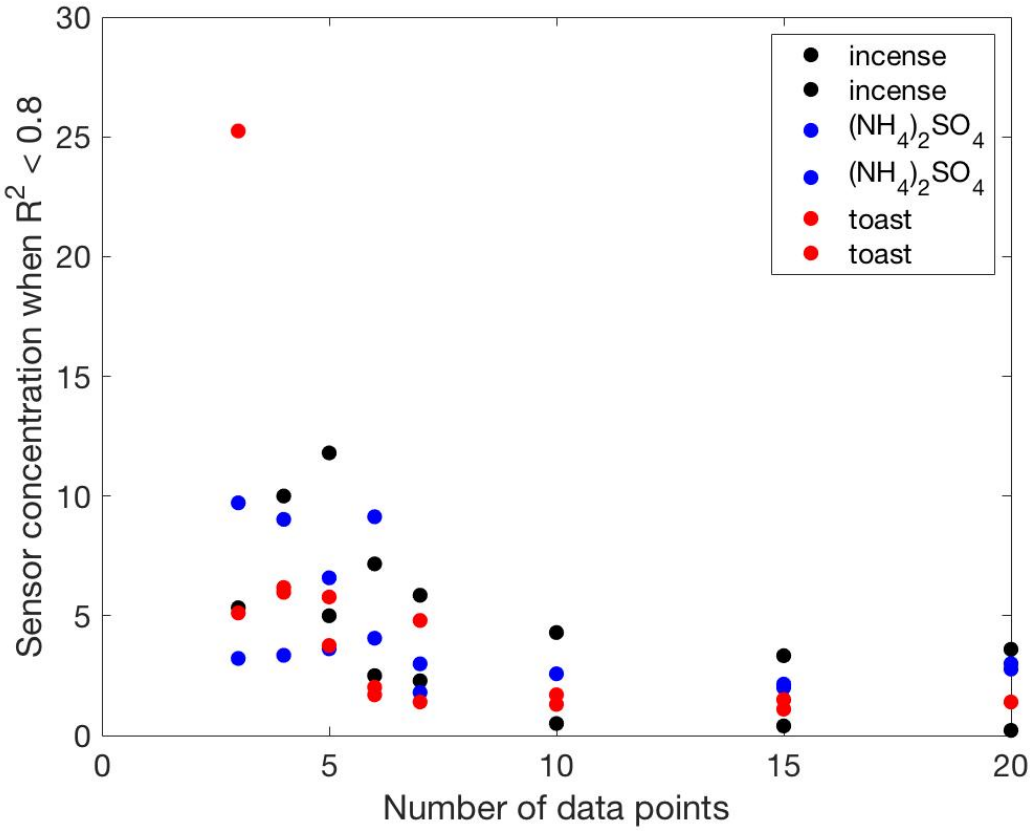

Figure 4.2: Effect of averaging time (or equivalently the number of data points used-each point is at one minute time resolution) on the apparent limit of quantification as defined as the concentration at which R^2 falls below 0.8.

We give two examples of typical sensor response in terms of running R^2 in Figures 4.3 and 4.4. Figures 4.3 and 4.4 show the running R^2 for a given sensor as a function of the reference instrument mass concentration. The abscissa value is the centroid of the range over which the running R^2 is calculated. The sensor in Figure 4.3 (BS2) shows a distinct drop in performance occurring around a concentration of approximately 30 $\mu g/m^3$. This concentration is greater than what is expected in many indoor environments, suggesting

the readings of at least some commercially-available low-cost sensors do not correlate with actual particle concentrations for many situations of interest.

This behavior was recorded for nearly all low-cost devices tested, although the concentration at which this sharp drop in performance occurred varied widely. For at least one device the drop occurred at a concentration less than 5 μg/m^3, as shown in Figure 4.4, suggesting good performance even at very low concentrations. Similar plots are given for other devices in Additional Tables and Figures.

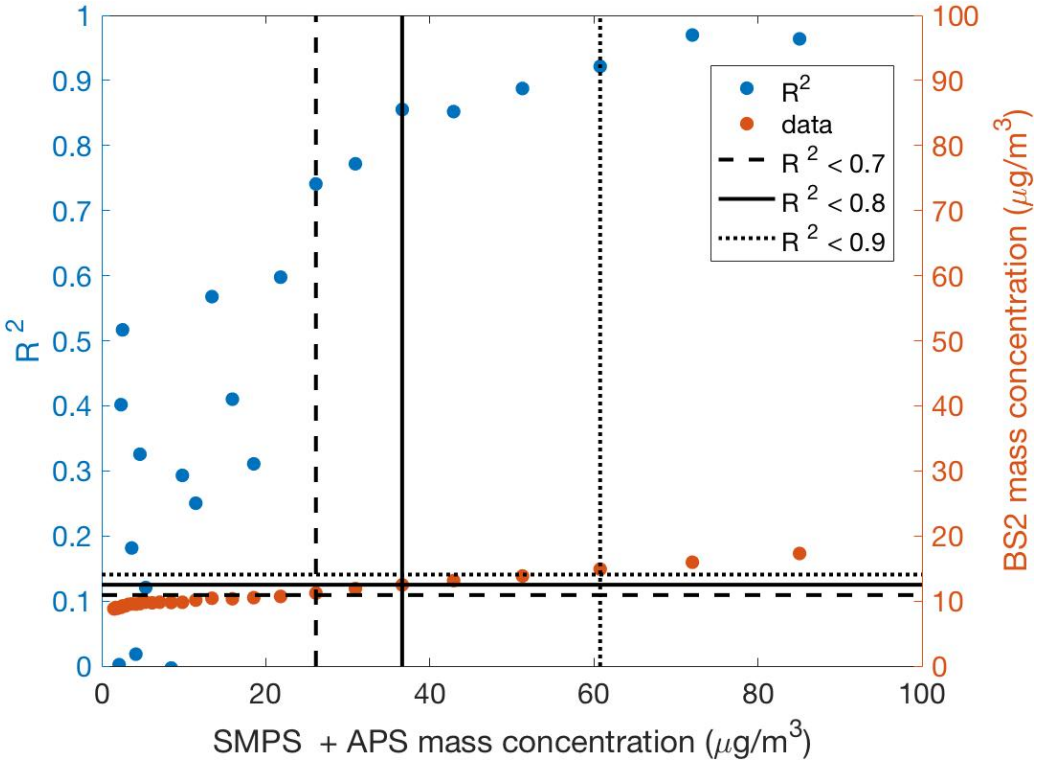

Figure 4.3: Relationship between running R^2 and reference particle mass concentration for BS2. The sensor mass concentration is provided as the right y-axis. Vertical lines relate R^2 and the reference mass concentration, while horizontal lines relate the reference mass concentration with the sensor mass concentration.

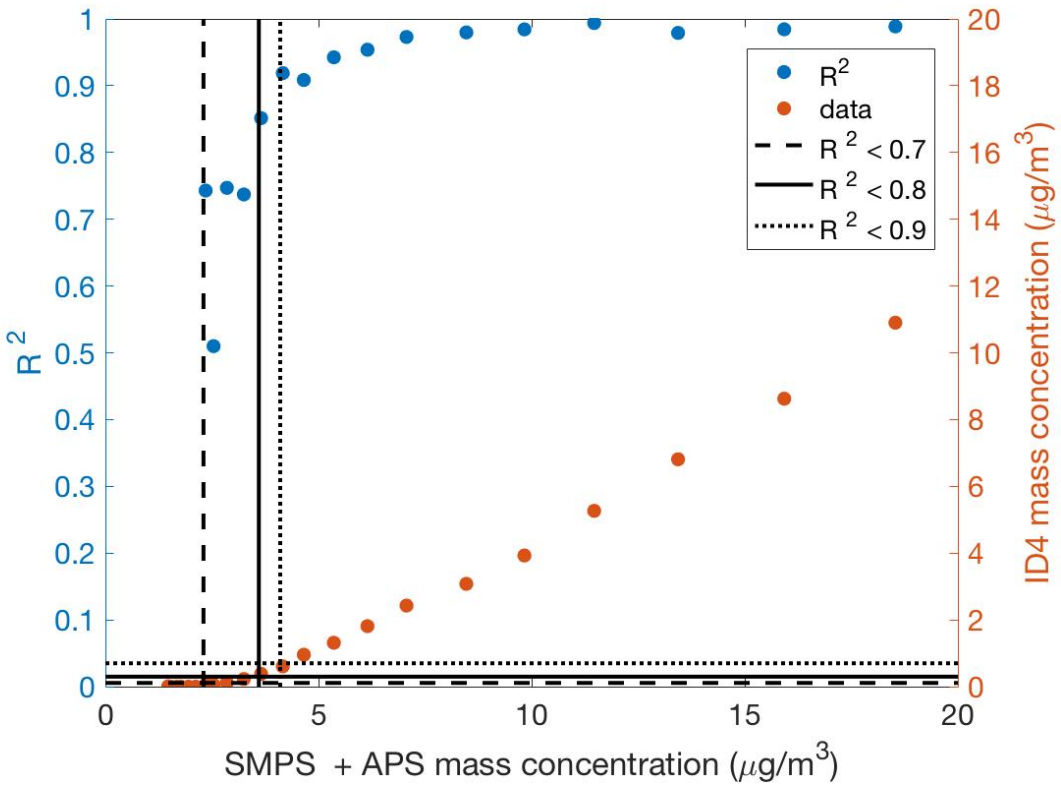

Figure 4.4: Relationship between running R^2 and reference particle mass concentration for ID4. The sensor mass concentration is provided as the right y-axis. Vertical lines relate R^2 and the reference mass concentration, while horizontal lines relate the reference mass concentration

Table 4.3: Limit of Quantification when using threshold of R^2 = 0.7, 0.8 and 0.9 for the three sources (average of 4 repeated experiments for the same source ± standard deviation) using 10 points using the *reference instrument concentration*:

	Incense (μg/m^3)			$(NH_4)_2SO_4$ (μg/m^3)			Toast (μg/m^3)		
R^2	***0.7***	***0.8***	***0.9***	***0.7***	***0.8***	***0.9***	***0.7***	***0.8***	***0.9***
ID1[a]	2.20±0.59	2.71±0.87	8.48±4.04	2.60±0.35	3.62±0.34	8.47±1.02	3.50±0.43	4.02±0.63	8.75±1.93
ID2[c]	2.78±0.69	3.69±1.12	5.74±2.12	3.26±0.84	3.87±1.03	4.94±1.62	4.32±0.38[d]	4.13±0.53[d]	5.06±0.72[d]
ID3[c]	2.16±0.46	2.66±0.52	4.03±1.08	3.53±0.77[d]	4.03±0.64[d]	5.02±0.79[d]	2.67±0.93[d]	3.83±1.80[d]	4.01±1.16[d]
ID4[b]	3.13±1.50[d]	3.35±1.86[d]	5.50±2.34[d]	4.12±0.49	4.73±1.05	5.90±0.70	2.85±1.01	3.69±1.18	5.75±1.04
ID5[c]	2.85±1.49[d]	3.81±1.72[d]	4.50±1.28[d]	3.82±0.64	4.70±1.66	6.55±1.30	4.01±1.04	4.70±1.19	7.19±2.80
BS1[b]	2.28±0.83[d]	2.30±0.42[d]	4.43±2.51[d]	8.72±4.21[d]	12.75±3.30[d]	13.67±3.72[d]	7.75±2.62[d]	10.33±4.42[d]	13.00±6.35[d]
BS2[c]	13.90±7.60[d]	15.57±8.30[d]	24.05±9.18[d]	6.36±2.34[d]	9.38±1.64[d]	11.42±2.41[d]	10.75±5.33[d]	12.35±5.44[d]	16.93±4.35[d]
BS3[b]	3.15±1.01[d]	4.41±1.42[d]	6.12±2.27[d]	4.30±1.46	4.51±1.42	4.58±1.39	4.02±0.91	5.29±1.45	6.30±1.41

Footnote a: only one unit was tested in this study over four replicate experiments. Therefore, the values represent the average of four experiments.

Footnote b: Two units were tested in this study over four replicate experiments. Values represent the average of eight (two x four) experiments.

Footnote c: Three units were tested in this study over four replicate experiments. Values represent the average of twelve (three x four) experiments.

Footnote d: For at least one experiment, the running R^2 is always greater than 0.95. These values are excluded from the average.

Table 4.4: Limit of Quantification using threshold of R^2 = 0.7, 0.8 and 0.9 for the three sources (average of 4 repeated experiments for the same source ± standard deviation) using 10 points using the *sensor concentration*:

	Incense (μg/m³)			*$(NH_4)_2SO_4$ (μg/m³)*			*Toast (μg/m³)*			*LOD*
R^2	***0.7***	***0.8***	***0.9***	***0.7***	***0.8***	***0.9***	***0.7***	***0.8***	***0.9***	
ID1$_a$	0.75±0.55	1.35±1.00	2.23±1.51	1.35±0.48	1.72±0.57	2.22±2.31	2.05±0.54	2.12±0.55	8.87±1.58	0.41
ID2$_c$	1.42±0.60	2.18±0.80	3.74±1.71	1.55±0.43	2.25±0.23	4.26±1.77	2.21±0.56$_d$	2.52±0.54$_d$	4.95±1.13$_d$	0.78
ID3$_c$	0.89±0.29	1.37±0.73	2.71±1.84	1.57±0.75$_d$	2.03±0.94$_d$	3.49±2.73$_d$	1.02±0.97$_d$	1.30±1.23$_d$	2.33±1.97$_d$	1.61
ID4$_b$	1.08±0.79$_d$	1.46±0.85$_d$	3.00±2.90$_d$	0.81±0.26	1.01±0.30	1.75±0.58	1.62±0.58	1.92±0.57	4.05±1.63	0.14
ID5$_c$	2.70±2.42$_d$	3.46±2.66$_d$	4.90±2.79$_d$	1.32±0.96	1.76±1.06	2.95±2.25	3.91±1.22	4.50±1.89	7.16±2.43	1.12
BS1$_b$	6.00±2.00$_d$	7.46±3.03$_d$	7.74±2.43$_d$	5.80±2.28$_d$	8.13±2.45$_d$	9.75±2.09$_d$	7.08±3.29$_d$	9.60±3.78$_d$	11.9±4.72$_d$	4.01
BS2$_c$	7.71±1.72$_d$	9.30±2.23$_d$	11.51±2.37$_d$	7.00±2.94$_d$	8.16±2.56$_d$	13.33±5.06$_d$	16.71±4.15$_d$	19.75±6.27$_d$	24.12±8.14$_d$	2.03
BS3$_b$	1.19±0.41$_d$	1.68±0.57$_d$	2.57±0.89$_d$	0.84±0.38	1.08±0.49	1.98±1.33	0.76±0.62	1.20±0.99	2.57±1.79	1.42

LOD was calculated from LOD = $M_{blank} + 3\sigma_{blank}$ under "zero air" test (CPC number < 200 #/cm^3), where M_{blank} is the average mass concentration for a given sensor under "zero air" conditions and σ_{blank} is the standard deviation for these conditions

Footnote a: only one unit was tested in this study over four replicate experiments. Therefore, the values represent the average of four experiments.

Footnote b: Two units were tested in this study over four replicate experiments. Values represent the average of eight (two x four) experiments.

Footnote c: Three units were tested in this study over four replicate experiments. Values represent the average of twelve (three x four) experiments.

Footnote d: For at least one experiment, the running R^2 is always greater than 0.95. These values are excluded from the average.

Table 4.3 shows the concentration as recorded by the reference instruments at which the running R^2 falls below each of three different thresholds (R^2=0.7, 0.8, 0.9) for each of three different sources, for each device tested. Table 4 gives the same information, but uses the sensor concentration as the reference. In other words, Table 4.3 provides values of LOQ using the actual concentration, while Table 4.4 provides values using the concentration that the sensor thinks is the actual concentration; these values differ because we did not conduct any calibrations of the sensors for this work.

To investigate whether the degradation to the running R^2 is influenced by the evolution of the particle size distribution in our chamber, we generated time series of the mode diameters and geometric standard deviations for each replicate of each source (Figures 4.22-4.27). From these figures, there appears to be no evidence that an evolving particle size distribution influenced our observations, so the changes in running R^2 appear to be related only to concentration decay.

We next present the results from the experimental investigation of the upper bound of the functional range by looking at the "running slope" of the relationship between one low-cost device response and the reference instrument response, as shown in Figure 4.5. A "perfect" sensor would have a slope of exactly 1 regardless of concentration. We expected that for each sensor there was a certain concentration at which this slope would begin to deviate from one, namely to move toward zero at which point the signal from the sensor can be considered saturated.

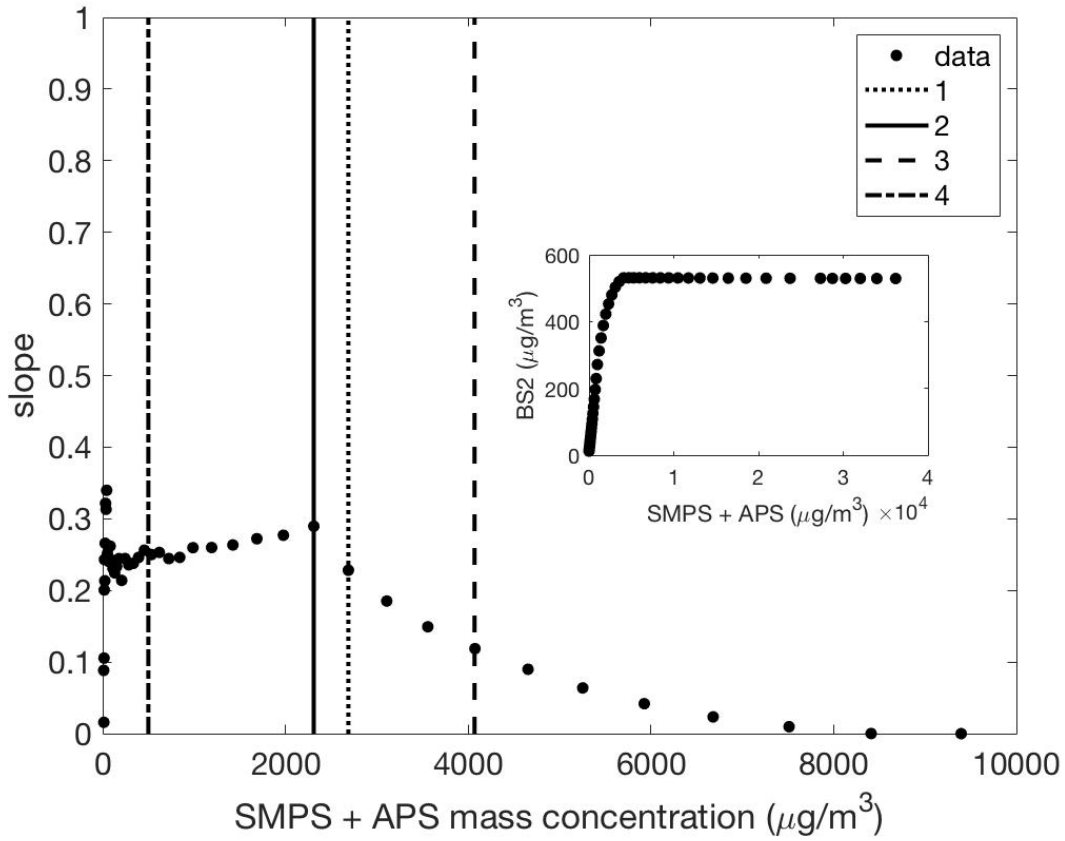

Figure 4.5: BS2 response during one decay test using toast as the PM source

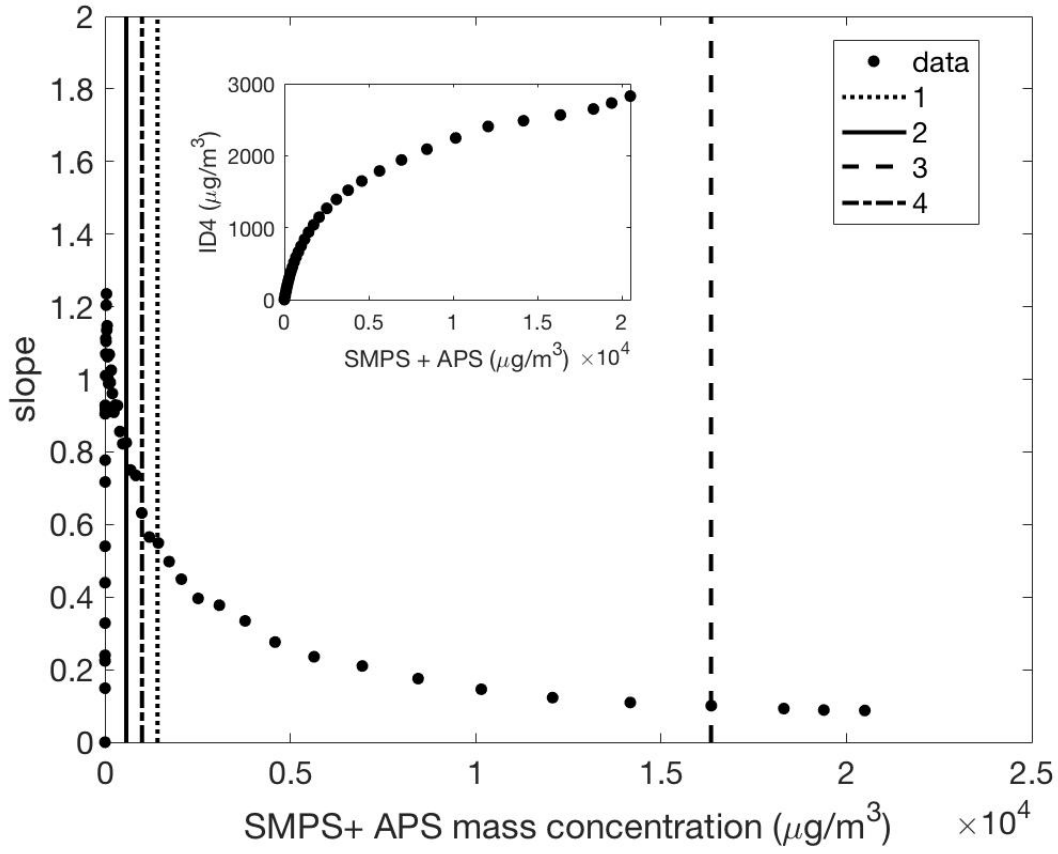

Figure 4.6: ID4 response during one decay test using incense as the PM source

We considered four definitions for the UB of the functional range as shown in Figure 4.5 and subsequent figures:

1) the concentration at which the derivative of the slope exceeds a certain threshold (e.g. 0.05) (the point at which the response deviates from linearity),

2) the concentration at which the slope continues to decrease for 5 consecutive points (the point at which the response deviates from linearity),

3) the concentration at which the slope is in the range of 0 ± 0.1 (the point at which sensor response is saturated), and

4) the manufacturer-reported maximum operating concentration.

In Figure 4.5, we see the running slope is approximately stable at 0.25 between 100-2,300 μg/m^3. We see clearly that at 2300 μg/m^3 the relationship ceases to be near linear and we see a sharp drop in the slope (definitions 1 and 2 of UB). The sensor response starts to become saturated at approximately 4,000 μg/m^3 (definition 3 of UB). It is worth noting that each of these definitions of the UB is greater than that reported by the manufacturer for this particular sensor. While the magnitude of the response of this particular sensor is approximately 25% of the reference instrument response, a simple linear calibration could convert this response to an accurate reading over a substantial range. On the other hand, Figure 6 shows another typical pattern of response (ID4). In this case the running slope is nearly continuously changing between very low concentrations and the point at which the signal becomes saturated, which does not occur until approximately 15,000 μg/m^3.

Table 4.5 shows the UB for each sensor tested, defined as the reference instrument mass concentration when each of the four definitions of UB is satisfied, with the corresponding sensor-reported mass concentration shown in parentheses. As is evident in Table 4.5, Definition 1 gave greater concentrations than Definition 2 for most devices. Except for BS2 and BS3, all devices deviated from linearity below 1000 μg/m^3. The saturation point for all sensors was greater than 10,000 μg/m^3 except for BS2, and these concentrations were all greater than the manufacturer maximum range. In Table 4.5, the concentration for toast particles were generally higher than the other sources for all sensors. This suggests that the sensors' functional ranges may behave differently for distinct particle sources, but a complete analysis of particle composition effects is outside the scope of this work.

Table 4.5: Four definitions of upper detection limit using incense as the PM source. (concentrations are given as “reference instrument mass concentration" (sensor mass concentration))

I: incense, T: Toast, A: Ammonium sulfate

		1: |dslope| > 0.05 (deviation from linearity)	**2: five consecutive decreasing slopes (deviation from linearity)**	**3: saturation point (slope within 0 ± 0.1) before this point**	**4:Manuf. reported maximum range**
ID1 [a]	I	2063±53(1340±14)	440±47(339±12)	16347±124(3894±124)	N/A
	T	3579±538(2741±223)	2689±312(1559±23)	28723±552(2908±424)	
	A	2310±248(910±162)	488±142(321±84)	slope always <0.1	
ID2 [c]	I	1251±198(1369±132)	441±127(366±62)	16394±328(4821±437)	≥ 1000
	T	2723±362(1623±182)	2639±634(1352±142)	14923±739(6379±274)	
	A	921± 268 (602±172)	472±157 (482±66)	slope always <0.1	
ID3 [c]	I	703±13(584±42)	1021±127(831±115)	11562±263(3844±153)	N/A
	T	3448±166(1321±98)	7429±426(4722±163)	32041±163(2548±134)	
	A	1191±68 (634±20)	921 ± 37 (342±48)	slope always <0.1	
ID4 [b]	I	1972±49(982±34)	711±82(527±52)	16923±102(2713±153)	≥ 1000
	T	4535±142(2012±132)	2421±105(1259±85)	21923±268(4282±183)	
	A	852±152(624±78)	592±72 (494±79)	8921± 276(1723±184)	
ID5 [c]	I	2258±82 (2713±731)	362±15 (620±47)	19263±1243 (6342±1356)	≥ 1000
	T	5283±73(2934±92)	1862±36 (1376±53)	17230±537(4326±273)	
	A	856± 72(921±74)	305±32 (437±33)	slope always <0.1	
BS1 [b]	I	1441±15(2002±14)	496±102(732±93)	2662± 82(2007±8)	2000
	T	1626±178(2001±2)	1021±148(723±39)	3062±83(2012±5)	
	A	1527±93(1612±94)	368±155(605±88)	5016±173(2006±3)	
BS2 [c]	I	1416±219(201±54)	2671±193(393±107)	4821± 52(522± 8)	500
	T	2401±172(300±52)	2691±152(437±47)	4611±225(517±7)	
	A	1097±681(163±102)	1253±98(152±58)	4392±135(522±2)	
BS3 [b]	I	3025±215(1715±43)	2202±291(1521±236)	18236±1423(7001±2332)	≥ 1000
	T	4501±209(1621±231)	4301±992(1736±342)	31356±7091(13302±3732)	
	A	1302±167(492±59)	789±193(281±74)	slope always <0.1	

Footnote a: only one unit was tested in this study over four replicate experiments.
Therefore, the values represent the average of four experiments.
Footnote b: Two units were tested in this study over four replicate experiments.
Values represent the average of eight (two x four) experiments.
Footnote c: Three units were tested in this study over four replicate experiments.
Values represent the average of twelve (three x four) experiments.

4.4 Conclusions and future work

In order to establish the functional range of commercially available low-cost particle sensors, we tested five types of commercial integrated devices (ID) and three types of "bare" low-cost PM sensors (BS) by exposing them to a range of concentrations of particles generated by three different sources. The following are the conclusions of these experiments:

- The time interval over which sensor output is averaged has a profound effect on the apparent limit of quantification at times less than approximately ten minutes. The apparent limit of quantification approached 70 $\mu g/m^3$ at averaging times less than five minutes, suggesting these commercially available devices are not able to give reliable information at such time scales. It also suggest that ten minutes may be the shortest time scale at which control decisions in buildings might be made based on signals from these low-cost particle sensors.
- We propose a definition of limit of quantification as the concentration at which the coefficient of determination between a given sensor's output and that of a reference instrument during a decay test falls below 0.8. Experiments show that this lower bound ranges from approximately 3-15 $\mu g/m^3$ among sensors tested for ten-minute sampling times. For those sensors have lower bound of limit of quantification less than 5 can be potentially used in a clean indoor environments (e.g., typical office building or non-kitchen locations in residences).
- We also proposed three definitions of the upper bound of the functional range based on the slope of a linear regression between the sensors and the reference instrument.

- Most experimentally derived definitions were greater than manufacturer-reported maximums for the sensors tested.
- The two definitions for sensor output deviation from linearity agreed reasonably well in most cases and were approximately 300-3,000 $\mu g/m^3$ for the sensors tested.
- Sensor responses became saturated at approximately 3,000-30,000 $\mu g/m^3$.

This work was done on a subset of the commercially available sensors and integrated devices and may or may not be representative of the entire market, although care was taken to select sensors that have generated interest in the indoor air community. In general, most of the tested sensors show low concentrations for their lower bound (roughly 3 $\mu g/m^3$), which indicates that these sensors can effectively detect the low particle concentration expected for indoor environments. However, there is a need for technical progress in manufacturing advanced low-cost PM sensors to be able to reliably conduct measurements in the cleanest indoor environments (<3 $\mu g/m^3$).

Furthermore, results from this chapter indicate that the sensors may respond differently to different PM sources. In Chapter 5, we will use the same PM source including $(NH_4)_2SO_4$, incense and toast as used in this chapter, and will add other PM sources such as Arizona Test Dust and Polystyrene Latex spheres to study a variety of different particle compositions; moreover, we will also explore the influence of particle size, which is inherently different for many of the sources in Chapters 3 and 4.

4.5 Additional Tables and Figures

Table 4.6: Bare sensor information

Sensor	Signal-to-Output Conversion Process	Intended Indoor Environment	Features
BS1	Light → photodiode → volt signal → photoelectric converter→ 32-bytes → MCU(4-bytes) → PM mass density	Air conditioners, air quality monitors, environmental monitoring, air cleaners, air quality detectors	20,000 hours of stable operation and continuous use
BS2	Light → photodiode → volt signal → amplified → volt signal → photoelectric converter → 32-bytes → MCU → PM mass density	Detecting dust in air, air purifier, air conditioner, air monitors, and distinguishing between smoke and house dust	
BS3	Light → phototransistor → volt signal → amplified → photoelectric converter → 32-bytes → MCU(12-bytes) → number concentrations → PM mass density	Can be in instruments related to the concentration of suspended particles in the air or other environmental improvement equipment	Six-sided shielding using an anti-interference material.

Table 4.7: Integrated device information

Sensor	Communication	Features
ID1	Cellular, WiFi, and Bluetooth, cloud-based storage.	Also provides CO_2, CH_2O, VOCs, temperature, humidity, and pressure.
ID2	Cellular networks, WiFi, Bluetooth, serial connector.	Weather resistant, casts to crowd-sourced mapping utility
ID3	Internal storage, serial connector.	
ID4	Serial connector.	
ID5	SD card, serial connector, and WiFi.	Also provides temperature, humidity, and pressure.

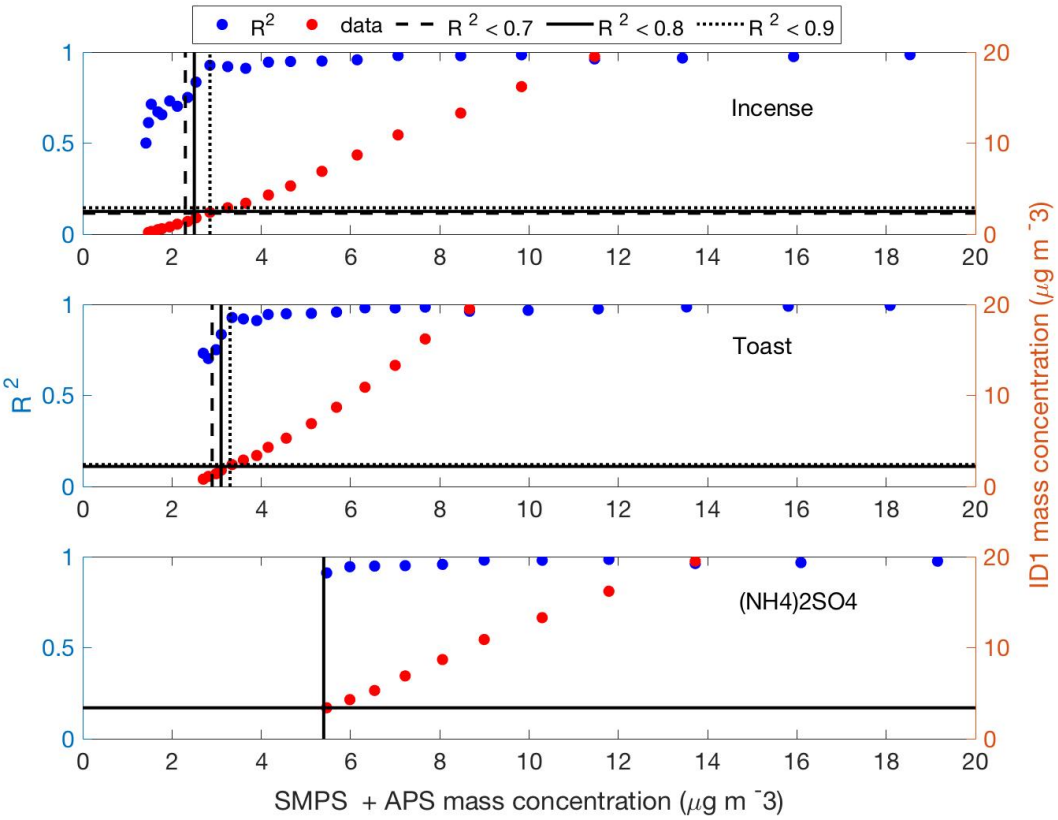

Figure 4.7: Running R^2 as a function of reference instrument concentration as measured for ID1.

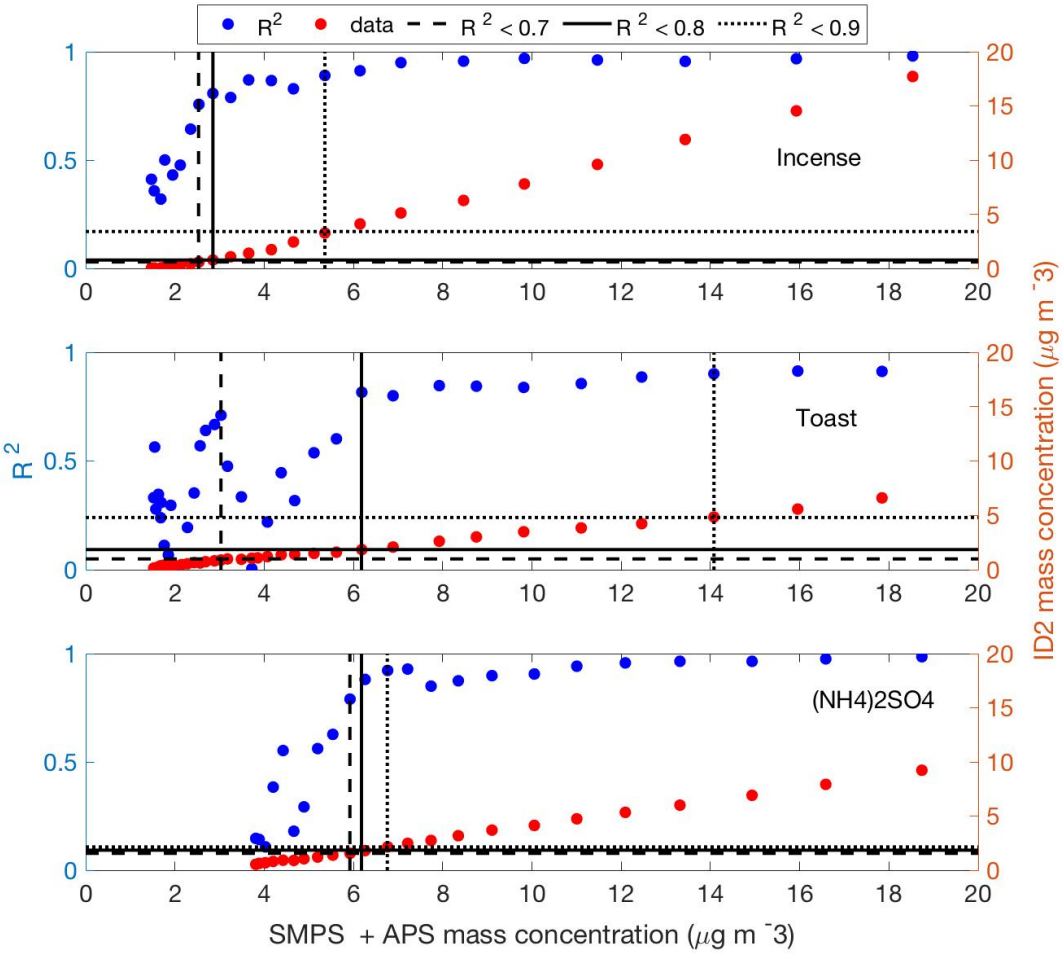

Figure 4.8: Running R^2 as a function of reference instrument concentration as measured for ID2.

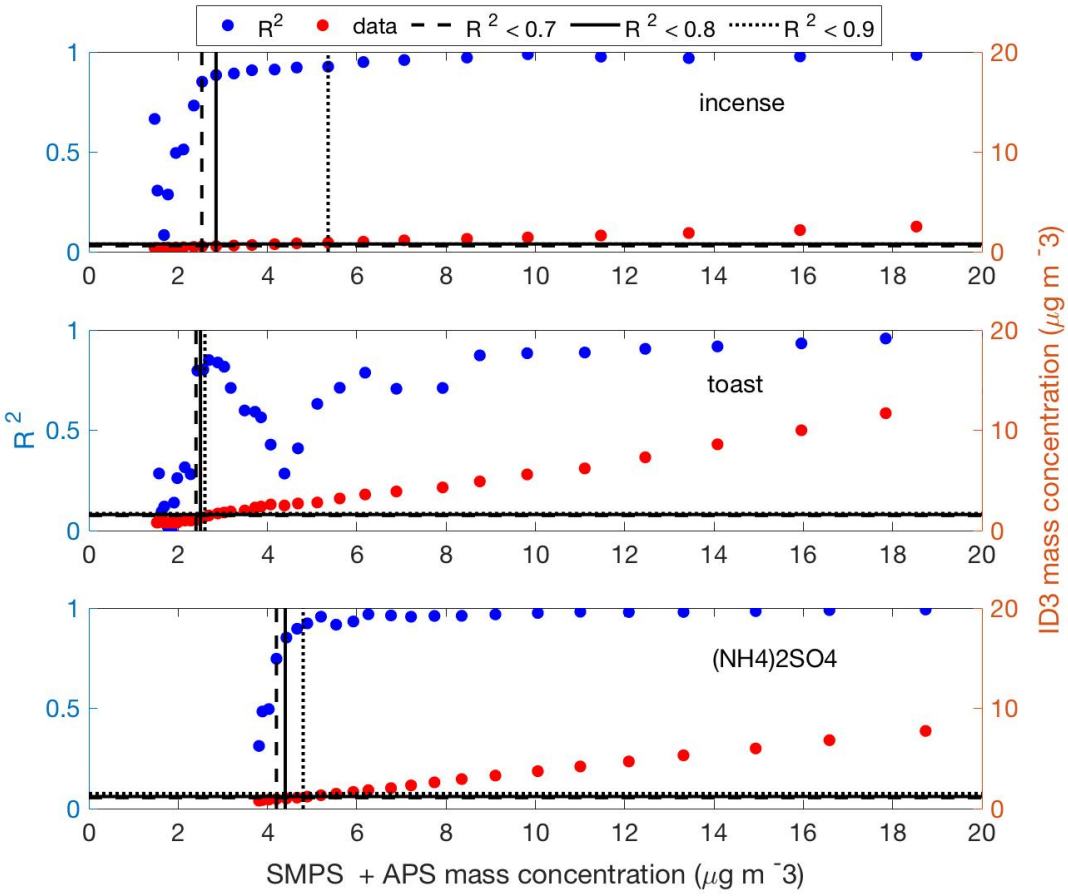

Figure 4.9: Running R^2 as a function of reference instrument concentration as measured for ID3.

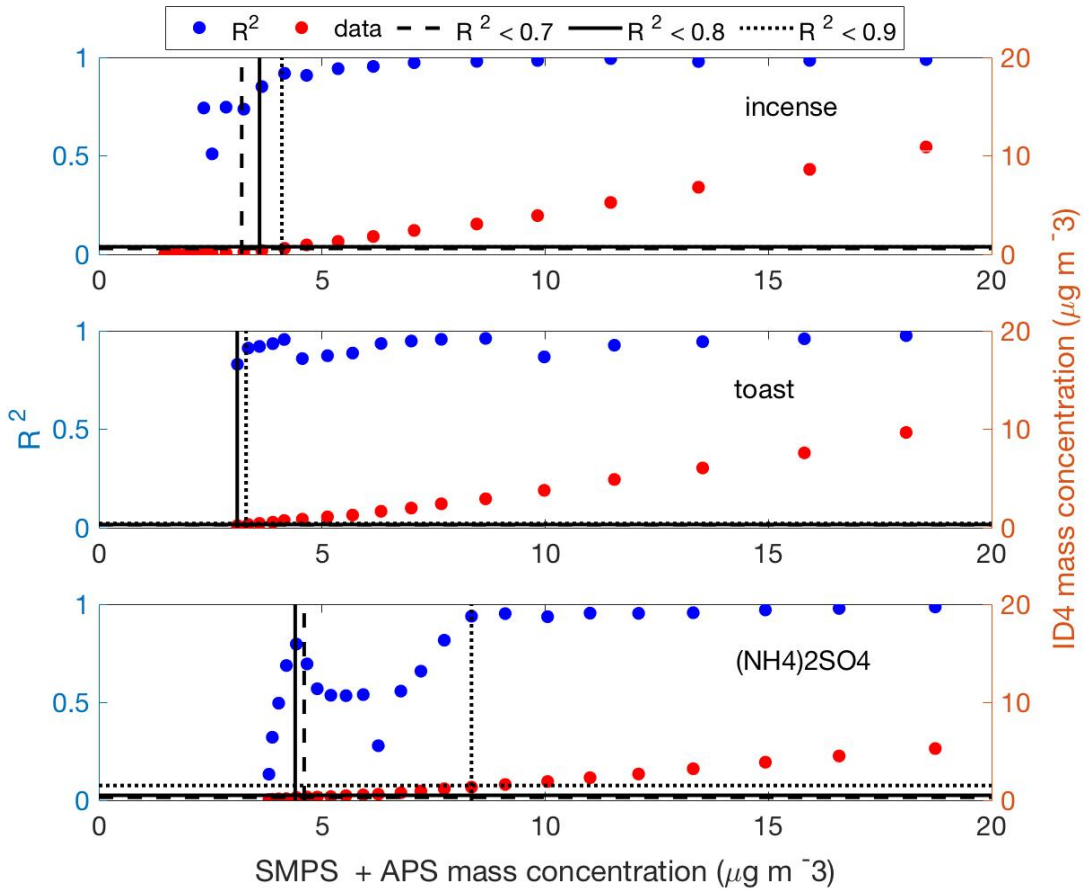

Figure 4.10: Running R^2 as a function of reference instrument concentration as measured for ID4.

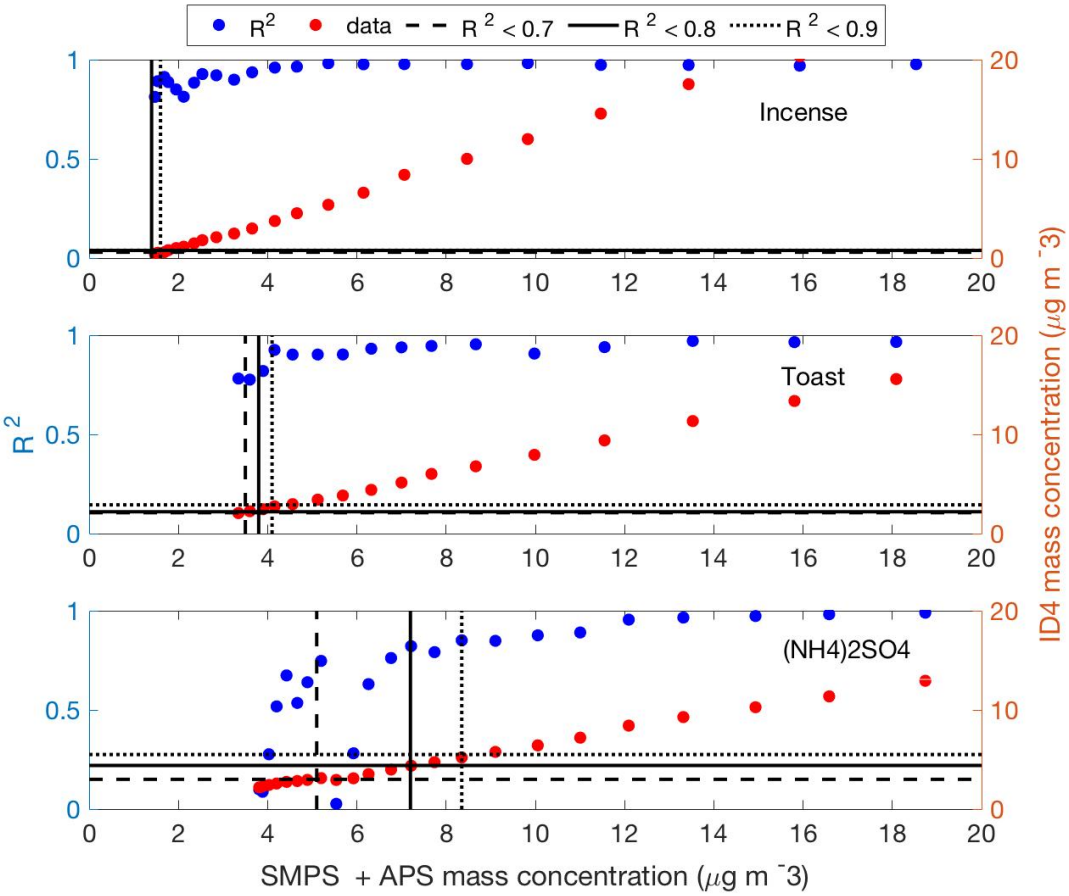

Figure 4.11: Running R^2 as a function of reference instrument concentration as measured for ID5.

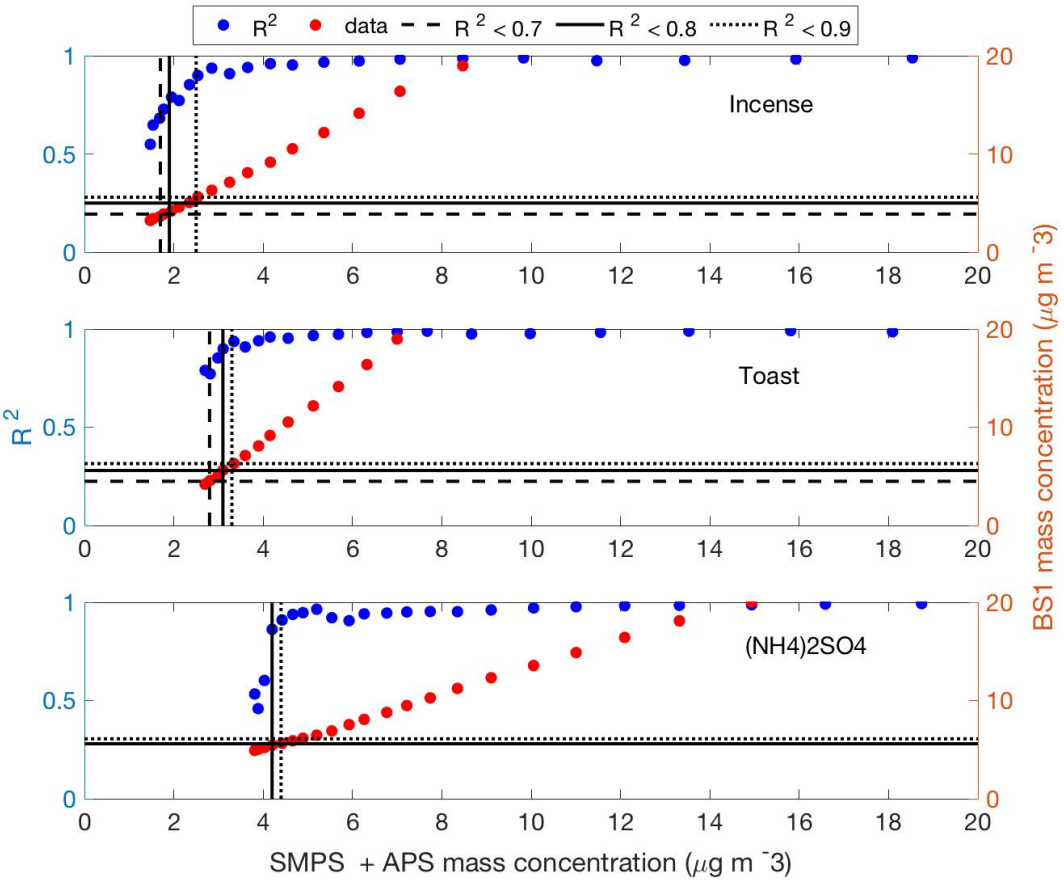

Figure 4.12: Running R^2 as a function of reference instrument concentration as measured for BS1.

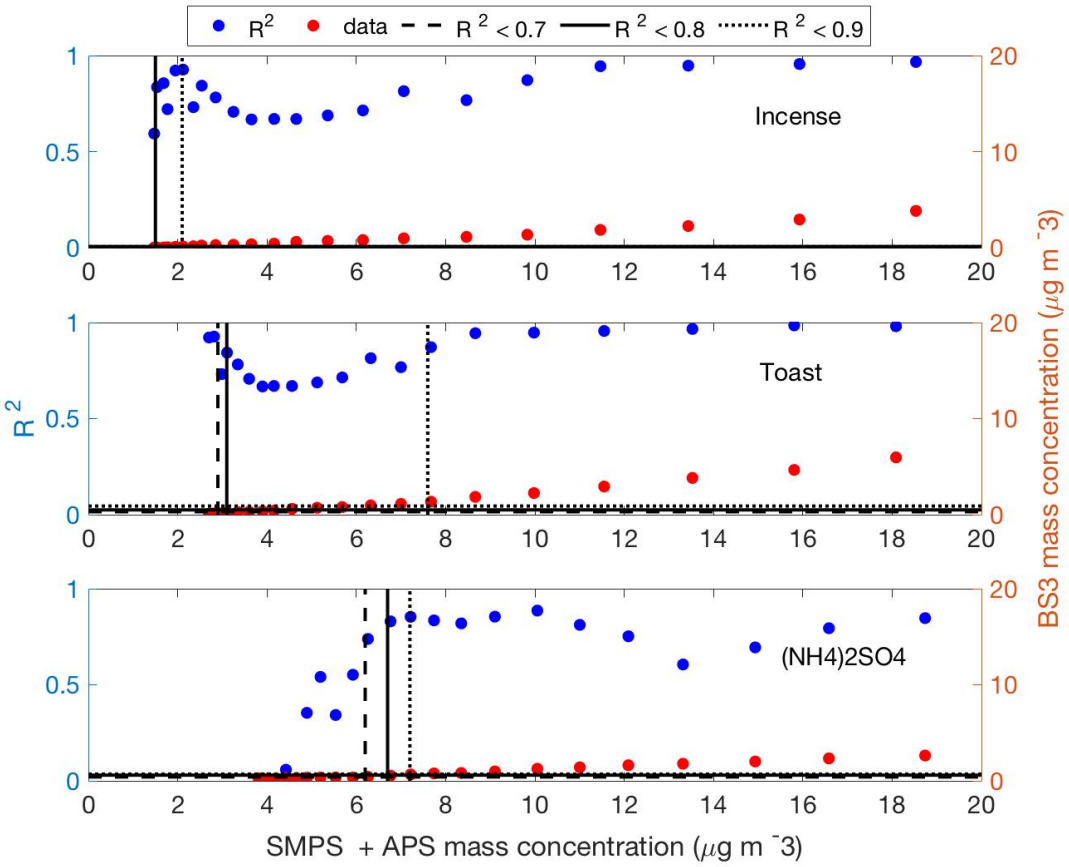

Figure 4.13: Running R^2 as a function of reference instrument concentration as measured for BS3.

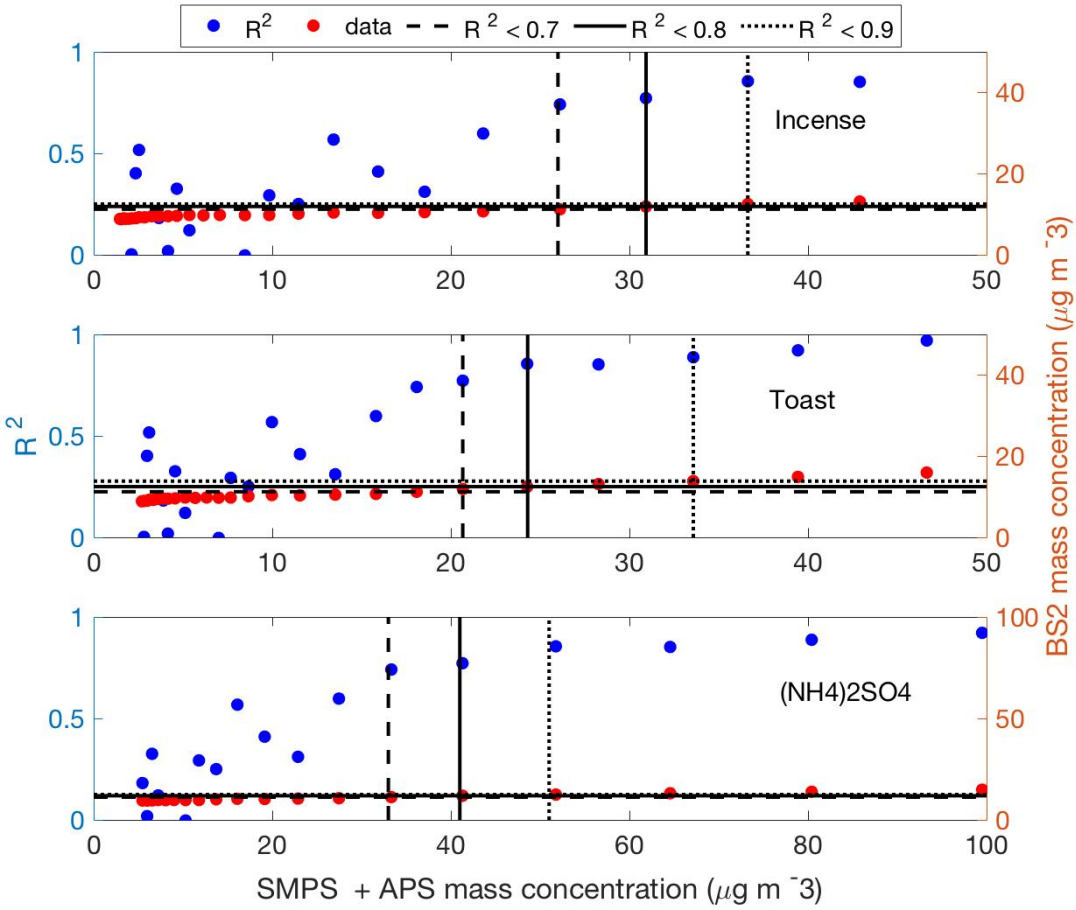

Figure 4.14: Running R^2 as a function of reference instrument concentration as measured for BS2.

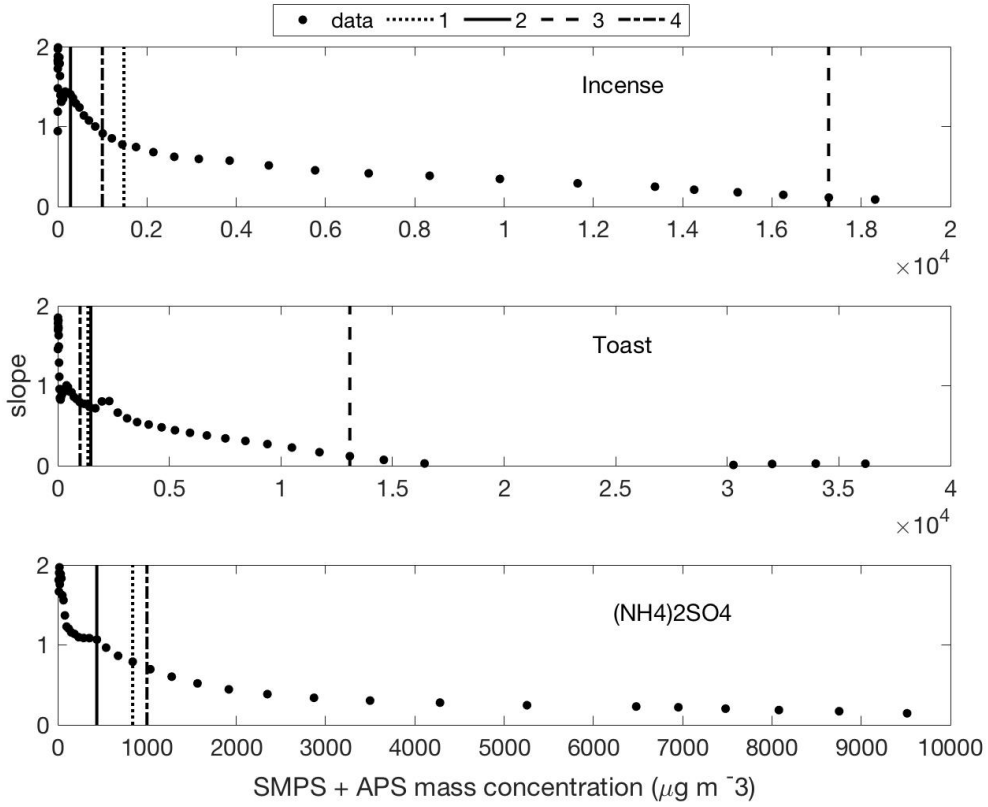

Figure 4.15: Running slope as a function of reference instrument concentration as measured for ID1.

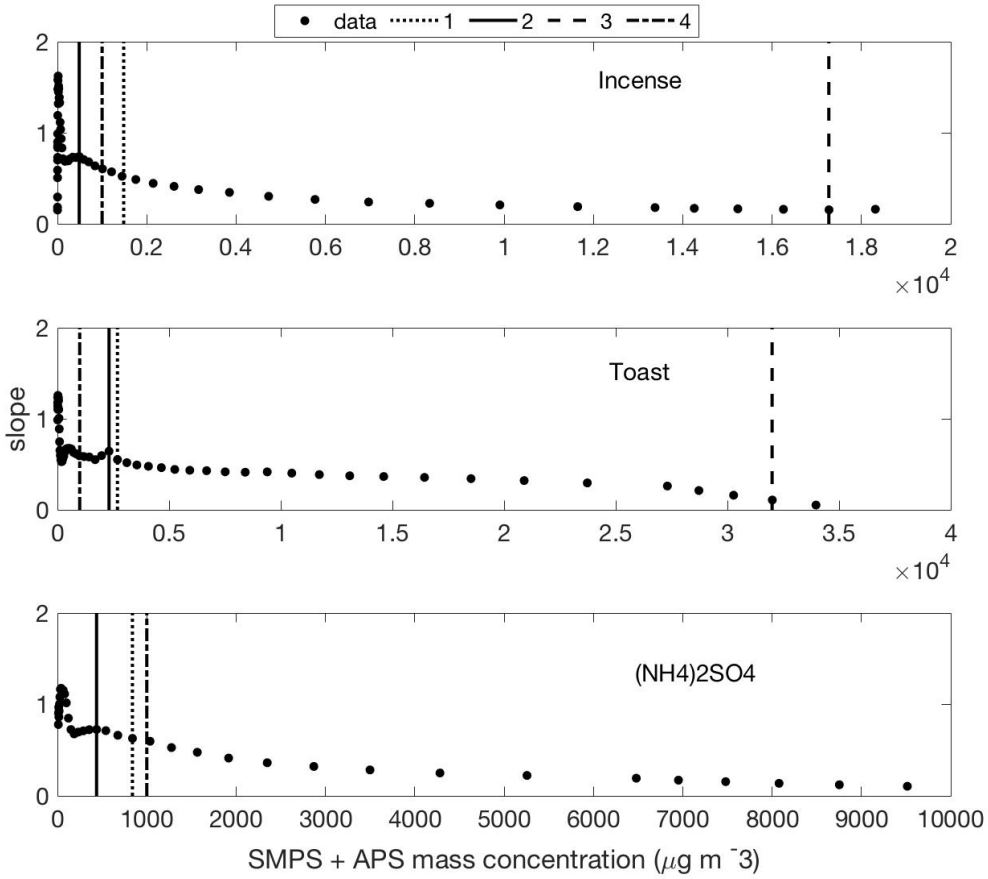

Figure 4.16: Running slope as a function of reference instrument concentration as measured for ID2.

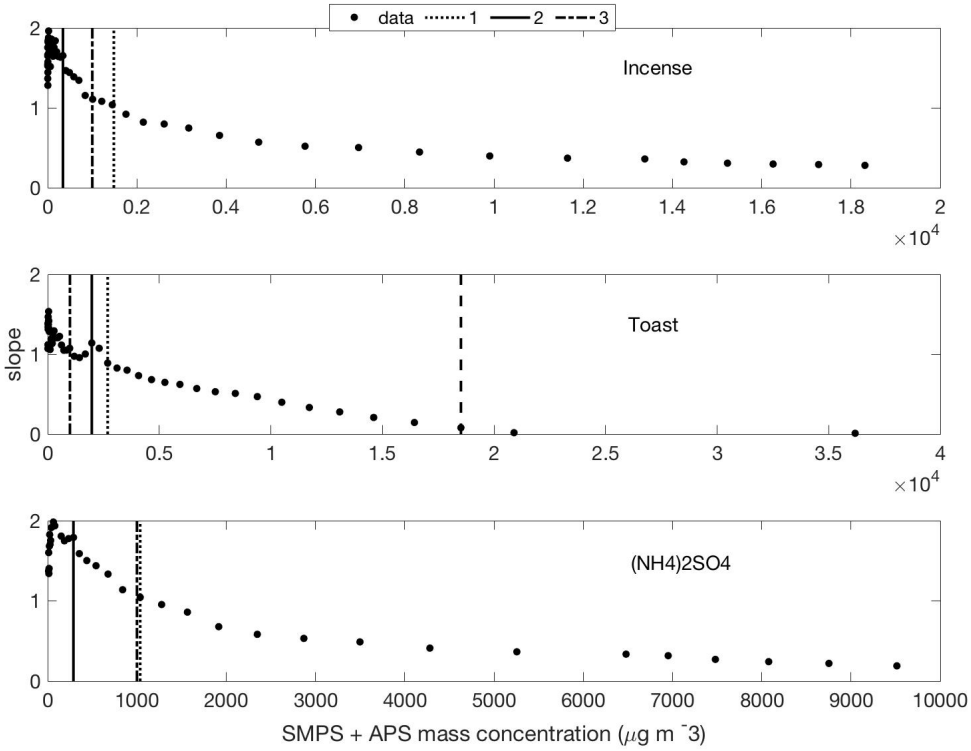

Figure 4.17: Running slope as a function of reference instrument concentration as measured for ID4.

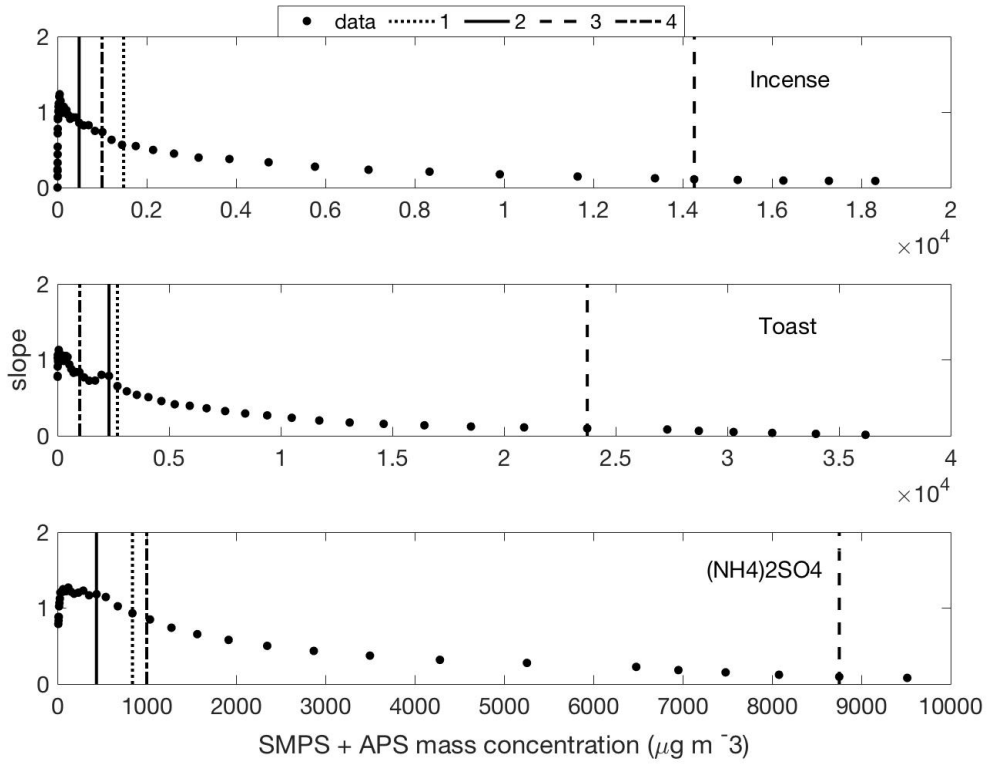

Figure 4.18: Running slope as a function of reference instrument concentration as measured for ID5.

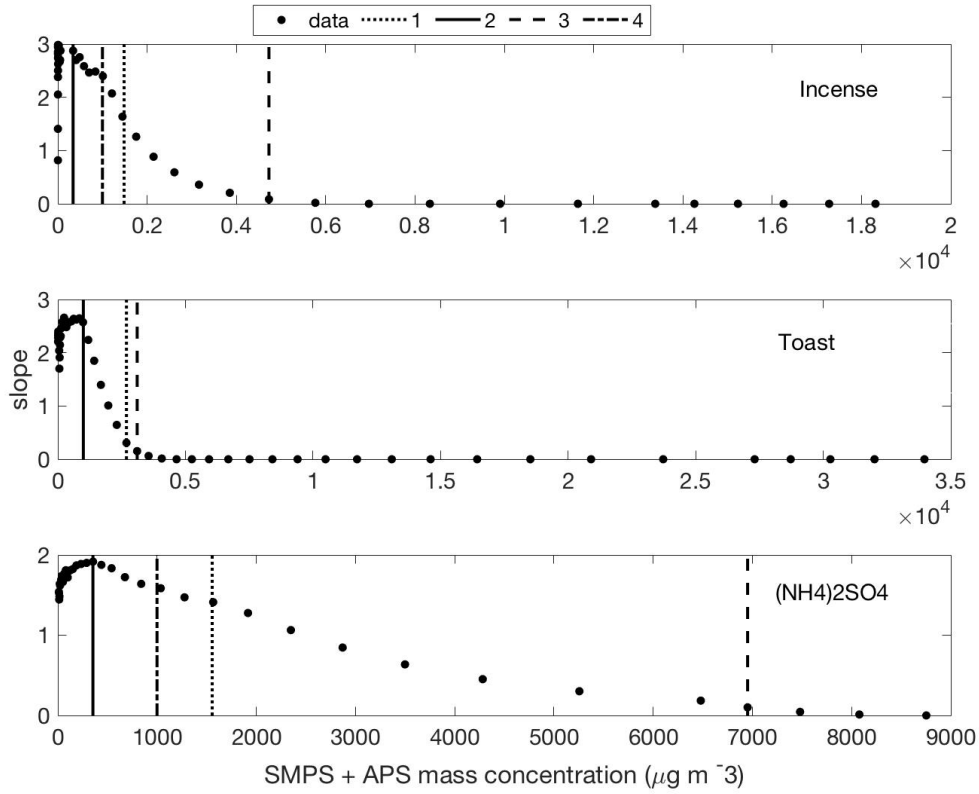

Figure 4.19: Running slope as a function of reference instrument concentration as measured for BS1.

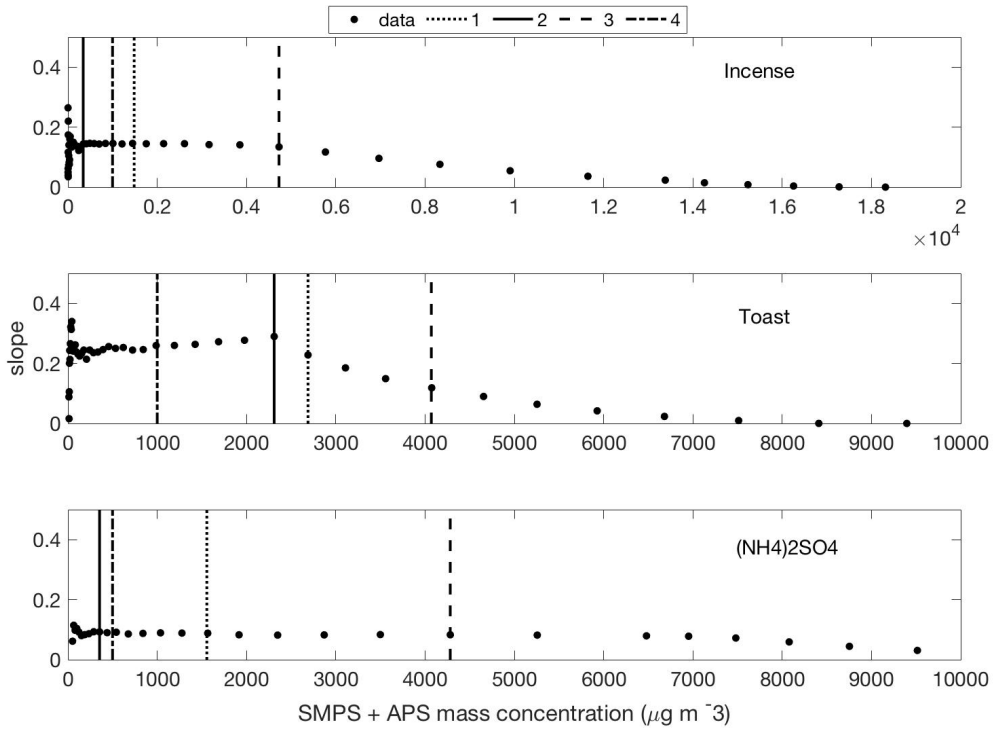

Figure 4.20: Running slope as a function of reference instrument concentration as measured for BS2.

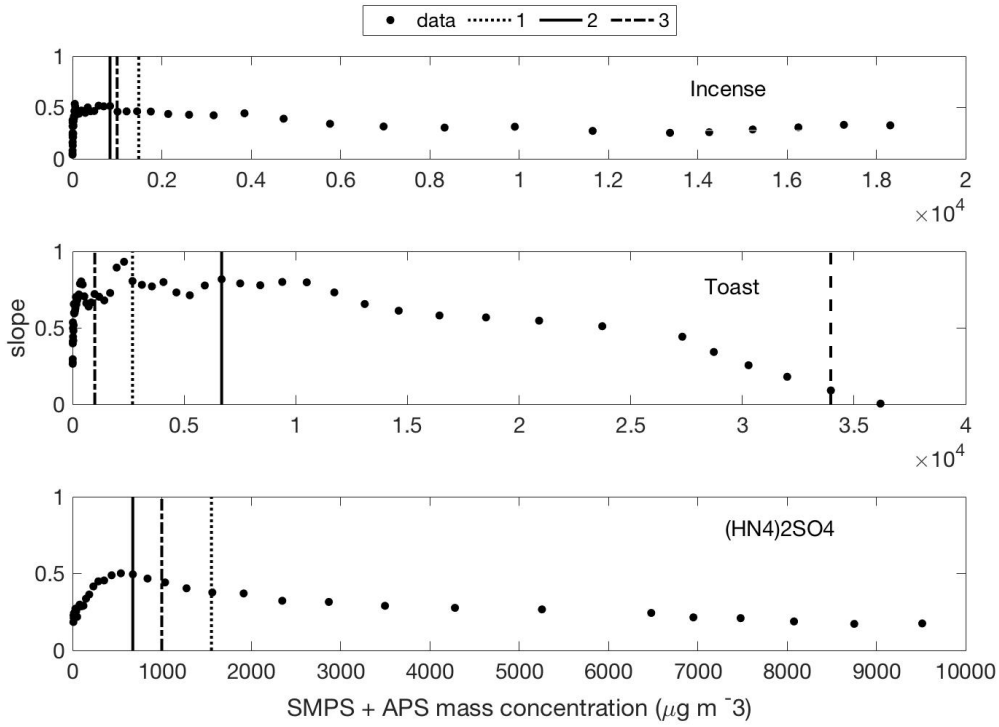

Figure 4.21: Running slope as a function of reference instrument concentration as measured for BS3.

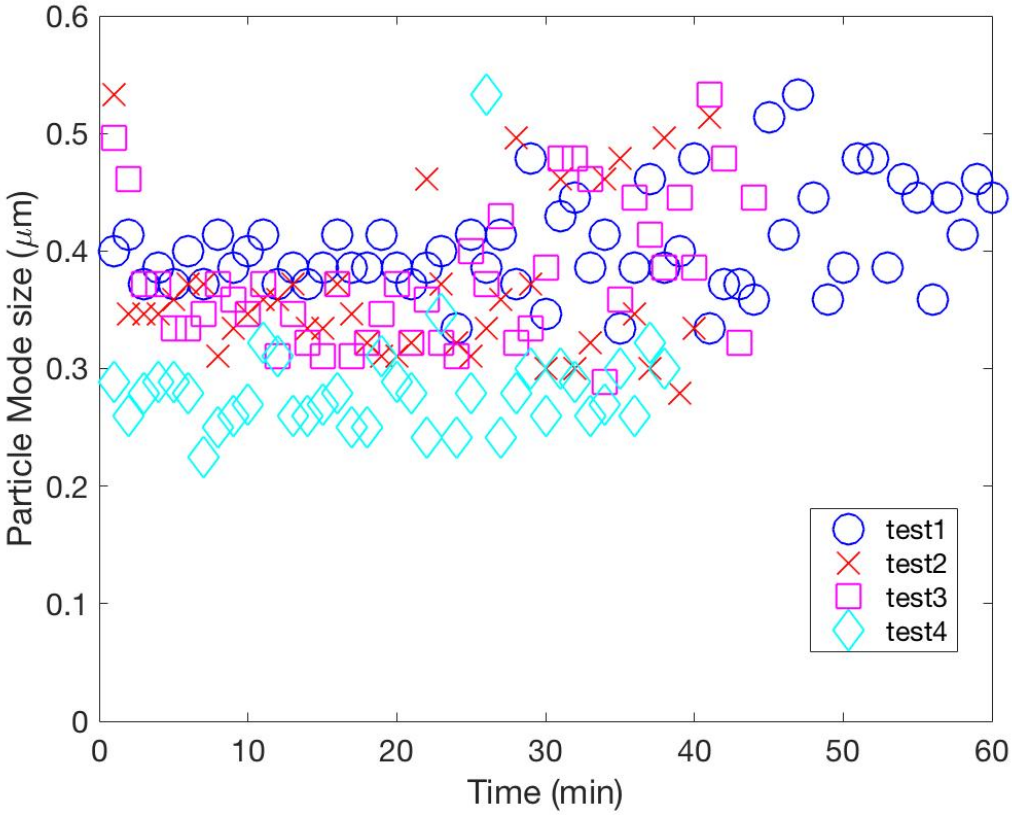

Figure 4.22: Mode size of particle during incense decay test (all 4 replicated tests)

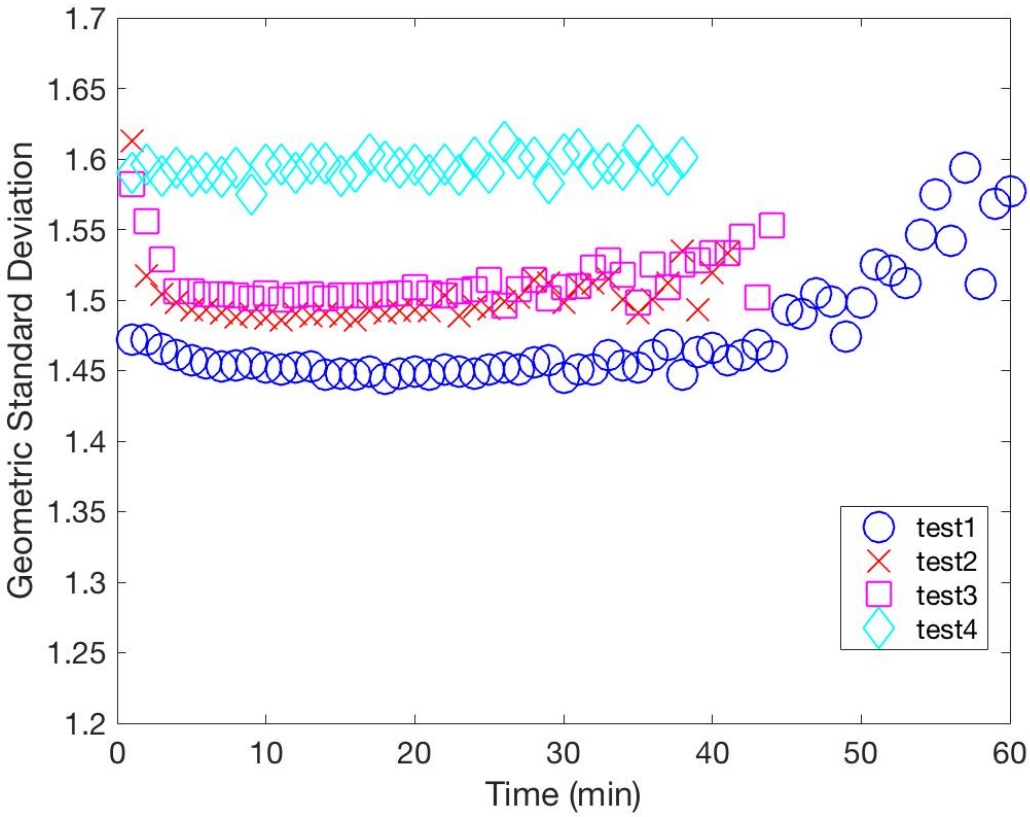

Figure 4.23: Geometric standard deviation of particle during incense decay test (all 4 replicated tests)

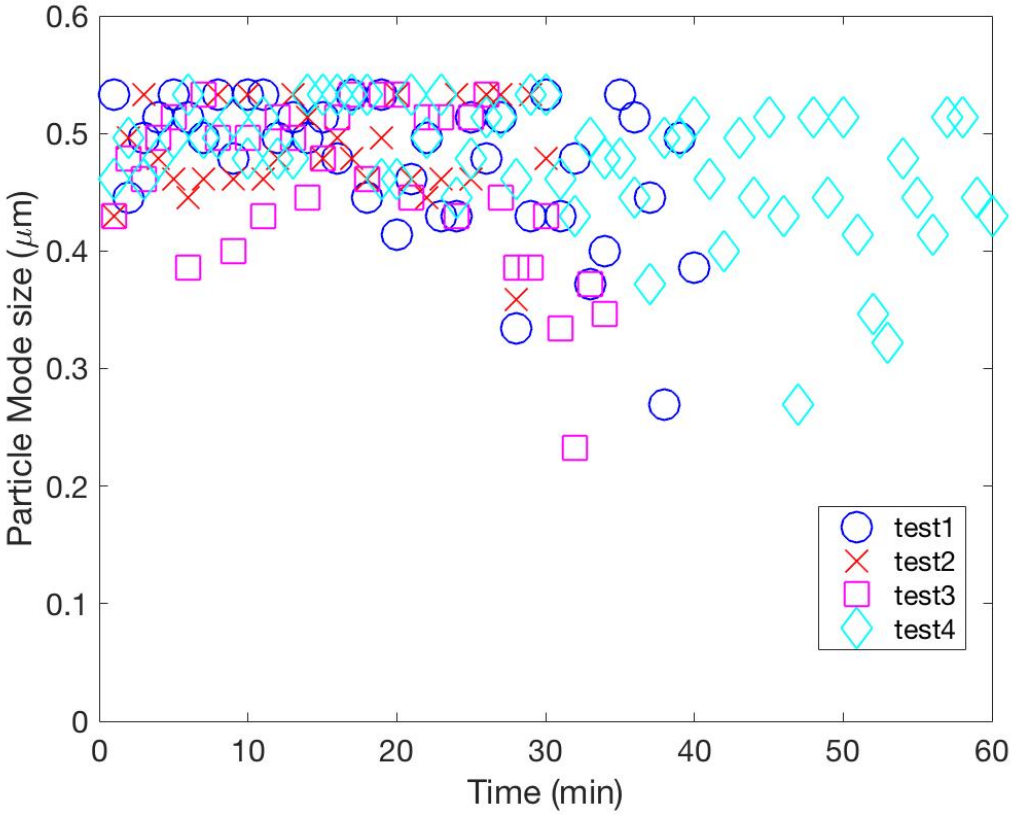

Figure 4.24: Mode size of particle during $(NH_4)_2SO_4$ decay test (all 4 replicated tests)

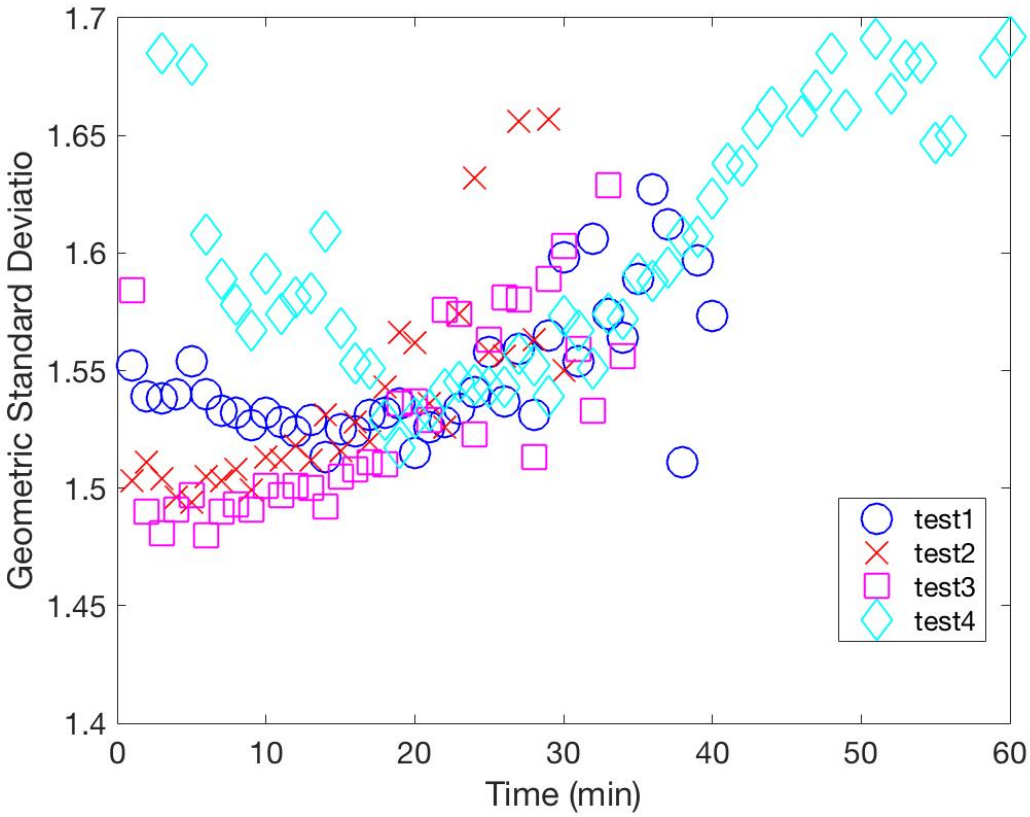

Figure 4.25: Geometric standard deviation of particle during $(NH_4)_2SO_4$ decay test (all 4 replicated tests)

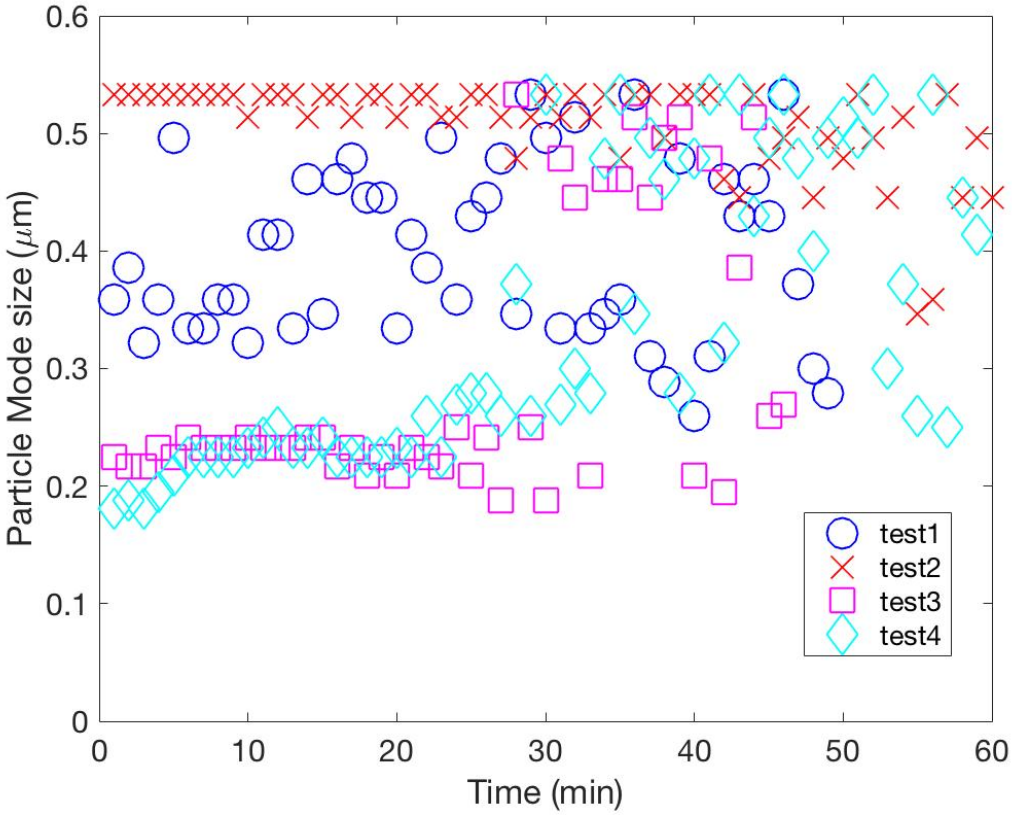

Figure 4.26: Mode size of particle during toast decay test (all 4 replicated tests)

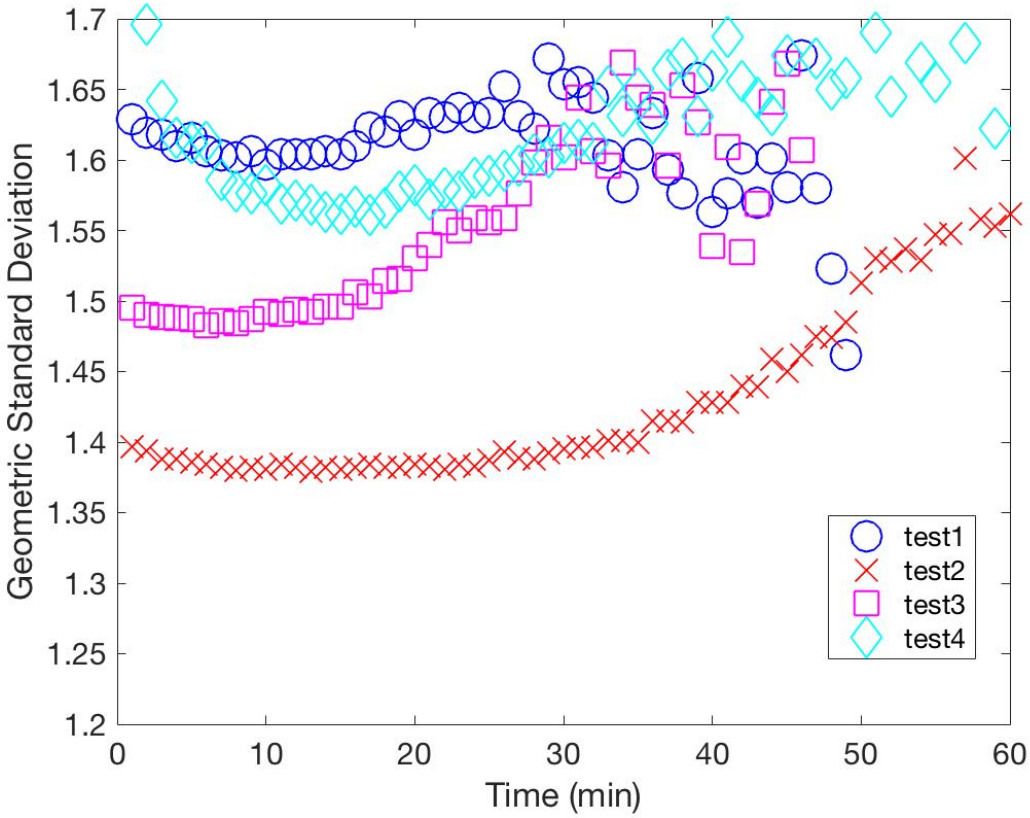

Figure 4.27: Geometric standard deviation of particle during toast decay test (all 4 replicated tests)

Simulation Results *(*Matthew Young conducted the simulation analysis)

In Figures 4.28 and 4.29 we show the results of the Monte Carlo analysis with 1,000 iterations (homes) simulated for each value of LOQ or UB. We see first in Figure B22 that according to this analysis, the effect of the upper bound on the deviation of the sensor-reported concentration from reality is minimal. For most sensors, the error was minimal-less than 10% in more than 95% of homes analyzed. Sensor ID3 is not shown because it exhibited a UB greater than our simulated range.

This suggests that the commercially available low-cost sensors analyzed in this work operate consistently at great enough concentrations for use in indoor environments. The definition of the sensor's UB was five consecutive decreasing slopes (deviation from linearity) averaged for each of the sources tested (incense, toast, ammonium sulfate).

The results are more varied in regards to the lower bound of the functional operating range, LOQ. The definition of the LOQ was the average concentration at which R^2 fell below 0.8 for each of the sources tested. For the worst-performing sensor we see that greater than 50% error is expected in more than 10% of homes according to this analysis.

In general, we find that the upper bound on the functional range results in minimal inaccuracy in exposure output, and the limitation on lower bound can result in as much as a 50% error in approximately 10% of U.S. homes. Therefore, all of the sensors tested likely have some utility for monitoring indoor PM exposure, although a subset will not provide accurate outputs in environments with lower PM concentrations.

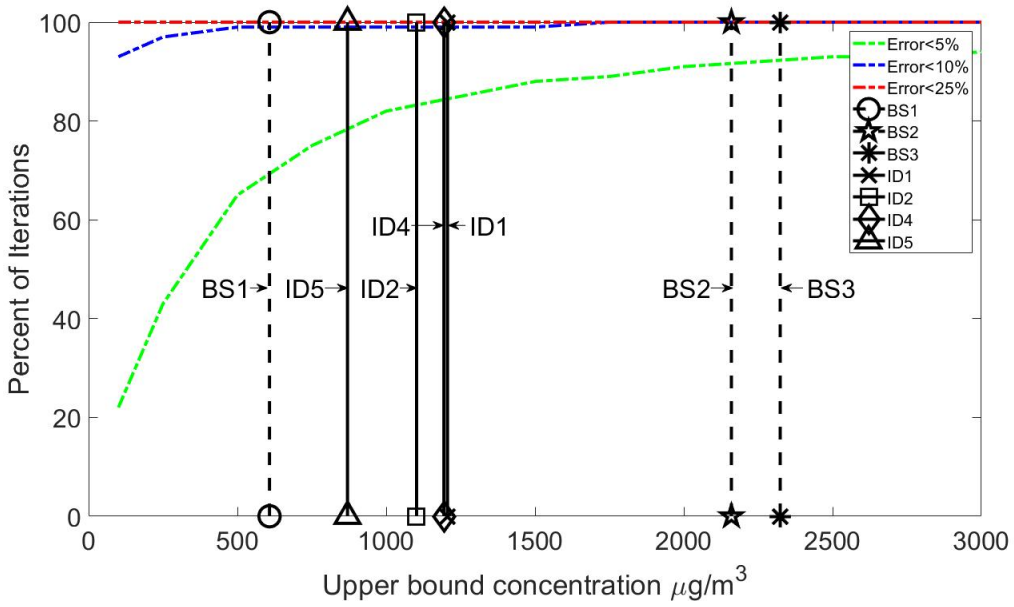

Figure 4.28: Percent of iterations (each iteration is one particular home) in which the exposure in a typical week as reported by a sensor with a particulate sensor saturation concentration exceeds each of three limits (5%, 10%, 25%). The sensor saturation concentrations for each sensor tested are also plotted. In this case sensor saturation concentration is defined as the average of the saturation concentration measured under exposure to three different sources. Sensor ID3 exhibited a sensor saturation concentration greater than our simulated range.

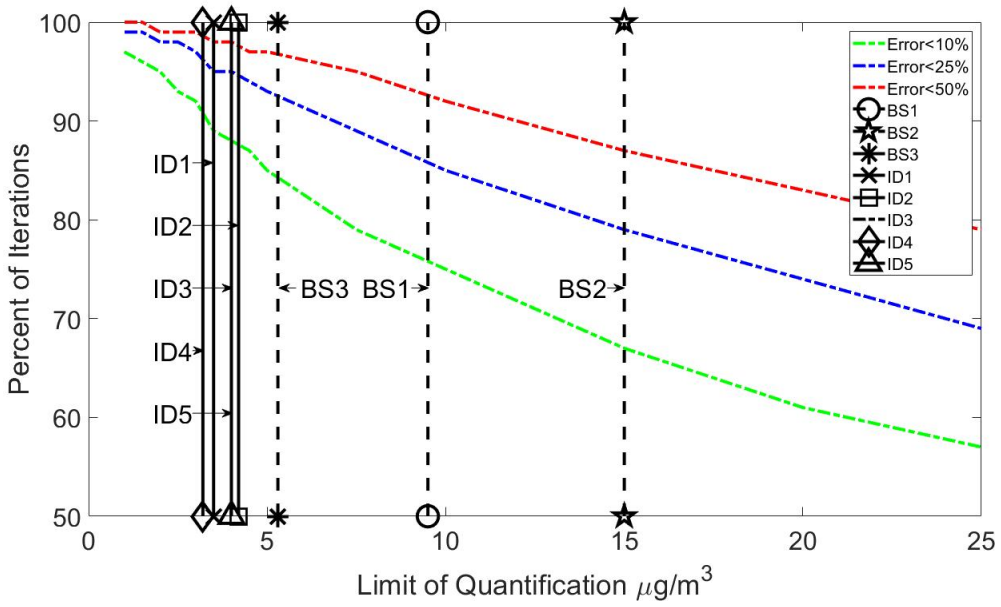

Figure 4.29: Percent of iterations (each iteration is one particular home) in which the exposure in a typical week as reported by a sensor with a particular limit of quantification exceeds each of three limits (10%, 25%, 50%). The sensor limits of quantification for each sensor tested are also plotted. In this case limit of quantification is defined as the average of the limits of quantification (R^2=0.8) measured under exposure to three different sources.

Chapter 5: Laboratory evaluation of the effects of particle size and composition on the performance of integrated devices containing Plantower particle sensors[3]

5.1 Introduction

Particulate matter (PM) is well-established as an airborne pollutant of concern, causing respiratory, lung, and cardiovascular diseases [e.g,, Guo et al. (2018)]. Recently, low-cost particle sensors have grown in popularity for estimating human exposure to ambient PM. Many of these sensors are nephelometers. In nephelometry, light is scattered by the particles as they pass through the sensor, and the scattered light intensity is quantified by a photodetector; the sensor then outputs an electrical signal, which can be related to a particle number or mass concentration using a calibration equation. Therefore, the accuracy of a given sensor may be related to the degree by which the particles scatter light. For example, the light scattering efficiency of a given particle is dependent on the particle's complex refractive index, its diameter, and the wavelength of incident light [e.g., Bohren and Huffman (Bohren & Huffman, 1983)]. These dependencies on both the particle's complex refractive index and diameter imply that low-cost particle sensors may respond differently when the particle composition and/or the particle size distribution is varied. We provide an overview of some previous work here.

---

[3] This chapter represents a draft manuscript, which was revised and published at https://doi.org/10.1080/02786826.2021.1905148

Regarding particle composition, Wang et al. (2015) observed that their sensors' output was greater for organic particles compared to inorganic salt particles, and the authors comment that these differences could be due to a greater proportion of light scattered by the organics than the inorganics. Similarly, Northcross et al. (2013) reported that the response of a Dylos sensor to three different particles sources (wood smoke, polystyrene latex spheres, ammonium sulfate) differed, as they observed different slopes in the sensor's response relative to a reference instrument. Sousan et al. (2016) and Liu et al. (2017) observed similarly variable responses for the Sharp GP2Y sensor using a variety of test aerosols. Liu et al. (2017) commented that the variable outputs related to different particle compositions may be due to differences in the sensors' optical chambers and calibration methods; in other words, a sensor's response to a given particle source may be related to the specific calibration material, an idea central to Hagan and Kroll (Hagan & Kroll, 2020).

The effects of particle size on a sensors' response has also been discussed in the literature. Both Wang et al. (2015) and Han et al. (2017) observed an increase in the slope between their tested sensors and the reference instruments with increasing particle size. Moreover, Sousan et al. (2016) found that the detection efficiency of the Dylos 1700 sensor was less than 5% for 0.3 μm particles, but increased to 60% for 1.3 μm and approximately 100% for particles larger than 3 μm. Conversely, Manikonda et al. (2016) found that the Dylos sensor overestimated PM_{10} when challenged with cigarette smoke but underestimated the concentration for $PM_{2.5}$, while Zamora et al. (2019) demonstrated that

Plantower sensors were most accurate for PM_1 (particle diameter < 1 μm) with worse performance for $PM_{2.5}$ (particle diameter < 2.5 μm) and PM_{10} (particle diameter < 10 μm). Interestingly, He et al. (2020) demonstrate that the Plantower sensor may be more accurate for 200 nm particles than 1 μm particles (cf., their Figure 8).

From previous studies, it is clear that both size and composition affect sensor performance. However, the trends are not completely consistent, which may be complicated by the difficulty in de-coupling size and composition effects for indoor sources (e.g., combustion sources may generate sub-micron particles, while dust resuspension may generate super-micron particles). To better understand size and composition effects, we conducted experiments in which we subjected five low-cost sensors, some of which have not previously been tested in such ways, to various particle sources, including both monodisperse and polydisperse aerosol populations.

The specific aims of our study were to 1) contribute to the body of knowledge relating to the relationship between particle composition and sensor performance; 2) probe the effect of particle size using monodisperse test aerosols; and 3) distinguish between size and composition effects and determine which effect is responsible for the variance in sensor performance.

5.2 Materials and Methods

5.2.1 Devices Tested

We tested a variety of optical particle sensors in this work, all of which contain at least one Plantower sensor. Consequently, each sensor outputs information related to PM_1,

$PM_{2.5}$, and PM_{10}. Details on each sensor and integrated device is provided in Table 5.1. The designation "BS" refers to the bare sensor, while "ID" refers to integrated devices containing the sensor. As in our previous work (Zou, Young, Chen, et al., 2020; Zou, Young, Wickey, et al., 2020), we used a TSI Scanning Mobility Particle Sizer (SMPS) Model 3938, comprised of a Model 3081 long DMA and a model 3775 Condensation Particle Counter (CPC), and an TSI Aerodynamic Particle Sizer (APS) Model 3321 as reference instruments.

Table 5.1. Summary of test sensors in this study[a]

Sensor	Type	Cost	Sensor	No. of Units	Mass Conc. Range ($\mu g\ m^{-3}$)
ID1	AirThinx IAQ	$699	BS3	1	0 - 500
ID2	Airbeam2	$200	Previous version of BS3	3	0 -1000
ID4	TSI Bluesky	N/A	Dual BS3	2	0 - 1000
ID5	Purple Air II	$229	Dual BS3	3	0 - 1000
BS3	PMS5003	$25	N/A	2	0 - 1000

a: To be consistent with our previous studies (Zou, Young, Chen, et al., 2020; Zou, Young, Wickey, et al., 2020)*, we use the same identification for the sensors as in those papers. ID3, BS1, and BS2 are excluded from the present work; ID3 does not contain a Plantower sensor, and BS1 and BS2 are produced by other manufacturers. All three of those report particle concentrations with less sizing information than any of those included in this work.*

5.2.2 Experimental Methodology

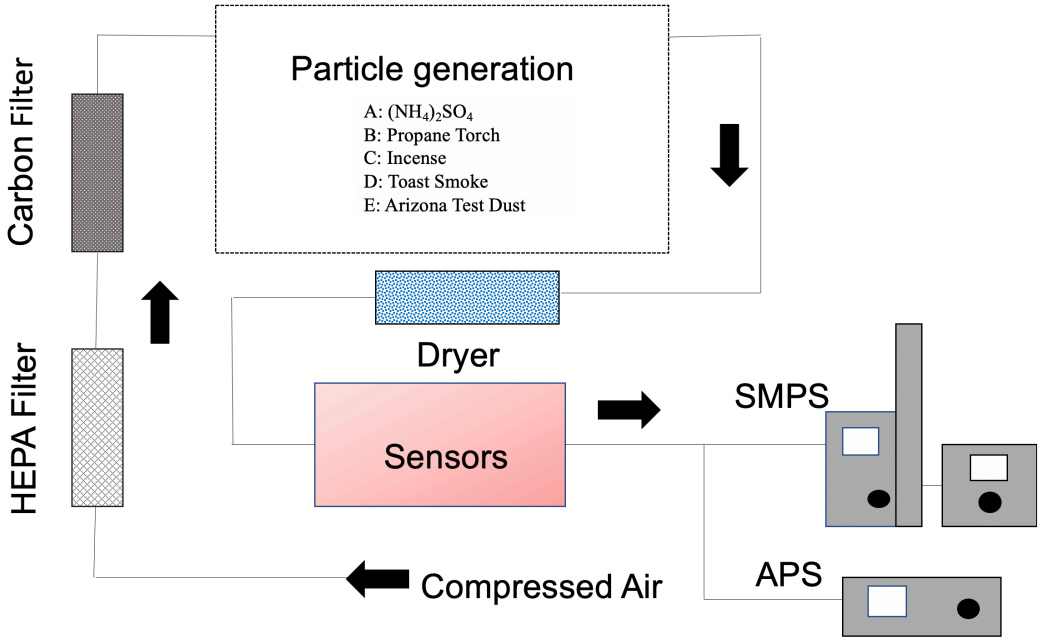

Figure 5.1. General experimental set up for decay tests. All sensors were co-located in the same chamber, labeled as "Sensors". For some experiments, the SMPS was split into a fixed-voltage DMA for size-selection upstream of that chamber and a CPC downstream of the chamber for particle counting.

We conducted three phases of experimental work to investigate how composition and size influence the sensors' responses, in order to try to de-couple these effects. We did not control for temperature or relative humidity in these experiments, but across all experiments, temperature was 26.0 ± 0.3 ºC and relative humidity was 20.9 ± 7.5% within the chamber.

In the first experimental phase, we placed all sensors into a 0.71 m x 0.48 m x 0.38 m (0.130 m^3) enclosed chamber (labeled as "Sensors" in Figure 5.1). We generated particles by atomizing aqueous ammonium sulfate [$(NH_4)_2SO_4$] solutions and operating a

propane torch, modified such that it produced greater quantities of soot. We dried the particles using a diffusion drier and then introduced the dried particles into a fixed-voltage DMA to introduce monodisperse particles (100, 200, 300, 400, 500, 600, 700 nm) into the chamber containing the sensors. The CPC was used to measure particle number concentrations downstream of the chamber. We converted CPC number concentrations to mass concentrations using values of particle density from the literature (see Data Analysis section) and assuming spherical particles. Typical mass concentrations of the size-selected particles ranged between 10 – 200 μg m^{-3} during these experiments. For each particle source, the experiments were conducted in triplicate for each particle size.

In the second phase, decay tests similar to Zou et al. (Zou, Young, Chen, et al., 2020) were conducted in a sealed Modular Blast Cabinet (Eastwood Inc.) with dimensions of 0.77 m x 0.52 m x 0.71 m and a 0.55 m x 0.25 m viewing window on the top. Coarse Arizona Test Dust (ATD; Powder Technology, Inc.) was placed in the bottom of the chamber and resuspended using the cabinet's blast gun, which was operated using HEPA-filtered and activated-carbon-denuded compressed air. Initial concentrations within the cabinet after the resuspension process were approximately 100 – 200 μg m^{-3}, and the concentration was allowed to naturally decay over the duration of the experiment. We repeated these decay experiments four times.

In the third phase, we re-examined earlier experiments from Zou et al. (Zou, Young, Chen, et al., 2020) in which three different particle sources were introduced into the 0.130 m^3 chamber. Those experiments used incense, atomized $(NH_4)_2SO_4$ solution, and burnt

toast smoke as the particle sources, but we also conducted new experiments using the modified propane torch as an additional source for this work. For each source, we generated a high concentration of particles (~100 – 1000 μg m^{-3}) in a separate chamber and dried the particles through a diffusion drier prior to introducing them to the chamber containing the sensors. After removing the particle source, the concentration inside the chamber naturally decayed to near zero. We repeated these decay experiments four times for each source.

5.2.3 Data Collection and Pre-Processing

The bare Plantower sensor was operated with an external microcontroller (i.e., Arduino) using a script written in the C programming language; this script also recorded the data in real-time into an output file. The output data from sensors were recorded at 1 Hz (based on the sensor capabilities) using serial communication software (Coolterm) with time logged from the computer clock. We received data from the integrated devices through cloud-based connectivity (e.g., ID1), serial communication (e.g., ID2, ID4) and SD card storage (e.g., ID5). Timestamps of data from the integrated devices vary based on the specific product and range between 1 and 80 seconds.

We averaged or interpolated the sensor data into 1-minute time intervals to match the sampling interval of the SMPS. SMPS and APS data were merged using the approach of Khlystov et al. (2004) and then converted from number distributions to mass distributions by assuming a spherical shape and assumed densities as follows: $(NH_4)_2SO_4$ is 1.77 g cm^{-3} (Zelenyuk et al., 2006); incense is 1.06 g cm^{-3} (Cheng et al., 1995; B. C. Singer & Delp, 2018); toast is 0.94 g cm^{-3} (B. C. Singer & Delp, 2018); propane torch is

1.9 g cm^{-3} (Khalizov et al., 2012); and ATD is 2.7 g cm^{-3} (B. C. Singer & Delp, 2018; Teipel et al., 2008).

Mass concentrations of PM_1, $PM_{1-2.5}$ and $PM_{2.5-10}$ of the reference instrument were calculated by integrating the merged size distribution from the SMPS and APS. Here, we use PM_1 to represent the integrated mass concentration for all diameters less than 1 μm, $PM_{1-2.5}$ to represent 1 μm to 2.5 μm, and $PM_{2.5-10}$ to represent 2.5 μm to 10 μm. We performed similar calculations with data from the sensors, as they report PM_1, $PM_{2.5}$, and PM_{10}. For the sensor data, $PM_{1-2.5}$ is the difference between $PM_{2.5}$ and PM_1, and $PM_{2.5-10}$ is the difference between PM_{10} and $PM_{2.5}$.

5.2.4 Data Analysis

Two often-used metrics in the evaluation of low-cost sensors are the coefficient of determination (R^2) of the linear regression between the low-cost PM sensor output and the reference instrument output (Karagulian et al., 2019) and the slope of this linear regression (Karagulian et al., 2019; Rai et al., 2017), both of which we used in this study. R^2 describes the correlation between the two outputs, and slope provides information on the relative magnitude of the outputs. R^2 and slope were calculated from least-squares linear regression models between the sensors and the reference instruments.

We first examined all slopes and R^2 values derived for the different sensors by pooling together the results from all experiments for each model to evaluate the similarities between the sensors. We then combined all sensors to investigate the composition and size

effects in order to try to discern a general trend in slopes and R^2 values. To do this, we used statistical tests applied to the slopes and R^2 values for each experimental condition (e.g., 300 nm $(NH_4)_2SO_4$ particles, 700 nm propane torch particles). The most useful of statistical test was Welch's t-test, a modification of the Student's t-test, which is typically used to test whether two populations with unequal variance and unequal sample size, such as the data analyzed in this work, have significantly unequal means. Therefore, the Welch's t-test was used to quantify whether the slopes and R^2 values varied significantly among different particle size bins, difference particle composition, and different sensor models.

We also conducted effect size calculations based on n-way analysis of variance. This was used to determine the contribution of particle size, particle composition, and their interaction to overall variability in the sensor outputs. We quantified fractional variance in the slopes explained by a given independent variable (ω^2) following:

$$\omega^2 = \frac{SSB - (a-1)MSE}{SST + MSE} \quad Eq.5.1$$

where SSB is sum of squares due to one of the independent variables, SST is the total sum of squares, MSE is mean square error, and a is the number of the total number of independent variables (i.e., size, composition, interaction).

5.3 Results and Discussion

5.3.1 Effect of Sensor Model

Before we investigated the effects of composition and size, we first examined the differences across different sensor models. As mentioned previously, all devices tested in this work are equipped with BS3 or a similar version of this Plantower sensor. The slopes and R^2 values from linear regressions between sensors and the reference instruments were calculated for each instance of each model and for each PM source. We combined all slopes for all particle sizes and compositions for each sensor type as box-and-whiskers in Figure 2 (left y-axis). Superimposed on this are the average R^2 value across all instances of each sensor (open circles; right y-axis). One notable observation is that the medians of the slope for all sensors are close to 1. This suggests that sensors may provide fairly accurate measurements in environments with a variety of particle sources. Slight differences may exist due to the proprietary algorithms that the manufacturers of the devices use to process and output raw data from BS3; alternatively, the difference could be related to the form factor of the integrated devices or some less obvious cause. Regardless, all of these sensors show relatively high average R^2 (0.68 – 0.72), implying good consistency in performance across this Plantower sensor "family".

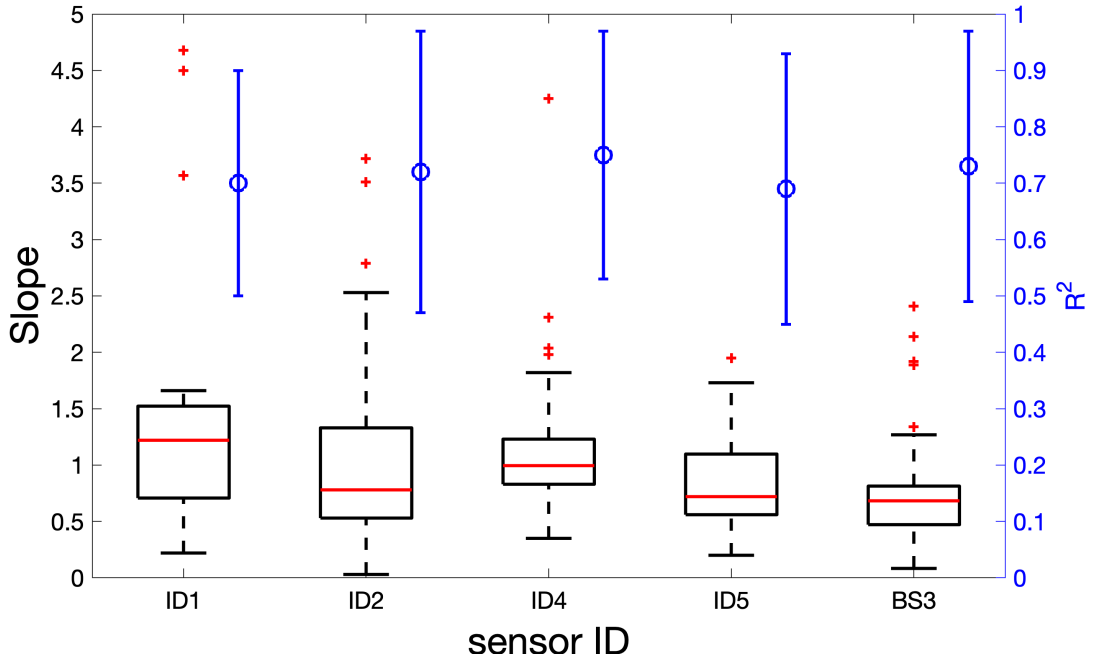

Figure 5.2. Slope and R^2 for each sensor combine all PM sources and all sizes. Boxes represent 25th and 75th percentiles, and whiskers represent the 1st and 99th percentiles, while markers represent the mean ± standard deviation with respect to R^2.

In order to establish this relationship quantitatively, and perhaps eliminate sensor model as a significant variable, we used Welch's t-test to examine the difference in slope between any two combinations of different sensors types. Table 5.2 summarizes the p-values calculated from each set of slopes from each type of sensors showed in Figure 5.3. Perhaps unsurprisingly given Figure 5.2, BS3 was shown to be significantly different than ID1, ID2, and ID4 at a 95% confidence level. Across the four IDs, the only statistical difference existed between the ID1/ID2 and ID1/ID5 pair. These differences, again, may be related to how each ID processes the raw signal and/or the form factor of the ID. However, we argue that although statistical differences exist, these may be irrelevant from a practical standpoint. Under this approximation of similarity, we combine the data across all sensors to investigate the composition and size effects in the following sections.

Table 5.2. p-values calculate from Welch's t-test (0.05 significant level) using the slopes for each type of sensors.

	ID1 (n=29)		ID2 (n =87)		ID4 (n= 58)		ID5 (n = 87)		BS3 (n = 58)	
	slope	R^2	slope	R^2	slope	R^2	slope	R^2	slope	R^2
ID1	--	--	**0.006**	0.532	0.055	0.623	**0.003**	0.781	**0.001**	0.686
ID2	--	--	--	--	0.320	0.682	0.156	0.592	**0.012**	0.695
ID4	--	--	--	--	--	--	0.847	0.523	**0.004**	0.823
ID5	--	--	--	--	--	--	--	--	0.196	0.446

5.3.2 Effect of Particle Source

We first provide an overview of the effect of particle source on sensor performance by combining all sensors across all particle size bins in Figure 5.3, considering slopes and R^2 values. The median slope is less than 1 (0.8) for the propane torch, but greater than 1 for incense, toast, and dust (1.3-1.5). It also appears as if sources with more homogenous composition (e.g., $(NH_4)_2SO_4$, ATD) have less variability compared to sources likely to have a more heterogeneous composition. For example, the interquartile ranges for slope and error bars in R^2 are larger for both incense and toast compared $(NH_4)_2SO_4$ and ATD. Consequently, the t-test results in Table 5.3 suggest that particle source does have a significant effect on sensor response, although one pair exhibit no statistical difference (incense/toast).

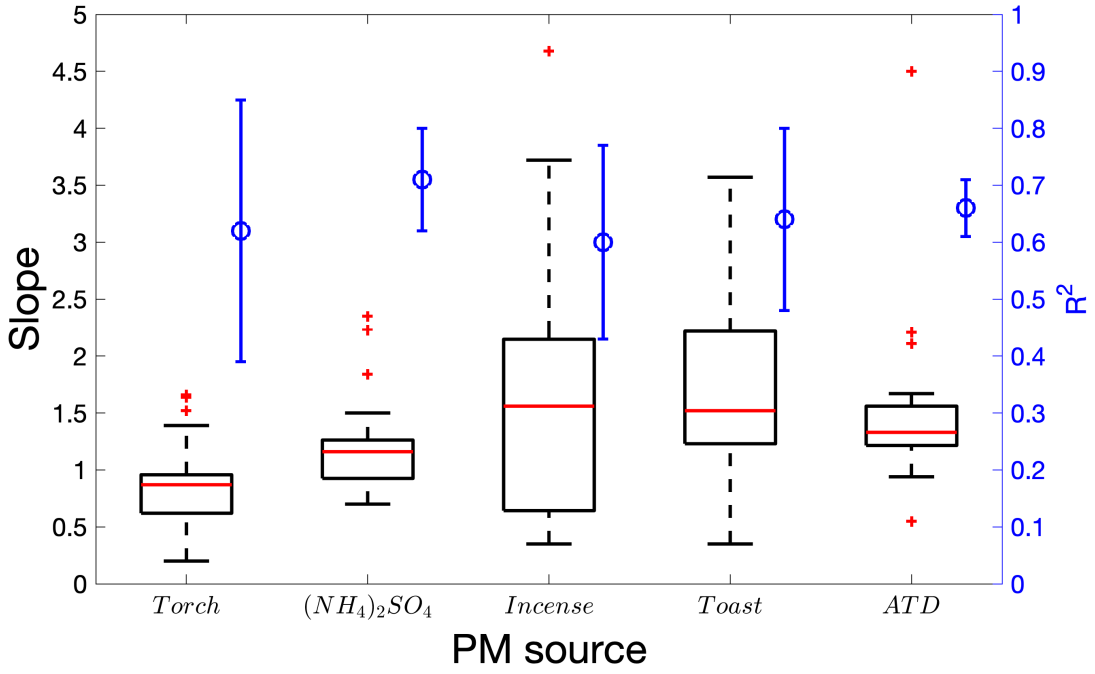

Figure 5.3**.** Slope and average R^2 for each PM sources combining all sensors and all sizes. Boxes, whiskers, and markers represent the same values as in Figure 2.

Table 5.3. p-values calculate from Welch's t-test (0.05 significant level) using the slopes for each sources.

	Propane torch (n = 33)		$(NH_4)_2SO_4$ (n = 33)		Incense (n =33)		Toast (n = 33)		ATD (n =33)	
	slope	R^2	slope	R^2	slope	R^2	slope	R^2	slope	R^2
Propane torch	--	--	**0.001**	0.391	**0.0006**	0.801	**<0.0001**	0.848	**<0.0001**	0.672
$(NH_4)_2SO_4$	--	--	--	--	**0.031**	0.361	**0.001**	0.512	**0.034**	0.151
Incense	--	--	--	--	--	--	0.592	0.355	**0.028**	0.334
Toast	--	--	--	--	--	--	--	--	**0.013**	0.601

Table 5.4. Average mass median diameter and geometric standard deviation for each PM source test, based on the merged SMPS + APS data.

	Mass median diameter		**Geometric standard deviation**	
	Mode 1	Mode 2	Mode 1	Mode 2
Incense - trial 1	153 nm	6.11 µm	1.85	1.25
Incense - trial 2	117 nm	7.91 µm	1.76	1.30
Incense - trial 3	189 nm	8.03 µm	1.98	1.33
Incense - trial 4	130 nm	6.93 µm	1.89	1.29
Toast - trial 1	132 nm	6.90 µm	1.92	1.21
Toast - trial 2	130 nm	6.88 µm	1.90	1.20
Toast - trial 3	131 nm	7.36 µm	1.95	1.28
Toast - trial 4	126 nm	8.21 µm	2.01	1.26
$(NH_4)_2SO_4$ - trial 1	494 nm	n/a	1.53	n/a
$(NH_4)_2SO_4$ - trial 2	486 nm	n/a	1.53	n/a
$(NH_4)_2SO_4$ - trial 3	468 nm	n/a	1.45	n/a
$(NH_4)_2SO_4$ - trial 4	490 nm	n/a	1.49	n/a
Propane torch - trial 1	318 nm	n/a	1.58	n/a
Propane torch - trial 2	309 nm	n/a	1.52	n/a
Propane torch - trial 3	272 nm	n/a	1.48	n/a
Propane torch - trial 4	285 nm	n/a	1.53	n/a
ATD - trial 1	2.7 µm*	n/a	1.85	n/a
ATD - trial 2	2.01 µm*	n/a	1.44	n/a
ATD - trial 3	1.24 µm*	n/a	1.35	n/a
ATD - trial 4	1.33 µm*	n/a	1.34	n/a

**Larger ATD particles likely settled out of the air prior to sampling. There is not strong evidence (e.g., Figure 3) that the reference instruments under-sampled these particles. Incense and toast include two modes in the size distribution, while other sources only have single mode.*

One complication in investigating the source effect with Figure 5.3 is that the size distributions for each particle source are different indicated by mass mean diameter and geometric standard deviation (Table 5.4). For example, both incense and toast generated bimodal mass distributions, with mass median diameters between ~100 – 200 nm and ~6 – 8 µm, while the propane torch particles had a single mode, with a mass median diameter of ~300 nm. The similarities between the particle size distributions is likely part of the reason why we found no statistical differences between incense and toast particles in Table 5.3; moreover, burning incense and toast may have similar combustion conditions (e.g., smoldering or pyrolysis), resulting in similar particle composition and optical properties. There are no apparent similarities in the size distributions for any other sources.

Consequently, we next focused on the effect of particle size. To do so, we apportioned the results into three size bins (PM_1, $PM_{1\text{-}2.5}$, and $PM_{2.5\text{-}10}$), shown in Figure 5. 4. For PM_1 (Figure 4a), the slopes for incense and toast are generally greater than the other four PM sources: the median values for incense and toast are approximately two times greater than the slopes for propane torch and $(NH_4)_2SO_4$. Moreover, the mean R^2 for incense, toast and propane torch are approximately 0.7-0.8, which is generally lower than the R^2 for $(NH_4)_2SO_4$ and ATD. The reason may partially be due to the fact that $(NH_4)_2SO_4$ and ATD (mostly silica and alumina) are sources of relatively homogeneous composition, whereas we expect the composition of incense, toast, and propane torch particles to be a mixture of organic and elemental carbon; moreover, the mixing state of these carbonaceous materials in those particles is unknown. In combination, heterogeneity may cause more variability in the sensors' output, but assessing the sensors' response to mixtures of particles is outside the scope of this work.

Conversely, in Figure 5.4b and 5.4c, there was no obvious difference in composition for $PM_{1\text{-}2.5}$ or $PM_{2.5\text{-}10}$. Incense again has the greatest variation in slopes, but in general, the difference of the median slopes between all sources are in the range of 0.5. The mean R^2 values in each panel are all consistent, so even if differences in magnitude exist across different aerosol sizes or compositions for the sensors, the influence on the correlation to the reference instruments is consistent.

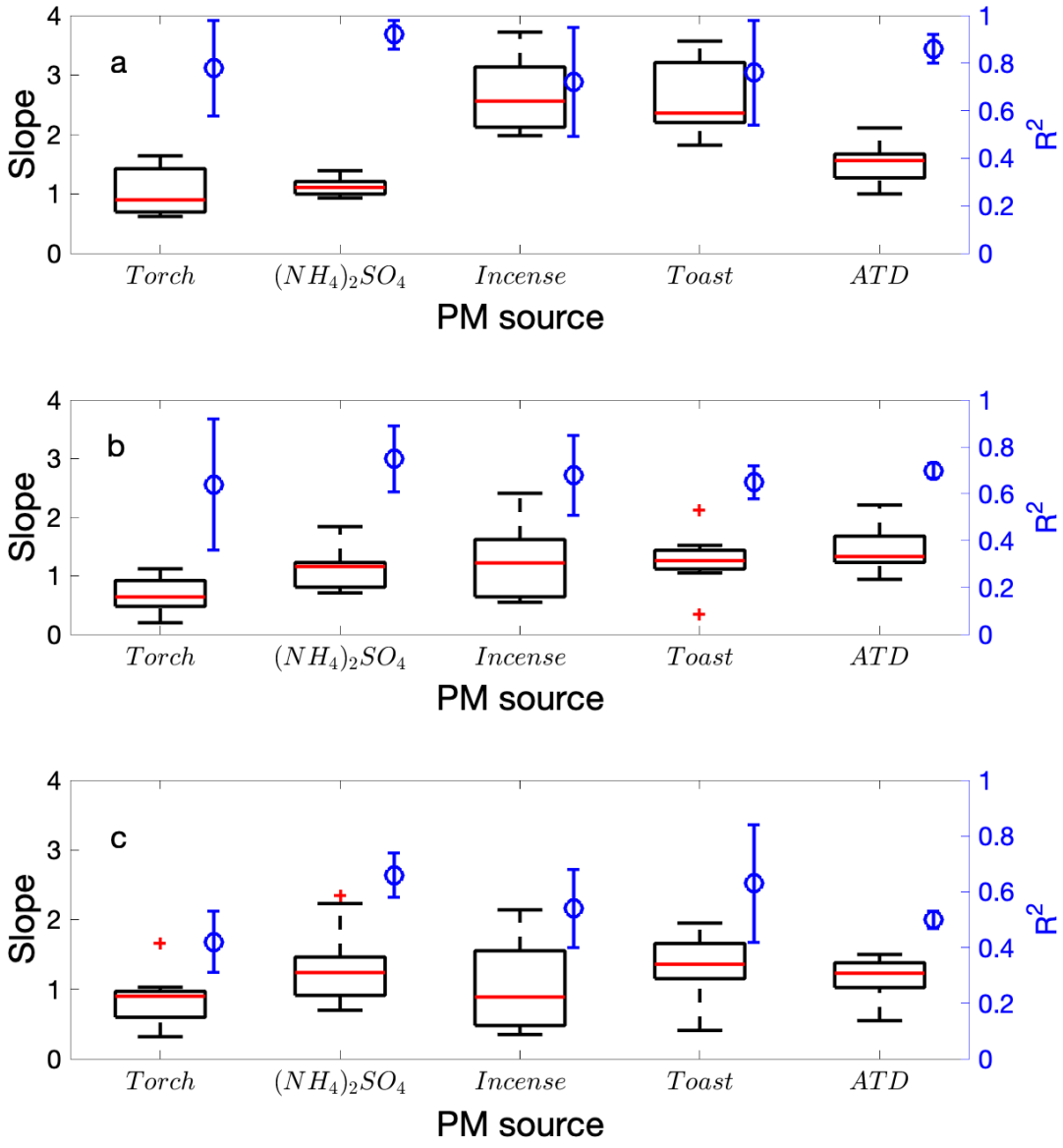

Figure 5.4. As in Figure 3, but with the data split into three size bins: (a) PM_1, (b) $PM_{1\text{-}2.5}$ and (c) $PM_{2.5\text{-}10}$.

We again used Welch's t-test to quantify the differences in slope among any combination of particle sources. Tables 5.5-5.7 summarize the p-values calculated from each set of slopes from different particle sources shown in Figure 5.4. For PM_1, the results were similar to those in Table 5.3, in that the only statistically similar pair was incense and toast. Conversely, for $PM_{1\text{-}2.5}$ and $PM_{2.5\text{-}10}$, the only statistically-significant differences

existed for pairs of sources including the propane torch. This result may be partially explained by Hagan and Kroll (2020), who use Mie theory to demonstrate that absorbing particles (e.g., soot) are more likely to result in sensor measurements that are biased low, relative to a "true" value.

Table 5.5. p-values calculate from Welch's t-test (0.05 significant level) for PM_1 using slopes and R^2

	Propane torch (n = 11)		$(NH_4)_2SO_4$ (n = 11)		Incense (n =11)		Toast (n = 11)		ATD (n =11)	
	slope	R^2	slope	R^2	slope	R^2	slope	R^2	slope	R^2
Propane torch	--	--	**0.003**	0.061	**<0.0001**	0.990	**<0.0001**	0.802	**<0.0001**	0.111
$(NH_4)_2SO_4$	--	--	--	--	**<0.0001**	**0.025**	**<0.0001**	**0.021**	**0.004**	0.121
Incense	--	--	--	--	--	--	0.631	0.752	**0.0001**	0.047
Toast	--	--	--	--	--	--	--	--	**0.0004**	**0.053**

Table 5.6. p-values calculate from Welch's t-test (0.05 significant level) for $PM_{1\text{-}2.5}$ using slopes and R^2

	Propane torch (n = 11)		$(NH_4)_2SO_4$ (n = 11)		Incense (n =11)		Toast (n = 11)		ATD (n =11)	
	slope	R^2	slope	R^2	slope	R^2	slope	R^2	slope	R^2
Propane torch	--	--	**0.023**	0.117	**0.014**	0.381	**0.004**	**0.004**	**0.01**	**0.002**
$(NH_4)_2SO_4$	--	--	--	--	0.523	0.392	0.329	0.428	0.031	0.185
Incense	--	--	--	--	--	--	0.858	0.398	0.207	0.055
Toast	--	--	--	--	--	--	--	--	0.263	0.051

Table 5.7. p-values calculate from Welch's t-test (0.05 significant level) for $PM_{2.5\text{-}10}$ using slopes and R^2

	Propane torch (n = 11)		$(NH_4)_2SO_4$ (n = 11)		Incense (n =11)		Toast (n = 11)		ATD (n =11)	
	slope	R^2	slope	R^2	slope	R^2	slope	R^2	slope	R^2
Propane torch			**0.044**	**<0.0001**	0.531	**0.009**	**0.018**	**0.004**	0.134	0.683
$(NH_4)_2SO_4$					0.248	**0.008**	0.942	0.251	0.631	**<0.0001**
Incense							0.228	0.241	0.251	0.253
Toast									0.689	**0.001**

5.3.3 Effect of Particle Size

The statistically-significant differences in between particle sources appear to have been driven by differences in particle size, especially since this effect appears to go away for $PM_{1\text{-}2.5}$ and $PM_{2.5\text{-}10}$ when we split the data into the three size fractions, as in Figure 5.4 and Tables 5.5-5.7. Moreover, our own Mie theory simulations based on Cappa et al. (Cappa et al., 2012) suggest that particle diameter, rather than complex refractive index (as a proxy for composition), is a stronger driver for variability in light scattering by particles (Figure 5.7).

Therefore, we further investigate the effect of particle size on sensor performance by combining data across all sensors for all particle sources (i.e., assuming that sensor model differences and composition effects are negligible relative to the size effects). The result of this is presented in Figure 5 as a box-and-whisker plot. The median slopes increase with increasing particle size from 100 nm to 700 nm before roughly plateauing between 700 nm and $PM_{2.5\text{-}10}$. These results are generally consistent with the "transfer functions" reported in He et al. (2020) for the Plantower 5003 sensor. Moreover, predictions of light scattering efficiency from Mie theory suggest a maximum as diameters approach 1 μm (Figure 5.8), suggesting that our observations are similar to this theoretical framework.

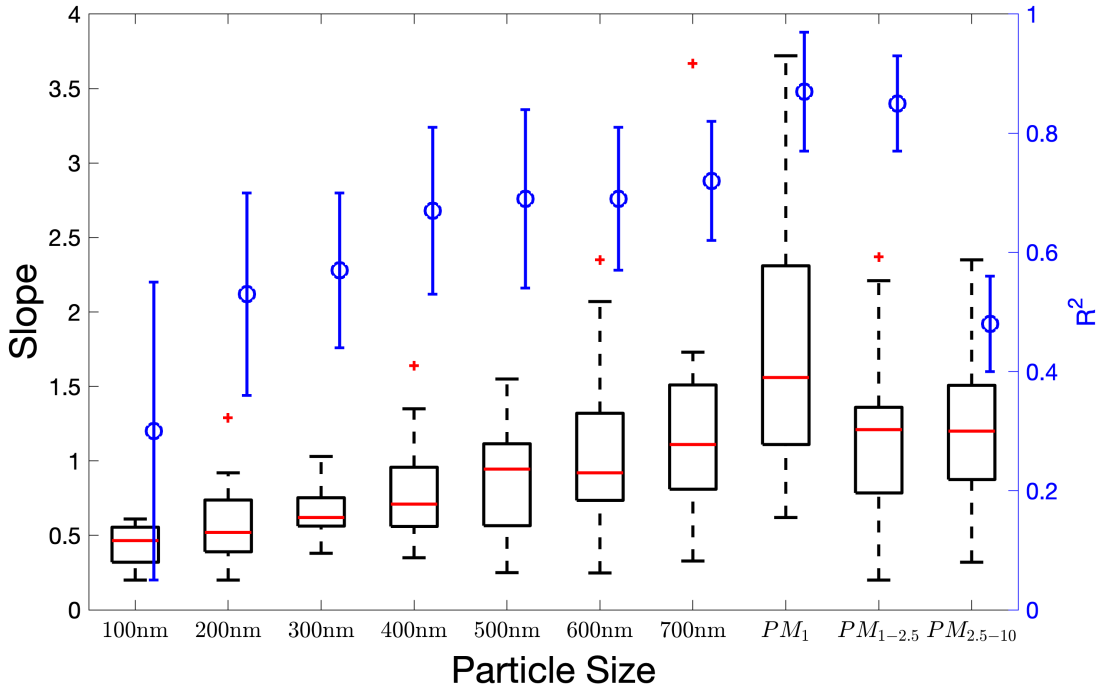

Figure 5.5. Slope and average R^2 for each particle size, combining data across all sources and sensors. Boxes, whiskers, and markers represent the same values as in Figures 2-5.

Similar to the pattern in measured slopes, the R^2 values show a generally increasing trend from 0.34 to 0.83 between 100 nm and $PM_{1\text{-}2.5}$, but it sharply decreases to 0.48 for $PM_{2.5\text{-}10}$; this trend is consistent with the study from Taylor (2016). We suspect that this degradation in R^2 is related to difficulties in sampling the larger particles, because of their relatively large inertia.

We again used Welch's t-test to examine the differences in slope between different size bins in Figure 5.5. Among any pair of size combinations, p-values are less than 0.05, indicating a significant size effect (not tabulated here). This effect of particle size on sensor performance is consistent with previous findings (Han et al., 2017; Zamora et al., 2019;

Liu et al., 2017; Manikonda et al., 2016; Rai et al., 2017; Sousan et al., 2016; Wang et al., 2015).

5.3.4 Decoupling Composition from Size

We next sought to analyze whether a composition effect existed independent of the size effect. As an illustrative example, in Figure 5.6 we present a summary of all results for a single sensor model (ID2). The slopes generally increase from 100 nm to 700 nm yet mostly remain below 1 for all sources; moreover, there is no obvious composition effect observed between 100 and 700 nm. However, for PM_1, the composition effect becomes more apparent. For example, the slope for incense is approximately 3 times greater than the slope for $(NH_4)_2SO_4$ for this size bin. For the larger size bins ($PM_{1\text{-}2.5}$ and $PM_{2.5\text{-}10}$), the slopes decrease slightly, and the apparent composition effects remain. Similar figures are provided for the other sensor models in the Additional Tables and Figures (see Figure 5.9 to Figure 5.12). While differences between the individual sensors exist, the general trends remain.

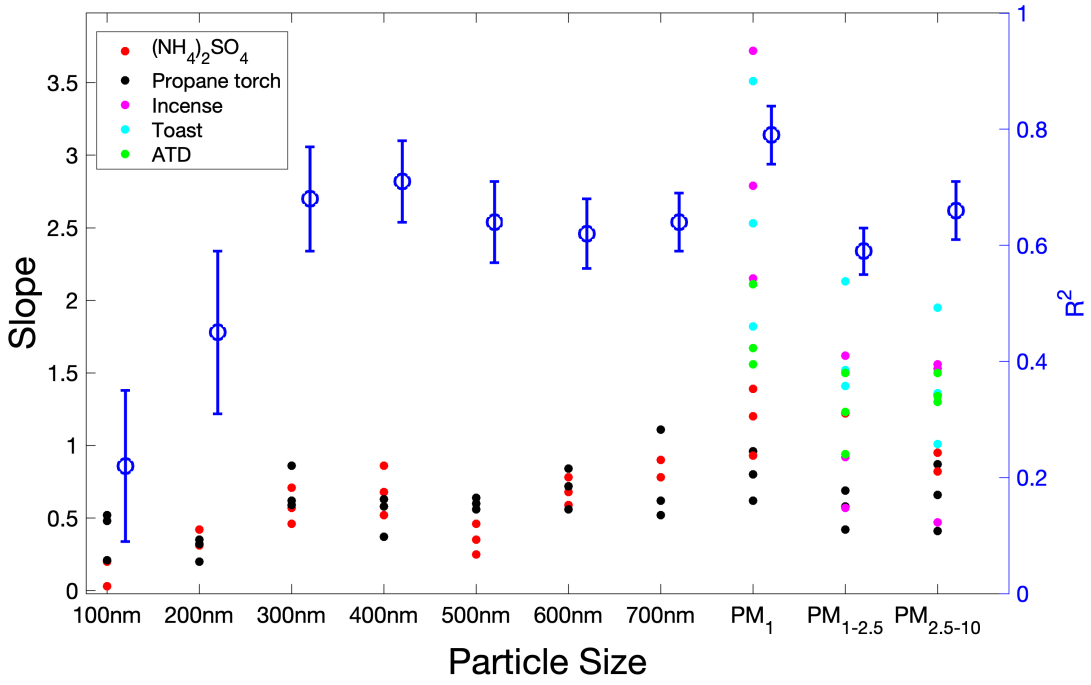

Figure 5.6. Slopes from experiments across different size bins for each particle source for ID2. Different solid markers represent different sensor instances.

To estimate the contribution of size, composition, and their interaction to the variance in the sensor output, we calculated ω^2 for each independent variable for each sensor. These results are presented in Table 5.8 using the slopes from each unique experiment as the dependent variable (i.e., data from Figure 5.6 was used in the calculation for ID2). This analysis of our empirical results suggests that particle size is a more important factor than its composition, with size typically accounting for roughly twice the variance than composition. However, the interaction between size and composition is clearly the dominant variable, which highlights the difficulty in discerning the effects of size and composition independently; this is perhaps not entirely surprising because light scattering by particles depends on both of these variables. Furthermore, this dominance by the size/composition interaction may suggest that identifying the source of the particles

may be a critical need for improved accuracy and that sensor calibrations with different sources based on the sensor's intended location for deployment may be necessary.

Table 5.8. Percent contribution to variance (ω^2) in the sensor output based on n-way analysis of variance.

	Size (%)	**Composition (%)**	**Size & composition interaction (%)**
ID1	5.6	3.5	10.2
ID2	9.1	5.6	12.4
ID4	13.2	6.0	20.8
ID5	12.3	6.3	19.8
BS3	9.2	5.5	17.5

5.4 Conclusions

In this study, we conducted laboratory experiments to evaluate size and composition effects on the performance of a Plantower particle sensor and four integrated devices that incorporate it. These efforts included experiments with five particle sources, and a subset of those experiments included monodisperse aerosols. Our major findings are:

1) There is an apparent source effect on the performance of the sensors, which appears to be related to particle size. For example, when combining all particle sizes, the median slopes for incense, toast, and ATD particles were roughly 1.5, while the median value for propane torch and $(NH_4)_2SO_4$ particles were closer to unity (Figure 5.3). When separated into the different size fractions (Figure 5.4), the median for the PM_1 size fraction for incense and toast particles increases to roughly 2.5, while the values for the $PM_{1\text{-}2.5}$ and $PM_{2.5\text{-}10}$ size fractions are more similar to the other three particle sources.

2) The sensors could generally detect particles as small as 100 nm. For example, the median slope across all sensors and sources for our monodisperse particle tests was roughly 0.5 for 100 nm particles (Figure 5.5). However, measurements at this small size were generally less precise, e.g., R^2 was roughly 0.35 ± 0.25 (mean ± standard deviation) for 100 nm particles, which is likely related to poor scattering efficiencies of those particles at the wavelength of light in the sensor.
3) While the means were statistically different, the median slopes were roughly unity for 500 – 700 nm monodisperse particles and for the $PM_{1\text{-}2.5}$ and $PM_{2.5\text{-}10}$ size fractions (Figure 5.5). The median value for the PM_1 fraction was roughly 1.5, likely related to the apparent source effect.
4) The mean R^2 values gradually increased from roughly 0.55 for 200 nm particles to roughly 0.70 for 700 nm particles and were greater than 0.80 for the PM_1 and $PM_{1\text{-}2.5}$ size fractions. There was a dramatic decrease in mean R^2 for the $PM_{2.5\text{-}10}$ size fraction (mean value of roughly 0.50), likely due to some combination of the difficulty in sampling these larger particles and the wave-like nature of scattered light by larger particles.
5) To decouple the competing effects of size and composition on the sensors' performance, we conducted an n-way analysis of variance to quantify the proportion of variance in the slopes that could be associated with size alone, composition alone, and the interaction between size and composition. Particle size alone explained roughly 6 – 13% of the variance, while particle composition alone explained roughly 3 – 6%. The interaction between particle size and composition

was clearly the dominant term as it was associated with roughly 10 – 21% of the variance.

Our results, along with other recent literature, demonstrate the need for improvements to calibration procedures and/or post-processing algorithms that consider the size and composition of the particles to improve sensor accuracy. For example, solid fuel combustion appears to consistently result in concentrations that are biased high [e.g., ~50% high for burning incense in our results and in Singer and Delp (2018); factor of ~2 high for wildfire smoke in Delp and Singer (2020) and Holder et al. (2020)], but for many particle sources, the discrepancies are not as extreme. This may imply the need for a database of source-specific correction factors that can be applied to Plantower-based sensors to improve exposure estimates, although our results show that composition alone explains the lowest fraction of the variance.

Accounting for particle size has the potential to remove roughly 10% of the variance in the sensor data, and in fact, Li et al. (2020) proposed the need for a size-specific calibration factor. For example, our results suggest that measurements of 200 nm particles may need to be increased by a factor of two, while measurements of 700 nm may need to be reduced by roughly 10%. Practically speaking, it is not this simple because real-world aerosol populations are rarely monodisperse, and while Plantower-based sensors do provide six channels of information across different particle sizes, He et al. (2020) comment that the sensors "always show a monotonically decreasing particle size distribution with increasing diameter …, regardless of the actual particle size distribution."

Therefore, the particle size distribution may need to be obtained through some external measurement in order to apply an accurate size-resolved correction equation.

However, our results suggest that accounting for either particle size or composition in isolation may be insufficient, since the interaction term between these two variables accounts for the largest fraction of the variance. Conceivably, a numerical post-processing algorithm, such as the framework developed in Hagan and Kroll (2020), could account for both isolated variables and their interaction. One challenge with this approach is that the complex refractive index and the particle size distribution are required inputs, and these input terms may be unknown *a priori*. While assumptions could be made regarding the input variables, incorrect assumptions could result in more, rather than less, error in the post-processed data.

5.5 Additional Tables and Figures

D.1 Mie theory modeling

To understand how particle diameter and composition may affect a sensor's response, we provide Mie theory simulations using code based on Cappa et al. (Cappa et al., 2012). In our simulations, we fix the wavelength of light to 650 nm, the approximate wavelength of the Plantower sensor (Hagan & Kroll, 2020), an input particle diameters range from 10 nm to 20 μm. We consider a range of complex refractive indices ($n = m + ik$), varying m between 1.3 and 2.0 and varying k between 10^{-6} and 10^{0}.

Simulation results are presented in Figures 5.7 and 5.8. In the left panel of Figure 5.7, we provide contours of predicted scattering efficiency as a function of particle diameter and real refractive index (m) with $k = 10^{-6}$; in the right panel, we fix m = 1.55 and vary the imaginary refractive index. In both cases, the predicted scattering efficiency is a much stronger function of particle diameter than the refractive index term. For example, at a fixed particle diameter, the scattering efficiency is roughly constant in either panel. This is presented in a slightly different manner in Figure 5.8, which includes five different curves corresponding to m ranging between 1.45 and 1.65. Although each curve is distinct, the underlying dependency as a function of particle diameter is roughly the same, and the majority of the variation can be attributed to the so-called "interference" and "ripple" structures (Bohren & Huffman, 1983). The maximum scattering efficiency is roughly consistent with our results in Figure 5.5 in the main text.

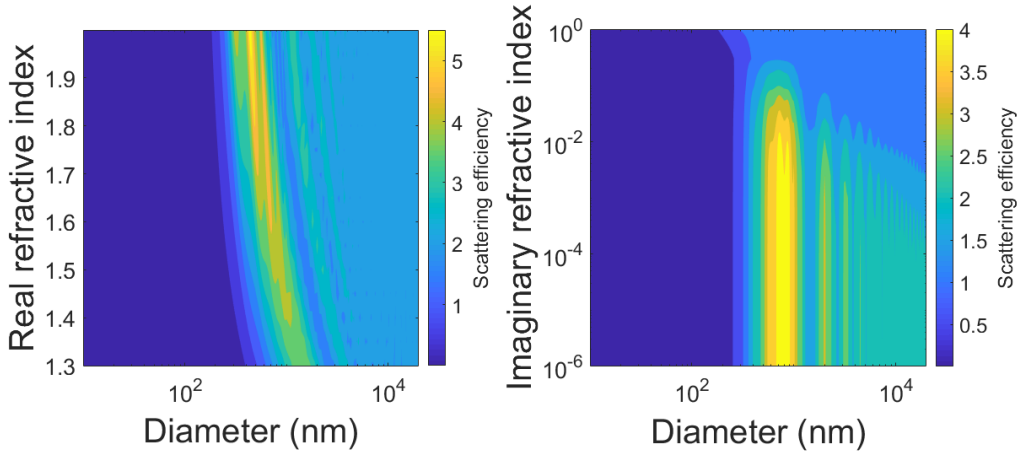

Figure 5.7: Mie theory simulations for variable real refractive index with the imaginary term fixed at 10^{-6} (left panel) and for variable imaginary refractive index with the real term fixed at 1.55 (right panel). Contours represent predicted scattering efficiencies.

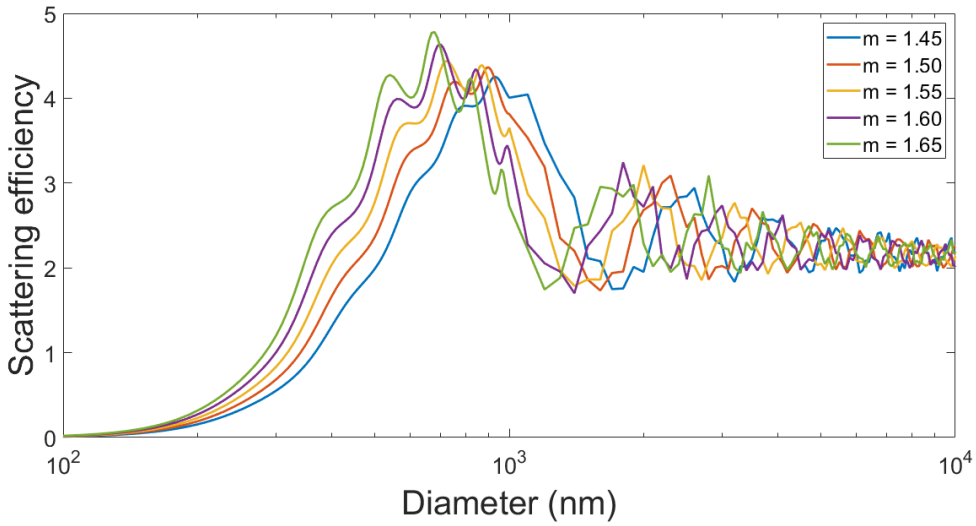

Figure 5.8: Mie theory simulations for non-absorbing particles with varying refractive indices. In all cases, there is a maximum in scattering efficiency between roughly 700 – 900 nm.

Individual Size/Composition Results

The following figures are analogous to Figure 5.6 in the main text. They include data for the other sensors tested.

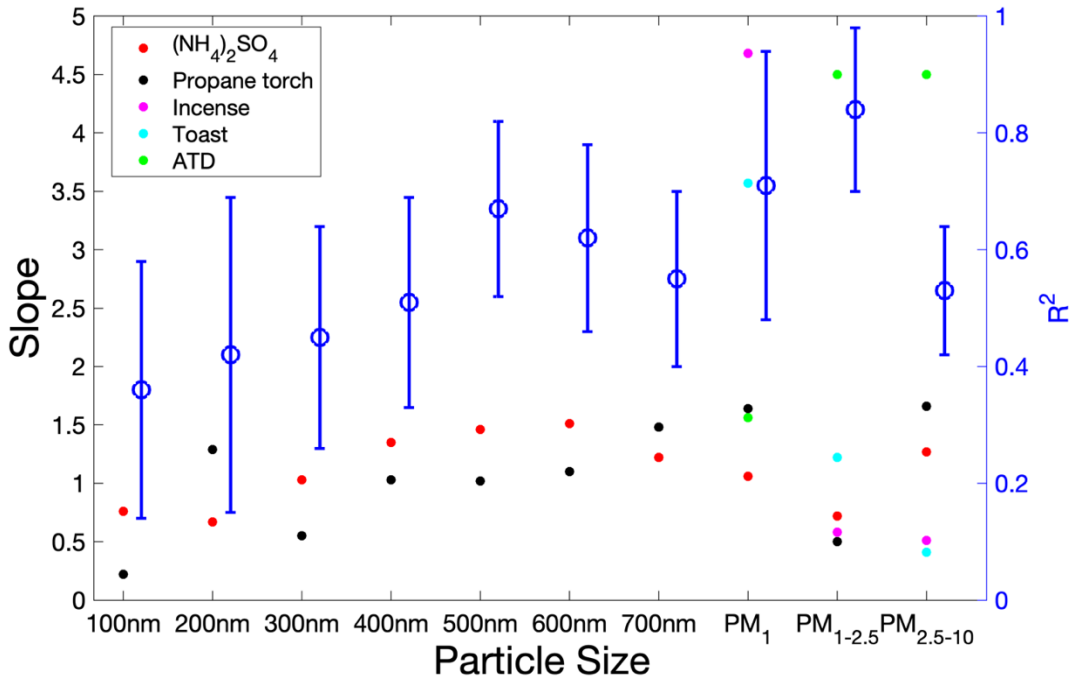

Figure 5.9: Slopes from decay tests using six different PM source for ID1 for different size bin

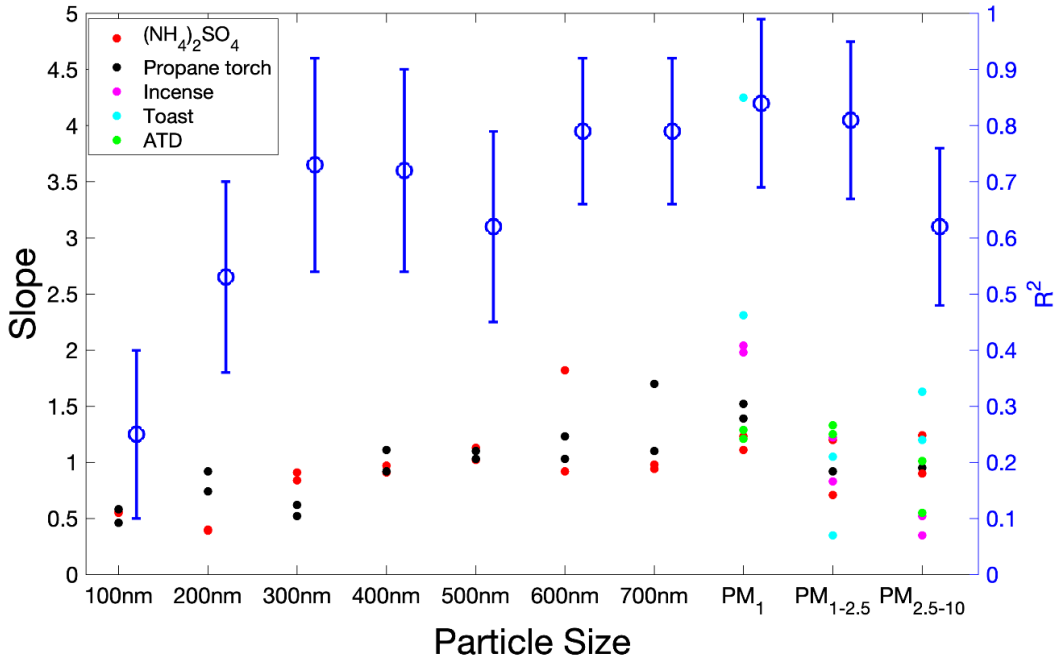

Figure 5.10: Slopes from decay tests using six different PM source for ID4 for different size bin

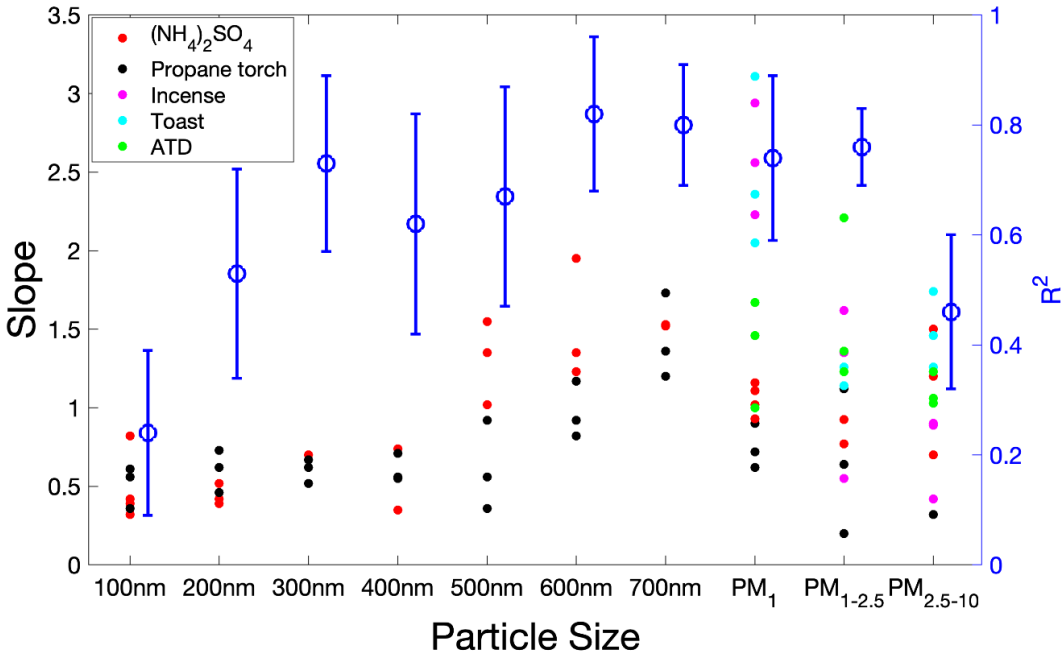

Figure 5.11: Slopes from decay tests using six different PM source for ID5 for different size bin

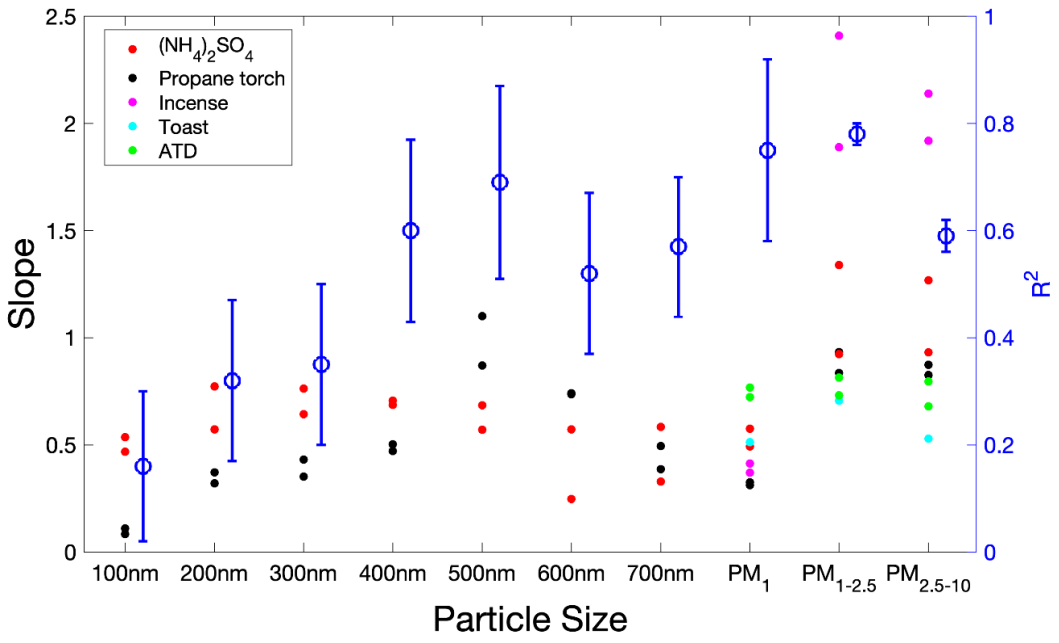

Figure 5.12: Slopes from decay tests using six different PM source for BS3 for different size bin

Chapter 6 A systematic investigation on the effects of temperature and relative humidity on the performance of eight low-cost particle sensors and devices[4]

6.1 Introduction

One promising area within the field of smart buildings is in smart monitoring, maintenance, and control of indoor environments. Low-cost air quality sensors can conceivably be used to ensure optimal operation of building air quality control systems and enable decision making based on reliable monitoring data. Chief among the airborne pollutants of interest for monitoring with these sensors is airborne particulate matter (PM). The link between PM exposure and numerous negative health outcomes is well established. Exposure to PM is linked to cardiovascular and respiratory disease (U.S. EPA 2018) and the majority of this exposure occurs indoors for Westerners, as this is where we spend the vast majority of our time (Klepeis, et al. 2011). Indoor sources of PM include combustion activities, outdoor penetration, mold, and airborne formation from gases emitted from cleaning products, furniture, or other building products (Li, Qingmei and Zhang 2017).

Numerous low-cost particle sensors have become commercially available recently for as little as $6 and may provide an inexpensive means to help assess and control PM exposure. These sensors usually consist of a light source (typically, a small LED) that is scattered by a stream of particles passing by it, and a small photoreceptor receiving this scattered light signal. Researchers have conducted many investigations of one or more

[4] This chapter is a published paper at https://doi.org/10.1016/j.jaerosci.2020.105715

aspects of the performance of these sensors, and mechanisms for deviation in performance from that of more expensive reference instruments have been identified. One of these mechanisms is the changes that occur at different psychrometric conditions.

There is little evidence that temperature has a substantial effect on the accuracy of low-cost sensors, within a reasonable range of temperatures, despite the fact that some sensors introduce air into the sensor via thermally-induced buoyancy via a resistive heater located within the sensor. Budde et al. (2013) noted a correlation between the output from a Sharp GP2Y sensor, which utilizes buoyancy-driven air, and temperature when each instance (one instance equals one unique sensor; multiple instances were tested in the study) of the sensor was held at a constant concentration of 0 $\mu g/m^3$, but this effect was slight. Zamora et al. (2019) conducted field and laboratory evaluations of the low-cost Plantower PMS A003 sensor, which contains a small internal fan to drive air flow, and found no observable effect of temperature on LCPMS performance.

With regards to humidity, though, several studies concluded that relative humidity (RH) has an impact on sensor performance. Badura et al. (2018) suggested four mechanisms may be responsible: hygroscopic growth leading to changes in particle diameter (Crilley et al., 2018); changes in the refractive index of particles, which can affect light scattering; moisture interference with electrical components, up to and including failure (Wang et al., 2015) and scattering of sensor LED light by moisture itself, which may occur at extreme RH (Jayaratne et al., 2018).

Several laboratory studies have measured relationships between RH and sensor output. Zamora et al. (2019) discovered that the accuracy of Plantower PMS A003 decreased at RH greater than 50%. Wang et al. (2015) found that the Sharp GP2Y sensor'

output increased as RH increased. Similar phenomena have been measured in the field. Han et al (2017) found that the PM2.5 and PM10 concentration were correlated to RH. Feenstra et al (2019) found increasing positive bias error for 12 particle sensors during field base monitoring as RH increased. Liu et al (2019) also noticed increase of sensor error at higher RH level (greater than 80% RH) for outdoor particle monitoring. Jayaratne et al. (2018) found that the Plantower PMS1003 mass concentration increased by 80% with RH increase from 78-89 % during field monitoring. In general, these studies all provide evidence that sensor output depends on RH.

In contrast, several studies concluded that neither temperature nor RH affect sensors' performance. Badura et al. (2018) tested 5 sensors in outdoor environments with temperatures ranging from -8 °C to +36 °C and RH ranging from 27% to 94% but found no effect. Malings et al. (2020) found little RH effect and attributed this to the plastic shell, which enclosed their sensors, trapping heat and reducing RH. Bulot et al. (2019) found that neither RH nor temperature had an influence on performance of multiple sensors in a school.

With these previous studies in mind, we conducted a series of experiments by varying temperature and humidity in a precisely controlled chamber, with eight different brands of low-cost particle sensors, some of which have not yet been tested in publicly available studies. Our primary objective in these investigations was to quantify the relationship between temperature and relative humidity for the range expected in building applications and the output of eight low-cost sensor models (relative to a reference instrument), some of which have not been previously analyzed in this manner.

6.2 Methodology

6.2.1 Sensors Tested

We tested three bare sensors and five integrated devices. We define bare sensors as small sensors, usually less than 10 cm along their longest edge, which output an electrical signal (analog or digital), that then must then be translated into something understandable by its users and/or by other devices. The bare sensors we are testing are exclusively optical sensors. Bare sensors tested as well as relevant specifications are given in Table 6.1. We refer to bare sensors as "BS" from here forward. Multiple instances were tested for each type of BS as shown in Table 6.1.

We refer to packaged devices that utilize bare sensors and fulfill the necessary conversion from raw sensor outputs to produce concentrations as "integrated devices". Many also offer built-in features such as Bluetooth or Wi-Fi connectivity, SD card storage, temperature and relative humidity sensors, other pollutant sensors, and/or compatibility with other smart devices like thermostats. Most of the integrated devices targeted towards residential consumers fall into the $200 – $300 price range. Bare sensors are incorporated into each of the integrated devices we are also testing. Specifications for the integrated devices tested are given in Table 6.2. We refer integrated devices as "ID" from here forward. Multiple instances were tested for each type of ID except for ID1, as shown in Table 6.2.

Table 6.1. Bare Sensors Tested

Sensor	Cost	Signal-to-Output Conversion Process	Intake	Manufacturer Reported Range	Use in Integrated Sensor(s)	Intended Indoor Environment	Previous Studies	No. of Units Tested
Honeywell HPM (BS1)	$30	Light → photodiode → volt signal → photoelectric converter→ 32-bytes → MCU(4-bytes) → PM mass density	Fan	0 μg/m^3 to 1000 μg/m^3	None	Air conditioners, air quality monitors, environmental monitoring, air cleaners, air quality detectors		2
Sharp GP2Y1010AU0F (BS2)	$15	Light → photodiode → volt signal → amplified → volt signal → photoelectric converter → 32-bytes → MCU → PM mass density	Resistor	0 μg/m^3 to 500 μg/m^3	Foobot, AirAssure, UB Air Sense	Detecting dust in air, air purifier, air conditioner, air monitors, and distinguishing between smoke and house dust	(Budde et al., 2013) (Weekly et al., 2013*) (Wang et al., 2015) (Hojaiji et al., 2017) (Liu et al., 2017a) (Sousan et al., 2016)	3
Plantower PMS5003 (BS3)	$25	Light → phototransistor → volt signal → amplified → photoelectric converter → 32-bytes → MCU(12-bytes) → number concentrations → PM mass density	Fan	Effective 0 μg/m^3 to 500 μg/m^3 Max 0 μg/m^3 to 1000 μg/m^3	TSI Bluesky, Purple Air II, AirBeam	Can be in instruments related to the concentration of suspended particles in the air or other environmental improvement equipment	(Kelly et al., 2017*) (Zheng et al., 2018) (Jayaratne et al., 2018) (Zamora et al., 2019)	2

*different version of sensor from same manufacturer tested in previous work

Table 6.2. Integrated Devices Tested

Sensor	Cost	Communication	Sensor	Features	Previous Studies	No. of Units Tested
AirThinx (ID1)	N/A	Cellular, WiFi, and Bluetooth. Uses Netronix© cloud-based storage.	Plantower	Also provides CO_2, formaldehyde, VOC, temperature, humidity, and pressure.		1
AirBeam2 (ID2)	$200	Cellular networks, WiFi, Bluetooth, serial connector.	Plantower PMS7003	Weather resistant, AirCasting App is managed by HabitatMap, a 501(c)(3) raising awareness about the impact of the environment on human health	(Sousan et al., 2017) (B. C. Singer & Delp, 2018)	3
Dylos DC1100 PRO (ID3)	$290	Internal storage, serial connector.	Dylos	The Dylos also uses its own computer program to interpret sensor readings that are stored internally.	(Northcross et al., 2013) (Williams, Kaufman, et al., 2014) (Steinle et al., 2013) (Polidori et al., 2016b) (Manikonda et al., 2016) (Jiao et al., 2016*) (Sousan et al., 2016*) (Han et al., 2017*) (Hojaiji et al., 2017)	3

Sensor	Cost	Communication	Sensor	Features	Previous Studies	No. of Units Tested
TSI BlueSky (ID4)	N/A	Serial connector.	Dual Plantower PMSA003			2
Purple Air II (ID5)	$229	SD card, serial connector, and WiFi.	Dual Plantower PMS5003	Also provides temperature, RH, and pressure.	(Polidori et al., 2016b) (B. C. Singer & Delp, 2018) (Feenstra et al., 2019)	3

*different version of sensor from same manufacturer tested in previous work

6.2.2 Experimental Setup

We subjected each of these sensors as well as reference instruments to particle sources in a series of environmental conditions and particle sources. A schematic of the experimental setup is shown in Figure 6.1. The low-cost sensors were placed inside a chamber with dimensions of 46" (L) x 62" (W) x 35" (H) (1.17 m x1.57 m x 0.89 m), built out of 4" (0.10 m) thick rigid insulation, labeled "Testing Chamber" in Figure 6.1. These sensors were elevated on wire racks to allow adequate airflow around them, similar to the setup in Zou et al. (2020a). A photograph of the interior of the testing chamber (insulation chamber) is given in Figure 6.2. Throughout all experiments, air was drawn from the testing chamber by our reference instruments: a TSI Scanning Mobility Particle Sizer (SMPS) Model 3938, which included a Model 3081 long DMA and a model 3775 Condensation Particle Counter (CPC); and a TSI Aerodynamic Particle Sizer (APS) Model 3321, as in previous work (Zou, Young, Chen, et al., 2020; Zou, Young, Wickey, et al., 2020). To avoid any additional bias, we did not pass the particles through a diffusion drier prior to detection by the SMPS and APS (i.e., the sensors and the reference instruments are both detecting "wet" particles).

Temperature and RH were controlled in the testing chamber by siphoning air from an automatically controlled four cubic foot (0.11 m^3) environmental chamber (ESPEC Inc.; labeled as "Controlled Environmental Chamber" in Figure 1) and injecting the conditioned air into the chamber housing the sensors through a pump. This was done rather than testing sensors directly in the conditioned chamber in order to prevent deposition of particles onto the evaporator and heating coils in the conditioned chamber. The flow rate of air pumped

into the testing chamber from the controlled environmental chamber was set to 6 L/min via two critical orifices in order to equal the flow rate drawn by the reference instruments. A thermistor and thin film capacitance humidity sensor (Fisher Scientific Traceable ±0.4 °C, ±1.5% RH) were placed inside the testing chamber to record psychrometric conditions.

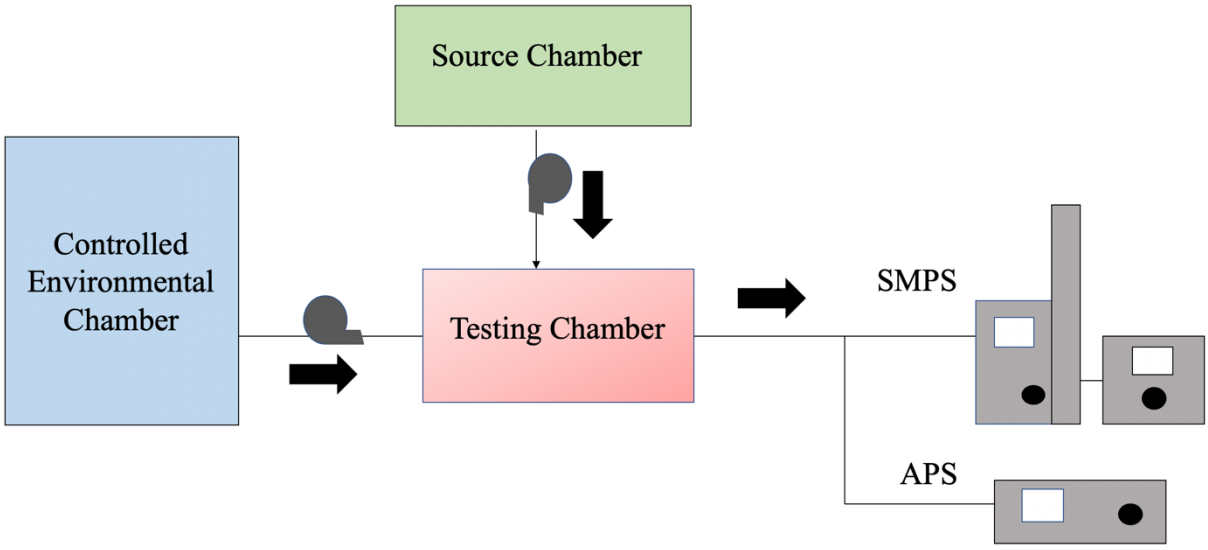

Figure 6.1: Schematic of the experimental setup

Figure 6.2: Photograph of interior of insulation testing chamber with sensors on racks.

6.2.3 Experimental Protocol

Twenty-five decay tests were conducted under different temperature and RH conditions, listed in Table 6.3. These conditions represent an optimized experimental matrix that simultaneously ensured good statistical properties in the outputs, covered the range of conditions in which we were interested for indoor environments, and included some repeated experimental conditions in order to evaluate the consistency of any response. Unlike outdoor investigations of temperature and RH effects, this optimized design resulted in temperature and RH effects that were uncorrelated.

We used incense and burnt toast smoke as two representative indoor particle sources. To generate incense particles, we used stick incense (sandalwood flavor), igniting it with a direct flame and then blowing out the flame to allow slow smoldering of the stick

to produce more smoke particles. We then put the stick into the source chamber prior to transfer into the testing chamber. To generate burnt toast smoke, we used a toaster to heat the bread several times until smoke was generated and placed the toaster inside the source chamber. Once the concentration reached a high concentration (roughly 100 to 1000 μg m^{-3}), the source was removed from the source chamber, and the particle concentration in the testing chamber was allowed to naturally decay. At the beginning of each test, we generated a high concentration of particles in yet another chamber, labeled "Source Chamber" in Figure 6.1, and pumped the particle-laden air into the testing chamber. We then stopped injecting the source, and let the concentration in the chamber naturally decay (mainly via extraction of chamber air by the reference instruments) until all sensors' concentration reached near zero. The only sinks within the chamber were gravitational settling, deposition on chamber walls and sensors, and removal of chamber air by the reference instruments. This procedure is similar to the decay tests conducted in Zou, Young, Chen, et al. (2020). Particle generation and behavior in the chamber was repeatable under similar chamber conditions. We provide one example of two repeated experiments with same T and RH condition in Additional Tables and Figures Figure 6.10; while there is some noise in the mass mode particle diameter, both the estimated mass concentration and the duration of the experiment are fairly consistent.

Table 6.3. Experimental conditions for decay tests

Run	T [°C]	RH [%]		**Run**	T [°C]	RH [%]		**Run**	T [°C]	RH [%]
1	20	40		**10**	30	15		**19**	40	30
2	30	60		**11**	40	30		**20**	25	10
3	20	60		**12**	35	75		**21**	40	40
4	30	90		**13**	35	45		**22**	40	30
5	30	30		**14**	20	25		**23**	20	25
6	30	90		**15**	27	75		**24**	15	30
7	20	90		**16**	30	30		**25**	15	20
8	22.5	75		**17**	40	90				
9	40	60		**18**	27.7	45				

6.2.4 Data Analysis

Because the low-cost devices and reference instruments had different sampling and averaging frequencies, we averaged all data into one-minute bins to allow direct comparison between all events. SMPS and APS data were merged using the approach of Khlystov et al. (2004). We assumed a spherical shape for particles from both sources (L. Wallace, 2007). To convert SMPS+APS data to mass concentrations, we assumed that the dry density of particles generated by incense was 1.06 g/cm^3 (Cheng et al., 1995; B. C. Singer & Delp, 2018), and toast is 0.94 g/cm^3 (B. C. Singer & Delp, 2018). Because both of these material densities are close to that of water (~1 g/cm^3), the hygroscopic uptake of water will have negligible effects on calculated wet particle mass concentrations (< 3% error for aerosol water contents up to 50%).

To evaluate the effect of temperature and RH on the sensors' outputs, we needed to establish a metric for describing accuracy. Most research on low-cost sensors evaluates sensors' performance by comparing low-cost sensor output to that of research grade instruments (Rai et al., 2017). Two often-used metrics are the coefficient of determination (R^2) of the linear regression between the low-cost PM sensor output and the reference instrument output (Karagulian et al., 2019) and the slope of this linear regression (Karagulian et al., 2019; Rai et al., 2017), both of which are used in this study. R^2 describes the correlation between the two outputs and the slope provides an indication of how the sensor concentration varies with changing reference instrument concentration. An ideal sensor would, therefore, have both R^2 and slope of unity. Each slope and R^2 that we present represent one decay test using one instance of the same type of sensor.

We sought to establish the relationship between T/RH and the slopes of the linear regression between the sensors and the reference instruments. In order to do this, we fit a linear, a quadratic and a two-factor interaction model for T/RH and slopes. We determined that a single-variable linear regression is more appropriate than a quadratic model or a two-factor interaction model for capturing this relationship. Model fitting parameters can be found in the Additional Tables and Figure (Table 6.6).

6.3 Results and discussion

In this section, we first present results illustrating the effect of each variable in isolation, and then we attempt to quantify the relative importance of each variable in determining sensor performance. Finally, we apply our correction algorithm to sensor outputs and assess the improvement.

6.3.1 Temperature effects

In Figure 6.3, we show an illustrative example of the response of one sensor's (ID2) response to incense during four decay tests under the same RH but different temperature conditions (panel a) and three repeated trials at 40 ^{o}C and 30% RH (panel b). The markers represent the average across three instances of this sensor, and the error bars represent the standard deviation among different instances of the same sensor. We highlight two features of Figure 6.3 that are generally true for most sensors tested:

1. Results of repetitions of experimental conditions track each other well (Figure 6.3b).

2. There is an apparent difference in data at different temperatures, but the results for one temperature for a given sensor type mostly falls within one standard deviation of the results for other temperatures especially at concentration lower than 100 µg/m^3, suggesting temperature may not be a significant determining variable for sensor output (Figure 6.3a).

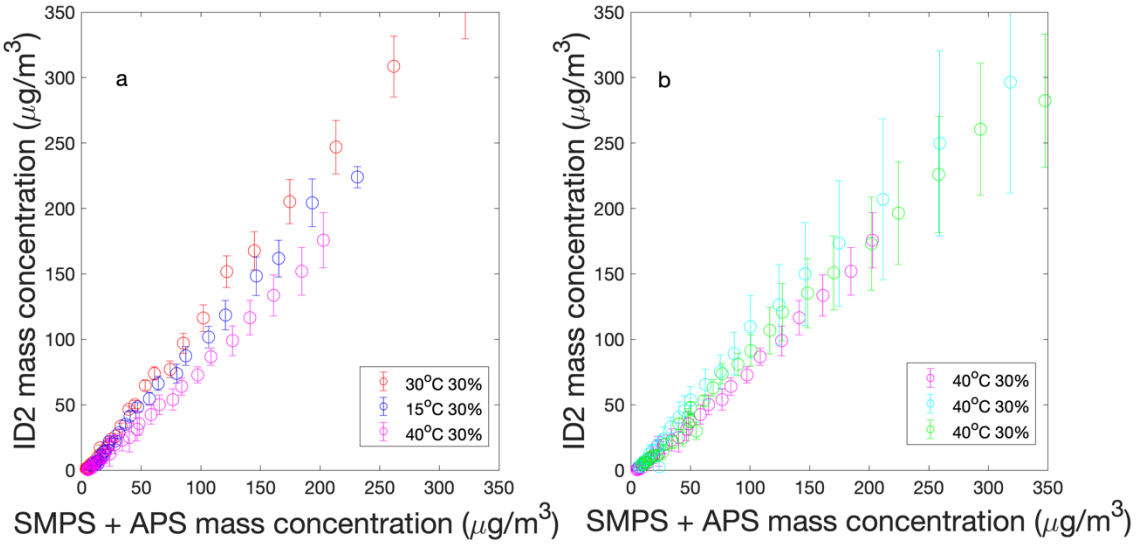

Figure 6.3: Example decay tests conducted under same RH but different temperature conditions (Figure 6.3 (a)) and repeated experiment conditions (Figure 6.3 (b)) using incense as the PM sources for the three ID2 sensors. Markers represent the mean, and error bars represent the standard deviation.

In order to quantify this second conclusion, we fit a linear regression to data from each experiment to obtain the slope and R^2 for that particular experiment (i.e., one combination of temperature and RH from Table 6.3). We then regressed 1) the slopes of all experiments and 2) the R^2 values of all experiments to the temperatures at which they were performed, to determine if temperature had a significant effect on slope or R^2 across the different experiments. We use p-value of the slope to indicate if the slopes are equal to

"0" at 0.01 significance level. An example of this is provided in Figures 6.4 and 6.5 for ID2 using incense as the particle source. In Figures 6.4 and 6.5, individual points are the R^2 and slope values (y-axis), respectively, from each experiment, as a function of the temperature at which the experiment was conducted (x-axis). The markers in Figures 6.4 and 6.5 are color-coded by RH.

The p-value of the resulting linear model shown in Figure 6.4 is 0.26 and its R^2 is practically zero, indicating very low confidence that effect of temperature on the sensors' correlation to the references instruments is distinguishable from pure chance. We show similar results for all sensors tested in Table 6.4.

In Figure 6.5, we show the results of similar hypothesis testing for the effect of temperature on slope of the linear regression between low-cost sensor output and that of reference instruments. Again, although there is an apparent increasing trend in the derived slopes with increasing temperature, the p-value (0.61) suggests that this is not significantly different from zero. Table 6.4 shows that the p-values for all instance of sensors are greater than 0.01, implying that there may be no relationship between temperature and slopes between sensors and instruments.

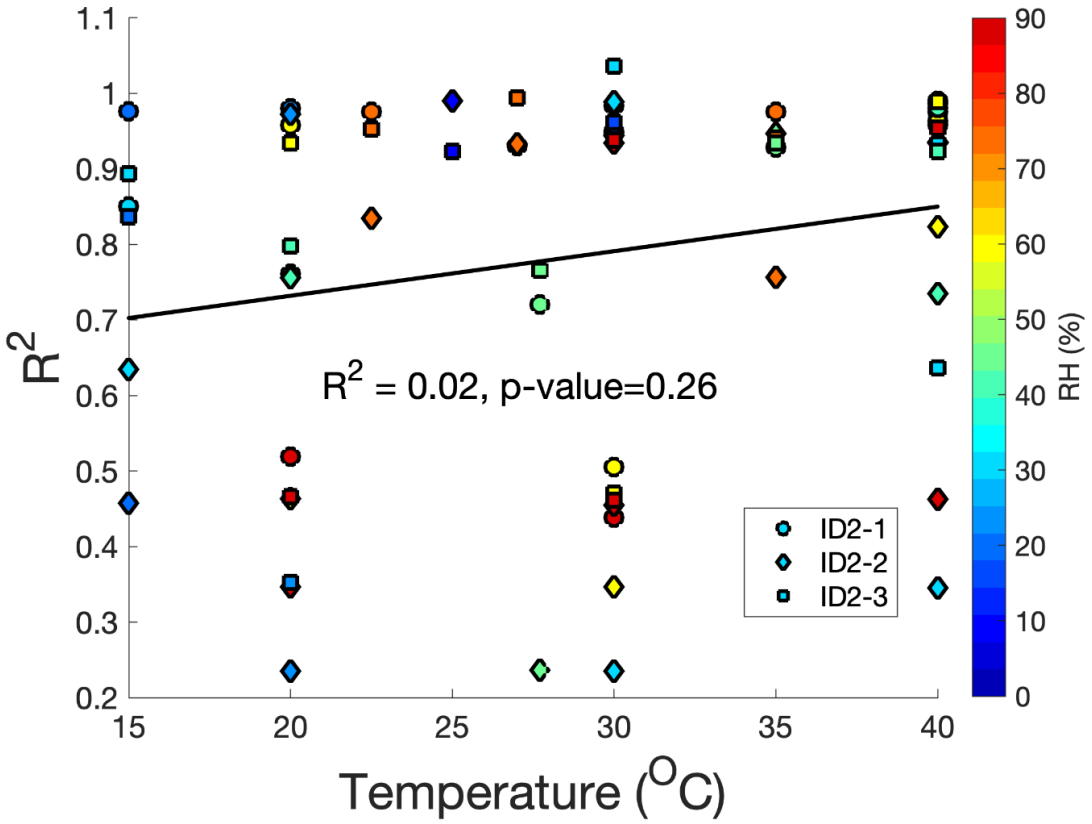

Figure 6.4: The relationship between temperature and the R^2 value from linear regression of each experiment for all three instances of ID2 and the reference instruments (SMPS+APS)

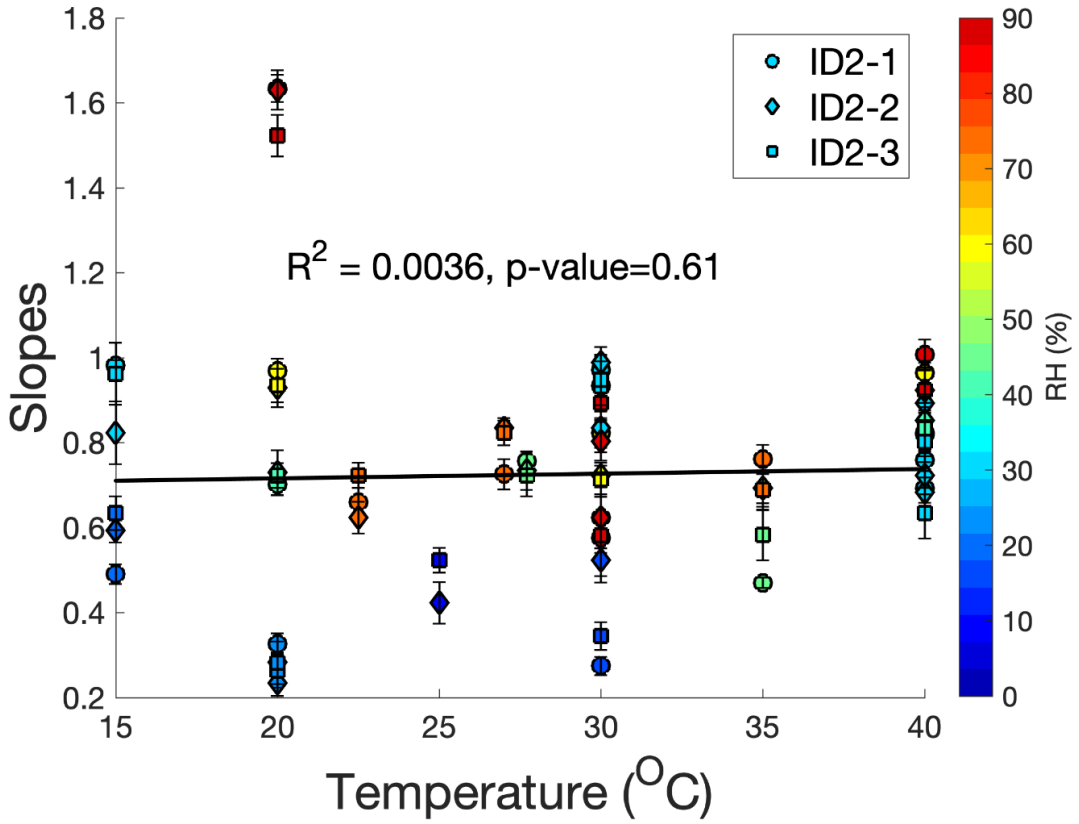

Figure 6.5: The relationship between temperature and slopes from linear regression of each experiment for all three instances of ID2 and the reference instruments (SMPS+APS). Error bars represent the standard error of the slope from linear regression.

Table 6.4: Slope, Standard error (SE), and p-values of a linear regression between Temperature and R^2 or slopes of individual experiments, using incense and toast as the source. Multiple entries for a given sensor represent different instances of that sensor

	Incense						**Toast**					
Comparison	**T vs. R^2**			**T vs. slope**			**T vs. R^2**			**T vs. slope**		
Sensor	slope	SE	p-value	slope	SE	p-value	Slope	SE	p-value	slope	SE	p-value
ID1	0.008	0.005	0.281	0.005	0.012	0.126	-0.005	0.005	0.345	-0.001	0.012	0.988
ID2	0.005 0.007 0.005	0.004 0.006 0.005	0.246 0.352 0.165	-0.003 0.004 0.001	0.007 0.006 0.006	0.960 0.504 0.827	0.001 0.001 0.002	0.005 0.001 0.001	0.832 0.943 0.901	0.001 0.010 0.008	0.007 0.009 0.008	0.825 0.891 0.903
ID3	0.009 0.007 0.006	0.004 0.005 0.005	0.065 0.073 0.039	0.002 0.001 -0.003	0.005 0.004 0.005	0.788 0.942 0.396	-0.007 -0.005 -0.002	0.008 0.003 0.004	0.268 0.268 0.549	0.005 0.004 -0.001	0.009 0.008 0.007	0.593 0.385 0.435
ID4	0.007 0.003	0.006 0.004	0.211 0.235	0.009 0.016	0.009 0.010	0.299 0.096	-0.007 -0.001	0.005 0.001	0.272 0.136	-0.004 -0.001	0.010 0.011	0.559 0.867
ID5	0.007 0.004 0.004	0.007 0.006 0.006	0.100 0.059 0.069	0.021 0.023 0.020	0.012 0.017 0.009	0.078 0.058 0.043	-0.004 -0.006 -0.001	0.005 0.004 0.004	0.634 0.190 0.328	-0.001 0.001 0.001	0.015 0.013 0.001	0.963 0.981 0.891
BS1	-0.004 -0.007	0.004 0.002	0.182 0.281	0.001 0.010	0.018 0.002	0.455 0.558	0.003 0.005	0.006 0.005	0.461 0.765	0.013 0.001	0.017 0.021	0.99 0.436
BS2	0.006 0.003 0.003	0.006 0.004 0.003	0.983 0.948 0.979	0.028 0.010 0.033	0.029 0.018 0.009	0.278 0.404 0.834	-0.016 -0.007 -0.007	0.009 0.007 0.007	0.520 0.379 0.168	0.001 0.003 0.001	0.003 0.002 0.005	0.227 0.879 0.382
BS3	0.002 0.003	0.006 0.004	0.567 0.695	-0.016 -0.002	0.008 0.009	0.835 0.161	-0.007 -0.004	0.006 0.004	0.13 0.41	-0.006 -0.004	0.001 0.013	0.777 0.469

6.3.2 RH effect

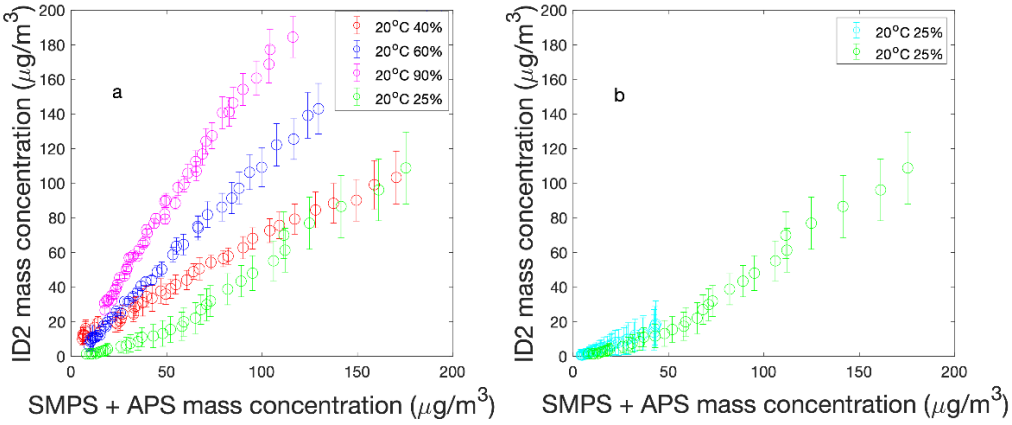

Figure 6.6: Example decay tests conducted under same temperature but different RH conditions (Figure 6.6 (a)) and repeated experiment condition (Figure 6.6 (b))using incense as the PM sources (ID2 sensors). Markers represent the mean, and error bars represent the standard deviation.

In Figure 6.6 we present results analogous to those in Figure 6.3, but with fixed temperature (at 20 °C) and varying RH between experiments, with two repeated trials at 25% RH in Figure 6.6b. Unlike in Figure 6.3, the differences between different experiments do not appear to agree within measurement uncertainty: the experiments at 90% RH had the greatest slope, followed by 60% RH, 40% RH, and 25% RH. Similar results were observed for all of the other sensors (see Table 6.7-6.12 in the Additional Tables and Figures).

Similar to the temperature experiments, we also evaluated how RH affects sensor performance by considering the relationship of RH to slope and R^2. Example results are

shown in Figures 6.7 and 6.8, and Table 6.5 provides a summary across all sensors. Figure 6.7 demonstrates the relationship between RH and R^2 for ID2 and suggests there is no statistically significant relationship between the RH and R^2 (p-values are all greater than 0.01) for this sensor. This trend holds true for all sensors tested (Table 6.5), with a single exception of one instance of one sensor (ID3) for one particular source (incense), which may indicate a problem with that one specific instance of that sensor. This suggests that although several previous works have shown a relationship between sensor performance and RH conditions, the correlation to reference instrument outputs does not seem to be significantly affected for the sensors and conditions tested.

We sought to clarify this further by looking at not just the correlation, but the magnitude of the low-cost sensor response, as quantified by the slope of the regression between the sensor signal and that of the reference instrument. Interestingly, as shown in Figure 6.8, RH has a clear, statistically-significant effect (p-value < 0.01) on the slope of the regression line between ID2 and the reference instruments for incense as the particle source. That is, the output from the sensor increased with increasing RH, which is consistent with previous studies (Han et al., 2017; Zamora et al., 2019; Liu et al., 2017b; Morawska et al., 2018; Wang et al., 2015).

Again, this trend holds true for other sensors tested, as shown in Table 6.5. Every sensor tested showed a significant effect for RH when subjected to toast smoke. Interestingly, several sensors showed no statistically-significant effect on RH versus slope for incense particles at 99% confidence level, but for toast smoke all sensors showed a significant effect; any potential explanation for this is purely speculative, so we do not elaborate here.

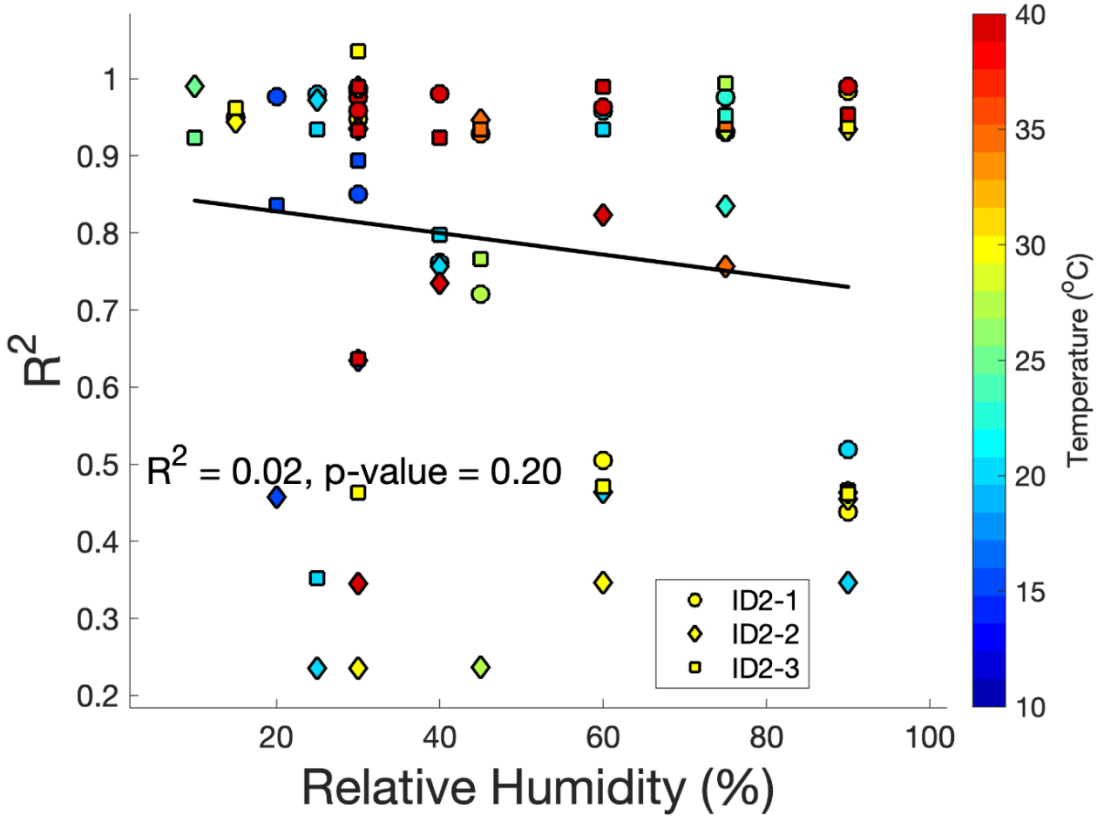

Figure 6.7: The relationship between RH and the R^2 value from linear regression of each experiment for all three instances of ID2 and the reference instruments (SMPS+APS)

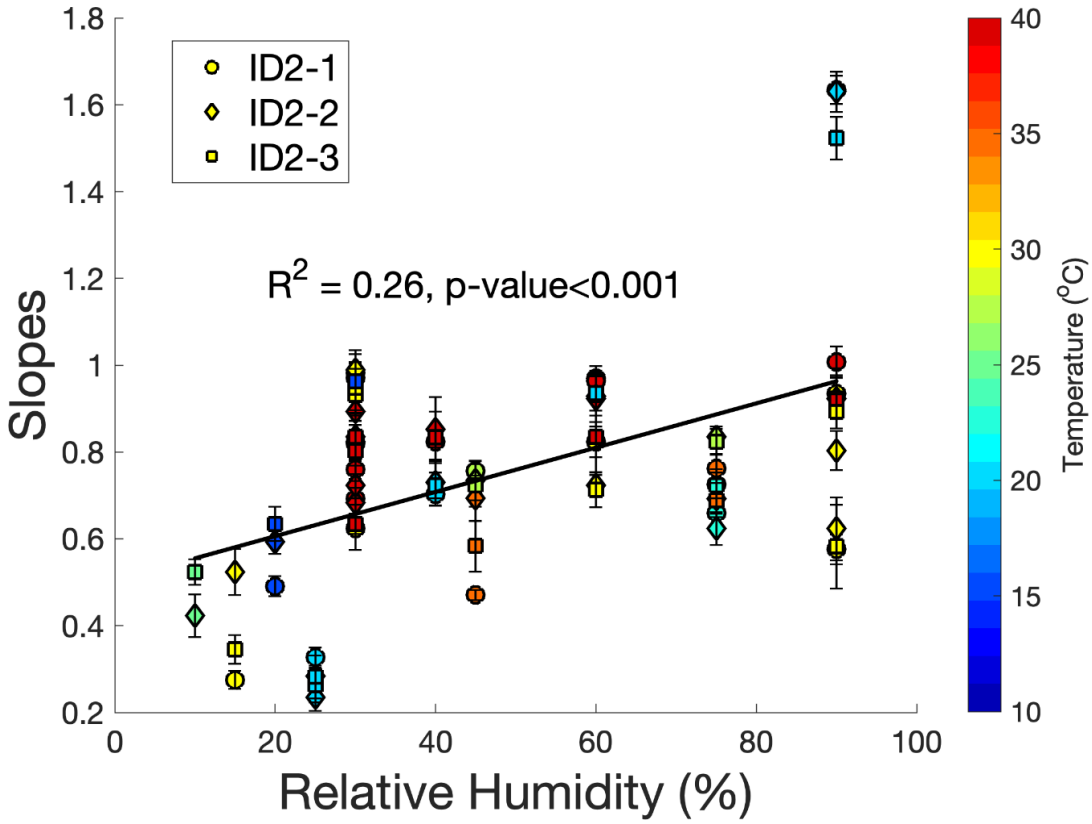

Figure 6.8: The relationship between RH and slopes from linear regression of each experiment for all three instances of ID2 and the reference instruments (SMPS+APS). Error bars represent the standard error of the slope from linear regression.

Table 6.5: Slope, Standard error (SE), and p-values of linear regression between RH and R^2, RH and slope using incense and toast as the PM sources. Multiple entries for a given sensor represent different instances of that sensor.

	incense						**toast**					
Comparison	**RH vs. R^2**			**RH vs. slope**			**RH vs. R^2**			**RH vs. slope**		
Sensor	slope	SE	p-value	slope	SE	p-value	slope	SE	p-value	slope	SE	p-value
ID1	-0.001	0.001	0.310	0.008	0.003	0.010	0.001	0.002	0.593	0.015	0.003	**1.5e-5**
ID2	-0.002	0.002	0.950	0.005	0.002	**0.003**	0.001	0.001	0.722	0.008	0.002	**1.4e-4**
	-0.001	0.002	0.203	0.005	0.001	**0.008**	0.001	0.001	0.836	0.014	0.001	**3.8e-4**
	-0.001	0.002	0.832	0.001	0.002	0.010	-0.001	0.001	0.635	0.010	0.002	**5.0e-5**
ID3	-0.001	0.002	0.990	-0.001	0.002	0.575	0.001	0.003	0.834	0.007	0.002	**5.0e-4**
	0.003	0.001	0.832	-0.001	0.001	0.623	0.001	0.001	0.938	0.004	0.003	**0.008**
	0.002	0.002	0.037	-0.001	0.001	0.452	-0.001	0.001	0.539	0.012	0.003	**0.006**
ID4	0.001	0.002	0.391	0.008	0.002	0.025	0.001	0.002	0.429	0.014	0.004	**4.1e-4**
	0.001	0.002	0.132	0.009	0.003	0.015	-0.001	0.001	0.643	0.017	0.004	**1.3e-4**
ID5	-0.001	0.002	0.623	0.011	0.003	0.036	0.001	0.001	0.864	0.015	0.004	**1.6e-4**
	-0.001	0.001	0.894	0.010	0.003	**0.002**	0.001	0.002	0.471	0.013	0.001	**1.0e-4**
	0.001	0.001	0.559	0.010	0.002	**0.007**	-0.001	0.002	0.792	0.020	0.004	**2.8e-4**
BS1	-0.001	0.001	0.469	0.001	0.001	0.024	-0.002	0.002	0.956	0.002	0.005	**1.9e-4**
	-0.001	0.002	0.963	0.011	0.005	0.036	0.001	0.001	0.992	0.021	0.001	**0.008**
BS2	-0.001	0.002	0.990	0.012	0.008	0.032	0.003	0.003	0.265	0.004	0.001	**0.006**
	0.001	0.002	0.981	0.023	0.005	0.052	0.002	0.003	0.483	0.002	0.002	**0.007**
	0.001	0.001	0.879	0.007	0.003	0.012	-0.001	0.002	0.167	0.002	0.001	**0.004**
BS3	-0.001	0.001	0.962	0.008	0.002	**0.007**	-0.001	0.002	0.990	0.012	0.003	**2.1e-4**
	0.001	0.002	0.932	0.009	0.002	**0.008**	0.001	0.001	0.981	0.014	0.004	**0.006**

6.3.3 Variability between Sensors, Sources, and Repeated Experiments

Our matrix of sensors combined with two particle sources and some repeated experimental conditions enables the investigation of variability in the relative response of the sensors to the reference instruments.

Variability between Experimental Conditions

To investigate the cause of the variability among experiments, we conducted an n-way analysis of variance (ANOVA) using input values from Tables 6.7 and Table 6.10. Table 6.7 and Table 6.10 include the average slopes from the linear regression between the sensors and the reference instrument under the 25 pairs of T/RH conditions for both incense and burnt toast smoke particles. The dependent variables were the slopes, and independent variables were the sensor used, the particle source, T, and RH. We then calculated the proportion of variance (ω^2):

$$\omega^2 = \frac{SSB - (a-1)MSE}{SST + MSE} \quad Eq.\ 6.1$$

where SSB is the sum of squares due to a given independent variable, a is the number of independent variables, MSE is the mean square error, and SST is the total sum of squares. Results of this analysis suggest that the sensor model, particle source, T, and RH accounted for 15.2%, 4.7%, 5.3%, and 11.1% of the variability, respectively.

These n-way ANOVA results suggest that the type of sensor used has the largest contribution to overall variance in our results, suggesting that although the sensors are all nephelometers, the form factor, wavelength of light, processing algorithm, and other "operating" differences can result in large variability. The results for RH and particle

source are consistent with our previous results in Chapter 5, suggesting that variations in the sensors' response can occur as RH varies or as the particle source varies. Variations in T account for roughly 5% of the variability in the slopes, which is inconsistent with our results in, e.g., Figure 6.5; however, there is some noise in, e.g., Figure 6.8, for a given RH. Therefore, T may account for a small, yet statistically insignificant, role in affecting the sensors' outputs.

6.3.3.1 Variability in Repeated Experiments

To quantify differences between repeated T and RH pairs (e.g., Experiments 14 and 23 in Table 6.3), we calculated the relative difference in the slopes for each sensor if there were two replicates or the relative standard deviation between the slopes if experiments were conducted in triplicate. These results are presented in Table E.6.8, separated by particle source. Generally, the results are more stable when $T < 40\ ^{o}C$, which could be related to the fact that the sensor manufacturers tend to report 40 ^{o}C as the upper bound of the sensors' working temperature; this fact could also contribute to the fractional variance for T in our n-way ANOVA results.

Some of this variability may be related to instance-to-instance variability for a given sensor, which can be estimated using results from Additional Tables and Figures Table 6.7 and 6.8, Table 6.10 and Table 6.11. For example, ID3 tends to have high variability in Table 6.7, and it also tends to have high "relative standard error" for both incense and toast smoke. In fact, we identified both ID3 and BS2 as having lower "manufacturer consistency" in previous work (Zou, Young, Wickey, et al., 2020). This instance-to-instance variability may also be part of the explanation for the large fraction of

"random" error in our n-way ANOVA (i.e., the error that cannot be explained by our independent variables).

6.3.3.2 Variability in Plantower-Based Sensors

Because four of our integrated devices incorporated some version of a Plantower sensor (ID1, ID2, ID4, and ID5), we investigated whether there were any systematic trends between those devices and BS3. To visualize this, we present the ratio of the slope from an integrated device to the slope from the bare sensor for a given experiment in Figure 6.9. Qualitatively, there is considerable noise among individual experiments (markers in the figure). To quantify these differences, we conducted significance testing. None of the slopes of the best-fit lines shown in the figure were significantly different from zero at a 99% confidence level. We also tested the mean values of the ratios presented in Figure 6.9 to determine if they were significantly different from unity. For ID1 and ID4, these means were not significantly different from unity at a 99% confidence level; however, for ID2 and ID5, they were significantly different. Consequently, our data suggests that while different form factors and proprietary algorithms can result in discrepancies between these Plantower-based sensors, but none of them appears to be disproportionately influenced by RH, relative to each other.

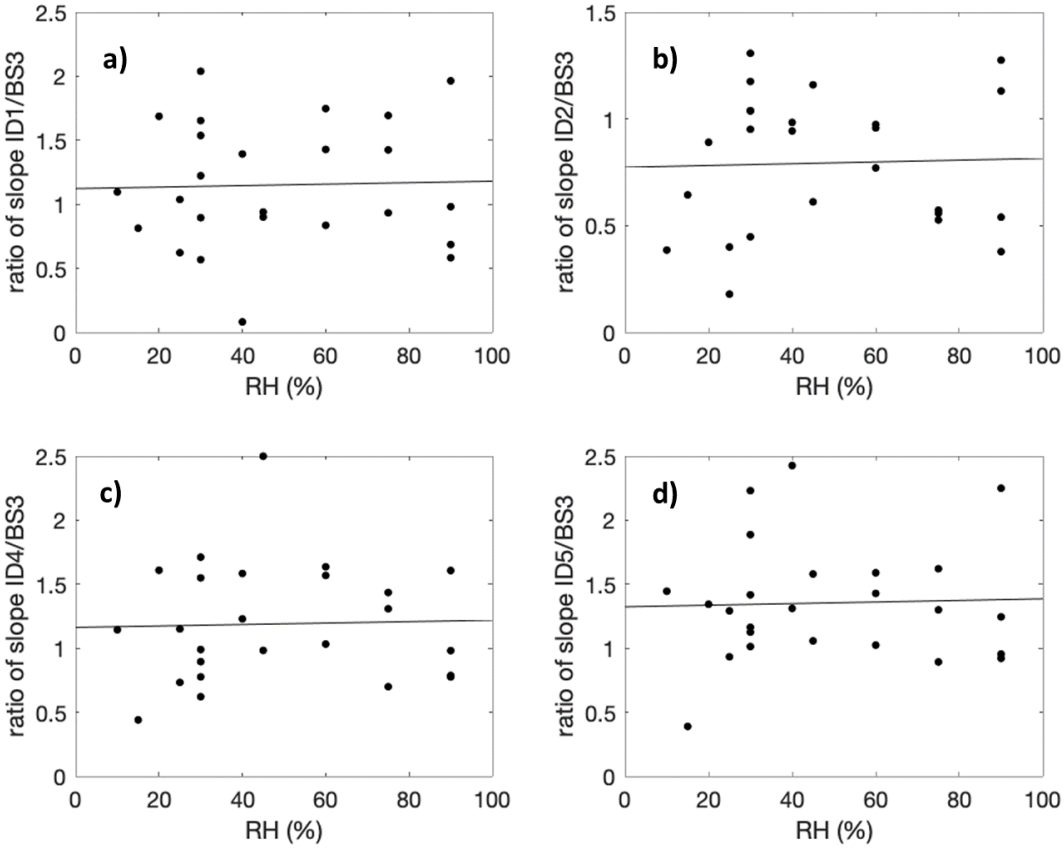

Figure 6.9. The relationship of the ratio of slopes between the integrated devices containing a Plantower sensor and the bare Plantower 5003 sensor (BS3) as a function of RH: a) ID1; b) ID2; c) ID4; and d) ID5. Note the different scales on the y-axes.

6.4 Conclusion

In this study we conducted an optimized matrix of twenty-five decay tests under different temperature and RH conditions using two common challenge sources and simultaneous measurement with reference instruments. Analysis of results showed a few interesting results:

1) No statistically significant relationship between temperature and low-cost sensor output emerged for any sensor tested in the range of 15 °C to 40 °C, suggesting this

variable may not be a large contributor to sensor performance degradation for indoor environments and likely does not need to be taken into consideration. This is largely in line with previous research on the subject.

2) Similarly, no significant relationship between the correlation of low-cost sensor output and humidity emerged from the tests conducted in the range of 10 % to 90 %. This suggests that while the magnitude of sensor output may change with humidity, the signal remains correlated to that of reference instruments and a simple calibration may improve performance.
3) There is a significant linear relationship between RH and the relative response of the low-cost particle sensors. This may be related to changes in the particles' complex refractive index as hygroscopic growth occurs, thus affecting the light-scattering measurements by the low-cost sensors.
4) In our n-way ANOVA, the sensor model appears to be the largest source of variability, implying that sensors produced by different manufacturers perform differently. Moreover, the agreement between the Plantower-based sensors (ID1, ID2, ID4, ID5, and BS3) is variable; however, none of these sensors are disproportionately affected by variations in RH.

For indoor particle sensor's application, there may be a need to monitoring temperature and RH for the correction on the sensor' output to provide more accurate measurement. For the correction of RH, Malings et al. (2020) and Tryner et al. (Tryner et al., 2020) both developed physics-based correction equations for low-cost particle sensors to account for uptake of water by particles at elevated RH. In this study, we did not explore the use of these correction equations for our sensors' data, since those corrections used

dried particles to obtain their reference concentrations, which our reference instruments sampled the humidified particles.

6.5 Additional Tables and Figures

Model Development and Statistical Tests

We sought to establish the significance of each variable of interest in determining the accuracy of the low-cost sensors. In order to do this, we fit linear and quadratic and two-factor interaction models for temperature and RH separately, with forms given below.

Linear models:

1a: $y = c_o + c_1 \cdot RH$

1b: $y = c_o + c_2 \cdot T$

Non-linear model (quadratic):

2a: $y = c_o + c_1 \cdot RH + c_3 \cdot RH^2$

2b: $y = c_o + c_2 \cdot T + c_4 \cdot T^2$

Two-factor-interaction model:

3: $y = c_o + c_1 \cdot RH + c_2 \cdot T + c_5 \cdot RH \cdot T$

The intent of this exercise was not to develop a predictive model, but to quantify the significance of each independent variable in determining sensor performance. Thus for each model, we calculated p-values as an indicator of the significance of the relationship between two environmental factors and sensor performance. For each model we calculated

adjusted R^2 values to adjust for the number of variables. we presents the result in Table 6.5. Adjusted R^2 are provided because it adjusts for the number of variables. Generally, we observed that the R^2/adjust R^2 of linear model for T and RH are lower than the quadratic model and the two-factors-interaction model for most of the sensors, highest R^2/ adjusted R^2 are observed for two-factors-interaction model. The reason of increase of R^2/adjusted R^2 is partially because quadratic model and the two-factor-interaction model are adding more variables, but the coefficient for these two models are not statistically significant. Thus, we believe that the linear model is more appropriate model than quadratic model and the two-factors-interaction model.

Table 6 6: Summary of model coefficients using linear, non-linear and two-factor interaction model to evaluate the relationship between sensor performance and temperature/RH from decay test using incense as the PM source (data from Table 6.7-6.12. The following equation were used to fit models (c_o-c_5 are the coefficients for models, R^2 is the coefficient of determination, p is p-values for the coefficients for c_1-c_5).

Sensor type		**c_o**	**c_1**	**c_2**	**c_3**	**c_4**	**c_5**	**R^2**	**R^2_{adj}**	**p**
Airthinx	1a	0.696	0.008					0.22	0.14	✓
	1b	0.481		0.021				0.10	0.06	×
	2a	0.634	0.011		-2.8e-5			0.18	0.10	×
	2b	-0.921		0.129		-1.8e-3		0.15	0.07	×
	3	0.858	-0.008	-0.005			5e-5	0.30	0.19	×
Airbeam-1	1a	0.314	0.006					0.35	0.33	✓
	1b	0.207		0.143				0.19	0.15	✓
	2a	-0.115	0.027		-1.9e-4			0.50	0.45	✓
	2b	0.170		0.017		-4.2e-5		0.19	0.12	×
	3	-0.045	-0.007	0.013			-2.8e-5	0.49	0.42	×
Airbeam-2	1a	0.466	0.004					0.28	0.25	✓
	1b	0.384		0.010				0.16	0.12	×
	2a	0.267	0.014		-9.2e-5			0.33	0.27	×
	2b	0.207		0.023		-2.3e-4		0.16	0.09	×
	3	0.166	0.006	0.011				0.40	0.31	×
Airbeam-3	1a	0.463	0.003					0.16	0.12	✓
	1b	0.321		0.010				0.16	0.13	✓
	2a	0.215	0.015		-1.2e-4			0.24	0.17	×
	2b	0.209		0.051		-6.9e-4		0.20	0.13	×
	3	0.393	0.001	-0.002			-1.5e-5	0.31	0.21	×
Dylos-1	1a	0.282	-0.001					0.01	0.03	×

Sensor type		c_o	c_1	c_2	c_3	c_4	c_5	R^2	R^2_{adj}	p
	1b	0.176		0.001				0.003	-0.02	×
	2a	0.237	0.001		-2.0e-5			0.01	-0.04	×
	2b	-0.726		0.070		-0.001		0.01	-0.07	×
	3	0.046	0.003	0.008			-1.4e-5	0.03	0.008	×
Dylos-2	1a	0.305	-1.9e-4					0.001	-0.10	×
	1b	0.285		3.7e-4				0.001	-0.04	×
	2a	0.024	0.002		-2.8e5			0.005	-0.04	×
	2b	-0.600		0.06		-0.001		0.01	-0.08	×
	3	0.071	0.005	0.008			-1.8e-5	0.02	0.01	×
Dylos-3	1a	0.339	-0.004					0.01	-0.11	×
	1b	0.413		-0.003				0.03	-0.03	×
	2a	0.306	8.9e-4		-1e-5			0.01	-0.01	×
	2b	-0.314		0.051		-9.6e-5		0.02	-0.07	×
	3	0.126	0.006	0.007		-2.5e-5		0.11	0.06	×
TSI-1	1a	0.714	0.007					0.30	0.28	✓
	1b	0.787		0.010				0.05	0.03	×
	2a	0.392	0.023		-1.4e-4			0.34	0.31	×
	2b	0.297		0.047		-6.3e-4		0.05	-0.03	×
	3	0.575	0.005	0.005			6e-5	0.33	0.23	×
TSI-2	1a	0.635	0.009					0.37	0.35	✓
	1b	0.630		0.016				0.11	0.07	×
	2a	0.392	0.026		-1.5e-4			0.42	0.36	×
	2b	-0.177		0.072		-9.8e-4		0.13	0.05	×
	3	0.878	0.004	-0.008			6e-5	0.49	0.42	×
PurpleAir-1	1a	0.740	0.011					0.32	0.29	✓
	1b	0.659		0.021				0.12	0.08	×
	2a	0.773	0.009		1.4e-4			0.32	0.26	×
	2b	0.213		0.052		-5.8e-4		0.13	0.05	×
	3	0.850	0.005	-0.002			4.9e-4	0.43	0.36	×
PurpleAir-2	1a	0.776	0.009					0.27	0.24	✓
	1b	0.575		0.022				0.16	0.12	×
	2a	0.450	0.025		-1.4e-4			0.30	0.23	×
	2b	0.616		0.197		-5.4e-5		0.16	0.08	×
	3	0.850	-0.005	-0.002			4.9e-4	0.43	0.35	×
PurpleAir-3	1a	0.833	0.009					0.32	0.29	✓
	1b	0.701		0.020				0.15	0.11	×
	2a	0.828	0.009		-2.2e-6			0.32	0.26	×
	2b	-0.005		0.074		-9.3e-4		0.17	0.09	×
	3	0.721	0.004	5.6e-4			2.8e-4	0.44	0.36	×
Honeywell-1	1a	0.047	0.001					0.18	0.14	✓
	1b	0.065		0.001				0.02	-0.01	×
	2a	0.024	0.002		-1e-5			0.18	0.11	×
	2b	-0.141		0.017		-2.7e-5		0.07	-0.001	×
	3	0.042	1.7e-4	1.6e-4			1.6e-5	0.20	0.08	×
Honeywell-2	1a	0.541	0.011					0.17	0.13	✓
	1b	0.792		0.010				0.01	-0.02	×
	2a	0.026	0.036		-2.3e-4			0.20	0.13	×
	2b	-0.824		0.133		-0.002		0.03	-0.03	×
	3	0.527	0.007	6e-4			1.3e-4	0.18	0.06	×
Sharp-1	1a	0.614	0.022					0.27	0.24	✓

Sensor type		c_o	c_1	c_2	c_3	c_4	c_5	R^2	R^2_{adj}	p
	1b	0.907		0.028				0.04	0.004	×
	2a	0.642	0.021		1.2e-5			0.27	0.20	×
	2b	-0.207		0.112		-0.001		0.04	-0.03	×
	3	0.672	0.008	-7e-3			4.7e-4	0.30	0.19	×
Sharp-2	1a	0.823	-0.002					0.28	0.25	✓
	1b	0.492		0.007				0.12	0.08	×
	2a	1.059	-0.013		1e-4			0.29	0.22	×
	2b	1.834		-0.094		0.001		0.15	0.04	×
	3	1.105	-0.014	-0.009			4.1e-4	0.37	0.28	×
Sharp-3	1a	0.809	1e-4					0.001	-0.002	×
	1b	0.719		0.003				0.06	0.02	×
	2a	0.829	-7e-3		8.9e-6			0.003	0.001	×
	2b	0.861		-0.007		1.9e-4		0.07	0.03	×
	3	0.702	0.003	2e-4			-6e-3	0.06	0.03	×
Plantower-1	1a	0.559	0.008					0.38	0.36	✓
	1b	0.963		-3e-4				<0.001	-0.04	×
	2a	0.663	0.003		4e-4			0.39	0.33	×
	2b	-0.771		0.131		-0.002		0.17	0.09	×
	3	0.247	0.017	0.011			-3.3e-5	0.43	0.35	×
Plantower-2	1a	0.553	0.008					0.48	0.46	✓
	1b	1.314		-0.011				0.08	0.04	×
	2a	0.792	-0.002		1e-4			0.51	0.47	×
	2b	-0.770		0.146		-0.002		0.34	0.28	×
	3	0.925	0.013	-0.011			-2e-4	0.62	0.57	×

Note:
✓ for p-value indicates that the p-value for coefficient a,b,c,d,and e for that model are less than 0.01
× for p-value indicates that the p-values for coefficient a,b,c,d,and e for that model are all greater than 0.01
p-value for m are not provided in the table because all p-value for m are less than 0.01

Results of linear regressions for individual experiments

Table 6.7: Average slopes from linear regression between sensor and reference instrument under 25 temperature and RH conditions using incense

Test #	T	RH	ID1	ID2	ID3	ID4	ID5	BS1	BS2	BS3
1	15.00	20.00	1.08	0.57	0.16	1.03	0.86	0.26	0.91	0.64
2	15.00	30.00	0.42	0.87	0.07	0.46	0.75	0.36	0.73	0.74
3	20.00	25.00	0.56	0.36	0.53	0.66	0.84	0.68	1.11	0.90
4	20.00	25.00	1.10	0.19	0.16	1.22	1.37	0.45	1.05	1.06
5	20.00	40.00	0.05	0.60	0.26	0.75	0.80	0.27	1.25	0.61
6	20.00	60.00	1.02	0.94	0.22	1.26	1.25	1.04	1.95	1.22
7	20.00	90.00	0.74	1.62	0.41	1.00	1.17	0.55	1.83	1.27
8	22.50	75.00	1.71	0.67	0.24	1.57	1.56	0.51	1.35	1.20
9	25.00	10.00	0.91	0.32	0.21	0.95	1.20	0.04	1.04	0.83
10	27.00	75.00	1.40	0.79	0.31	1.05	1.34	1.66	3.61	1.50
11	27.70	45.00	1.09	0.74	0.31	1.19	1.28	0.48	1.47	1.21
12	30.00	15.00	0.48	0.38	0.19	0.26	0.23	0.17	0.70	0.59
13	30.00	30.00	1.26	0.98	0.35	0.80	1.46	0.74	1.20	1.03

14	30.00	30.00	2.10	1.07	1.13	1.02	1.16	1.39	1.85	1.03
15	30.00	60.00	1.10	0.75	0.25	1.26	1.10	0.51	1.00	0.77
16	30.00	90.00	1.07	0.59	0.15	1.21	1.49	0.68	1.50	1.56
17	30.00	90.00	1.60	0.88	0.26	1.60	2.03	0.75	1.70	1.63
18	35.00	45.00	0.47	0.58	0.12	1.25	0.79	0.31	0.76	0.50
19	35.00	75.00	2.10	0.71	0.28	1.78	2.01	0.40	1.83	1.24
20	40.00	30.00	0.60	0.30	0.20	0.60	0.78	0.44	0.75	0.67
21	40.00	30.00	0.86	0.68	0.12	0.89	1.16	0.13	1.00	0.52
22	40.00	30.00	1.23	0.83	0.31	1.24	1.51	0.57	1.57	0.80
23	40.00	40.00	1.24	0.84	0.29	1.41	2.16	1.05	2.24	0.89
24	40.00	60.00	1.66	0.91	0.20	1.49	1.51	0.49	1.51	0.95
25	40.00	90.00	1.65	0.95	0.17	1.35	1.89	1.22	2.73	0.84

Table 6.8: Average standard error for the slopes from linear regression between sensor and reference instrument under 25 temperature and RH conditions using incense.

Test #	**T**	**RH**	**ID1**	**ID2**	**ID3**	**ID4**	**ID5**	**BS1**	**BS2**	**BS3**
1	15.00	20.00	1.08	0.07	0.10	0.00	0.07	0.30	0.10	0.06
2	15.00	30.00	0.42	0.08	0.06	0.16	0.05	0.47	0.26	0.18
3	20.00	25.00	0.56	0.07	0.09	0.03	0.09	0.79	0.09	0.02
4	20.00	25.00	1.10	0.18	0.06	0.02	0.04	0.55	0.04	0.08
5	20.00	40.00	0.05	0.08	0.18	0.11	0.05	0.31	0.59	0.10
6	20.00	60.00	1.02	0.02	0.03	0.00	0.09	1.26	0.17	0.14
7	20.00	90.00	0.74	0.25	0.18	0.44	0.21	0.64	0.46	0.08
8	22.50	75.00	1.71	0.05	0.05	0.10	0.07	0.59	0.55	0.01
9	25.00	10.00	0.91	0.28	0.10	0.03	0.15	0.02	0.03	0.13
10	27.00	75.00	1.40	0.06	0.03	0.04	0.17	1.92	1.88	0.00
11	27.70	45.00	1.09	0.02	0.16	0.06	0.22	0.56	0.11	0.04
12	30.00	15.00	0.48	0.13	0.09	0.04	0.11	0.24	0.23	0.07
13	30.00	30.00	1.26	0.08	0.11	0.00	0.10	0.87	0.24	0.01
14	30.00	30.00	2.10	0.09	0.21	0.14	0.22	1.60	0.75	0.02
15	30.00	60.00	1.10	0.06	0.14	0.01	0.06	0.63	0.30	0.13
16	30.00	90.00	1.07	0.03	0.05	0.59	0.07	0.80	0.06	0.05
17	30.00	90.00	1.60	0.07	0.02	0.03	0.12	0.85	0.62	0.04
18	35.00	45.00	0.47	0.11	0.06	0.02	0.15	0.36	0.21	0.13
19	35.00	75.00	2.10	0.04	0.06	0.13	0.10	0.46	0.10	0.06
20	40.00	30.00	0.60	0.11	0.08	0.04	0.06	0.54	0.40	0.02
21	40.00	30.00	0.86	0.05	0.08	0.05	0.07	0.12	0.10	0.09
22	40.00	30.00	1.23	0.07	0.06	0.03	0.05	0.66	0.64	0.45
23	40.00	40.00	1.24	0.01	0.05	0.06	0.19	1.25	1.25	0.14
24	40.00	60.00	1.66	0.07	0.05	0.10	0.05	0.57	0.54	0.08
25	40.00	90.00	1.65	0.05	0.07	0.16	0.08	1.42	1.67	0.20

Table 6.9: Average R^2 from linear regression between sensor and reference instrument under 25 conditions using incense.

Test #	T	RH	ID1	ID2	ID3	ID4	ID5	BS1	BS2	BS3
1	15.00	20.00	0.92	0.76	0.60	0.96	0.75	0.89	0.85	0.96
2	15.00	30.00	0.55	0.79	0.78	0.75	0.63	0.84	0.76	0.80
3	20.00	25.00	0.98	0.23	0.89	0.63	0.98	0.86	0.73	0.54
4	20.00	25.00	0.99	0.00	0.71	0.95	0.96	0.92	0.90	0.95
5	20.00	40.00	0.66	0.77	0.59	0.77	0.73	0.80	0.81	0.73
6	20.00	60.00	0.99	0.79	0.58	0.96	0.89	0.92	0.90	0.97
7	20.00	90.00	0.60	0.44	0.76	0.75	0.77	0.49	0.82	0.79
8	22.50	75.00	0.93	0.92	0.90	0.95	0.96	0.91	0.72	0.99
9	25.00	10.00	0.99	0.00	0.53	0.72	0.98	0.61	0.83	0.94
10	27.00	75.00	0.97	0.95	0.58	0.96	0.61	0.74	0.66	0.97
11	27.70	45.00	0.49	0.57	0.48	0.83	0.79	0.44	0.39	0.53
12	30.00	15.00	0.97	0.95	0.68	0.51	0.60	0.46	0.65	0.99
13	30.00	30.00	0.95	0.55	0.90	0.92	0.91	0.77	0.85	0.73
14	30.00	30.00	0.97	1.00	0.65	0.21	0.95	0.49	0.94	0.99
15	30.00	60.00	1.00	0.44	0.86	0.72	0.81	0.34	0.69	0.71
16	30.00	90.00	0.64	0.45	0.81	0.78	0.87	0.67	0.57	0.57
17	30.00	90.00	0.98	0.95	0.86	0.94	0.92	0.95	0.88	0.92
18	35.00	45.00	0.39	0.94	0.74	0.66	0.60	0.48	0.61	0.33
19	35.00	75.00	0.93	0.89	0.70	0.99	0.97	0.16	0.95	0.99
20	40.00	30.00	0.96	0.77	0.88	0.96	0.91	0.91	0.93	0.99
21	40.00	30.00	0.97	0.84	0.89	0.99	0.94	0.62	0.86	0.58
22	40.00	30.00	0.99	0.95	0.86	0.97	0.99	0.83	0.93	0.91
23	40.00	40.00	0.97	0.88	0.90	0.95	0.95	0.91	0.93	0.98
24	40.00	60.00	0.99	0.93	0.86	0.99	0.96	0.81	0.94	0.98
25	40.00	90.00	0.98	0.80	0.86	0.96	0.92	0.91	0.96	0.96

Table 6.10: Average slopes from linear regression between sensor and reference instrument under 25 temperature and RH conditions using burnt toast smoke.

Test #	T	RH	ID1	ID2	ID3	ID4	ID5	BS1	BS2	BS3
1	15.00	20.00	0.36	0.23	0.12	0.54	0.69	0.39	0.02	0.33
2	15.00	30.00	0.44	0.34	0.36	0.43	0.51	0.73	0.04	0.30
3	20.00	25.00	0.62	0.50	0.16	0.67	0.74	1.00	0.07	0.76
4	20.00	25.00	0.98	0.79	0.53	1.18	1.39	1.94	0.18	1.39
5	20.00	40.00	0.38	0.36	0.19	0.47	0.55	0.82	0.02	0.26
6	20.00	60.00	1.71	0.85	0.21	1.74	1.46	1.30	0.07	1.21
7	20.00	90.00	0.38	0.32	0.18	0.42	0.49	0.81	0.04	0.25
8	22.50	75.00	0.59	0.53	0.56	0.55	0.87	1.21	0.19	0.96
9	25.00	10.00	0.61	0.41	0.28	0.85	0.95	1.81	0.15	0.98
10	27.00	75.00	0.24	0.31	0.02	0.32	0.49	0.34	0.11	0.20
11	27.70	45.00	0.47	0.51	0.37	0.37	0.72	0.82	0.14	0.37
12	30.00	15.00	0.47	0.44	0.30	0.41	0.60	0.68	0.08	0.80
13	30.00	30.00	0.26	0.48	0.15	0.28	0.61	0.33	0.02	0.21
14	30.00	30.00	1.40	0.84	0.26	1.26	2.26	1.42	0.16	0.84
15	30.00	60.00	1.38	NaN	0.18	1.54	2.13	2.49	0.21	1.47
16	30.00	90.00	2.10	1.49	1.28	1.62	1.89	2.41	0.31	2.26
17	30.00	90.00	0.49	0.77	0.09	0.67	0.97	0.58	0.03	0.54
18	35.00	45.00	0.73	0.89	0.42	0.61	0.66	1.19	0.12	0.55
19	35.00	75.00	0.28	0.35	0.31	0.68	0.30	0.52	0.24	0.85
20	40.00	30.00	0.42	0.30	0.12	0.30	0.51	0.26	0.01	0.04
21	40.00	30.00	0.69	0.50	0.16	0.73	0.85	0.85	0.05	0.47
22	40.00	30.00	0.38	0.47	0.50	0.65	0.79	0.90	0.19	0.52
23	40.00	40.00	0.83	0.76	0.38	0.84	1.46	2.29	0.28	0.77
24	40.00	60.00	0.98	0.69	0.42	0.84	1.23	2.34	0.35	0.80
25	40.00	90.00	1.02	0.87	0.52	0.93	1.41	2.24	0.29	0.53

Table 6.11: Average standard error for slopes from linear regression between sensor and reference instrument under 25 temperature and RH conditions using burnt toast smoke.

Test #	T	RH	ID1	ID2	ID3	ID4	ID5	BS1	BS2	BS3
1	15.00	20.00	0.36	0.00	0.16	0.21	0.23	0.01	0.01	0.09
2	15.00	30.00	0.44	0.04	0.18	0.04	0.14	0.08	0.01	0.06
3	20.00	25.00	0.62	0.10	0.07	0.17	0.18	0.00	0.02	0.02
4	20.00	25.00	0.98	0.12	0.38	0.02	0.15	0.02	0.10	0.18
5	20.00	40.00	0.38	0.05	0.07	0.04	0.08	0.02	0.02	0.07
6	20.00	60.00	1.71	0.34	0.02	0.33	0.15	0.01	0.03	0.02
7	20.00	90.00	0.38	0.03	0.06	0.03	0.16	0.02	0.01	0.06
8	22.50	75.00	0.59	0.05	0.05	0.22	0.10	0.04	0.07	0.00
9	25.00	10.00	0.61	0.07	0.06	0.01	0.02	0.04	0.04	0.00
10	27.00	75.00	0.24	0.20	0.01	0.11	0.11	0.08	0.16	0.06
11	27.70	45.00	0.47	0.07	0.13	0.24	0.25	0.10	0.11	0.04
12	30.00	15.00	0.47	0.09	0.08	0.03	0.17	0.11	0.04	0.02
13	30.00	30.00	0.26	0.40	0.12	0.02	0.21	0.01	0.01	0.03
14	30.00	30.00	1.40	0.03	0.08	0.06	0.20	0.02	0.05	0.04
15	30.00	60.00	1.38	NaN	0.06	0.08	0.16	0.59	0.08	0.07
16	30.00	90.00	2.10	0.06	0.07	0.46	0.60	0.08	0.05	0.06
17	30.00	90.00	0.49	0.28	0.13	0.12	0.02	0.28	0.02	0.08
18	35.00	45.00	0.73	0.56	0.02	0.17	0.07	0.07	0.08	0.06
19	35.00	75.00	0.28	0.07	0.45	0.12	0.09	0.02	0.31	0.00
20	40.00	30.00	0.42	0.04	0.19	0.14	0.07	0.12	0.01	0.03
21	40.00	30.00	0.69	0.14	0.07	0.18	0.11	0.37	0.00	0.04
22	40.00	30.00	0.38	0.30	0.41	0.29	0.36	0.14	0.15	0.45
23	40.00	40.00	0.83	0.12	0.13	0.00	0.73	0.09	0.02	0.10
24	40.00	60.00	0.98	0.23	0.45	0.21	0.82	0.02	0.50	0.10
25	40.00	90.00	1.02	0.09	0.40	0.01	0.08	0.14	0.10	0.05

Table 6.12: Average R^2 from linear regression between sensor and reference instrument under 25 conditions using burnt toast smoke.

Test #	T	RH	ID1	ID2	ID3	ID4	ID5	BS1	BS2	BS3
1	15.00	20.00	0.78	0.75	0.73	0.91	0.91	0.43	0.50	0.90
2	15.00	30.00	0.94	0.97	0.94	0.99	0.95	0.95	0.81	0.94
3	20.00	25.00	0.99	0.95	0.95	0.95	0.95	0.96	0.95	0.95
4	20.00	25.00	0.91	0.93	0.86	0.95	0.92	0.94	0.97	0.96
5	20.00	40.00	0.96	0.94	0.95	0.98	0.94	0.94	0.94	0.99
6	20.00	60.00	0.93	0.94	0.94	0.96	0.96	0.57	0.92	0.97
7	20.00	90.00	0.96	0.97	0.95	0.95	0.95	0.99	0.98	0.94
8	22.50	75.00	0.99	0.99	0.95	0.96	0.98	0.99	1.00	0.99
9	25.00	10.00	0.97	0.95	0.96	0.99	0.98	0.54	0.30	0.96
10	27.00	75.00	0.97	0.94	0.54	0.96	0.97	0.98	0.92	0.94
11	27.70	45.00	0.98	0.97	0.89	0.94	0.98	0.95	0.97	0.95
12	30.00	15.00	0.95	0.98	0.93	0.84	0.94	0.89	0.97	0.93
13	30.00	30.00	0.98	0.91	0.94	0.98	0.59	0.99	0.96	0.95
14	30.00	30.00	0.43	0.71	0.55	0.63	0.88	0.25	0.29	0.53
15	30.00	60.00	0.92	NaN	0.88	0.93	0.76	0.94	0.89	0.88
16	30.00	90.00	0.95	0.96	0.93	0.92	0.94	0.95	0.62	0.80
17	30.00	90.00	0.99	0.95	0.62	0.95	0.96	0.95	0.21	0.99
18	35.00	45.00	0.93	0.95	0.95	0.98	0.82	0.80	0.89	0.92
19	35.00	75.00	0.18	0.70	0.55	0.57	0.98	0.43	0.27	0.92
20	40.00	30.00	0.58	0.95	0.74	0.90	0.95	0.83	0.29	0.21
21	40.00	30.00	0.98	0.95	0.66	0.94	0.95	0.93	0.40	0.86
22	40.00	30.00	0.95	0.95	0.87	0.97	0.85	0.99	0.94	0.98
23	40.00	40.00	0.96	0.97	0.91	0.95	0.98	0.99	0.78	0.99
24	40.00	60.00	0.99	0.96	0.87	0.97	0.99	0.98	0.98	0.96
25	40.00	90.00	0.99	0.97	0.86	0.96	0.95	1.00	0.78	0.99

Table 6.13: Repeatability of experimental conditions. If n = 2, the value represents the relative difference, while if n = 3, the value represents the relative standard deviation. All values are expressed as percentages (%).

Source	T (ºC)	RH (%)	n	ID1	ID2	ID3	ID4	ID5	BS1	BS2	BS3
Incense	20	25	2	16.2	15.4	26.8	14.8	11.9	10.1	1.4	4.1
	30	30	2	12.5	2.2	26.3	6.1	5.7	15.2	10.6	0.0
	30	90	2	9.9	9.8	13.4	6.9	7.6	2.4	3.1	1.0
	40	30	3	35.3	45.2	45.4	35.2	31.7	59.5	37.9	21.1
Toast	20	25	2	11.3	11.2	26.8	13.7	15.2	16.0	22.0	14.7
	30	30	2	34.3	13.6	13.4	31.8	28.7	31.1	38.9	30.0
	30	90	2	31.0	15.9	43.4	20.7	16.0	30.6	41.1	30.7
	40	30	3	33.9	25.4	80.3	40.8	25.3	53.1	98.0	76.8

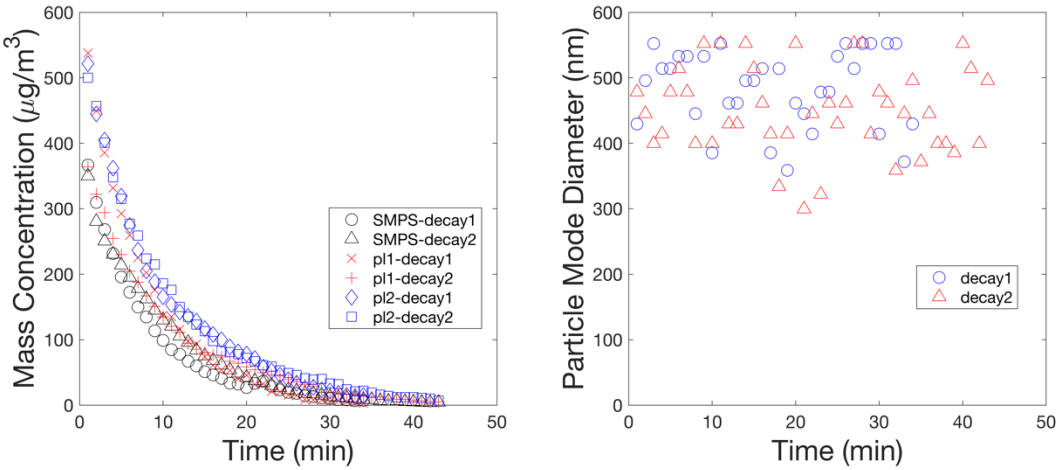

Figure 6.10: Sample data for two decay tests at 30 ºC and 90% RH using incense as the particle source. *Left panel*: Estimated mass concentrations for the combined SMPS+APS (SMPS) and both instances of the bare Plantower sensor (pl1 and pl2). *Right panel*: Mass mode diameter from the SMPS+APS size distributions.

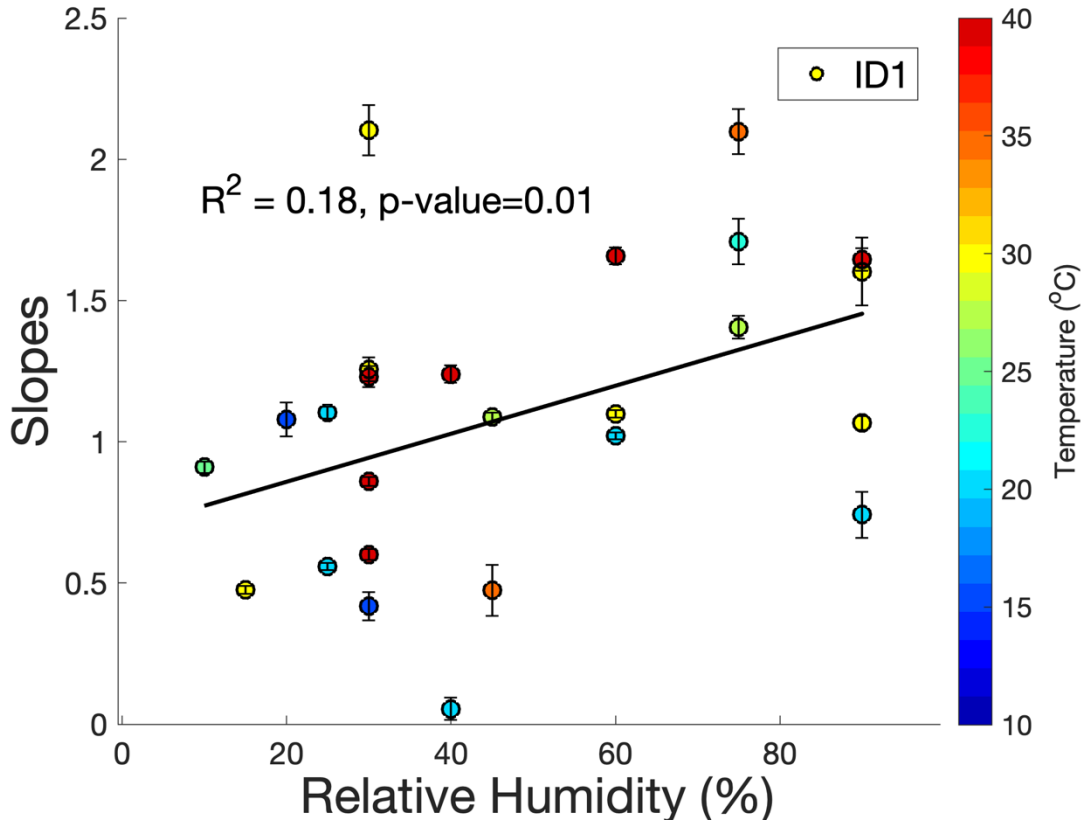

Figure 6.11: The relationship between RH and slopes from linear regression of each experiment during incense decay tests for ID1 (one instance) and the reference instruments (SMPS+APS). Error bars represent the standard error of the slope from linear regression.

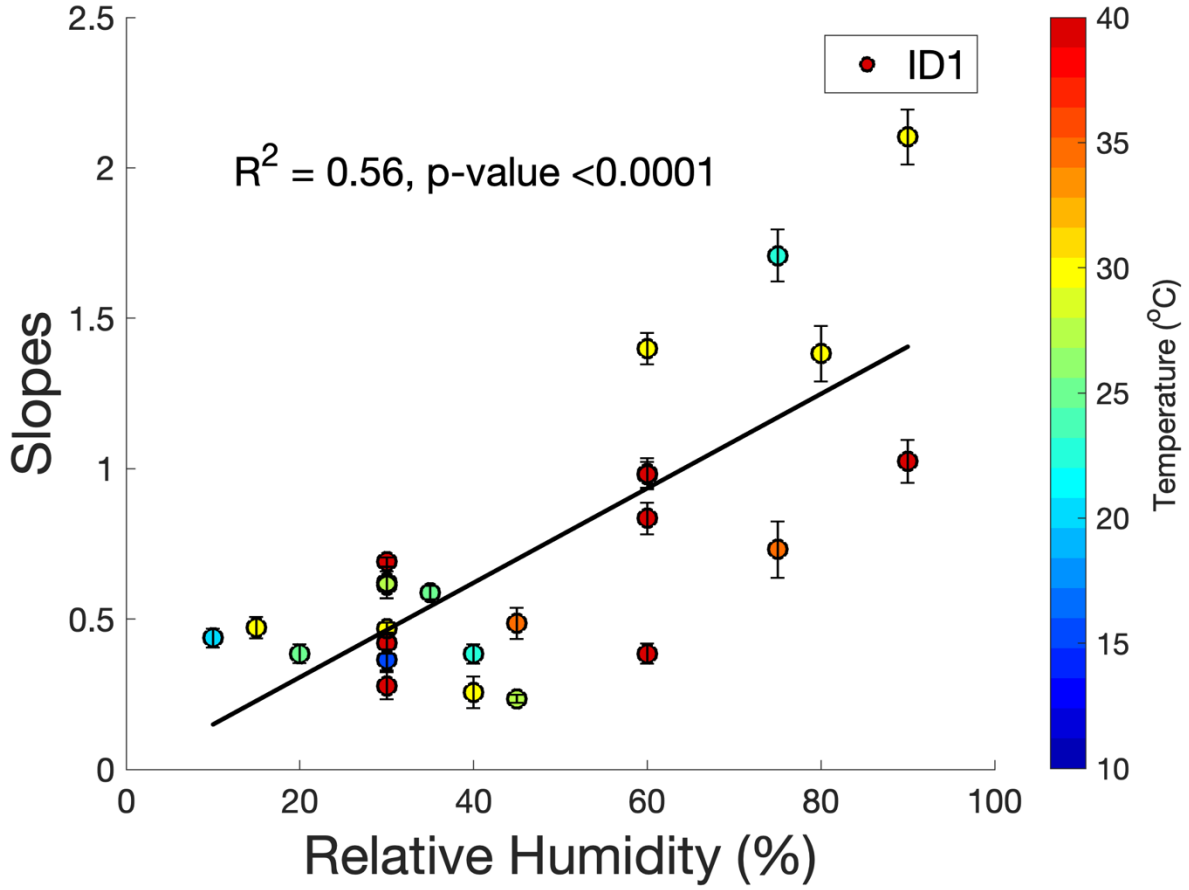

Figure 6.12: The relationship between RH and slopes from linear regression of each experiment during burning toast decay tests for ID1 (one instance) and the reference instruments (SMPS+APS). Error bars represent the standard error of the slope from linear regression.

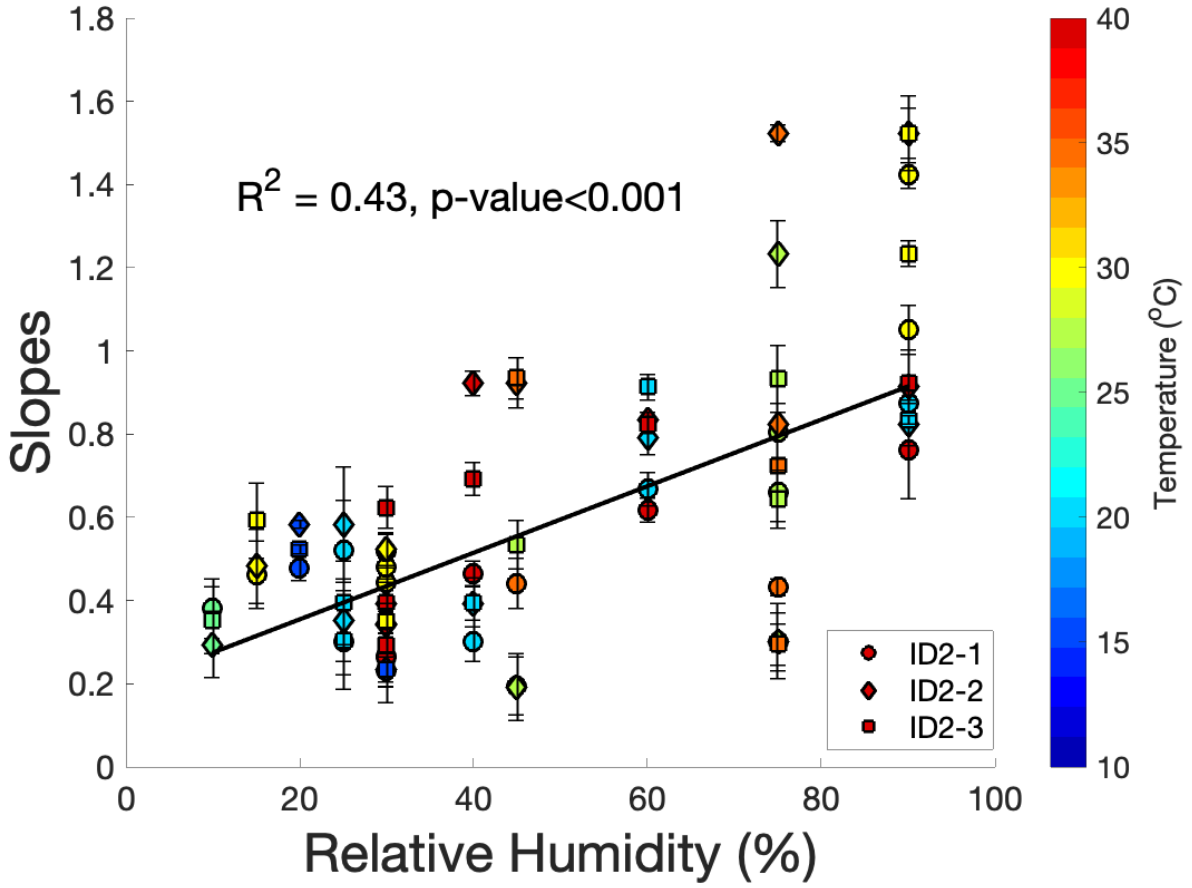

Figure 6.13: The relationship between RH and slopes from linear regression of each experiment during burning toast decay tests for all three instances of ID2 and the reference instruments (SMPS+APS). Error bars represent the standard error of the slope from linear regression. The linear regression line is fit to all the slopes from three instances.

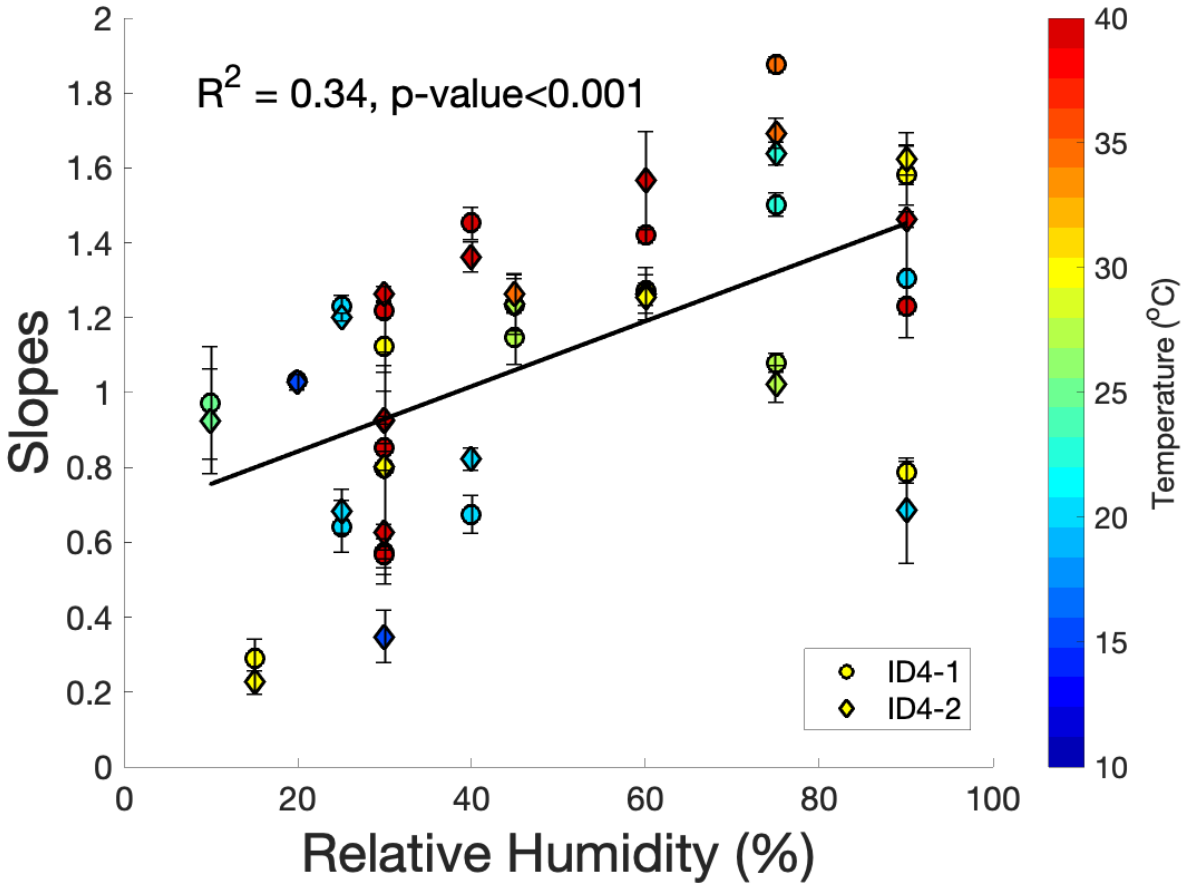

Figure 6.14: The relationship between RH and slopes from linear regression of each experiment during incense decay tests for both instances of ID4 and the reference instruments (SMPS+APS). Error bars represent the standard error of the slope from linear regression. The linear regression line is fit to all the slopes from two instances.

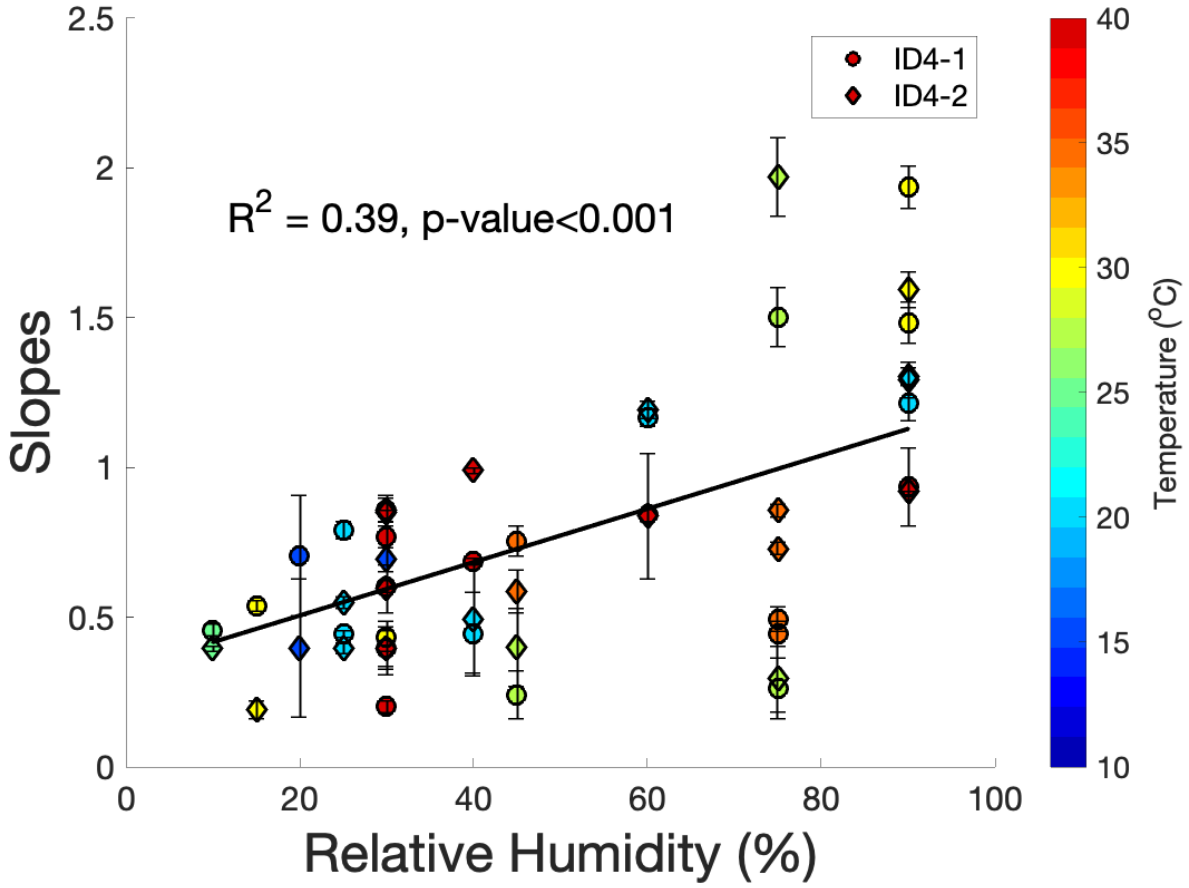

Figure 6.15: The relationship between RH and slopes from linear regression of each experiment during burning toast decay tests for both instances of ID4 and the reference instruments (SMPS+APS). Error bars represent the standard error of the slope from linear regression. The linear regression line is fit to all the slopes from two instances.

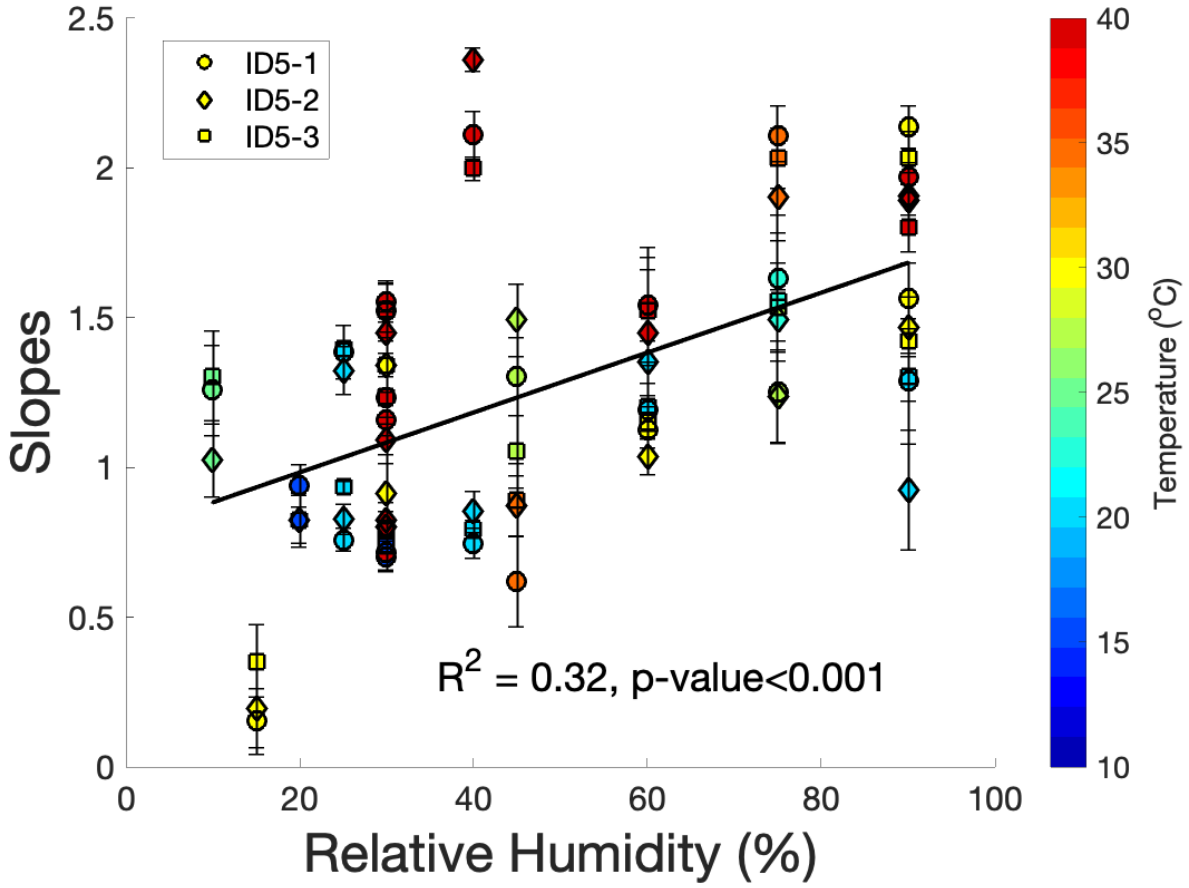

Figure 6.16: The relationship between RH and slopes from linear regression of each experiment during incense decay tests for all three instances of ID5 and the reference instruments (SMPS+APS). Error bars represent the standard error of the slope from linear regression. The linear regression line is fit to all the slopes from three instances.

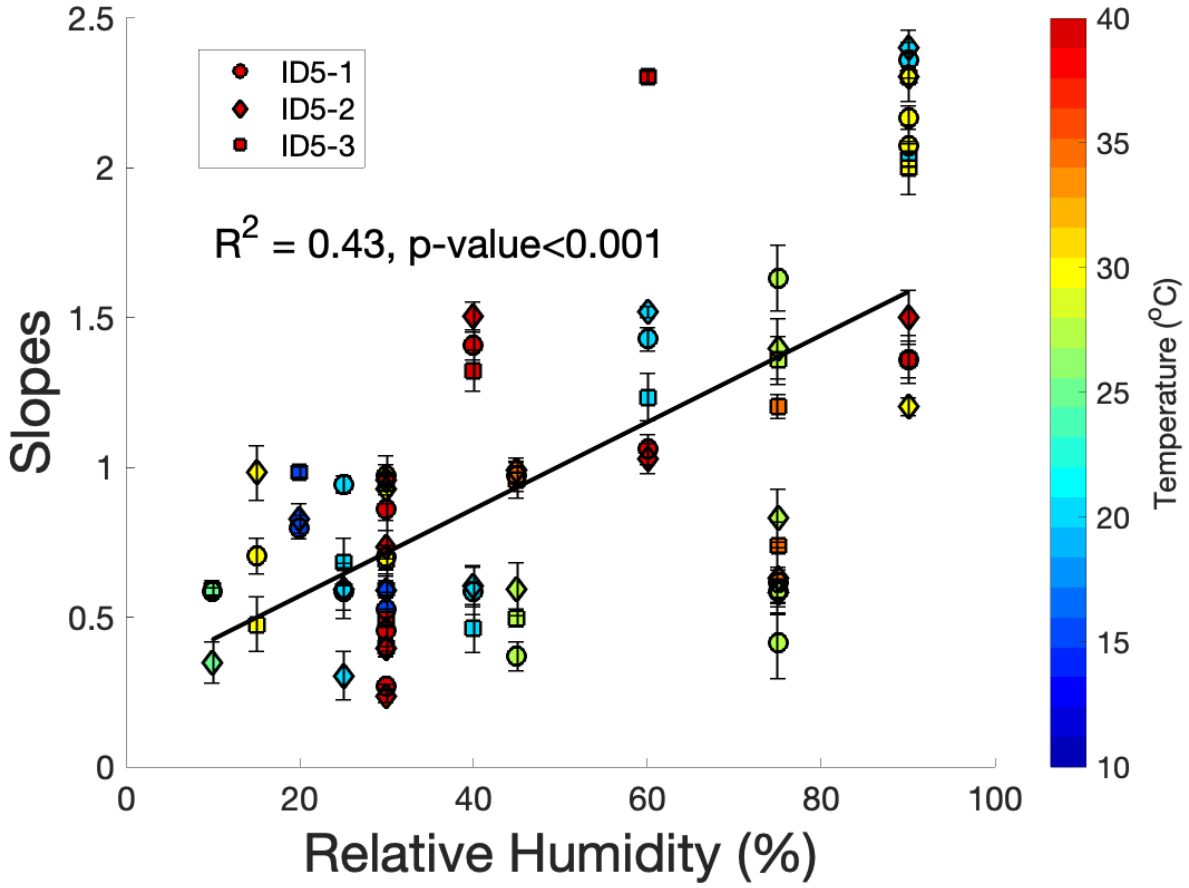

Figure 6.17: The relationship between RH and slopes from linear regression of each experiment during burning toast decay tests for all three instances of ID5 and the reference instruments (SMPS+APS). Error bars represent the standard error of the slope from linear regression. The linear regression line is fit to all the slopes from three instances.

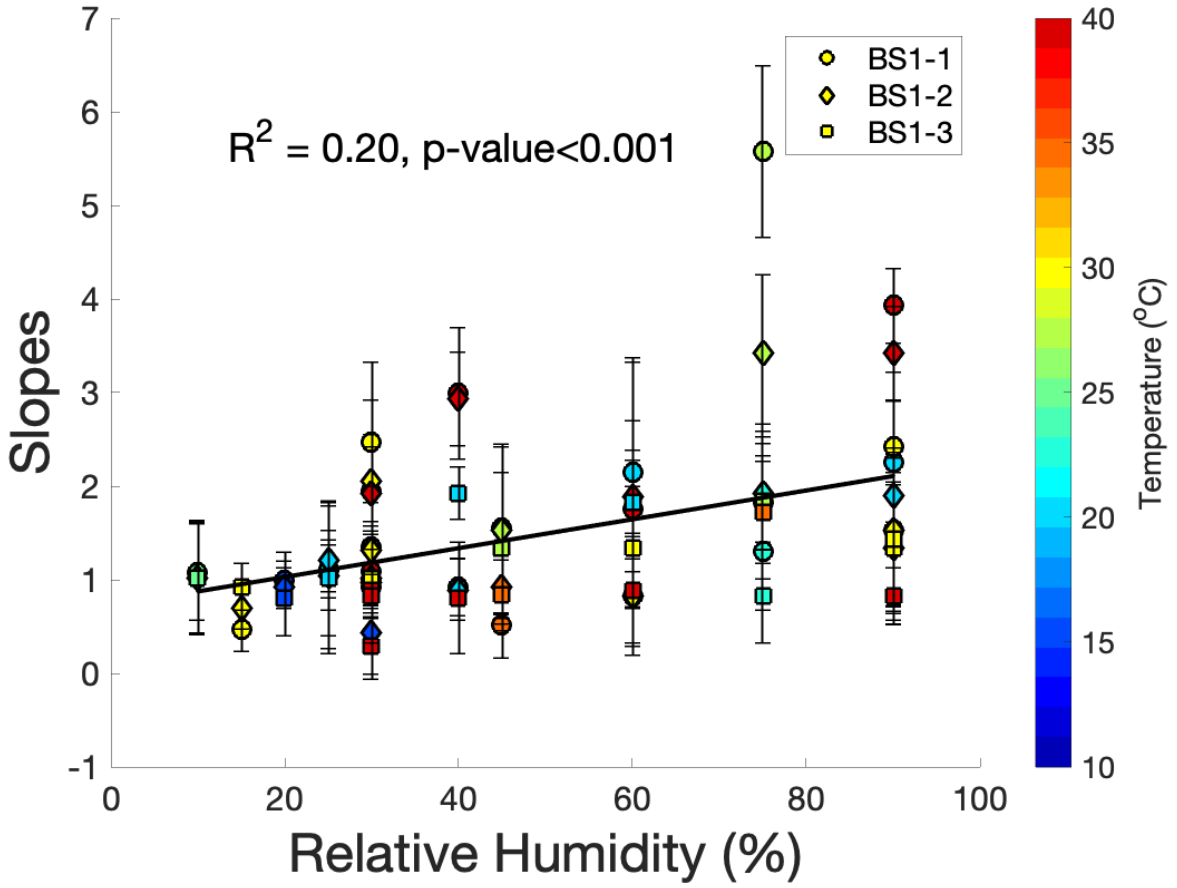

Figure 6.18: The relationship between RH and slopes from linear regression of each experiment during incense decay tests for all three instances of BS1 and the reference instruments (SMPS+APS). Error bars represent the standard error of the slope from linear regression. The linear regression line is fit to all the slopes from three instances.

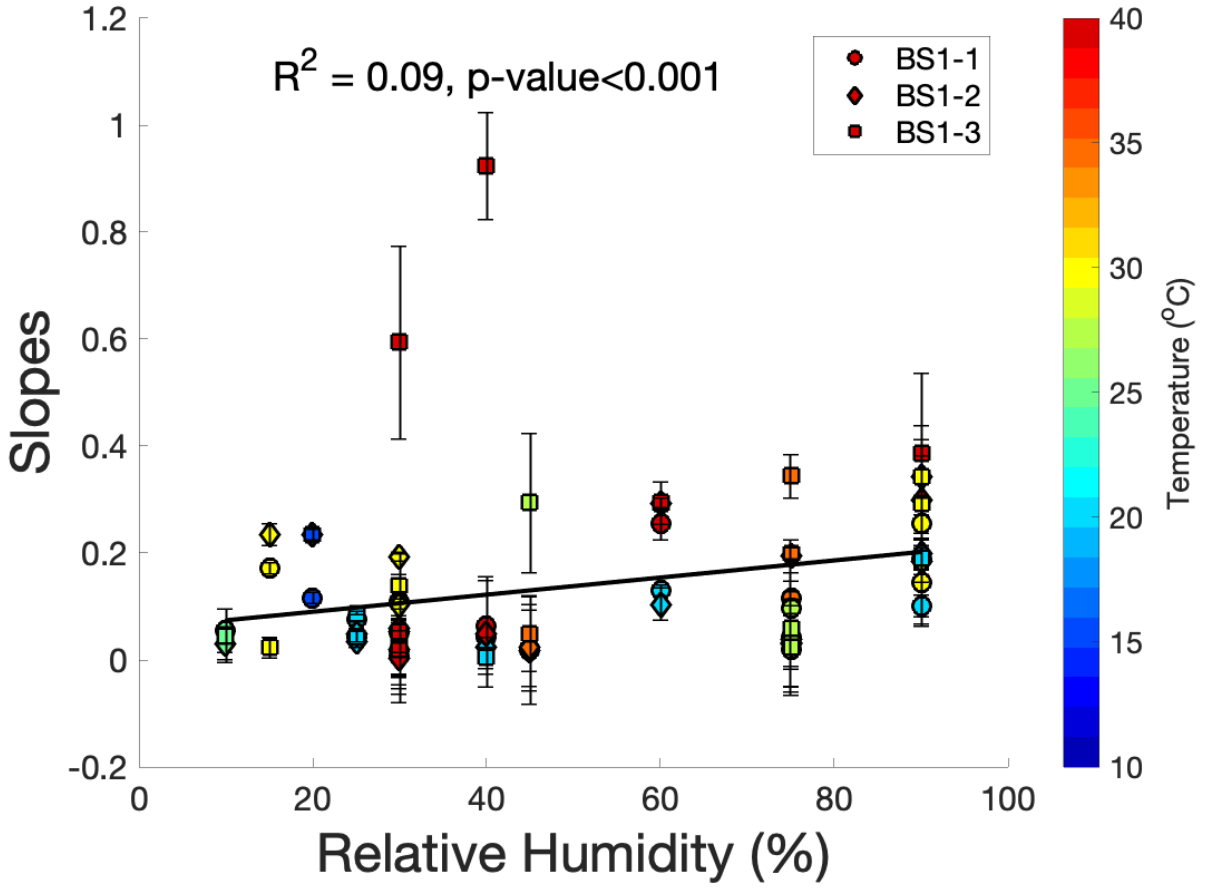

Figure 6.19: The relationship between RH and slopes from linear regression of each experiment during burning toast decay tests for all three instances of BS1 and the reference instruments (SMPS+APS). Error bars represent the standard error of the slope from linear regression. The linear regression line is fit to all the slopes from three instances.

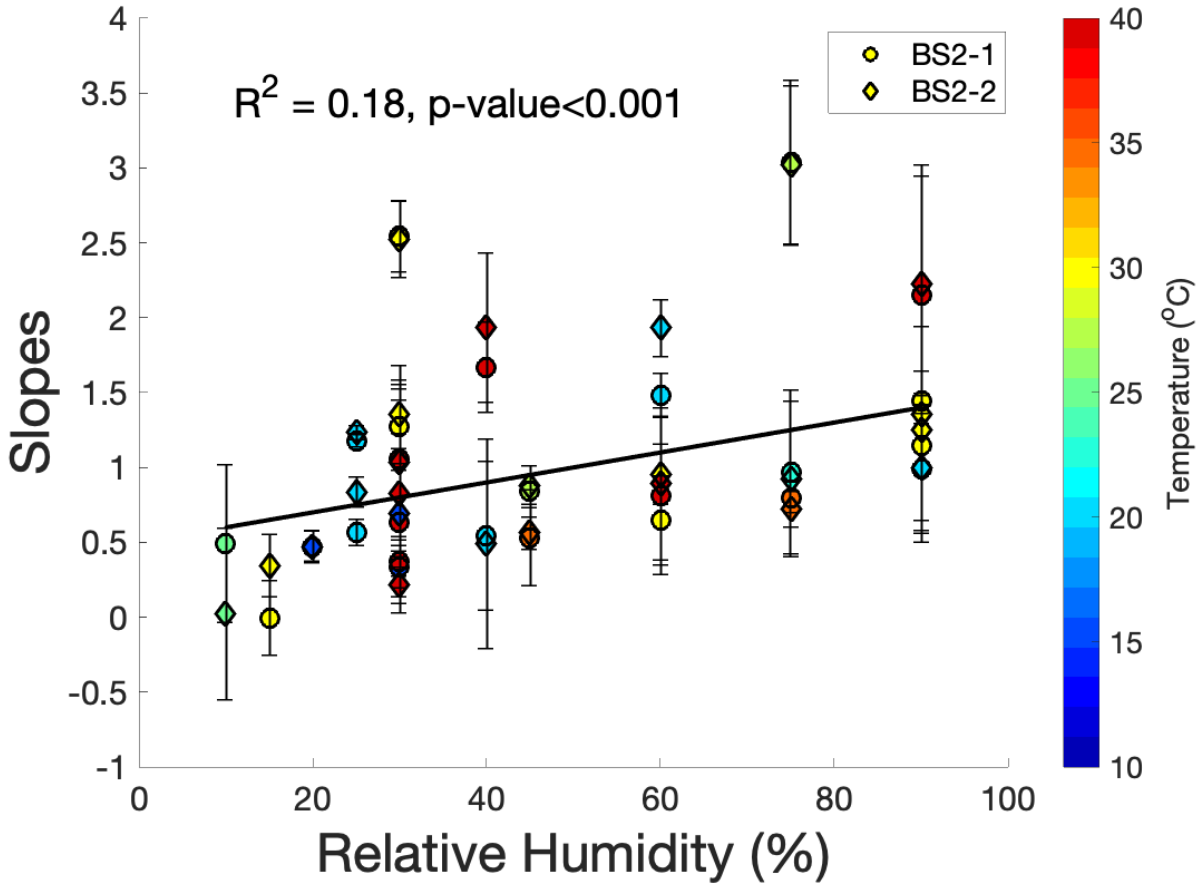

Figure 6.20: The relationship between RH and slopes from linear regression of each experiment during incense decay tests for all two instances of BS2 and the reference instruments (SMPS+APS). Error bars represent the standard error of the slope from linear regression. The linear regression line is fit to all the slopes from two instances.

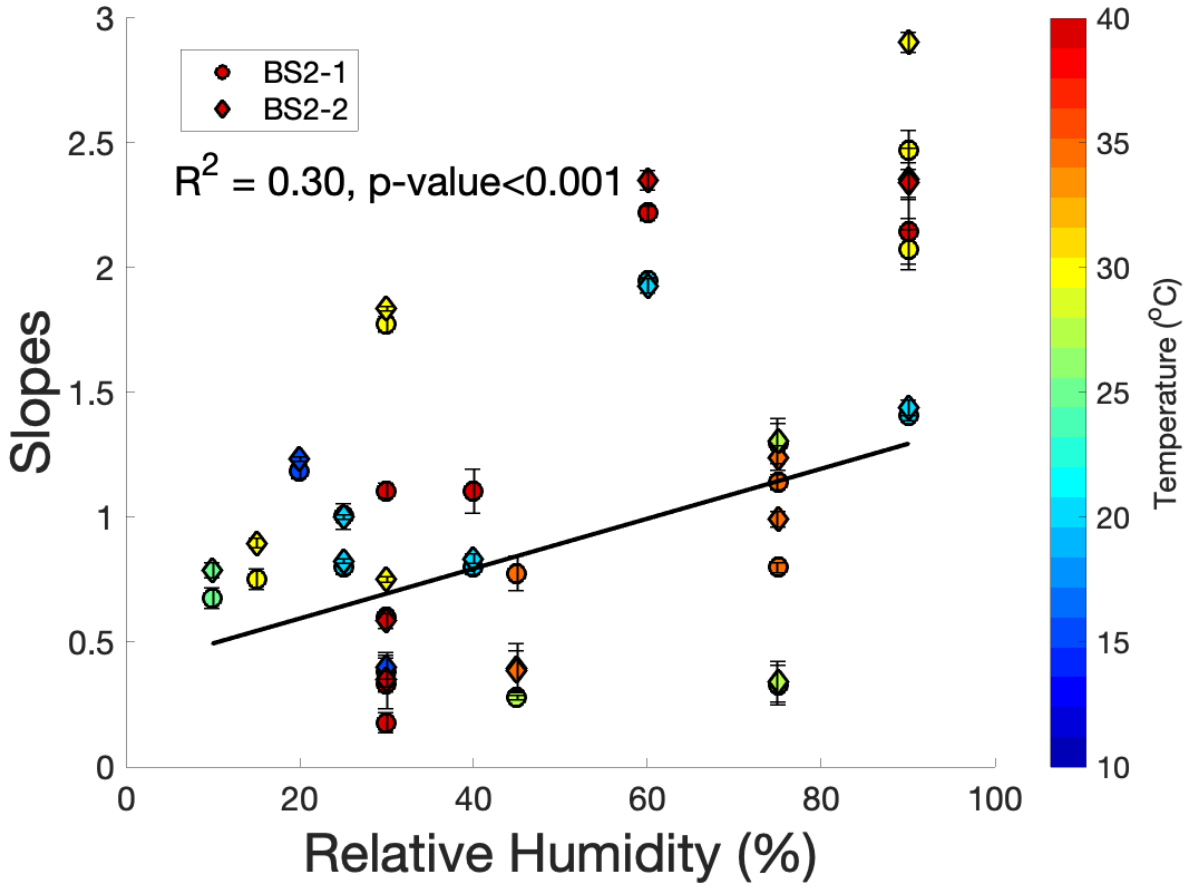

Figure 6.21: The relationship between RH and slopes from linear regression of each experiment during burning toast decay tests for all two instances of BS2 and the reference instruments (SMPS+APS). Error bars represent the standard error of the slope from linear regression. The linear regression line is fit to all the slopes from two instances.

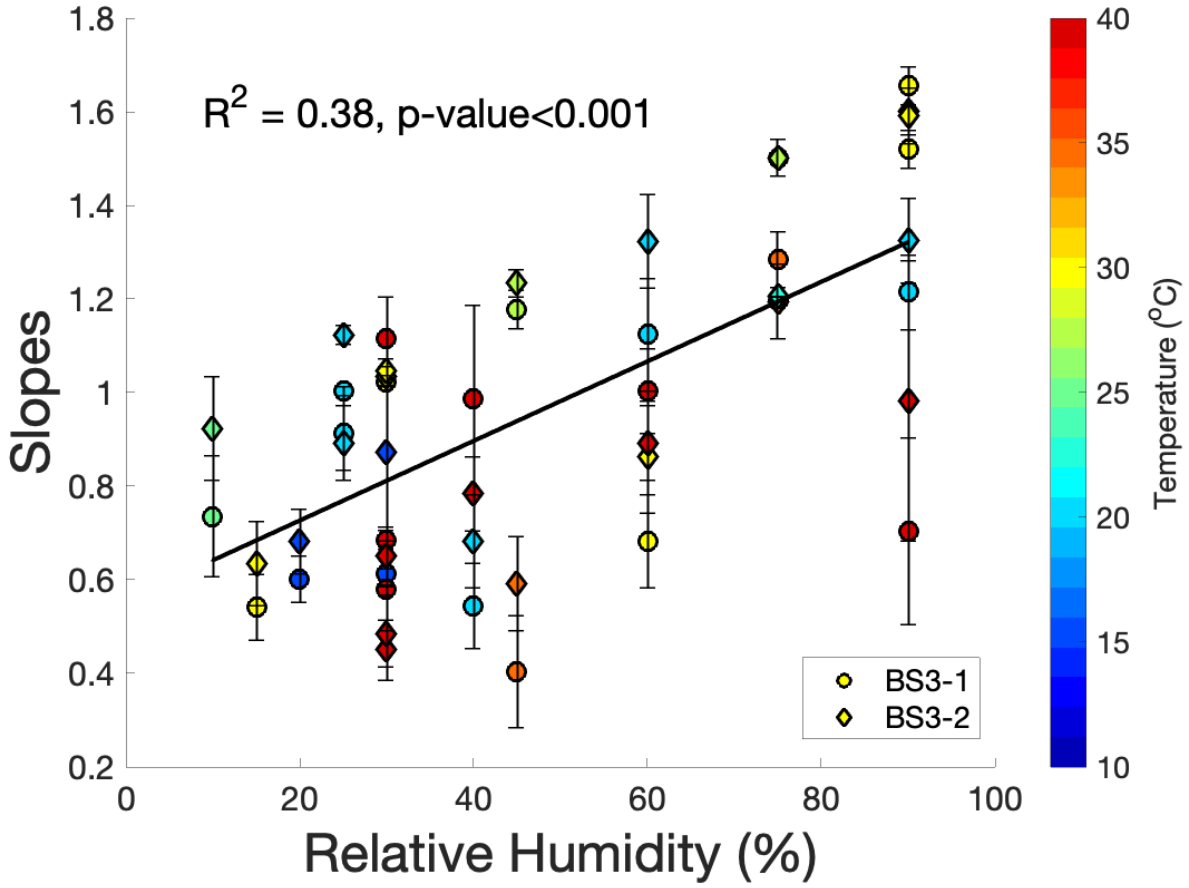

Figure 6.22: The relationship between RH and slopes from linear regression of each experiment during incense decay tests for all two instances of BS3 and the reference instruments (SMPS+APS). Error bars represent the standard error of the slope from linear regression. The linear regression line is fit to all the slopes from two instances.

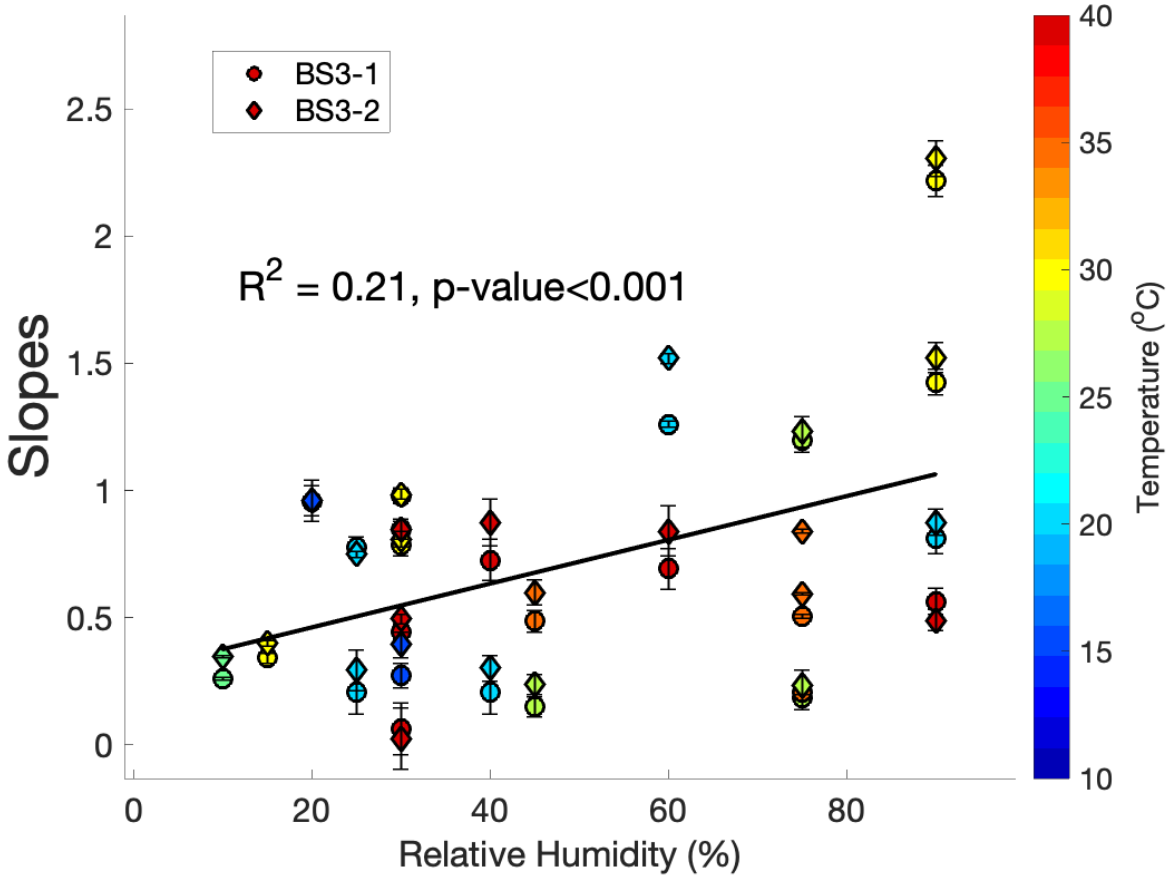

Figure 6.23: The relationship between RH and slopes from linear regression of each experiment during burning toast tests for all two instances of BS3 and the reference instruments (SMPS+APS). Error bars represent the standard error of the slope from linear regression. The linear regression line is fit to all the slopes from two instances.

Chapter 7: Summary and future studies

7.1 Summary

Low-cost air quality sensors are emerging technologies on the market, and their relatively inexpensive prices and portability make them more accessible for residential or commercial use than traditional air monitoring instruments. However, uncertainties in their performance remain. This study focused on the use of low-cost gaseous sensors to characterize spatial patterns in an urban area and the evaluation of factors that affect low-cost particle sensors' performance.

In this thesis, Chapter 2 describes the field application of low-cost gaseous sensors for outdoor monitoring. We deployed sensors on a transit bus to monitor on-road traffic-related air pollution. Through the regular and repeated traversals along routes made by the bus, we obtained sensor data to explore the consistency of the spatial and temporal patterns observed for different air pollutants. Although our efforts were a pilot-scale study, they suggest that an air quality monitoring network using sensors deployed on transit buses may be a promising application for characterizing the underlying spatial and temporal pattern of air pollution within urban areas.

Chapter 3 focuses on the field application of using low-cost particle sensor within an emulated indoor residential environment. We investigated the ability of particle sensors to detect residential particle emission events and found that all of sensors could respond to each events. However, the magnitude of the response by sensors varied for different particle sources. The results of this study can provide information regarding how well the

sensors may characterize exposure to real-world indoor particles. Our simultaneous characterization of the particle size distributions of these (and other) particle sources suggested that the size of the particles can affect the sensors' performance. We further evaluated this effect of particle size as well as particle composition as summarized subsequently in Chapter 5.

In Chapter 4, we proposed a definition for the limits of quantification (i.e., the maximum and minimum particle concentrations between which reliable data may be obtained) for each of the tested low-cost particle sensors through controlled laboratory experiments. Experiments show that the lower bound (minimum) range from 3 to 15 $\mu g/m^3$ and higher bound (maximum) range from 300 to 3,000 $\mu g/m^3$ for the sensors tested. We found that these limits (both upper and lower bound) may be unlikely to affect most of the sensors' performance for most indoor environments. However, lower R^2 values between the reference instruments and some of the sensors were observed for "background" conditions during the experiments described in Chapter 3, which is likely attributable to the particle concentration falling below the sensors' lower limit of quantification, implying that they may not provide high-quality data when particle concentrations are low.

Chapter 5 describes the effects of particle size and particle composition on the performance of low-cost particle sensors. We conducted laboratory experiments to separate these two factors and found that particle size appears to have a more dominant effect on the sensors' response to the particles than composition, although the interaction between size and composition is more dominant than size or composition alone. This implies that if the sampled particles within a given environment are substantially different than the calibration particles, the sensor's output may be inaccurate. Results from this chapter can

also, in part, explain why the slopes and R^2 between the sensors and the reference instruments were highly variable for different particle sources, as described in Chapter 3. This implies that accurate exposure assessments may be difficult when indoor particle sources vary.

Chapter 6 investigates how two environmental factors, temperature and relative humidity (RH), affect the performance of low-cost particle sensors. We conducted laboratory experiments under different temperature and RH conditions within the range that might be expected for the indoor environment. We found that there is a statistically significant, positive linear relationship between the slopes of the linear fit between sensors' measurements and research-grade instruments' measurements as RH varies. This indicates that RH may result in a positive bias to the sensors' reported particle concentrations (likely related to changes to the particles' diameters or refractive indices). We obtained no strong evidence that temperature has a significant effect on the sensors' performance. These results may suggest the need for a co-located RH sensor that is deployed alongside the low-cost particle sensors to enable corrections for this RH effect, either in near-real-time or during data post-processing.

In general, low-cost gaseous sensors can provide higher spatial air quality measurements in outdoor environments, and low-cost particle sensors can provide information about indoor air quality that is largely unmonitored. Even if a low-cost particle sensor cannot provide accurate measurements within the indoor environment, they appear to have utility for event detection, or in other words, as an indicator that particles have been emitted within a given environment. For those particle sensors that can provide fairly accurate measurements, they may have utility in exposure studies.

7.2 Future studies

There is still work that needs to be done to better understand applications and limitations of low-cost sensors for air quality monitoring. In Chapter 2, we learned that low-cost sensors deployed on a transit bus can provide high resolution spatial measurements. This approach may have practical utility in future applications, but additional work is required to providing data to support air pollution modeling and air quality information services. One extension of the work in Chapter 2 could be the inclusion of a particle sensor to provide information about PM concentrations as well as the gas-phase pollutants.

In the context of our evaluation of particle sensors in Chapters 4 through 6 along with other literature, there does not appear to be a standard approach for evaluating the particle sensors, which may explain why discrepancies exist among different studies. Therefore, a standard procedure for the evaluation of the sensors may be necessary. Such a standard protocol should be developed for the calibration and evaluation of these sensors in order to understand biases that may exist (and their causes) and to improve the accuracy of a given sensor through robust calibrations. For example, a calibration protocol should be followed by the manufacturer when testing all types of sensors. The protocol should explain how the calibration was conducted including details related to the testing environment, testing period and concentration levels; this should also prescribe a specific reference instrument (or instruments) for calibration. Requiring such a transparent standard protocol would also improve quality assurance and quality control by encouraging the

manufacturers to test their sensors, which should reduce discrepancies, like we observed in Chapter 3 and others have reported previously, across sensors from the same manufacturer.

Correction methods for data post-processing for low-cost sensor are necessary to provide accurate measurements. As discussed in Chapter 5 and Chapter 6, several factors including particle size, particle composition and RH affect the sensors' performance. Our study only focused on the evaluation of how these factors affect sensor performance, as we did not develop correction methods as an outcome of our work. Further studies are needed to provide robust correction methods for these factors (size, composition, RH) simultaneously in order to provide more accurate data by reducing systematic biases. For example, experiments (similar to the decay tests from Chapter 4 and Chapter 5) can be conducted by perturbing five variables: particle size, particle composition, RH, temperature and sensor type. A multiple regression model can be developed for the calibrations as in previous studies (Malings et al., 2020; Si et al., 2019), in which the dependent variable is the reference instrument concentration and the independent variables are the low-cost sensor's concentration, particle size, particle composition, relative humidity, temperature and sensor type. This model may have similar functional form across different sensors, but the coefficients for the calibration equations may be different for each sensor. This model can also demonstrate which variable(s) can significantly affect the sensors' performance and provide a means of evaluating how the interaction between any two variables affects the sensors' performance. The outcome of the correction would to be that low-cost particle sensors will require a co-located RH sensor to account for the RH effects, and another recommendation may be to use low-cost optical particle counters

to account for particle size effects. RH sensors are relatively inexpensive, and while inexpensive optical particle counters may cost ~$1,000, this is still much lower in cost than the reference instruments that we used in this study.

The ideas discussed above are focused on enhancing the utility of low-cost gaseous sensors in the outdoor environment and on improving confidence in the data collected by low-cost particle sensors within the indoor environment. This dissertation has further demonstrated the potential of low-cost sensors to be deployed as supplemental measurements for regulatory monitoring, on transit systems to provide higher resolution spatiotemporal data, and in buildings to provide air quality measurements that are largely non-existent indoors. These applications can lead to a number of beneficial outcomes, including changing human behavior (e.g., avoid air pollution "hotspots"), providing data for personal exposure and epidemiologic studies evaluating air quality models, and aiding in the understanding of the atmospheric transport of air pollutants (e.g., smoke from wildland fires). In addition, networks of low-cost sensors may provide data that enable the development statistical models which could provide air quality forecasts.

Bibliography

Agency, U. S. E. P. (2010). *Characterization of Low-Cost NO 2 Sensors*. *2*.

Apte, J. S., Messier, K. P., Gani, S., Brauer, M., Kirchstetter, T. W., Lunden, M. M., Marshall, J. D., Portier, C. J., Vermeulen, R. C. H., & Hamburg, S. P. (2017). High-Resolution Air Pollution Mapping with Google Street View Cars: Exploiting Big Data. *Environmental Science and Technology*, *51*(12), 6999–7008. https://doi.org/10.1021/acs.est.7b00891

Atkinson, R. W., Butland, B. K., Anderson, H. R., & Maynard, R. L. (2018). Long-term concentrations of nitrogen dioxide and mortality. *Epidemiology*, *29*(4), 460–472. https://doi.org/10.1097/EDE.0000000000000847

Austin, E., Novosselov, I., Seto, E., & Yost, M. G. (2015). Laboratory evaluation of the Shinyei PPD42NS low-cost particulate matter sensor. *PLoS ONE*, *10*(9), 1–17. https://doi.org/10.1371/journal.pone.0137789

Badura, M., Batog, P., Drzeniecka-Osiadacz, A., & Modzel, P. (2018). Evaluation of low-cost sensors for ambient PM2.5 monitoring. *Journal of Sensors*, *2018*. https://doi.org/10.1155/2018/5096540

Barkjohn, K. K., Bergin, M. H., Norris, C., Schauer, J. J., Zhang, Y., Black, M., Hu, M., & Zhang, J. (2020). Using low-cost sensors to quantify the effects of air filtration on indoor and personal exposure relevant PM2.5 concentrations in Beijing, China. *Aerosol and Air Quality Research*, *20*(2), 297–313. https://doi.org/10.4209/aaqr.2018.11.0394

Beckett, W. S. (1991). Ozone, air pollution, and respiratory health. *Yale Journal of Biology and Medicine*, *64*(2), 167–175.

Bohren, C., & Huffman, D. (1983). *Absorption and Scattering of Light by Small Particles* (D. R. Huffman (ed.)). Wiley-Interscience.

Brauer, M. (2010). How Much, How Long, What, and Where: Air Pollution Exposure Assessment for Epidemiologic Studies of Respiratory Disease. *Proceedings of the American Thoracic Society*, *7*(2), 111–115. https://doi.org/10.1513/pats.200908-093RM

Brienza, S., Galli, A., Anastasi, G., & Bruschi, P. (2015). A low-cost sensing system for cooperative air quality monitoring in urban areas. *Sensors (Switzerland)*, *15*(6), 12242–12259. https://doi.org/10.3390/s150612242

Budde, M., & Beigl, M. (2016). Advances in Smartphonebased Fine Dust Sensing. *Scientific Research Abstracts*, *5*(23), 24649147. https://doi.org/10.14644/dust.2014.038

Budde, M., El Masri, R., Riedel, T., & Beigl, M. (2013). Enabling low-cost particulate matter measurement for participatory sensing scenarios. *Proceedings of the 12th International Conference on Mobile and Ubiquitous Multimedia, MUM 2013*, *Mum*. https://doi.org/10.1145/2541831.2541859

Bulot, Florentin M.J., Johnston, S. J., Basford, P. J., Easton, N. H. C., Apetroaie-Cristea, M., Foster, G. L., Morris, A. K. R., Cox, S. J., & Loxham, M. (2019). Long-term field comparison of multiple low-cost particulate matter sensors in an outdoor urban environment. *Scientific Reports*, *9*(1), 1–13. https://doi.org/10.1038/s41598-019-43716-3

Bulot, Florentin Michel Jacques, Russell, H. S., Rezaei, M., Johnson, M. S., Ossont, S. J. J., Morris, A. K. R., Basford, P. J., Easton, N. H. C., Foster, G. L., Loxham, M., & Cox, S. J. (2020). Laboratory comparison of low-cost particulate matter sensors to measure transient events of pollution. *Sensors (Switzerland)*, *20*(8). https://doi.org/10.3390/s20082219

Cappa, C. D., Onasch, T. B., Massoli, P., Worsnop, D. R., Bates, T. S., Cross, E. S., Davidovits, P., Hakala, J., Hayden, K. L., Jobson, B. T., Kolesar, K. R., Lack, D. A., Lerner, B. M., Li, S.-M., Mellon, D., Nuaaman, I., Olfert, J. S., Petaja, T., Quinn, P. K., … Zaveri, R. A. (2012). Radiative Absorption Enhancements Due to the Mixing State of Atmospheric Black Carbon. *Science*, *337*(6098), 1078–1081. https://doi.org/10.1126/science.1223447

Castell, N., Dauge, F. R., Schneider, P., Vogt, M., Lerner, U., Fishbain, B., Broday, D., & Bartonova, A. (2017). Can commercial low-cost sensor platforms contribute to air quality monitoring and exposure estimates? *Environment International*, *99*, 293–302. https://doi.org/10.1016/j.envint.2016.12.007

Chan, W. R., Logue, J. M., Fisk, X. W. N. E. K. W. J., & Singer, B. C. (2018). *Quantifying fine particle emission events from time- - resolved measurements : Method description and application to 18 California low- - income apartments*. *January 2017*, 89–101. https://doi.org/10.1111/ina.12425

Cheng, Y. S., Bechtold, W. E., Yu, C. C., & Hung, I. F. (1995). Incense Smoke: Characterization and Dynamics in Indoor Environments. *Aerosol Science and Technology*, *23*(3), 271–281. https://doi.org/10.1080/02786829508965312

Christian Kjær Jensen. (2016). *Assessing the applicability of low-cost electrochemical*

gas sensors for urban air quality monitoring. *March*, 181. https://doi.org/PNR61

Crilley, L. R., Shaw, M., Pound, R., Kramer, L. J., Price, R., Young, S., Lewis, A. C., & Pope, F. D. (2018). Evaluation of a low-cost optical particle counter (Alphasense OPC-N2) for ambient air monitoring. *Atmospheric Measurement Techniques*, *11*(2), 709–720. https://doi.org/10.5194/amt-11-709-2018

Crilley, L. R., Singh, A., Kramer, L. J., Shaw, M. D., Alam, M. S., Apte, J. S., Bloss, W. J., Ruiz, L. H., Fu, P., Fu, W., Gani, S., Gatari, M., Ilyinskaya, E., Lewis, A. C., Ng'ang'a, D., Sun, Y., Whitty, R. C. W., Yue, S., Young, S., & Pope, F. D. (2019). *Effect of aerosol composition on the performance of low-cost optical particle counter correction factors*. *October*, 1–21. https://doi.org/10.5194/amt-2019-370

Cross, E. S., Lewis, D. K., Williams, L. R., Magoon, G. R., Kaminsky, M. L., Worsnop, D. R., & Jayne, J. T. (2017). Use of electrochemical sensors for measurement of air pollution: correcting interference response and validating measurements. *Atmospheric Measurement Techniques Discussions*, 1–17. https://doi.org/10.5194/amt-2017-138

Curto, A., Donaire-Gonzalez, D., Barrera-Gómez, J., Marshall, J. D., Nieuwenhuijsen, M. J., Wellenius, G. A., & Tonne, C. (2018). Performance of low-cost monitors to assess household air pollution. *Environmental Research*, *163*, 53–63. https://doi.org/10.1016/j.envres.2018.01.024

Dacunto, P. J., Klepeis, N. E., Cheng, K. C., Acevedo-Bolton, V., Jiang, R. T., Repace, J. L., Ott, W. R., & Hildemann, L. M. (2015). Determining PM2.5 calibration curves for a low-cost particle monitor: Common indoor residential aerosols. *Environmental Sciences: Processes and Impacts*, *17*(11), 1959–1966.

https://doi.org/10.1039/c5em00365b

Delp, W. W., & Singer, B. C. (2020). Wildfire Smoke Adjustment Factors for Low-Cost and Professional PM2.5 Monitors with Optical Sensors. *Sensors*, *20*(13), 3683. https://doi.org/10.3390/s20133683

Feenstra, B., Papapostolou, V., Hasheminassab, S., Zhang, H., Boghossian, B. Der, Cocker, D., & Polidori, A. (2019). Performance evaluation of twelve low-cost PM2.5 sensors at an ambient air monitoring site. *Atmospheric Environment*, *216*(February), 116946. https://doi.org/10.1016/j.atmosenv.2019.116946

Gao, Y., Dong, W., Guo, K., Liu, X., Chen, Y., Liu, X., Bu, J., & Chen, C. (2016). Mosaic: A low-cost mobile sensing system for urban air quality monitoring. *Proceedings - IEEE INFOCOM*, *2016-July*, 1–9. https://doi.org/10.1109/INFOCOM.2016.7524478

Geller, M. D., Chang, M., Sioutas, C., Ostro, B. D., & Lipsett, M. J. (2002). Indoor/outdoor relationship and chemical composition of fine and coarse particles in the southern California deserts. *Atmospheric Environment*, *36*(6), 1099–1110. https://doi.org/10.1016/S1352-2310(01)00340-5

Gil-Castiñeira, F., González-Castaño, F. J., Duro, R. J., & Lopez-PeñTa, F. (2008). Urban pollution monitoring through opportunistic mobile sensor networks based on public transport. *CIMSA 2008 - IEEE Conference on Computational Intelligence for Measurement Systems and Applications Proceedings*, *July*, 70–74. https://doi.org/10.1109/CIMSA.2008.4595835

Gonzalez, A., Boies, A., Swason, J., & Kittelson, D. (2019). Field Calibration of Low-Cost Air Pollution Sensors. *Atmospheric Measurement Techniques Discussions*,

2050(August), 1–17. https://doi.org/10.5194/amt-2019-299

Guo, C., Zhang, Z., Lau, A. K. H., Lin, C. Q., Chuang, Y. C., Chan, J., Jiang, W. K., Tam, T., Yeoh, E. K., Chan, T. C., Chang, L. Y., & Lao, X. Q. (2018). Effect of long-term exposure to fine particulate matter on lung function decline and risk of chronic obstructive pulmonary disease in Taiwan: a longitudinal, cohort study. *The Lancet Planetary Health*, *2*(3), e114–e125. https://doi.org/10.1016/S2542-5196(18)30028-7

Hagan, D. H., & Kroll, J. H. (2020). *Assessing the accuracy of low-cost optical particle sensors using a physics-based approach*. *June*, 1–36.

Han, I., Symanski, E., & Stock, T. H. (2017). Feasibility of using low-cost portable particle monitors for measurement of fine and coarse particulate matter in urban ambient air. *Journal of the Air and Waste Management Association*, *67*(3), 330–340. https://doi.org/10.1080/10962247.2016.1241195

Harrison, R. M., Thornton, C. A., Lawrence, R. G., Mark, D., Kinnersley, R. P., & Ayres, J. G. (2002). Personal exposure monitoring of particulate matter, nitrogen dioxide, and carbon monoxide, including susceptible groups. *Occupational and Environmental Medicine*, *59*(10), 671–679. https://doi.org/10.1136/oem.59.10.671

Hasenfratz, D. (2015). *Enabling Large-Scale Urban Air Quality Monitoring with Mobile Sensor Nodes*. *22481*, 166.

He, M., Kuerbanjiang, N., & Dhaniyala, S. (2020). Performance characteristics of the low-cost Plantower PMS optical sensor. *Aerosol Science and Technology*, *54*(2), 232–241. https://doi.org/10.1080/02786826.2019.1696015

Hojaiji, H., Kalantarian, H., Bui, A. A. T., King, C. E., & Sarrafzadeh, M. (2017).

Temperature and humidity calibration of a low-cost wireless dust sensor for real-time monitoring. *SAS 2017 - 2017 IEEE Sensors Applications Symposium, Proceedings*, 1–6. https://doi.org/10.1109/SAS.2017.7894056

Holder, A. L., Mebust, A. K., Maghran, L. A., McGown, M. R., Stewart, K. E., Vallano, D. M., Elleman, R. A., & Baker, K. R. (2020). Field Evaluation of Low-Cost Particulate Matter Sensors for Measuring Wildfire Smoke. *Sensors*, *20*(17), 4796. https://doi.org/10.3390/s20174796

Holstius, D. M., Pillarisetti, A., Smith, K. R., & Seto, E. (2014). Field calibrations of a low-cost aerosol sensor at a regulatory monitoring site in California. *Atmospheric Measurement Techniques*, *7*(4), 1121–1131. https://doi.org/10.5194/amt-7-1121-2014

Jayaratne, R., Liu, X., Thai, P., Dunbabin, M., & Morawska, L. (2018). The influence of humidity on the performance of a low-cost air particle mass sensor and the effect of atmospheric fog. *Atmospheric Measurement Techniques*, *11*(8), 4883–4890. https://doi.org/10.5194/amt-11-4883-2018

Jerrett, M., Donaire-Gonzalez, D., Popoola, O., Jones, R., Cohen, R. C., Almanza, E., de Nazelle, A., Mead, I., Carrasco-Turigas, G., Cole-Hunter, T., Triguero-Mas, M., Seto, E., & Nieuwenhuijsen, M. (2017). Validating novel air pollution sensors to improve exposure estimates for epidemiological analyses and citizen science. *Environmental Research*, *158*(March), 286–294. https://doi.org/10.1016/j.envres.2017.04.023

Ji, X., Bihan, O. Le, Ramalho, O., Martinon, L., & Nicolas, M. (2010). *Characterization of particles emitted by incense burning in an experimental house*. 147–158.

https://doi.org/10.1111/j.1600-0668.2009.00634.x

Jiao, W., Hagler, G., Williams, R., Sharpe, R., Brown, R., Garver, D., Judge, R., Caudill, M., Rickard, J., Davis, M., Weinstock, L., Zimmer-Dauphinee, S., & Buckley, K. (2016). Community Air Sensor Network (CAIRSENSE) project: Evaluation of low-cost sensor performance in a suburban environment in the southeastern United States. *Atmospheric Measurement Techniques*, *9*(11), 5281–5292. https://doi.org/10.5194/amt-9-5281-2016

Karagulian, F., Barbiere, M., Kotsev, A., Spinelle, L., Gerboles, M., Lagler, F., Redon, N., Crunaire, S., & Borowiak, A. (2019). Review of the performance of low-cost sensors for air quality monitoring. *Atmosphere*, *10*(9). https://doi.org/10.3390/atmos10090506

Karami, M., Mcmorrow, G. V., & Wang, L. (2018). Continuous monitoring of indoor environmental quality using an Arduino- based data acquisition system. *Journal of Building Engineering*, *19*(January), 412–419. https://doi.org/10.1016/j.jobe.2018.05.014

Kelly, K. E., Whitaker, J., Petty, A., Widmer, C., Dybwad, A., Sleeth, D., Martin, R., & Butterfield, A. (2017). Ambient and laboratory evaluation of a low-cost particulate matter sensor. *Environmental Pollution*, *221*, 491–500. https://doi.org/10.1016/j.envpol.2016.12.039

Khalizov, A. F., Hogan, B., Qiu, C., Petersen, E. L., & Zhang, R. (2012). Characterization of soot aerosol produced from combustion of propane in a shock tube. *Aerosol Science and Technology*, *46*(8), 925–936. https://doi.org/10.1080/02786826.2012.683839

Khlystov, A., Stanier, C., & Pandis, S. N. (2004a). An algorithm for combining electrical mobility and aerodynamic size distributions data when measuring ambient aerosol. *Aerosol Science and Technology*, *38*(SUPPL. 1), 229–238. https://doi.org/10.1080/02786820390229543

Khlystov, A., Stanier, C., & Pandis, S. N. (2004b). An Algorithm for Combining Electrical Mobility and Aerodynamic Size Distributions Data when Measuring Ambient Aerosol Special Issue of Aerosol Science and Technology on Findings from the Fine Particulate Matter Supersites Program. *Aerosol Science and Technology*, *38*(sup1), 229–238. https://doi.org/10.1080/02786820390229543

Kim, K. H., Kabir, E., & Kabir, S. (2015). A review on the human health impact of airborne particulate matter. *Environment International*, *74*, 136–143. https://doi.org/10.1016/j.envint.2014.10.005

Klepeis, N. E., Nelson, W. C., Ott, W. R., Robinson, J. P., Tsang, A. M., Switzer, P., Behar, J. V., Hern, S. C., & Engelmann, W. H. (2001). The National Human Activity Pattern Survey (NHAPS): A resource for assessing exposure to environmental pollutants. *Journal of Exposure Analysis and Environmental Epidemiology*, *11*(3), 231–252. https://doi.org/10.1038/sj.jea.7500165

Kolb, R. W. (2018). National Ambient Air Quality Standards (NAAQS). *The SAGE Encyclopedia of Business Ethics and Society*, *4*, 1–2. https://doi.org/10.4135/9781483381503.n817

KS, & KL. (2014). *Teledyne API – Model T400 Photometric Ozone Analyzer*. *September*. http://www.teledyne-api.com/

Kumar, P., Morawska, L., Martani, C., Biskos, G., Neophytou, M., Di Sabatino, S., Bell,

M., Norford, L., & Britter, R. (2015). The rise of low-cost sensing for managing air pollution in cities. *Environment International*, *75*, 199–205. https://doi.org/10.1016/j.envint.2014.11.019

Kumar, P., Skouloudis, A. N., Bell, M., Viana, M., Carotta, M. C., Biskos, G., & Morawska, L. (2016). Real-time sensors for indoor air monitoring and challenges ahead in deploying them to urban buildings. *Science of the Total Environment*, *560–561*(April), 150–159. https://doi.org/10.1016/j.scitotenv.2016.04.032

Kuula, J., Mäkelä, T., Aurela, M., Teinilä, K., Varjonen, S., Gonzales, O., & Timonen, H. (2019). Laboratory evaluation of particle size-selectivity of optical low-cost particulate matter sensors. *Atmospheric Measurement Techniques Discussions*, *December*, 1–21. https://doi.org/10.5194/amt-2019-422

Lattimer, B. Y. (2008). Fire Safety Science – Proceedings of the Ninth International Symposium, International Association for Fire Safety Science. *Ninth International Symposium, International Association for Fire Safety Science*.

Levy Zamora, M., Xiong, F., Gentner, D., Kerkez, B., Kohrman-Glaser, J., & Koehler, K. (2019). Field and Laboratory Evaluations of the Low-Cost Plantower Particulate Matter Sensor [Research-article]. *Environmental Science and Technology*, *53*(2), 838–849. https://doi.org/10.1021/acs.est.8b05174

Lewis, A. C., Lee, J. D., Edwards, P. M., Shaw, M. D., Evans, M. J., Moller, S. J., Smith, K. R., Buckley, J. W., Ellis, M., Gillot, S. R., & White, A. (2016). Evaluating the performance of low cost chemical sensors for air pollution research. *Faraday Discussions*, *189*, 85–103. https://doi.org/10.1039/c5fd00201j

Lewis, A., & Edwards, P. (2016). Validate personal air-pollution sensors. *Nature*,

535(7610), 29–31. https://doi.org/10.1038/535029a

Li, J., Li, H., Ma, Y., Wang, Y., Abokifa, A. A., Lu, C., & Biswas, P. (2018). Spatiotemporal distribution of indoor particulate matter concentration with a low-cost sensor network. *Building and Environment*, *127*(September 2017), 138–147. https://doi.org/10.1016/j.buildenv.2017.11.001

Li, J., Mattewal, S. K., Patel, S., & Biswas, P. (2020). Evaluation of Nine Low-cost-sensor-based Particulate Matter Monitors. *Aerosol and Air Quality Research*, *20*(2), 254–270. https://doi.org/10.4209/aaqr.2018.12.0485

Lim, C. C., Kim, H., Vilcassim, M. J. R., Thurston, G. D., Gordon, T., Chen, L. C., Lee, K., Heimbinder, M., & Kim, S. Y. (2019). Mapping urban air quality using mobile sampling with low-cost sensors and machine learning in Seoul, South Korea. *Environment International*, *131*(June), 105022. https://doi.org/10.1016/j.envint.2019.105022

Lin, C., Gillespie, J., Schuder, M. D., Duberstein, W., Beverland, I. J., & Heal, M. R. (2015). Evaluation and calibration of Aeroqual series 500 portable gas sensors for accurate measurement of ambient ozone and nitrogen dioxide. *Atmospheric Environment*, *100*(2), 111–116. https://doi.org/10.1016/j.atmosenv.2014.11.002

Liu, D., Zhang, Q., Jiang, J., & Chen, D. R. (2017). Performance calibration of low-cost and portable particular matter (PM) sensors. *Journal of Aerosol Science*, *112*(May), 1–10. https://doi.org/10.1016/j.jaerosci.2017.05.011

Liu, H. Y., Schneider, P., Haugen, R., & Vogt, M. (2019). Performance assessment of a low-cost PM 2.5 sensor for a near four-month period in Oslo, Norway. *Atmosphere*, *10*(2), 1–19. https://doi.org/10.3390/atmos10020041

Long, C. M., Suh, H. H., & Koutrakis, P. (2000). Characterization of indoor particle sources using continuous mass and size monitors. *Journal of the Air and Waste Management Association*, *50*(7), 1236–1250. https://doi.org/10.1080/10473289.2000.10464154

Malings, C., Tanzer, R., Hauryliuk, A., Saha, P. K., Robinson, A. L., Presto, A. A., & Subramanian, R. (2020). Fine particle mass monitoring with low-cost sensors: Corrections and long-term performance evaluation. *Aerosol Science and Technology*, *54*(2), 160–174. https://doi.org/10.1080/02786826.2019.1623863

Manikonda, A., Zíková, N., Hopke, P. K., & Ferro, A. R. (2016). Laboratory assessment of low-cost PM monitors. *Journal of Aerosol Science*, *102*, 29–40. https://doi.org/10.1016/j.jaerosci.2016.08.010

Masson, N., Piedrahita, R., & Hannigan, M. (2015). Quantification method for electrolytic sensors in long-term monitoring of ambient air quality. *Sensors (Switzerland)*, *15*(10), 27283–27302. https://doi.org/10.3390/s151027283

Mazaheri, M., Clifford, S., Yeganeh, B., Viana, M., Rizza, V., Flament, R., Buonanno, G., & Morawska, L. (2018). Investigations into factors affecting personal exposure to particles in urban microenvironments using low-cost sensors. *Environment International*, *120*(January), 496–504. https://doi.org/10.1016/j.envint.2018.08.033

McMurry, P. H., & Stolzenburg, M. R. (1989). On the sensitivity of particle size to relative humidity for Los Angeles aerosols. *Atmospheric Environment (1967)*, *23*(2), 497–507. https://doi.org/10.1016/0004-6981(89)90593-3

Mead, M. I., Popoola, O. A. M., Stewart, G. B., Landshoff, P., Calleja, M., Hayes, M., Baldovi, J. J., McLeod, M. W., Hodgson, T. F., Dicks, J., Lewis, A., Cohen, J.,

Baron, R., Saffell, J. R., & Jones, R. L. (2013). The use of electrochemical sensors for monitoring urban air quality in low-cost, high-density networks. *Atmospheric Environment*, *70*, 186–203. https://doi.org/10.1016/j.atmosenv.2012.11.060

Miller, D. J., Actkinson, B., Padilla, L., Griffin, R. J., Moore, K., Lewis, P. G. T., Gardner-Frolick, R., Craft, E., Portier, C. J., Hamburg, S. P., & Alvarez, R. A. (2020). Characterizing Elevated Urban Air Pollutant Spatial Patterns with Mobile Monitoring in Houston, Texas. *Environmental Science & Technology*. https://doi.org/10.1021/acs.est.9b05523

Moltchanov, S., Levy, I., Etzion, Y., Lerner, U., Broday, D. M., & Fishbain, B. (2015). On the feasibility of measuring urban air pollution by wireless distributed sensor networks. *Science of the Total Environment*, *502*, 537–547. https://doi.org/10.1016/j.scitotenv.2014.09.059

Morawska, L., Thai, P. K., Liu, X., Asumadu-Sakyi, A., Ayoko, G., Bartonova, A., Bedini, A., Chai, F., Christensen, B., Dunbabin, M., Gao, J., Hagler, G. S. W., Jayaratne, R., Kumar, P., Lau, A. K. H., Louie, P. K. K., Mazaheri, M., Ning, Z., Motta, N., … Williams, R. (2018). Applications of low-cost sensing technologies for air quality monitoring and exposure assessment: How far have they gone? *Environment International*, *116*, 286–299. https://doi.org/10.1016/j.envint.2018.04.018

Mukherjee, A., Brown, S. G., Mccarthy, M. C., Pavlovic, N. R., Stanton, L. G., Snyder, J. L., Andrea, S. D., & Hafner, H. R. (2019). *Network of Low-Cost Sensors*.

Mukherjee, A., Stanton, L. G., Graham, A. R., & Roberts, P. T. (2017). Assessing the utility of low-cost particulate matter sensors over a 12-week period in the Cuyama

valley of California. *Sensors (Switzerland)*, *17*(8). https://doi.org/10.3390/s17081805

Munir, S., Mayfield, M., Coca, D., Jubb, S. A., & Osammor, O. (2019). Analysing the performance of low-cost air quality sensors, their drivers, relative benefits and calibration in cities—a case study in Sheffield. *Environmental Monitoring and Assessment*, *191*(2). https://doi.org/10.1007/s10661-019-7231-8

Nieuwenhuijsen, M. J., Wellenius, G. A., Tonne, C., & Marshall, J. D. (2018). Performance of low-cost monitors to assess household air pollution. *Environmental Research*, *163*(January), 53–63. https://doi.org/10.1016/j.envres.2018.01.024

Northcross, A. L., Edwards, R. J., Johnson, M. A., Wang, Z. M., Zhu, K., Allen, T., & Smith, K. R. (2013). A low-cost particle counter as a realtime fine-particle mass monitor. *Environmental Sciences: Processes and Impacts*, *15*(2), 433–439. https://doi.org/10.1055/s-0035-1545797

Pan, Z., & Singh, R. P. (2001). *Physical and Thermal Properties of Ground Beef During Cooking*. *444*, 437–444.

Patel, S., Li, J., Pandey, A., Pervez, S., Chakrabarty, R. K., & Biswas, P. (2017). Spatio-temporal measurement of indoor particulate matter concentrations using a wireless network of low-cost sensors in households using solid fuels. *Environmental Research*, *152*(July 2016), 59–65. https://doi.org/10.1016/j.envres.2016.10.001

Patton, A. P., Perkins, J., Zamore, W., Levy, J. I., Brugge, D., & Durant, J. L. (2014). Spatial and temporal differences in traffic-related air pollution in three urban neighborhoods near an interstate highway. *Atmospheric Environment*, *99*, 309–321. https://doi.org/10.1016/j.atmosenv.2014.09.072

Piedrahita, R., Xiang, Y., Masson, N., Ortega, J., Collier, A., Jiang, Y., Li, K., Dick, R. P., Lv, Q., Hannigan, M., & Shang, L. (2014). The next generation of low-cost personal air quality sensors for quantitative exposure monitoring. *Atmospheric Measurement Techniques*, *7*(10), 3325–3336. https://doi.org/10.5194/amt-7-3325-2014

Polidori, A., Papapostolou, V., & Zhang, H. (2016a). *Laboratory Evaluation of Low-Cost Air Quality Sensors: Laboratory Setup and Testing Protocol*.

Polidori, A., Papapostolou, V., & Zhang, H. (2016b). *Laboratory Evaluation of Low-Cost Air Quality Sensors*. *August*. http://www.aqmd.gov/docs/default-source/aq-spec/protocols/sensors-lab-testing-protocol6087afefc2b66f27bf6fff00004a91a9.pdf?sfvrsn=2

Rai, A. C., Kumar, P., Pilla, F., Skouloudis, A. N., Di Sabatino, S., Ratti, C., Yasar, A., & Rickerby, D. (2017). End-user perspective of low-cost sensors for outdoor air pollution monitoring. *Science of the Total Environment*, *607–608*, 691–705. https://doi.org/10.1016/j.scitotenv.2017.06.266

Rissler, J., Messing, M. E., Malik, A. I., Nilsson, P. T., Erik, Z., Bohgard, M., Sanati, M., Pagels, J. H., Rissler, J., Messing, M. E., Malik, A. I., Nilsson, P. T., Erik, Z., Rissler, J., Messing, M. E., Malik, A. I., Nilsson, P. T., Nordin, E. Z., Bohgard, M., … Pagels, J. H. (2013). *Effective Density Characterization of Soot Agglomerates from Various Sources and Comparison to Aggregation Theory Effective Density Characterization of Soot Agglomerates from Various Sources and Comparison to Aggregation Theory*. *6826*. https://doi.org/10.1080/02786826.2013.791381

Roberts, T. J., Saffell, J. R., Oppenheimer, C., & Lurton, T. (2014). Electrochemical

sensors applied to pollution monitoring: Measurement error and gas ratio bias - A volcano plume case study. *Journal of Volcanology and Geothermal Research*, *281*, 85–96. https://doi.org/10.1016/j.jvolgeores.2014.02.023

Sadighi, K., Coffey, E., Polidori, A., Feenstra, B., Lv, Q., Henze, D. K., & Hannigan, M. (2018). Intra-urban spatial variability of surface ozone in Riverside, CA: Viability and validation of low-cost sensors. *Atmospheric Measurement Techniques*, *11*(3), 1777–1792. https://doi.org/10.5194/amt-11-1777-2018

Sayahi, T., Butterfield, A., & Kelly, K. E. (2019). Long-term field evaluation of the Plantower PMS low-cost particulate matter sensors. *Environmental Pollution*, *245*, 932–940. https://doi.org/10.1016/j.envpol.2018.11.065

Schieweck, A., Uhde, E., Salthammer, T., Salthammer, L. C., & Morawska, L. (2018). Smart homes and the control of indoor air quality. *Renewable and Sustainable Energy Reviews*, *94*(February), 705–718. https://doi.org/10.1016/j.rser.2018.05.057

Shum, L. V., Rajalakshmi, P., Afonja, A., McPhillips, G., Binions, R., Cheng, L., & Hailes, S. (2011). On the development of a sensor module for real-time pollution monitoring. *2011 International Conference on Information Science and Applications, ICISA 2011*. https://doi.org/10.1109/ICISA.2011.5772355

Si, M., Xiong, Y., Du, S., & Du, K. (2019). Evaluation and Calibration of a Low-cost Particle Sensor in Ambient Conditions Using Machine Learning Technologies. *Atmospheric Measurement Techniques Discussions*, 1–25. https://doi.org/10.5194/amt-2019-393

Singer, B. C., & Delp, W. W. (2018). Response of consumer and research grade indoor air quality monitors to residential sources of fine particles. *Indoor Air*, *28*(4), 624–

639. https://doi.org/10.1111/ina.12463

Singer, Brett C, Coleman, B. K., Destaillats, H., Hodgson, A. T., Lunden, M. M., Weschler, C. J., & Nazaroff, W. W. (2006). *Indoor secondary pollutants from cleaning product and air freshener use in the presence of ozone*. *40*, 6696–6710. https://doi.org/10.1016/j.atmosenv.2006.06.005

Sousan, S., Koehler, K., Hallett, L., & Peters, T. M. (2016). Evaluation of the Alphasense optical particle counter (OPC-N2) and the Grimm portable aerosol spectrometer (PAS-1.108). *Aerosol Science and Technology*, *50*(12), 1352–1365. https://doi.org/10.1080/02786826.2016.1232859

Sousan, S., Koehler, K., Hallett, L., & Peters, T. M. (2017). Evaluation of consumer monitors to measure particulate matter. *Journal of Aerosol Science*, *107*(October 2016), 123–133. https://doi.org/10.1016/j.jaerosci.2017.02.013

Spinelle, L., Gerboles, M., Villani, M. G., Aleixandre, M., & Bonavitacola, F. (2014). Calibration of a cluster of low-cost sensors for the measurement of air pollution in ambient air. *Proceedings of IEEE Sensors*, *2014-Decem*(December), 21–24. https://doi.org/10.1109/ICSENS.2014.6984922

Spinelle, L., Gerboles, M., Villani, M. G., Aleixandre, M., & Bonavitacola, F. (2015). Field calibration of a cluster of low-cost available sensors for air quality monitoring. Part A: Ozone and nitrogen dioxide. *Sensors and Actuators, B: Chemical*, *215*, 249–257. https://doi.org/10.1016/j.snb.2015.03.031

Steinle, S., Reis, S., & Sabel, C. E. (2013). Quantifying human exposure to air pollution-Moving from static monitoring to spatio-temporally resolved personal exposure assessment. *Science of the Total Environment*, *443*, 184–193.

https://doi.org/10.1016/j.scitotenv.2012.10.098

Sun, L., Wong, K. C., Wei, P., Ye, S., Huang, H., Yang, F., Westerdahl, D., Louie, P. K. K., Luk, C. W. Y., & Ning, Z. (2016). Development and application of a next generation air sensor network for the Hong Kong marathon 2015 air quality monitoring. *Sensors (Switzerland)*, *16*(2). https://doi.org/10.3390/s16020211

Suriano, D., Prato, M., Pfister, V., Cassano, G., Camporeale, G., Dipinto, S., & Penza, M. (2015). *Stationary and Mobile Low-Cost Gas Sensor-Systems for Air Quality Monitoring Applications*. 4–7. https://doi.org/10.5162/4EuNetAir2015/15

Taylor, M. D., Nourbakhsh, I. R., Steinfeld, A., Presto, A., & Longhurst, J. (2016). *Calibration and Characterization of Low-Cost Fine Particulate Monitors and their Effect on Individual Empowerment*. 146. https://www.ri.cmu.edu/pub_files/2016/12/m_taylor_robotics_2016.pdf%0Ahttp://repository.cmu.edu/cgi/viewcontent.cgi?article=1971&context=dissertations

Taylor, P., Turpin, B. J., Lim, H., Turpin, B. J., & Lim, H. (2010). *Aerosol Science and Technology Species Contributions to PM2 . 5 Mass Concentrations : Revisiting Common Assumptions for Estimating Organic Mass Species Contributions to PM2 . 5 Mass Concentrations : Revisiting Common Assumptions for Estimating Organic Mas*. *January 2012*, 37–41.

Teipel, U., Winter, H., Cäsar, J., & Gromov, A. (2008). Characterization of Test Dust for Product Qualification. *Bulk Solids & Power -Science & Technology*, *3*(4), 155–161.

Tryner, J., L'Orange, C., Mehaffy, J., Miller-Lionberg, D., Hofstetter, J. C., Wilson, A., & Volckens, J. (2020). Laboratory evaluation of low-cost PurpleAir PM monitors and in-field correction using co-located portable filter samplers. *Atmospheric*

Environment, *220*(June 2019), 117067. https://doi.org/10.1016/j.atmosenv.2019.117067

Varela, G., Paz-Lopez, A., Duro, R. J., Lopez-Peña, F., & González-Castaño, F. J. (2009). An integrated system for urban pollution monitoring through a public transportation based opportunistic mobile sensor network. *Proceedings of the 5th IEEE International Workshop on Intelligent Data Acquisition and Advanced Computing Systems: Technology and Applications, IDAACS'2009*, *September*, 148–153. https://doi.org/10.1109/IDAACS.2009.5343007

Velasco, A., Ferrero, R., Gandino, F., Montrucchio, B., & Rebaudengo, M. (2016). A mobile and low-cost system for environmental monitoring: A case study. *Sensors (Switzerland)*, *16*(5). https://doi.org/10.3390/s16050710

Vu, T. V., Ondracek, J., Zdímal, V., Schwarz, J., Delgado-Saborit, J. M., & Harrison, R. M. (2017). Physical properties and lung deposition of particles emitted from five major indoor sources. *Air Quality, Atmosphere and Health*, *10*(1), 1–14. https://doi.org/10.1007/s11869-016-0424-1

Wallace, L. (2007). *Indoor Sources of Ultrafine and Accumulation Mode Particles : Size Distributions , Size-Resolved Concentrations , and Source Strengths Indoor Sources of Ultrafine and Accumulation Mode Particles : Size Distributions , Size-Resolved Concentrations ,. 6826*. https://doi.org/10.1080/02786820600612250

Wallace, L. A., Wheeler, A. J., Kearney, J., Van Ryswyk, K., You, H., Kulka, R. H., Rasmussen, P. E., Brook, J. R., & Xu, X. (2011). Validation of continuous particle monitors for personal, indoor, and outdoor exposures. *Journal of Exposure Science and Environmental Epidemiology*, *21*(1), 49–64. https://doi.org/10.1038/jes.2010.15

Wallace, L., Williams, R., Rea, A., & Croghan, C. (2006). Continuous weeklong measurements of personal exposures and indoor concentrations of fine particles for 37 health-impaired North Carolina residents for up to four seasons. *Atmospheric Environment*, *40*(3), 399–414. https://doi.org/10.1016/j.atmosenv.2005.08.042

Wang, Y., Li, J., Jing, H., Zhang, Q., Jiang, J., & Biswas, P. (2015). Laboratory Evaluation and Calibration of Three Low-Cost Particle Sensors for Particulate Matter Measurement. *Aerosol Science and Technology*, *49*(11), 1063–1077. https://doi.org/10.1080/02786826.2015.1100710

Weekly, K., Rim, D., Zhang, L., Bayen, A. M., Nazaroff, W. W., & Spanos, C. J. (2013). Low-cost coarse airborne particulate matter sensing for indoor occupancy detection. *IEEE International Conference on Automation Science and Engineering*, 32–37. https://doi.org/10.1109/CoASE.2013.6653970

Wen, T. H., Jiang, J. A., Sun, C. H., Juang, J. Y., & Lin, T. S. (2013). Monitoring street-level spatial-temporal variations of carbon monoxide in urban settings using a wireless sensor network (WSN) framework. *International Journal of Environmental Research and Public Health*, *10*(12), 6380–6396. https://doi.org/10.3390/ijerph10126380

WHO. (2010). Exposure to air pollution: a major public health concern. *WHO Document Production Services, Geneva*.

Williams, R., Kaufman, A., Hanley, T., Rice, J., & Garvey, S. (2014). *Evaluation of field-deployed low cost PM sensors*. *December*, 76. https://doi.org/EPA/600/R-14/464 (NTIS PB 2015-102104)

Williams, R., Kilaru, V. J., Snyder, E. G., Kaufman, A., Dye, T., Rutter, A., Russell, A.,

& Hafner, H. (2014). Air Sensor Guidebook. *Epa/600/R-14/159*, *1*, 1–5. https://cfpub.epa.gov/si/si_public_record_report.cfm?dirEntryId=277996&simpleSearch=1&searchAll=air+sensor+guidebook

Xing, Y. F., Xu, Y. H., Shi, M. H., & Lian, Y. X. (2016). The impact of PM2.5 on the human respiratory system. *Journal of Thoracic Disease*, *8*(1), E69–E74. https://doi.org/10.3978/j.issn.2072-1439.2016.01.19

Yu, C. C., & Hung, I. F. (1995). Incense smoke: Characterization and dynamics in indoor environments. *Aerosol Science and Technology*, *23*(3), 271–281. https://doi.org/10.1080/02786829508965312

Yu, C. H., Fan, Z., Lioy, P. J., Baptista, A., Greenberg, M., & Laumbach, R. J. (2016). A novel mobile monitoring approach to characterize spatial and temporal variation in traffic-related air pollutants in an urban community. *Atmospheric Environment*, *141*, 161–173. https://doi.org/10.1016/j.atmosenv.2016.06.044

Zelenyuk, A., Cai, Y., & Imre, D. (2006). From Agglomerates of Spheres to Irregularly Shaped Particles: Determination of Dynamic Shape Factors from Measurements of Mobility and Vacuum Aerodynamic Diameters. *Aerosol Science and Technology*, *40*(3), 197–217. https://doi.org/10.1080/02786820500529406

Zheng, T., Bergin, M. H., Johnson, K. K., Tripathi, S. N., Shirodkar, S., Landis, M. S., Sutaria, R., & Carlson, D. E. (2018). Field evaluation of low-cost particulate matter sensors in high-and low-concentration environments. *Atmospheric Measurement Techniques*, *11*(8), 4823–4846. https://doi.org/10.5194/amt-11-4823-2018

Zikova, N., Hopke, P. K., & Ferro, A. R. (2017). Evaluation of new low-cost particle monitors for PM2.5concentrations measurements. *Journal of Aerosol Science*,

105(May 2016), 24–34. https://doi.org/10.1016/j.jaerosci.2016.11.010

Zimmerman, N., Presto, A. A., Kumar, S. P. N., Gu, J., Hauryliuk, A., Robinson, E. S., Robinson, A. L., & Subramanian, R. (2018). A machine learning calibration model using random forests to improve sensor performance for lower-cost air quality monitoring. *Atmospheric Measurement Techniques*, *11*(1), 291–313. https://doi.org/10.5194/amt-11-291-2018

Zou, Y., Young, M., Chen, J., Liu, J., May, A., & Clark, J. D. (2020). Examining the functional range of commercially available low-cost airborne particle sensors and consequences for monitoring of indoor air quality in residences. *Indoor Air*, *30*(2), 213–234. https://doi.org/10.1111/ina.12621

Zou, Y., Young, M., Wickey, M., May, A., & Clark, J. D. (2020). Response of eight low-cost particle sensors and consumer devices to typical indoor emission events in a real home (ASHRAE 1756-RP). *Science and Technology for the Built Environment*, *26*(2), 237–249. https://doi.org/10.1080/23744731.2019.1676094